APPLICATION OF
GEOGRAPHIC INFORMATION SYSTEMS
TO LANDSLIDE HAZARD ZONATION

C. J. van Westen

STELLINGEN

behorende bij het proefschrift

APPLICATION OF GEOGRAPHIC INFORMATION SYSTEMS TO LANDSLIDE HAZARD ZONATION

van

Cornelis Johannes van Westen

1. Onderzoek naar aardverschuivingsgevaar heeft zelden geresulteerd in gevarenkaarten.
   "Natural hazard means the probability of occurrence within a specified period of time and within a given area of a potentially damaging phenomenon"
   D.J. Varnes (1984) "Landslide hazard zonation: a review of principles and practice". Commission on Landslides of the IAEG, UNESCO, Natural Hazards No.3.

2. Het gebruik van Geografische Informatie Systemen in het onderzoek naar aardverschuivingsgevaar is het meest nuttig voor onervaren aardwetenschappers.

3. Het toepassen van onderzoeksmethoden die de verschillende factoren, welke van invloed zijn op het voorkomen van aardverschuivingen, onafhankelijk beoordelen, resulteert in een grote overschatting van het aardverschuivingsgevaar.

4. Indien de juistheid van een gevarenkaart wordt getoetst aan het voorkomen van aardverschuivingen in het gekarteerde gebied, is er sprake van een cirkelredenering.

5. Geomorfologische kaarten dienen gemaakt te worden op basis van veldwerk, voorafgegaan door fotointerpretatie, en niet door fotointerpretatie, gevolgd door een veld "check".

6. Het verdient aanbeveling een geomorfologische gevarenkartering vergezeld te doen gaan van een gedetailleerde beschrijving van de gehanteerde besluitvormingscriteria.

7. De aantrekkelijkheid van een A.I.O. aanstelling zou sterk verhoogd kunnen worden, bij gelijkblijvend budget en rendement, door het salaris met 1/2 te verhogen en 1/3 minder plaatsen toe te wijzen.

8. Zeeland is de provincie met de meeste historische aardverschuivingen in Nederland.
   "Zeeuwse zandkorrels gewonnen in zonnebrand en hemeldauw op de berghellingen van Midden Europa, weggesleurd door de zondvloed en neergeploft in het kille sombere diep, niet gekomen tot rust, maar trillen nog na, breed uitvloeiend als enige schok hen opjaagt uit de schijnbare eeuwslaap"
   R.P.J.Tuteyn Nolthenius, Worstelend Zeeland, 1898.
   Ing. M.H. Wilderom, Tussen Afsluitdammen en Deltadijken, Deel 4, Zeeuws Vlaanderen, 567 pp.

9. De uitdrukking "Acts of God", die gebruikt wordt voor het vóórkomen van natuurrampen, zou evengoed gebruikt kunnen worden voor het voorkómen van natuurrampen.

10. Men moet voorzichtigheid betrachten bij het gebruik van het werkwoord "gissen" als aanduiding voor het werken met Geografische Informatie Systemen (GIS), vooral in een instituut dat zich bezighoud met "luchtkaartering".

Enschede, januari 1993

APPLICATION OF GEOGRAPHIC INFORMATION SYSTEMS
TO LANDSLIDE HAZARD ZONATION

APPLICATION OF GEOGRAPHIC INFORMATION SYSTEMS TO LANDSLIDE HAZARD ZONATION

TOEPASSING VAN GEOGRAFISCHE INFORMATIE-SYSTEMEN IN DE ZONERING VAN AARDVERSCHUIVINGSGEVAAR

Proefschrift ter verkrijging van de graad van doctor
aan de Technische Universiteit Delft,
op gezag van de Rector Magnificus, prof. drs. P.A. Schenck,
in het openbaar te verdedigen ten overstaan van een commissie
aangewezen door het College van Dekanen
op 1 februari 1993 te 16.00 uur

door

Cornelis Johannes van Westen,

geboren te Terneuzen,
doctorandus Fysische Geografie

SUMMARY

The objective of landslide hazard zonation is subdivision of an area into zones with an equal susceptibility to or probability for the occurrence of mass movements. Many different methods have been proposed in the literature. These methods have in common the combination and integration of a series of input maps, which is a time-consuming process if done manually.

This study evaluates the applicability of geographic information systems (GIS), which are computerized systems for the handling of geographical data, for landslide hazard assessment. An inventory was made of the currently available methods, in order to compare these and to give recommendations for the use of specific methods for specific situations. Nine different methods are discussed in chapter 2: mass movement distribution analysis, mass movement density analysis, mass movement activity analysis, geomorphological hazard analysis, qualitative hazard analysis, univariate statistical analysis, multivariate statistical analysis, deterministic slope instability analysis, and mass movement frequency analysis. The potential and the specific requirements for input data for each of these methods are treated. Three scales of analysis are distinguished: a regional scale (<1:100,000), a medium scale (1:50,000-1:25,000) and a large scale (>1:10,000). Recommendations are given as to which method is applicable at each of the scales, and how a GIS could be incorporated.

The methods have been tested in the Rio Chinchina area in the Cordillera Central in Colombia, near the city of Manizales. Study areas were selected for each of the three scales mentioned above, and data sets were collected. Chapter 3 gives an introduction to the specific aspects of the the study area related to the occurrence of mass movements, such as the geological setting, the faulting pattern and seismic activity, the presence of mantles of volcanic ash, the climatic situation, deforestation, coffee cultivation, road construction, and urbanization. Several examples of mass movement phenomena are described.

Issues related to the collection of data for landslide hazard assessment using GIS are discussed in chapter 4. For each of the three scales, the minimum requirements for data types and volumes, and standards for data collection are presented. Interpretation of aerial photography and satellite imagery is the main source of information for many of the input maps, and should be carried out in a well structured manner, with the use of clear criteria and photo checklists. Emphasis is placed on the use of multitemporal aerial photo interpretation to evaluate changes in mass movement activity and landuse patterns. Fieldwork techniques were developed which include the use of checklists for the description of mass movement phenomena, and the collection of soil and rock data, also using simple field tests.

The use of geographic information systems requires a special approach to data collection and data management. Chapter 5 deals with the special aspects of data entry and data manipulation for landslide hazard assessment using a GIS. The structure of the map data bases and the attribute data bases is given for the three different scales. Examples are given of pre-analysis data manipulation, with special emphasis on the construction of an engineering geological map and the application of a groundwater model at the large scale.

In chapter 6 all methods of analysis are tested with data sets from the Rio Chinchina area. The results of the analyses are discussed and the problems which were encountered are outlined. Special emphasis is given to univariate statistical analysis, as this is concluded to be the most useful method to combine the field knowledge of the earth scientist with the computational capabilities of the GIS. Qualitative analytical methods usually do not fully benefit from the GIS capabilities and are considered to be very dependent on the subjective judgement of the earth scientist. However, when limited input data are available, they are the only feasible methods. They may result in high-quality hazard maps, if made by experienced geomorphologists. Multivariate analysis techniques meet problems associated with the sampling of variables. Deterministic models require very detailed input data which cannot be provided when working over large areas.

An evaluation of error sources is given in chapter 7. The most error-prone maps are based on subjective image-interpretation. However, errors in existing maps and field observations may also be considerable. Heavy emphasis should be given in future work to the development of standards for data collection, and a clear differentiation in the input maps of factual and inferred data.

In conclusion, GIS is considered to be a useful tool in assessment of landslide hazard (chapter 8). It is, however, a tool which, apart from its potential for data manipulation, updating, and analysis, confronts the user with the importance of detailed, accurate, and reliable input maps and ample field experience.

i

CONTENTS

CHAPTER 1: INTRODUCTION

CHAPTER 1: INTRODUCTION

Mass movements in mountainous terrain are natural degradational processes, and one of the most important landscape building factors. Most of the terrain in mountainous areas has been subjected to slope failure at least once, under the influence of a variety of causal factors, and triggered by events such as earthquakes or extreme rainfall.

Mass movements become a problem when they interfere with human activity. The frequency and the magnitude of slope failures can increase due to human activities, such as deforestation or urban expansion. In developing countries this problem is especially great due to rapid non-sustainable development of natural resources. Developing countries suffer some 95% of total disaster-related fatalities, which are estimated to number on the order of 225,000 per year (A.Hansen, 1984). Economic losses attributable to natural hazards in developing countries may represent as much as 1-2% of gross national product (Fournier D'Albe, 1976). Losses due to mass movements are estimated to be one quarter of the total losses due to natural hazards (A.Hansen, 1984).

These statistics illustrate well the importance of hazard mitigation. Indeed, the decade 1990-2000 has been designated the "International Decade for Natural Disaster Reduction" by the general assembly of the United Nations.

Mitigation of landslide disasters can be successful only when detailed knowledge is obtained about the expected frequency, character, and magnitude of mass movement in an area. The zonation of landslide hazard must be the basis for any landslide mitigation project and should supply planners and decision makers with adequate and understandable information. Analysis of landslide hazard is a complex task, as many factors can play a role in the occurrence of mass movements (see Crozier, 1986 for a comprehensive treatment of causes). The analysis requires a large number of input parameters, and techniques of analysis may be very costly and time-consuming. The increasing availability of computers during the last decades has created opportunities for a more detailed and rapid analysis of landslide hazard.

This study deals with the application of a relatively new tool for earth scientists in landslide hazard zonation: the use of computerized systems for the handling of geographical data, known as geographic information systems (GIS).

The main objective of this research is to develop a methodology for landslide hazard zonation using a PC-based GIS. This main objective can be divided into a number of specific objectives:

- Collection of information on existing methods for landslide hazard assessment (chapter 2).
- Identification of different scales of analysis and definition of their characteristic requirements and potentials (chapter 2).
- Identification of input data needed for each method of analysis (chapter 2 and 4).
- Design of procedures for data entry, data base construction and data analysis within a GIS for the execution of the various methods (chapter 5).
- Testing of each method using the same basic data set (chapter 6), obtained from the Rio Chinchina study area in central Colombia (chapter 3).
- Evaluation of potential sources of error in input data and analysis methods (chapter 6 and 7).

1

- Comparison of the various methods and recommendation of optimal methods for each scale of analysis (chapter 7 and 8).

The methodological framework which is presented should be understandable for earth scientists, without extensive knowledge of geographical information systems. For this reason some general aspects of GIS are treated.

Although the methodology is tested, and results for different techniques are compared for the Rio Chinchina study area, the main objective is not to produce a hazard map for this particular region.

Most of the hazard maps resulting from the various techniques will be presented in a reduced format, in order to reduce reproduction costs. Maps at their original scale can be obtained from the author on request.

CHAPTER 2: BACKGROUND

This chapter provides an overview of the concepts involved in the assessment of slope instability hazard. A general overview of the available methods to assess slope instability hazard is presented, together with a more in-depth discussion of GIS-based methods. But first a brief introduction of the concepts of *hazard*, *vulnerability* and *risk* is presented.

2.1 Hazard, vulnerability, and risk

Mass movement is defined as "the outward or downward gravitational movement of earth material without the aid of running water as a transporting agent" (Crozier, 1986). Although by definition the term *landslide* is used only for mass movements occurring along a well-defined sliding surface, it has been used as the most general term for all mass movements, including those that involve little or no sliding. In this study the terms *mass movement*, *landslide*, *slope movement* and *slope failure* are used synonymously.

To differentiate between the terms *hazard*, *vulnerability* and *risk*, the following definitions (given by Varnes, 1984) have become generally accepted:

Natural hazard (H):	the probability of occurrence of a potentially damaging phenomenon within a specified period of time and within a given area.
Vulnerability (V):	the degree of loss to a given element or set of elements at risk (see below) resulting from the occurrence of a natural phenomenon of a given magnitude. It is expressed on a scale from 0 (no damage) to 1 (total loss).
Specific risk (Rs):	the expected degree of loss due to a particular natural phenomenon. It may be expressed by the product of H and V.
Elements at risk (E):	the population, properties, economic activities, including public services, etc. at risk in a given area.
Total risk (Rt):	the expected number of lives lost, persons injured, damage to property, or disruption of economic activity due to a particular natural phenomenon. It is therefore the product of specific risk (Rs) and elements at risk (E): $Rt = (E)*(Rs) = (E)*(H*V)$.

Landslide hazard is commonly shown on maps, which display the spatial distribution of hazard classes (landslide hazard zonation). *Zonation* refers to "the division of the land in 'homogeneous' areas or domains and their ranking according to degrees of actual/potential hazard caused by mass movement" (Varnes, 1984). Landslide hazard zonation requires a detailed knowledge of the processes that are or have been active in an area, and on the factors leading to the occurrence of the potentially damaging phenomenon. This is considered the task of earth scientists. Vulnerability analysis requires detailed knowledge of the population density, infrastructure, and economic activities, in addition to the hazard. Therefore, this part of the analysis is done mainly by persons from other disciplines, such as urban planning, social geography, and economics.

Fully worked out examples of risk analysis on a quantitative basis are still scarce in the literature (Einstein, 1988; Kienholz, 1992; Innocenti, 1992), because of the difficulties in defining quantitatively both hazard and vulnerability. Hazard analysis is seldom executed in accordance with the definition given above, since the probability of occurrence of potentially damaging phenomena is extremely difficult to determine for larger areas. The determination of actual probabilities requires analysis of triggering factors, such as earthquakes or rainfall,

or the application of complex models. In most cases, however, there is no clear relationship between these factors and the occurrence of landslides. Therefore, the legend classes used in most hazard maps do not give more information than relative indications, such as high, medium, and low hazard.

This study is restricted to the analysis of landslide hazard.

2.2 Hazard mapping/hazard analysis

An ideal map of slope instability hazard should provide information on the spatial probability, temporal probability, type, magnitude, velocity, runout distance, and retrogression limit of the mass movements predicted in a certain area (Hartlén and Viberg, 1988). The most straightforward type of hazard map is a landslide inventory map displaying present and past landslides. Assessment of the areal extent of landslides and their evolution in the recent past can be made with the use of multitemporal photo interpretation and geomorphological fieldwork. However, in landslide hazard zonation one should take care with this approach for the following reasons:

1. Landslides may have occurred in the past under conditions different from those that prevail today, such as a different climatic regime or different land-use conditions.
2. The method gives information on those areas where landslides are observed presently, but does not provide a hazard prediction for areas that were free of landslides when the photos were taken.

Prediction of hazard in areas presently free of landslides requires different methods, based on the assumption that hazardous phenomena that have occurred in the past can provide useful information for the prediction of occurrences in the future. Therefore, *mapping* these phenomena and the factors thought to be of influence is very important in hazard zonation. Two general approaches are used for such mapping:

1. Many of the geomorphology-based hazard zonation studies can be called *hazard mapping* studies, since the hazard is basically assessed in the field during mapping. This method is also called the *direct approach* (A.Hansen, 1984).
2. *Indirect methods* calculate the importance of the combinations of parameters occurring in landslide locations, and extrapolate the results to landslide-free areas with similar combinations, mostly by statistical techniques (A.Hansen, 1984).

Another useful division in techniques for assessment of slope instability hazard is given by Hartlén and Viberg (1988), who differentiate between *relative hazard* and *absolute hazard assessment techniques*. The relative hazard assessment techniques differentiate the likelihood of occurrence of mass movements for different areas on the map, without giving exact values. Absolute hazard maps display an absolute value for the hazard, either as a factor of safety or a probability of occurrence. A combination is also possible, indicating the probability that the factor of safety is below one.

Absolute hazard assessment techniques can be divided into three main groups (Carrara, 1983; Hartlén and Viberg, 1988):

1. *White box models*, based on physical models (slope stability and hydrological models), also referred to as *deterministic models*;
2. *Black box models*, not based not on physical models but on statistical analysis;
3. *Grey box models*, based partly on physical models and partly on statistics.

2.3 General trends in landslide hazard zonation

A large amount of research on hazard zonation has been done over the last 30 years as the consequence of an urgent demand for slope instability hazard mapping. Overviews of the various slope instability hazard zonation techniques can be found in Cotecchia (1978), Brabb (1984), A. Hansen (1984), Varnes (1984), and Hartlén and Viberg (1988). Initially the investigations were oriented mainly toward problem solving at the scale of site investigation and development of deterministic models. A wide variety of deterministic slope stability methods is now available to the engineer. Good reviews of these can be found in Lambe and Whitman (1969), Chowdury (1978, 1984), Hoek and Bray (1981), Graham (1984), Bromhead (1986), and Anderson and Richards (1987).

The large regional variability of geotechnical variables such as cohesion, angle of internal friction, thickness of layers, or depth to groundwater, is inconsistent with the homogeneity of data required in deterministic models. The site investigation approach provides an unacceptable cost/benefit ratio for engineering projects over larger areas during the planning and decision-making phases due to the high cost and time requirements of data collection. Several types of landslide hazard zonation techniques have been developed to tackle such problems encountered in the application of deterministic modelling. A summary of the various trends in the development of techniques is given in table 2.1. Each of the main groups highlighted in table 2.1 is described in more detail in the following paragraphs.

Type of landslide hazard analysis	Main characteristic
A. Distribution analysis	Direct mapping of mass movement features resulting in a map which gives information only for those sites where landslides have occurred in the past
B. Qualitative analysis	Direct, or semi-direct, methods in which the geomorphological map is renumbered to a hazard map, or in which several maps are combined into one using subjective decision rules, based on the experience of the earth scientist
C. Statistical analysis	Indirect methods in which statistical analyses are used to obtain predictions of the mass movement hazard from a number of parameter maps
D. Deterministic analysis	Indirect methods in which parameter maps are combined in slope stability calculations
E. Landslide frequency analysis	Indirect methods in which earthquake and/or rainfall records or hydrological models are used for correlation with known landslide dates, to obtain threshold values with a certain frequency

Table 2.1: General trends in landslide hazard zonation methods.

A. Landslide distribution analysis

The most straightforward approach to landslide hazard mapping is a *landslide inventory map*, based on aerial photo interpretation, ground survey, and/or a data base of historical occurrences of landslides in an area. The final product gives the spatial distribution of mass movements, represented either at scale or as points (Wieczorek, 1984). Mass movement inventory maps are the basis for most of the other landslide hazard zonation techniques. They can, however, also be used as an elementary form of hazard map, because they display where in an area a particular type of slope movement has occurred. They provide information only for the period shortly preceding the date the aerial photos were taken or the fieldwork was conducted. They provide no insight into the temporal changes in mass movement distribution.

Many landslides that occurred some time before the photographs were taken may have become undetectable. Therefore a refinement is the construction of *landslide activity maps*, based on multitemporal aerial photo interpretation (Canutti et al., 1979, 1985, 1986). To study the effects of the temporal variation of a variable such as land use, landslide activity maps are indispensable.

Landslide distribution can also be shown in the form of a *density map*. Wright et al. (1974) presented a method to calculate landslide densities using counting circles. The resulting density values are interpolated and presented by means of *landslide isopleths*. Although the method does not investigate the relationship between mass movements and causal factors, it is useful in presenting landslide densities quantitatively.

B. Qualitative hazard analysis

In *geomorphological methods*, mapping of mass movements and their geomorphological setting is the main input factor for hazard determination. The basis for this approach was outlined by Kienholz (1977), who developed a method to produce a combined hazard map based on the mapping of "silent witnesses (Stumme Zeugen)". In this method the degree of hazard is evaluated at each site in the terrain. The decision rules are therefore difficult to formulate, as they vary from place to place. Because the hazard analysis is in fact accomplished "in the mind of the geomorphologist", geomorphological methods are considered subjective. In this study the terms *objective* and *subjective* are used to indicate whether the various steps taken in the determination of the degree of hazard are verifiable and reproducible by other researchers, or whether they depend upon the personal judgement of the researcher. The term subjective is not intended as a disqualification. Subjective analysis may result in a very reliable map when it is executed by an experienced geomorphologist and objective analysis may result in an unreliable map when it is based on an oversimplification of the real situation. Some examples of geomorphological hazard maps can be found in Carrara and Merenda (1974), Brunsden et al. (1975), Malgot and Mahr (1979), Kienholz (1977,1978,1980,1984), Kienholz et al. (1983,1988), Grunder (1980), Ives and Messerli (1981), Rupke et al. (1987, 1988), Perrot (1988), Hermelin (1990,1992), Hearn (1992) and Seijmonsbergen (1992).

To overcome the problem of the "hidden rules" in geomorphological mapping, other qualitative methods have been developed based on *qualitative map combination*. Stevenson (1977) developed an empirical hazard rating system for an area in Tasmania. On the basis of his expert knowledge on the causal factors of slope instability, he assigned weighting values to different classes in a number of parameter maps. This method of qualitative map combination has become very popular in slope instability zonation. The problem with this method is that the exact weighting of the various parameter maps is often based on insufficient field knowledge of the important factors, which will lead to unacceptable generalizations. The term "blind weighting" for this was suggested by Gee (1992).

C. Statistical hazard analysis

Aiming at a higher degree of objectivity and better reproducibility of the hazard zonation, which is important for legal reasons, statistical techniques have been developed for the assessment of landslide hazard. These quantitative methods have benefitted strongly from the availability of computers. Brabb et al. (1972) presented a method for quantitative *landslide*

6

susceptibility analysis at a regional scale, which is based on landslide occurrence, substrate material type, and slope angle. Geological units are grouped according to their landslide density and relative susceptibility values are assigned. Combining these values with a slope map produces final susceptibility classes. The method is easy to use, although it is usually not sufficient to use only the factors of rock type and slope angle.

Carrara et al. (1977b,1978) introduced a method for *multivariate statistical analysis* of mass movement data. Two main approaches of multivariate analysis exist:
1. Statistical analysis of point data obtained from checklists of causal factors associated with individual landslide occurrences (Neuland, 1976; Carrara et al., 1977b; Lessing et al., 1983; Corominas et al., 1992; Othman et al, 1992).
2. Statistical analysis performed on terrain units covering the whole study area. For each of the units data on a number of geological, geomorphological, hydrological, and morphometrical factors is collected and analyzed using multiple regression or discriminant analysis (Carrara et al.,1978,1990,1991; Carrara,1983,1988a,b,1992).

These methods are rather time-consuming, for both data collection and data processing. Several other statistical methods have been applied in landslide hazard analysis, such as the *information value method* (Yin and Yan, 1988; Kobashi and Suzuki, 1988), the *logical message model* (Runqiu and Yuanguo, 1992), and *probabilistic modelling* (Gonzalez, 1992; Sabto, 1991).

D. Deterministic hazard analysis

Despite problems related to collection of sufficient and reliable input data, deterministic models are increasingly used in hazard analysis over larger areas. They are applicable only when the geomorphological and geological conditions are fairly homogeneous over the entire study area and the landslide types are simple. The advantage of these "white box models" is that they have a physical basis. The main problem with these method is the high degree of oversimplification. This method is usually applied for translational landslides using the infinite slope model (Ward et al., 1982; Brass et al., 1989; Murphy and Vita-Finzi, 1991). The methods generally require the use of groundwater simulation models (Okimura and Kawatani, 1986). Stochastic methods are sometimes used for selection of input parameters (Mulder and van Asch, 1988; Mulder, 1991; Hammond et al., 1992).

E. Landslide frequency analysis

Most of the methods mentioned so far do not result in real hazard maps as defined by Varnes (1984). Assessing the probability of occurrence at a certain location within a certain time period is possible only when a relationship can be found between the occurrence of landslides and the frequency of triggering factors, such as rainfall or earthquakes. Especially for rainfall-related landslides, various techniques have been developed which determine threshold values of *antecedent rainfall* (Crozier, 1986; Keefer et al., 1987; Capecchi and Focardi, 1988).

7

2.4 Geographic information systems

A geographic information system (GIS) is defined as a "powerful set of tools for collecting, storing, retrieving at will, transforming and displaying spatial data from the real world for a particular set of purposes" (Burrough, 1986). The first experimental computerized GIS's were developed as early as the 1960's, but the real boom came in the 1980's, with the increasing availability of "cheap" (personal) computers. It is estimated that by 1986 more than 4000 different systems had been developed around the world (Burrough, 1986). There are still relatively few books devoted to GIS and none is dedicated specifically to geological applications. For an introduction to GIS the reader is referred to Burrough (1986) and Aronoff (1989). Other textbooks are by Penquet and Marble (1990), Rhind and Mounsey (1990), Tomlin (1990), and Bill and Frisch (1991). Generally a GIS consists of the following components:

- data input and verification;
- data storage and data base manipulation;
- data transformation and analysis;
- data output and presentation;

Differences between GIS systems are related to the following features:

- type of data structure (vector versus raster);
- data compression techniques (Quadtrees, run-length coding);
- two-dimensional versus three-dimensional;
- mainframe, mini-, and microcomputer hardware;
- user interfaces (pop-up menus, mouse-driven, help options, etc.).

For the work reported in this study a representative GIS system was used, which contains the standard routines offered by most GIS. The Integrated Land and Watershed Information System (ILWIS) was developed at ITC. It combines conventional GIS procedures with image processing capabilities and a relational data base, which also serves as an interface to external software packages (Valenzuela, 1988). Table 2.2 gives an overview of the various modules within the system (ITC, 1992). ILWIS is basically a raster system, as most of the analytical tools operate in the raster module. Vector data analysis is used only in network analysis. The core of the system is the calculation program in the Spatial Modelling Module. This program performs spatial analysis on multiple-input raster maps and connected attribute data tables for map overlay, reclassification, and various other spatial functions. It incorporates logical, arithmetical, conditional, and neighbourhood operations, including iteration. Modelling in ILWIS is facilitated by the ability to use batch files for automatic execution of lists of commands, and by the use of functions and macros for the calculation program. The system runs on an IBM-AT 80286, 80386, 80386SX, 80486, or compatible computer with an appropriate mathematical co-processor and high resolution graphics board. The system uses two screens: a monochromatic screen for text display and a colour monitor for display of images. The ILWIS system was been developed for use on a personal computer (PC), to make it available in most developing countries, where mainframe or minicomputers are still scarce (Valenzuela, 1988).

The advantages of the use of GIS as compared to conventional techniques are treated extensively by Burrough (1986) and Aronoff (1989). The advantages of GIS for assessing landslide hazard include:

- The much larger variety of hazard analysis techniques that becomes attainable. Due to the speed of calculation, complex techniques requiring a large number of map crossings and table calculations become feasible.
- The possibility to improve models, by evaluating their results and adjusting the input variables. The users can achieve the best results in a process of trial and error, by running the models several times, whereas it is difficult to use these models even once in the conventional manner. Therefore more accurate results can be expected.
- In the course of a landslide hazard assessment project the input maps derived from field observations can be updated rapidly when new data are collected. Also after the completion of the project the data can be used by others in an effective manner.

The disadvantages of GIS for assessing landslide hazard include:

- The large amount of time needed for data entry. Digitizing is especially time-consuming.
- The danger of placing too much emphasis on the data analysis as such, at the expense of data collection and manipulation based on professional experience. It is possible to use many different techniques of analysis, but often the necessary data are missing. In other words: the tools are available but cannot be used due to the lack, or uncertainty, of input data.

MODULE	Function	Explanation
INPUT MODULE	Data Conversion Digitizing	Conversion of vector, raster or table files in several formats Entry of maps. Screen digitizing is also possible
VECTOR MODULE	Network Copy & Merge Change Projection Display & Change Rasterizing	Performing of stream ordering analysis Copying or merging of vector files to other files Conversion of segment data from one projection to another Displaying, recoding, transforming, labelling of vector data Conversion of points, segments, or polygons to raster maps
RASTER: VISUALIZATION MODULE	Display & Store ColorLut PixelInfo Display3D Define Windows	Displaying or storing of raster maps on/from the colour screen Selecting, manipulating, and creating colour lookup tables Reading information for the same pixel from maps and tables Displaying maps in three dimensions (3-D) Defining windows of raster maps on the colour screen
RASTER: SPATIAL MODELLING	Calculation Crossing Distance Interpolation Geometric Trans	Performing of spatial analysis on sets of maps and tables Crossing of two raster maps and aggregating results Calculating distances and Thiessen polygons Interpolating from points, raster maps, or isolines Resampling of a map to a geo-referenced coordinate system
RASTER: IMAGE PROCESSING	Transfer function Stretch Colour composite Filter Statistics Sampling	Creating, loading, or editing of transfer functions Stretching or compressing images Creating colour composites using three images Enhancing of satellite images Calculating histograms and multiband statistics Sampling, clustering, classification, and density slicing
TABLE MODULE	Table Calculation Special Tables	Manipulating of tabular data with many functions Creating and editing of 2-D tables and classification tables
POINTS MODULE	Vector to points Raster to points Points to raster	Converting segment maps to point tables Converting raster maps to point tables Converting point tables to raster maps
OUTPUT MODULE	Conversions Annotation Output	Converting ILWIS vector/raster/tables to other formats Creating, displaying, or updating legends, symbols, and text Plotting and printing of maps and graphs

Table 2.2: Schematic overview of modules and routines of the ILWIS system (ITC, 1992).

2.5 GIS in landslide hazard analysis

The development of GIS has greatly increased the applicability of techniques for landslide hazard assessment. The first applications of simple, self-programmed, prototype GIS in the analysis of landslide hazard zonation date from the late 1970's. Newman et al. (1978) reported on the feasibility of producing landslide susceptibility maps using computers. Carrara et al. (1978) reported results of multivariate analysis applied on grid cells with a ground resolution of 200 x 200 m using approximately 25 variables. Huma and Radulescu (1978) reported an example from Romania of a qualitative hazard analysis including the factors of mass movement occurrence, geology, structural geological conditions, hydrological conditions, vegetation, slope angle, and slope aspect. Radbruch-Hall et al. (1979) have written their own software to produce small-scale (1:7,500,000) maps with 6,000,000 pixels showing hazards, unfavourable geological conditions, and areas where construction or land development may exacerbate existing hazards. The maps were made by qualitative overlay of several input maps.

During the 1980's the use of GIS for slope instability mapping increased sharply due to the development of commercial GIS systems, such as ARC/INFO, Intergraph, SPANS and IDRISI, and the increasing availability of PCs. The majority of case studies presented in the literature on this subject deal with qualitative hazard mapping. The importance of geomorphological input data is stressed in the methods used by Kienholz et al. (1988), who used a GIS for a qualitative mountain hazard analysis; detailed aerial photo interpretation was used as a basis. The authors state that due to the lack of good models and geotechnical input data, the use of a relatively simple model based on geomorphology seems to be the most realistic method. Most examples of qualitative hazard analysis with GIS are very recent (Stakenborg, 1986; Mani and Gerber, 1992; Bertozzi et al., 1992; Kingsbury et al, 1992). Many examples are presented in the proceedings of the "First International Symposium on the use of Remote Sensing and GIS for Natural Risk Assessment", held in Bogotá, Colombia, in March 1992 (Mendivelso et al., 1992; Osejo, 1992; Vargas, 1992; Peralta, 1992; Mora and Vahrson, 1992; Simões et al, 1992).

Examples of landslide susceptibility analysis with GIS reported since the 1970's have come mainly from the United States Geological Survey (USGS) in Menlo Park, California, where Brabb and his team have proceeded with their work and extended it, taking into account additional factors besides landslides, geology, and slope (Brabb, 1984, 1987; Brabb et al., 1989). Other examples of quantitative univariate statistical analysis with GIS are rather scarce (Lopez and Zinck, 1992; Choubey and Litoria, 1990; Choubey et al., 1991). This is rather strange, since one of the strong advantages of using a GIS is the capability to test the importance of each factor, or combinations of factors, and assign quantitative weighting values based on mass movement density.

Recent examples of multivariate statistical analysis using GIS have been presented mainly by Carrara and his team. Their work has developed from the use of large rectangular grid cells as the basis for analysis (Carrara et al., 1978; Carrara, 1983, 1988a) towards the use of morphometric units (Carrara et al., 1990, 1991; Carrara, 1988b, 1992). The method itself has not undergone major changes. The statistical model is built-up in a "training area", where the spatial distribution of landslides is (or should be) well known (Carrara, 1988a). In the next step the model is extended to the whole study area or "target area", based on the assumption that the factors that cause slope failure in the training area are the same as in the target area.

Another example of multivariate analysis using a GIS is presented by Bernknopf et al. (1988). They applied multiple regression analysis to a data set, using presence/absence of landslides as the dependent variable and the factors used in a slope stability model (soil depth, soil strength, slope angle) as independent variables. Water table data and cohesion data were not taken into account. The resulting regression function is transformed so that landslide probability can be calculated for each pixel.

Deterministic modelling of landslide hazard using GIS has become rather popular. Most examples deal with infinite slope models, since they are simple to use for each pixel separately (Brass et al., 1989; Murphy and Vita-Finzi, 1991). Hammond et al. (1992) presented methods in which the variability of the factor of safety is calculated from selected input variables following the Monte Carlo technique. This implies a large number of repeated calculations, which require the use of a GIS.

Another useful application of GIS has been the prediction of rockslides by comparing discontinuity measurements within structurally homogeneous regions with slope angle and aspect for each pixel (Wagner et al., 1988, Wentworth et al., 1987, Essa Nuru, 1992). The method is feasible only in structurally simple areas, however.

A relatively new development in the use of GIS for slope instability assessment is the application of so-called "neighbourhood analysis". Most of the conventional GIS techniques are based on "map overlaying", which allows only for the comparison of different maps at the same pixel locations. Neighbourhood operations allow as well evaluation of the neighbouring pixels around a central pixel, and can be used in the automatic extraction from a digital elevation model (DTM) of such morphometric and hydrological features as slope angle, slope aspect, downslope and cross-slope convexity, ridge and valley lines, catchment area, stream ordering, and the contributing area for each pixel. Zevenbergen and Thorne (1987) presented a method for the automatic extraction of slope angle, slope aspect, and downslope and cross-slope convexity. An overview of the algorithms applied in the extraction of morphometric parameters from DTMs is given by Gardner et al (1990). Neighbourhood analysis has proved to be very useful in analysis of landslide hazard (Wadge, 1988). Carrara identified automatically the homogeneous units he used as the basis for a multivariate analysis from a detailed DTM. The morphometric and hydrological parameters used in that analysis were also extracted automatically (Carrara et al., 1990; Carrara, 1988b). Niemann and Howes (1991) performed a statistical analysis based on automatically extracted morphometric parameters (slope angle, slope aspect, downslope and cross-slope convexity and drainage area), which they grouped into homogeneous units using cluster analysis. Various authors (Okimura and Kawatani, 1986; Brass et al., 1989) have used neighbourhood analysis in the modelling of groundwater tables over time, as one of the input factors in infinite slope modelling. Van Dijke and van Westen (1990) applied a simple type of neighbourhood analysis to model the runout distances for rockfall blocks.

A recent development in the use of GIS for slope instability zonation is the application of expert systems. Pearson et al. (1991) developed an expert system in connection with a GIS in order to "remove the constraints that the users should have a considerable experience with GIS". A prototype interface between a GIS (ARC/INFO) and an expert system (Nexpert Object) was developed and applied for translational landslide hazard mapping in an area in Cyprus. The question remains, however, whether the rules used in the expert system apply only to this specific area, or whether they are universally applicable.

In sections 2.3 and 2.5 many different techniques for landslide hazard zonation were presented. One of the objectives of this study is to compare different methods of landslide hazard zonation and to give recommendations as to which method is most appropriate considering the working scale and the amount, type and quality of input data. Similar work on this topic is under development by Gee (1992) who applied nine landslide hazard zonation methods to a single area in the Korokoro hills near Wellington, New Zealand. The hazard maps were tested quantitatively using data derived from a major landslide event which occurred in 1976. Most of the zonation methods were found to produce maps with a similar ability to predict relative landslide susceptibility.

In the following sub-sections the techniques for landslide hazard zonation will be presented systematically for their use in a GIS. For each method a schematic working scheme is given. An overview of the required input data is given and the various steps using GIS are mentioned briefly. A recommendation is also given regarding the most appropriate working scale (regional: <1:100,000, medium: 1:25,000 - 1:50,000 and large: ≥ 1:10,000). A more detailed description of the working scales will be given in section 2.6.

2.5.1 Landslide distribution analysis

In most of the methodologies for landslide hazard assessment a mass movement distribution map is the most important input map, as it shows the distribution of the phenomena that one wants to predict. The input consists of a field-checked photo interpretation map of landslides for which recent, relatively large scale, aerial photos have been used, combined with a table containing landslide parameters, obtained from a checklist. GIS can perform an important task in transferring the digitized photo interpretation to the topographic base map projection using a series of control points and camera information (Bargagli, 1991).

The GIS procedure followed is:
- Digitizing of the mass movement phenomena, each with its own unique label and a six-digit code containing information on the landslide type, subtype, activity, depth, and site vegetation, and on whether the unit is a landslide scarp or body;
- Recoding of the landslide map with the parameters for type or subtype into maps displaying only one type of process.

The method is most appropriate at medium or large scales. At the regional scale, the construction of a mass movement distribution map is very time-consuming and too detailed for procedures of general regional zoning. Nevertheless, when possible it is advisable to prepare such a map also for the regional scale, although with less detail.

Some important considerations that arise in this method are:
- The accuracy of interpretation of mass movement phenomena from aerial photos depends on the skill of the interpreter, and the interpretation is subjective. Detailed fieldwork is very important. More comments related to this will be given in section 7.3.1;
- GIS in this technique is used only to store the information and to display maps in different forms (e.g. only the scarps, only slides, only active slides). Although the actual analysis is very simple, the use of a GIS system is of great advantage in this method. The user can select specific combinations of mass movement parameters and obtain a better insight into the spatial distribution of the various landslide types.

The method is schematically represented in figure 2.1
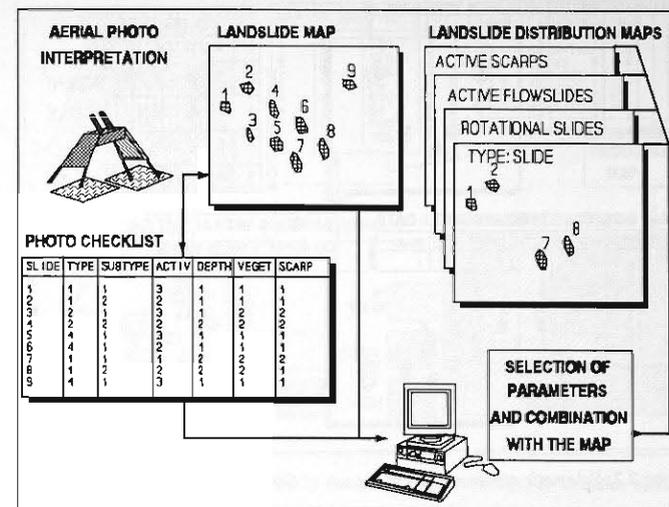
Figure 2.1: Schematic representation of the use of GIS for analysis of landslide distribution. The code numbers of the photo-checklist are explained in section 4.3.2.2.

2.5.2 Landslide activity analysis

The code for mass movement activity (see section 4.3.2.2) which is given to each mass movement phenomena can also be used in combination with mass movement distribution maps from earlier dates for to analyze mass movement activity. Depending on the type of terrain which is studied, time intervals of 5 to 20 years can be selected. This method of interval analysis offers numbers or percentages of reactivated, new, or stabilized landslides.

The following GIS procedures are used:
- The digitized map of recent mass movements is used as the basis for the digitizing of maps from earlier dates. This is done in order to make sure that the landslides, which were already present at earlier dates are digitized in the same position;
- Calculation of the differences in activity between two different dates, by comparison of the data from the checklists combined with the map data;
- Calculation of all landslides which were initiated or reactivated in the period between the two photo-coverages.

The most appropriate scales are the medium and the large scales, for the reason of the required detail of input maps, discussed in 2.5.1. The main problems with the landslide activity method are that it is very time-consuming, and that it is difficult to prevent inconsistencies between interpretations from the various dates. The information derived from aerial photos from earlier dates cannot be checked in the field, and will result in greater inaccuracies. The method is represented schematically in figure 2.2.
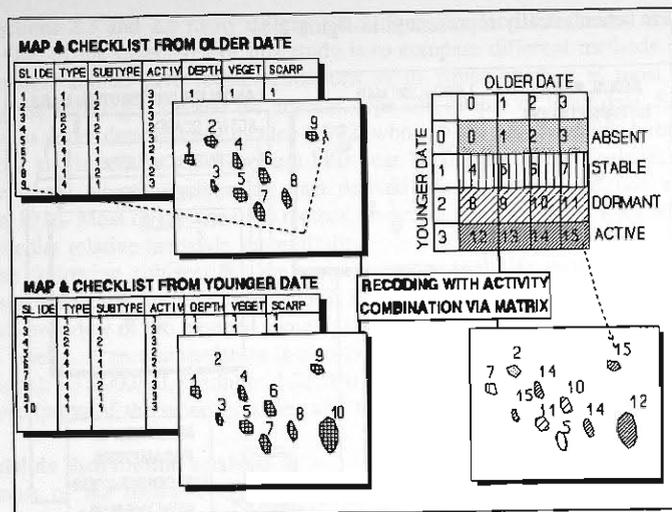
Figure 2.2: Schematic representation of the use of GIS for analysis of landslide activity.

2.5.3 Landslide density analysis

Mass movement information can also be presented as a percentage cover within mapping units. These mapping units may be terrain mapping units (TMUs), geomorphological units, geological units, etc. This method is also used to test the importance of each parameter individually for the occurrence of mass movements. The required input data consist of a mass movement distribution map, and a land-unit map. If the method is used to test the importance of specific parameter classes, the user decides, on the basis of his field experience, which individual parameter maps, or combination of parameter maps will be used.

The following GIS procedures are used for mass movement density analysis:

- Calculation of a bit map (presence/absence) for the specific movement type for which the analysis is carried out;
- Combination of the selected parameter map with the bit map through map crossing;
- Calculation of the area percentage per parameter class occupied by landslides.

With a small modification, the number of landslides can be calculated instead of the areal density. In that case a bit map is not made, and the mass movement map itself, in which each polygon has a unique code, is crossed with the parameter map (see also section 6.3.3.1).

A special form of mass movement density mapping is isopleth mapping. The method uses a large, moving, counting circle which calculates the landslide density for each circle centre. The result is a contour map of landslide density. The scale of the pixels and the size of the filter used define the values in the resulting density map. Except for the creation of a bit map, the procedure for landslide isopleth mapping is rather different (see section 6.1.4).

The method is most appropriate on the medium and large scales for the reasons discussed in section 2.5.1. The method is represented schematically in figure 2.3.
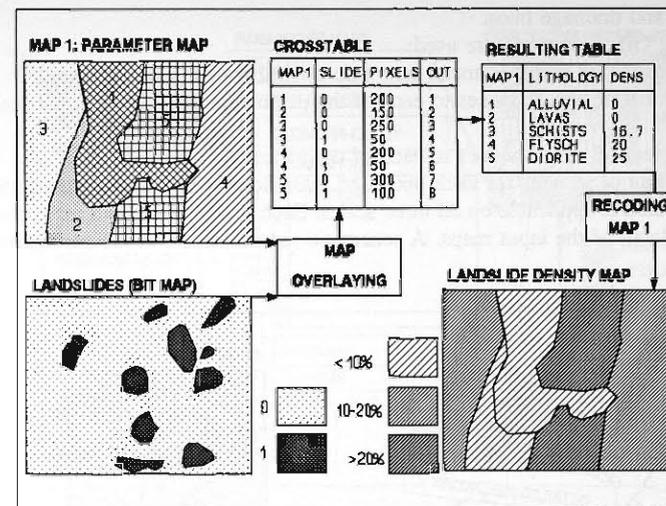
Figure 2.3: Schematic representation of the use of GIS for analysis of landslide density.

2.5.4 Geomorphological landslide hazard analysis

In geomorphological hazard analysis the hazard map is made by the mapping geomorphologist, using his site-specific knowledge, obtained through photo-interpretation and fieldwork. The map can be made either directly in the field, or by recoding the geomorphological map. The criteria on which he bases hazard class designations are not formalized in generally applicable rules and may vary from polygon to polygon. GIS can be used in this type of work as a drawing tool, allowing rapid recoding of units, and correction of units which were coded erroneously. GIS is not used as a tool for the analysis of the important parameters related to the occurrence of mass movements. The method can be applied at regional, medium or large scales in a relatively short time period. It does not require the digitizing of many different maps. However, the detailed fieldwork requires a considerable amount of time as well. The accuracy of the resulting hazard map will depend completely on the skill and experience of the geomorphologist. Geomorphological maps of the same area made by different geomorphologists may vary considerably, as will be shown in section 7.3.2. A schematic representation of the method is given in figure 2.4.

2.5.5 Qualitative landslide hazard analysis

The basis for this method of hazard mapping is the field knowledge of the earth scientist who decides which parameters are important for the occurrence of mass movements. Qualitative weighting values are assigned to each class of a parameter map, and each parameter map receives a different weight itself. The weight values are not derived quantitatively, but are estimated from field knowledge of the causal factors. Depending on the detail of the study several input maps can be used, among which the most important are geomorphology, mass movement occurrences, slope angle, geology, land use, and distance to

faults, roads, and drainage lines.

The following GIS procedures are used:

- Classification of each parameter map into a number of relevant classes;
- Assignment of weight values to each of the parameter classes (e.g., on a scale of 1 to 10);
- Assignment of weight values to each of the parameter maps;
- Calculation of weights for each pixel and classification in a few hazard classes.

The method is applicable on all three scales. Each scale has its own requirements as to the required detail of the input maps. A schematic representation of the method is given in figure 2.5.
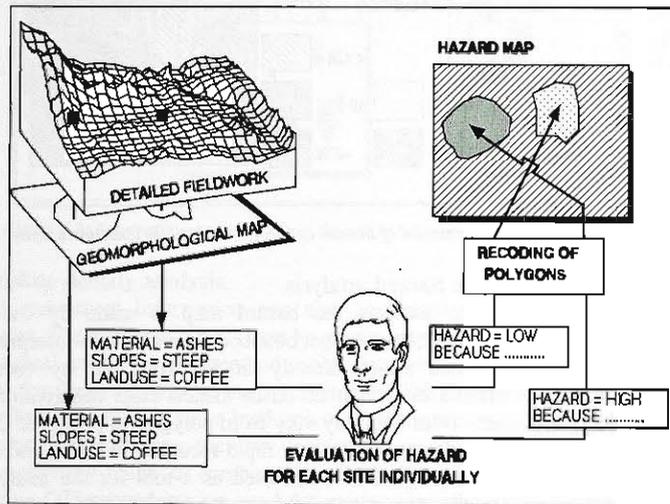
Figure 2.4: Schematic representation of the use of GIS for geomorphological hazard analysis.

2.5.6 Univariate statistical landslide hazard analysis

In this method, crossing of parameter maps and calculation of landslide densities form the core of the analysis. The importance of each parameter, or specific combinations of parameters, can be analyzed individually. Using normalized values (landslide density per parameter class in relation to the landslide density over the whole area), a total hazard map can be made by addition of the weights for individual parameters. The weight values can also be used to design decision rules, which are based on the experience of the earth scientist. It is also possible to combine various parameter maps into a map of homogeneous units, which is then crossed with the landslide map to give a density per unique combination of input parameters.

GIS is very suitable for use with this method, which involves a large number of map crossings and manipulation of attribute data. This method requires the same input data as the qualitative method discussed in the previous section.
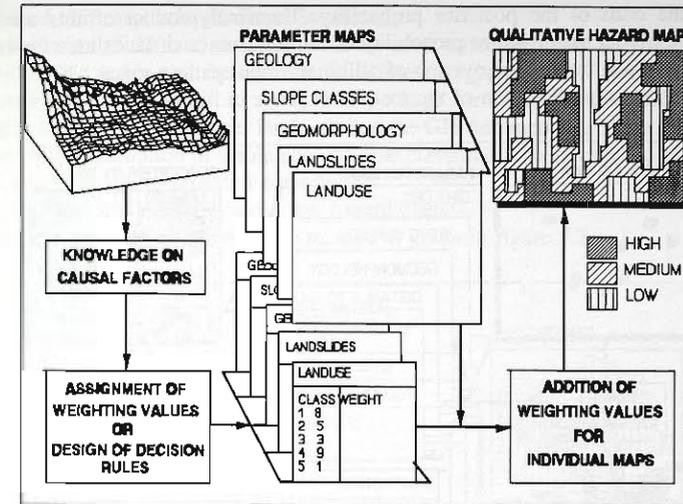
Figure 2.5: Schematic representation of the use of GIS for qualitative map combination.

It should be stressed that the selection of parameters has also an important subjective element in this method. The following GIS procedures are used:

- Classification of each parameter map into a number of relevant classes;
- Combination of the selected parameter maps with the landslide map via map crossing;
- Calculation of weighting values based on the cross table data;
- Assignment of weighting values to the various parameter maps, or design of decision rules to be applied to the maps, and classification of the resulting scores in a few hazard classes.

The medium scale is most appropriate for this type of analysis. The method is not detailed enough to apply at the large scale, and at the regional scale the necessary landslide occurrence map is difficult to obtain.

Several specific univariate statistical methods exist which are based on the same principles, but use different indexes:

The information value method (Yin and Yan, 1988) is a statistical technique that requires a data base of parameters collected for different land units. The analysis is based on the presence (1) or absence (0) of landslides at a certain location or within a land unit. It can be used for both alpha-numerical and numerical data. The presence or absence of parameters is also calculated. The relative importance for the occurrence of landslides of each parameter is calculated in terms of an information value, which is the log of the landslide density per parameter, as compared to the overall landslide density.

In *the weights of evidence method* (Bonham-Carter et al., 1990) point phenomena (landslides) are regarded along with several terrain factors. These factors are translated into binary input maps. Weights are assigned to the binary maps using Bayes rules for conditional probability. These weights are added to the log of the odds of the prior probability, to give

the log of the odds of the posterior probability. The final product of this analysis is a predictor map giving the posterior probability of the occurrence of landslides for each pixel, which is based upon the unique overlap of all binary input pattern maps.

A schematic representation of the method is given in figure 2.6.
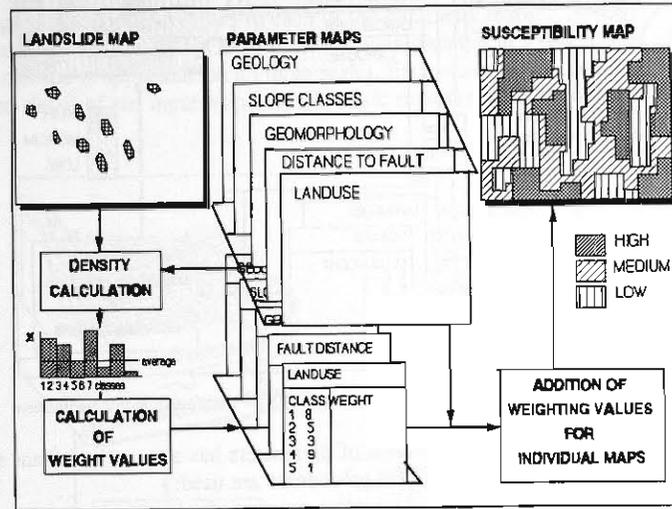
Figure 2.6: Schematic representation of the use of GIS for univariate statistical analysis.

2.5.7 Multivariate statistical landslide hazard analysis

Multivariate statistical analyses of important factors related to landslide occurrence may give the relative contribution of each of these factors to the total hazard within a defined land unit. The analyses are based on the presence or absence of mass movement phenomena within these land units, which may be catchment areas, interpreted geomorphological units or other kinds of terrain units.

Several multivariate methods have been proposed in the literature. Most of these, such as discriminant analysis or multiple regression, require the use of external statistical packages. GIS is used to sample parameters for each land unit. However, with PC-based GIS systems, the large volume of data may become a problem. The method requires a landslide distribution map and a land unit map. A large number of parameters is used, comparable to those mentioned in section 2.5.5. The different classes of a parameter map are considered as individual parameters result in a large matrix.

The following GIS procedures are used:
- Determination of the list of factors that will be included in the analysis. As many input maps (such as geology) are of an alpha-numerical type, they must be converted to numerical maps. These maps can be converted to presence/absence values for each land-unit, or presented as percentage cover, or the parameter classes can be ranked according to increasing mass movement density. By crossing the parameter maps with

the land-unit map, a large matrix is created;
- Combination of the land-unit map with the mass movement map via map crossing and dividing the stable and the unstable units into two groups;
- Exportation of the matrix to a statistical package for subsequent analysis;
- Importation of the results per land-unit into the GIS and recoding of the land-units. The frequency distribution of stable and unstable classified units is checked to see whether the two groups are separated correctly;
- Classification of the map into a few hazard classes.

A schematic representation of the method is given in figure 2.7.
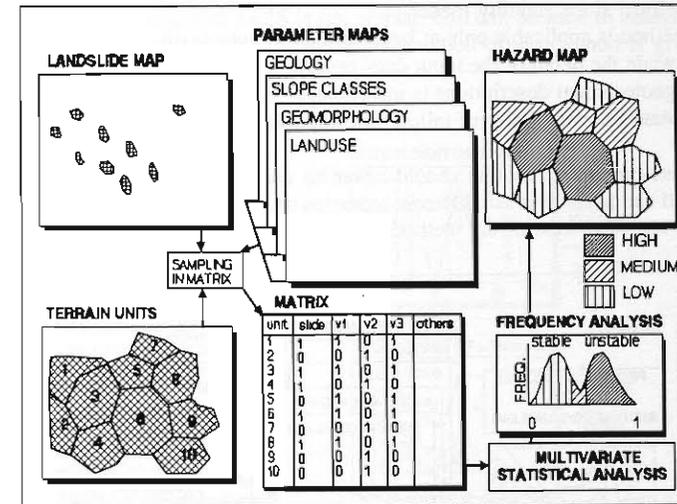
Figure 2.7: Schematic representation of the use of GIS for multivariate statistical analysis.

Although these techniques can be applied at different scales, the use becomes quite restricted at the regional scale, where an accurate input map of landslide occurrences may be not available, and where most of the important parameters cannot be collected with satisfactory accuracy. At large scales, different factors will have to be used (such as water-table depth, soil layer sequences and thicknesses). These data are very difficult to obtain even for relatively small areas. Therefore the medium scale is considered most appropriate for this technique.

2.5.8 Deterministic landslide hazard analysis

The methods described so-far give no information on the stability of a slope as expressed in terms of its factor of safety. For such a type of information slope stability models are required. These models require input data on: soil layer thickness, soil strength, depth below the terrain surface of potential sliding surfaces, slope angle, and pore pressure conditions to be expected on the slip surfaces.

The following parameter maps should be available in order to be able to use such models:
• A material map, showing both the distribution at ground surface and in the vertical profile, with accompanying data on soil characteristics;
• A groundwater level map, based on a groundwater model or on field measurements;
• A detailed slope angle map, derived from a very detailed DTM.

For the application of GIS in deterministic modelling several approaches can be followed:
• The use of an infinite slope model, which calculates the safety factor for each pixel;
• Selection of a number of profiles from the DTM and the other parameter maps which are exported to external slope stability models.
• Sampling of data at predefined grid-points, and exportation of these data to a three-dimensional slope stability model.

The method is applicable only at large scales and over small areas. At the regional and the medium scale the detail of the input data, especially concerning groundwater levels, soil-profile, and geotechnical descriptions is insufficient. The variability of the input data can be used to calculate the probability of failure in connection with the return period of triggering events.

The resulting safety factors should never be used as absolute values. They are only indicative and can be used to test different scenarios of slip surfaces and groundwater depths. A schematic representation of the method is given in figure 2.8.
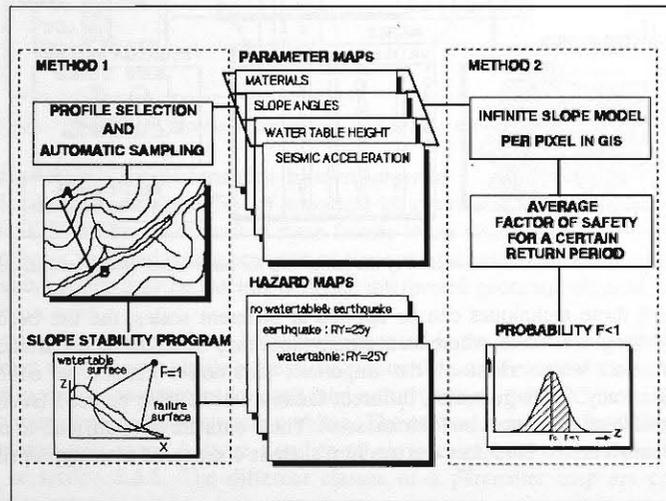
Figure 2.8: Schematic representation of the use of GIS in deterministic analysis.

2.5.9 Landslide frequency analysis

The probability of mass movement occurrence at a certain place within a certain time period can only be determined when a relationship can be found between the occurrence of landslides and the frequency of triggering factors, such as rainfall or earthquakes. The most

promising technique is the calculation of antecedent rainfall, which is the accumulated amount of precipitation over a specified number of days preceding the day on which a landslide occurred (Crozier, 1986). This way a rainfall threshold value can be calculated.

The following input data are required:
• Daily rainfall records;
• Landslide records (taken from insurance companies, newspapers, or fire/rescue departments).

The method is most appropriate at medium and large scales. At the regional scale it may be difficult to correlate known landslides at one location with rainfall records from a different location in the area. The spatial component is usually not taken into account in this analysis, and therefore the use of a GIS is not crucial. GIS can be used to analyze the spatial distribution of rainfall, however. A schematic presentation of the method is given in figure 2.9.
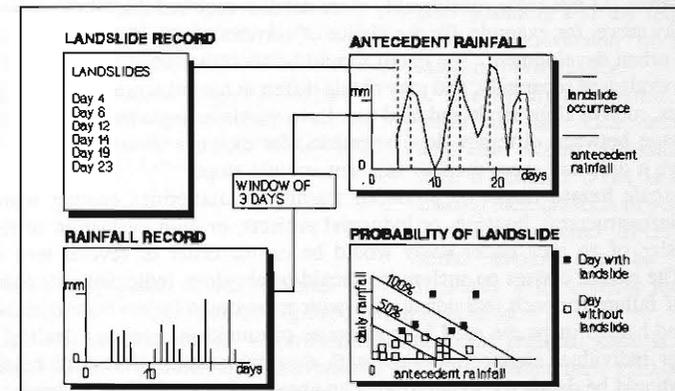
Figure 2.9: Schematic representation of the use of GIS in antecedent rainfall analysis. The window of 3 days relates to the summation of rainfall over the last three days.

2.6 Scales of analysis

Before starting any data collection, an earth scientist working on a hazard analysis project will have to answer a number of interrelated questions:
• What is the aim of the study?
• What scale and with what degree of precision must the result be presented?
• What are the available resources in the form of money and manpower?

Selecting the working scale for a slope instability analysis project is determined by the purpose for which it is executed. The following scales of analysis, which were presented in the International Association of Engineering Geologists (IAEG) monograph on engineering geological mapping (IAEG, 1976), can also be distinguished in landslide hazard zonation (Malgot and Mahr, 1979):

- Synoptic or regional scale (< 1:100,000);
- Medium scale (1:25,000 - 1:50,000);
- Large scale (1:5,000 - 1:10,000);
- Detailed maps (> 1:5,000).

Regional-scale hazard analysis is used to outline problem areas with potential slope instability. The maps are mainly intended for agencies dealing with regional (agricultural, urban, or infrastructural) planning. The areas to be investigated are very large, on the order of 1000 square kilometres or more, and the required detail of the map is low. The maps indicate regions where severe mass movement problems can be expected to threaten rural, urban, or infrastructural projects. Terrain units with areas of at least several tens of hectares are outlined. Within these units the degree of hazard is assumed to be uniform.

Medium-scale hazard maps are made mainly for agencies dealing with intermunicipal planning or companies dealing with feasibility studies for large engineering works (such as dams, roads, railroads). The areas to be investigated will have areas of several hundreds of square kilometres. At this scale considerably more detail is required than at the regional scale. The maps may serve, for example, for the choice of corridors for infrastructural construction or zones for urban development. The detail should be such that adjacent slopes in the same lithology are evaluated separately, and may obtain different hazard scores, depending on other characteristics, such as slope angle and land use. Even within a single terrain unit a distinction should be made between different slope segments, for example a concave part of a slope should receive a different score than an adjacent straight slope.

Large-scale hazard maps are produced mainly for authorities dealing with detailed planning of infrastructural, housing, or industrial projects, or with evaluation of risk within a city. The size of an area under study would be on the order of several tens of square kilometres. The hazard classes on such maps should be absolute, indicating, for example, the probability of failure for each individual units with areas down to less than a hectare.

Detailed hazard maps are used by companies or municipal agencies dealing with risk evaluation for individual engineering sites with maximum areas of several hectares. The information should be detailed enough to give an absolute hazard indication for terrain areas measuring down to 25 square meters across. Detailed site mapping at scales larger than 1:5,000, in combination with geotechnical testing and groundwater level measurement should provide sufficient information for the application of deterministic slope stability models.

Although the selection of the scale of analysis is usually determined by the intended application of its results, the choice of technique for mapping landslide hazard remains open. The choice depends on the type of problem, the availability of geotechnical and other data, the availability of financial resources, and time restrictions, as well as on the knowledge and experience of the research team. Furthermore, a number of factors related to the use of GIS in hazard analysis should be considered as described below.

1. *Image interpretation*. Aerial photo interpretation maps can be made at all scales, if aerial photos and/or satellite imagery are available at the appropriate scale. For detailed geomorphological mapping, or outlining of landslide phenomena, the imagery should generally be at a scale larger than 1:25,000 (Rengers et al., 1992). The number of aerial photos needed to cover an area stereoscopically is given in table 2.3, based on the size of the area and on the photo-scale (the useful area per photo for stereovision is estimated at 35%, taking into account overlap and sidelap). Brabb et al. (1989) prepared a landslide distribution map for the entire state of New Mexico (with an area of 121,122 km^2) using 1:30,000-scale aerial photos. The number of photos that had to be interpreted, was calculated as approximately 7500.

As can be seen from table 2.3, for regional mapping (areas of 1000 km^2 or more) medium- or large scale photography requires interpretation of too many photographs and an unacceptable amount of time for photo-interpretation and field-checking. For this reason, methods based on the use of detailed landslide occurrence maps are not considered feasible for large areas at the regional scale.

Size of the area (km²)	Aerial photo-scale	Useful area per photo (km²)	Number of photos
1000	1:50,000 (small)	35% of 126 = 44.3	23
1000	1:25,000 (medium)	35% of 31.6 = 11.1	90
1000	1:10,000 (large)	35% of 5.06 = 1.7	565

Table 2.3: Required number of aerial photos for stereoscopic coverage of an area at different photographic scales (assuming a photo-size of 22.5 x 22.5 cm).

2. *Amount of digitizing work*. Most of the map data must be entered via manual digitizing, which is very tedious and time consuming. The use of scanners is still less attractive due to the extensive editing that has to be done after scanning and the required raster-to-vector conversion of hand drawn maps of poor quality.

3. *Use of digital terrain models*. For many of the GIS techniques for landslide hazard assessment (section 2.5), a detailed DTM is essential. At small scales, creation of accurate DTMs is tedious. Stereo SPOT images or aerial photos can be used in a photogrammetrical process, or contour lines with sufficiently small contour intervals and a scale of 1:50,000 to 1:25,000 can be digitized and interpolated.

4. *Generalization problems*. A problem related to the regional scale is that it often becomes impossible to outline mass movements at scales smaller then 1:50,000. This has important consequences for all GIS procedures based on map crossing.

Area (km²)	Pixel size (m)	Number of pixels	Volume of Byte map	Volume of Integer map
10	20*20	158 * 158	25 Kb	50 Kb
100	20*20	500 * 500	0.25 Mb	0.5 Mb
1000	20*20	1581*1581	2.5 Mb	5.0 Mb
1000	10*10	3163*3163	10 Mb	20 Mb

Table 2.4: File volumes as determined by the size of the study area, the pixel size, and the data type.

5. *Quantitative data collection*. For maps linked to an attribute data base containing field and laboratory test data, it is very difficult to obtain relevant data for large areas at small scales. Parameters that are very important when using deterministic models, such as water-table depth, detailed soil profile data, or geotechnical parameters, are too variable to be used at medium or regional scales, unless the area is very homogenous. For this reason, the use of deterministic models is limited to the large and very large scales.

6. *Amount of storage space.* Depending on the data type (byte or integer), the size of the area, and the selected pixel-size, the volume of data that has to be stored on disk may cause problems. Both storage of input maps and of inter-mediate and final results of analysis may exceed the storage capacity, especially if a PC-based GIS system is used. Table 2.4 gives examples of some file sizes.

2.7 Phases of landslide hazard analysis using GIS.

The following phases can be distinguished in the process of mass movement hazard analysis using GIS:

1. Choice of the working scale and the methods of analysis which will be applied;
2. Collection of existing maps and reports with relevant data;
3. Interpretation of images and creation of new input maps;
4. Design of the data base and definition of the way in which data should be collected and stored;
5. Fieldwork to verify the photo-interpretation and to collect relevant quantitative data;
6. Laboratory analysis of soil and rock samples for classification;
7. Digitizing of maps and attribute data;
8. Validation of the entered data;
9. Manipulation and transformation of the raw data to a form which can be used in the analysis;
10. Analysis of data for preparation of hazard maps;
11. Evaluation of the reliability of the output maps and inventory of the errors which may have occurred during the previous phases.
12. Final production of hazard maps and adjoining report.

Most of these phases will be treated in more detail in chapters 4-7. There is a logical order of the various phases, although some may overlap considerably. Phases 7 to 11 are carried out behind the computer. Data base design (phase 4) occurs before computer-work starts, and even before fieldwork, because it determines the way in which the input data are collected in the field.

Table 2.5 gives a relative indication of the amount of time spent for each of the twelve mentioned phases at each of three scales. The time amounts are expressed as a percentage of the time spent on the entire process, and are an estimation based on the author's experience. Absolute time estimates are not given, since these depend on too many variable factors, such as the amount of available input data, the size of the study area, and the experience of the investigator(s).

Activity	Regional scale		Medium scale		Large scale	
	CONV	GIS	CONV	GIS	CONV	GIS
1 Choice of scale and methods	<5	<5	<5	<5	<1	<5
2 Collection of existing data	<5	<5	<5	<5	8	8
3 Image interpretation	50	50	30	30	10	20
4 Data base design	0	<5	0	<5	0	<5
5 Fieldwork	<5	<5	7	7	10	20
6 Laboratory analysis	0	0	0	<5	0	10
7 Data entry	0	20	0	30	0	15
8 Data validation	0	<5	0	5	0	5
9 Data manipulation	0	<5	0	5	0	5
10 Data analysis	30	10	48	10	61	10
11 Error analysis	0	<5	0	<5	0	<5
12 Final map production	10	<5	10	<5	10	<5

Table 2.5: Percentage of the time spent in the various phases of a landslide hazard assessment project using GIS, and conventional methods at different scales (CONV, conventional methods; GIS, GIS-based methods).

The given percentages are not independent of the size of the study area and the total time available for the execution of a hazard assessment project. The percentage for image interpretation and for data entry increases for larger study areas.

Working with a GIS increases considerably the time needed for the pre-analysis phases, due mainly to the tedious job of hand digitizing input maps. Time needed for data analysis, however, is not more than 10 percent in the GIS approach against almost half using conventional techniques. Many of the analysis techniques are almost impossible to execute without a GIS (see chapter 6). Working with GIS reduces considerably the time needed to produce the final maps, which are no longer drawn by hand. On the other side the production of a cartographical acceptable output product with GIS is more difficult than one would expect.

The percentage of time needed for image interpretation using the GIS approach decreases from the regional scale to the large scale, and fieldwork and laboratory analysis become more important. Data entry requires most time at the medium scale due to the large number of parameter maps that have to be digitized. Because analysis is based on only one basic data layer of TMUs, the time needed for data entry on the regional scale is much lower.

CHAPTER 3: THE RIO CHINCHINA STUDY AREA

In this chapter an introduction is given to the study area where the various GIS-based methods for assessing landslide hazard were tested. A general outline is given of the three study areas at the different scales of analysis. Important factors leading to slope instability in the area are described and the various mass movement types occurring in the area are discussed and illustrated with case studies.

3.1 General information

3.1.1 Choice of study area

The catchment of the Rio Chinchina with a surface area of 722 km^2 and a perimeter of 159 km is located on the western slope of the central Andean mountain range (Cordillera Central) in the Caldas Department in Colombia (see figure 3.1). The Cordillera Central, with a maximum elevation of 5750 m (Nevado del Huila), is located between the two main Andean rivers of Colombia: the Rio Magdalena in the east, and the Rio Cauca in the west.
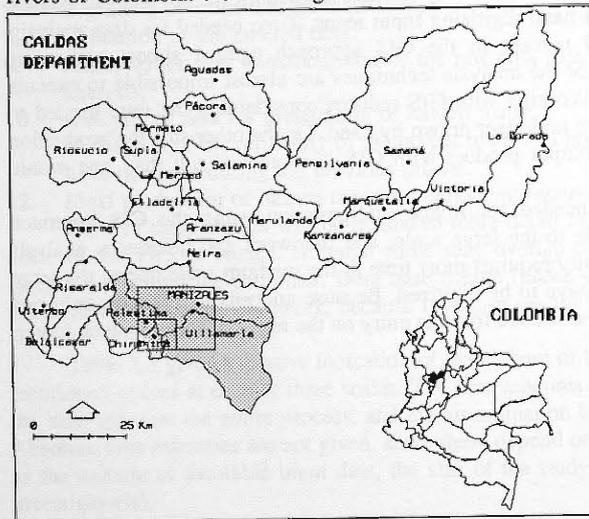
Figure 3.1: Location of the study area.

The Rio Chinchina area was chosen as the study area to test the methodology developed in this work because of its following characteristics:

1. The severity of natural hazards in the area, combined with intensive industrial and agricultural activity and a high population density, has caused considerable damage and loss of lives in the past. The area is susceptible to mass movement, earthquake, and volcanic hazards. Tables 3.1- 3.3 summarize the occurrence and damage of natural disasters in recorded history. The largest disaster in the Rio Chinchina area took place on 13 November 1985, when a lahar, triggered by an eruption of the glacier-covered Nevado del Ruiz, caused the death of about 2000 persons and destroyed all bridges over the Rio Claro and Rio Chinchina (Florez, 1986; Romero et al., 1989). The last major earthquake, which killed 50 persons in Pereira and Manizales and caused considerable property damage, occurred on 23 November 1979. Landslide casualties and material damage are reported almost annually, both in urban and rural areas. Table 3.1 summarizes landslide damage for the period 1960-1987 in the city of Manizales. The road network also suffers from severe mass movement problems. The so called "triangulo vial" (road triangle) between Manizales, La Manuela, and Chinchina is considered by the Ministry of Public Works to be one of the main problem areas in the Colombian road network (Baez et al., 1988).

2. The availability of maps, aerial photos, and reports. Imagery and topographic maps, as well as a wide range of thematic maps from different years and at different scales, are available for most parts of the area.

Year	Persons killed	Persons injured	Persons evacua-ted	Homes dama-ged
1960	10	9	0	6
1961	0	0	20	3
1962	9	16	54	28
1963	5	6	134	46
1964	1	3	12	12
1965	58	0	72	107
1966	0	0	125	31
1967	20	6	622	89
1968	6	0	0	1
1969	8	4	537	73
1970	0	0	121	20
1971	10	8	1027	165
1972	0	0	20	36
1973	0	0	22	4
1974	4	17	566	86
1975	8	0	26	1
1976	1	1	90	8
1977	0	0	26	1
1978	4	0	160	29
1979	0	0	4	2
1980	0	0	0	0
1981	6	10	1272	445
1982	23	11	617	149
1983	0	0	0	0
1984	8	7	1336	48
1985	0	0	0	0
1986	8	12	283	0
1987	4	0	10	78
Total	193	110	7156	1468

Table 3.1: Summary of casualties and damage due to landslides in Manizales between 1960 and 1987.

Date	Magni-tude	Depth (km)	Lat. ° W	Long ° N
09/02/1878	5.3	–	75.5	5.1
31/01/1900	8.9	25	81.5	1.0
10/04/1911	7.2	100	74.0	5.1
04/02/1938	7.0	160	75.5	5.1
22/05/1942	5.75	130	74.7	4.1
14/02/1952	6.75	44	76.4	7.5
10/11/1957	5.5	52	75.1	7.3
12/12/1957	6.75	100	76.0	7.0
12/03/1960	6.1	60	77.0	7.5
20/12/1961	6.9	175	75.6	4.6
18/02/1962	5.6	41	75.0	6.9
30/07/1962	6.9	59	75.9	5.4
20/12/1962	5.5	127	76.2	5.2
09/02/1967	6.3	60	74.9	2.9
26/09/1970	6.1	8	77.6	6.2
02/12/1970	5.7	38	76.1	7.4
03/04/1973	6.2	158	75.6	4.7
24/04/1973	5.5	113	75.8	5.2
24/04/1973	6.3	50	76.1	5.0
23/11/1979	6.3	106	76.2	4.8
12/12/1979	6.4	33	76.0	4.7

Table 3.2: Mayor earthquakes which have affected Manizales between 1878 and 1979 (Page (ed), 1982).

Date	Damage
12-03-1595	Agricultural land
19-02-1845	Armero (± 1000 victims)
13-11-1985	Armero (± 25,000 victims), Rio Claro (± 2000 victims)

Table 3.3: Historic eruptions of the Nevado del Ruiz, and indication of damage (INGEOMINAS, 1985).

Overviews of the study areas at the regional and medium scale are shown in figures 3.2, 3.3, and 3.4. Some characteristics of the three types of hazards are represented in figures 3.5, 3.6, and 3.7. A block diagram, made by combination of SPOT data with a digital terrain model for the Manizales area is given in figure 3.8.

3.1.2 The regional-scale study area

The study area for the regional scale comprises the entire catchment area of the Rio Chinchina (see figure 3.2). The elongated catchment receives part of its water from the second highest mountain of the Cordillera Central: the glacier-covered Nevado del Ruiz volcano (5200 m). The lowest point of the catchment is its outlet in the Rio Cauca (830 m). The catchment is drained by two main rivers: the Rio Claro, which originates from the glaciers of the Nevado del Ruiz and the adjacent Santa Isabel volcanoes and the Rio Chinchina, which originates in the northeastern part of the catchment. The Rio Chinchina, with a length of 77 km, is one of the major tributaries of the Rio Cauca. The area contains one major city, Manizales, which is the capital of the Caldas Department, and three villages, Villamaria, Chinchina, and Palestina. Within the area are several small hamlets such as Arauca, La Plata, La Manuela, Rio Claro, and Llanito. East of Manizales are two isolated settlements, which belong to the municipality of Manizales: La Nubia, where the airport is located, and Malteria, where most of the industrial activity of Manizales is concentrated. The eastern part of the area is relatively uninhabited due to its steep morphology and high altitudes. The most populated rural region is found to the west of Manizales, where extensive coffee cultivation takes place at altitudes between 1000 and 2000 m. Between Manizales and Chinchina the area is crossed by the Romeral fault zone, one of the major fault zones in Colombia.
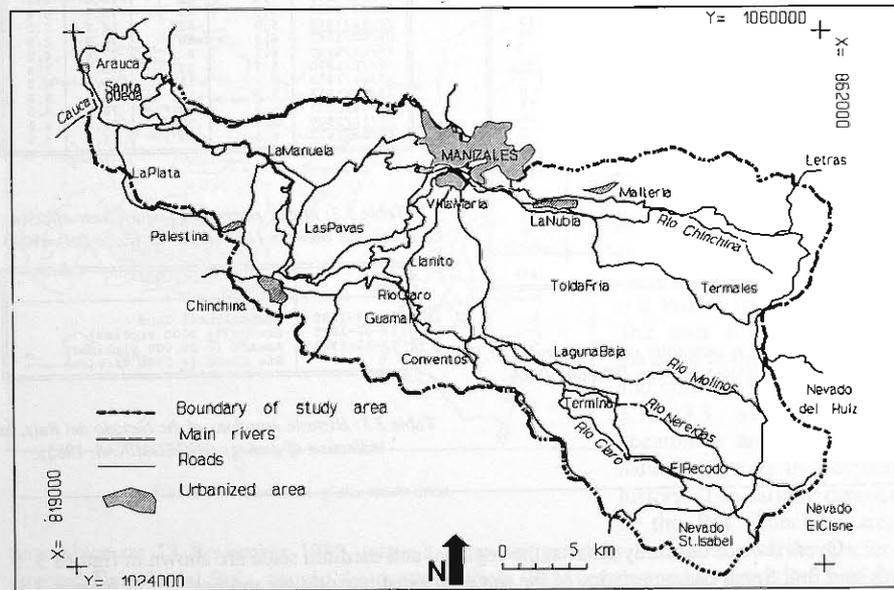
Figure 3.2: Study area for the regional-scale analysis.
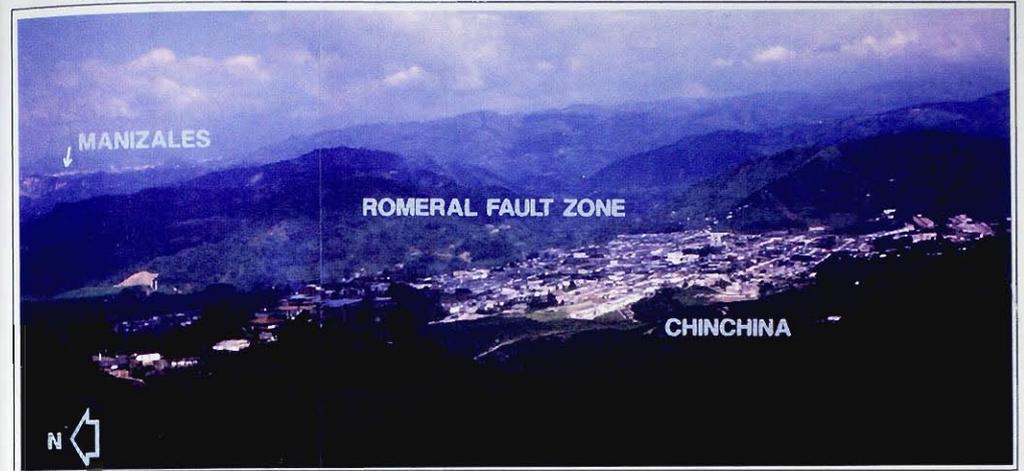
Figure 3.3: Overview of the medium scale study area, with Chinchina in the foreground and Manizales in the background.

Figure 3.4: The city of Manizales (foreground) with the active Nevado del Ruiz volcano (background).
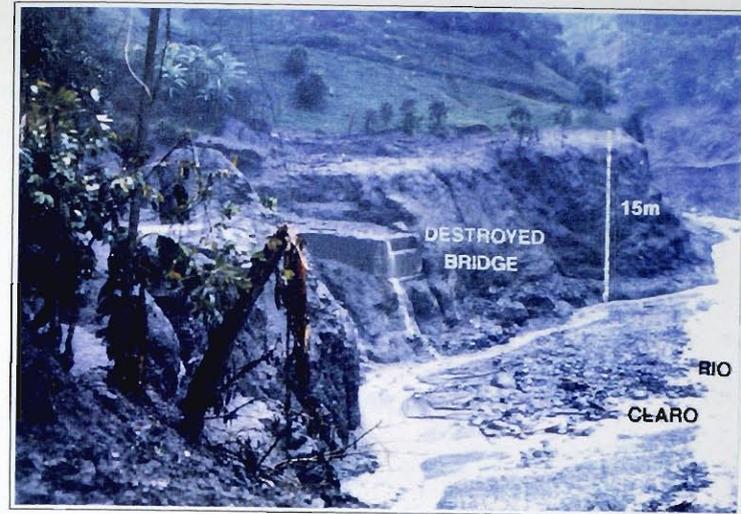
Figure 3.5: Volcanic hazards in the Rio Chinchina catchment. Lahar from 13 November 1985 destroyed many bridges within the Rio Claro valley and reached heights of up to 30 m.
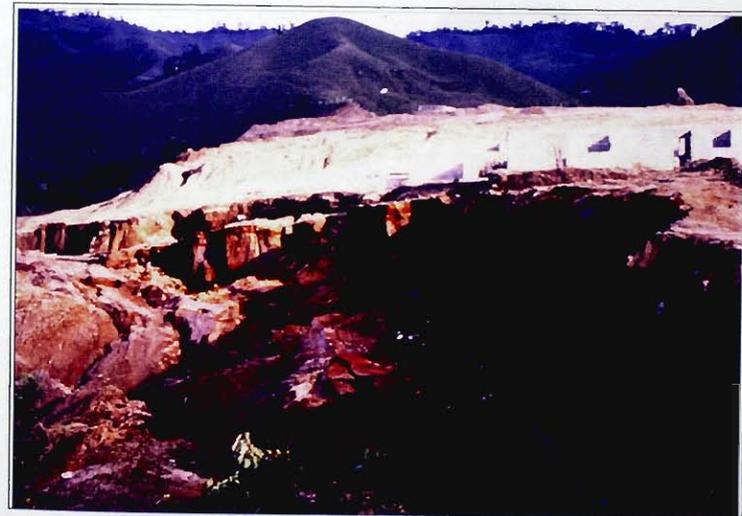
Figure 3.6: Seismic hazards in the Rio Chinchina catchment. Damage to newly constructed township in Manizales (Barrio Soferino) caused by a landslide triggered by the earthquake of 23 November 1979.

28b
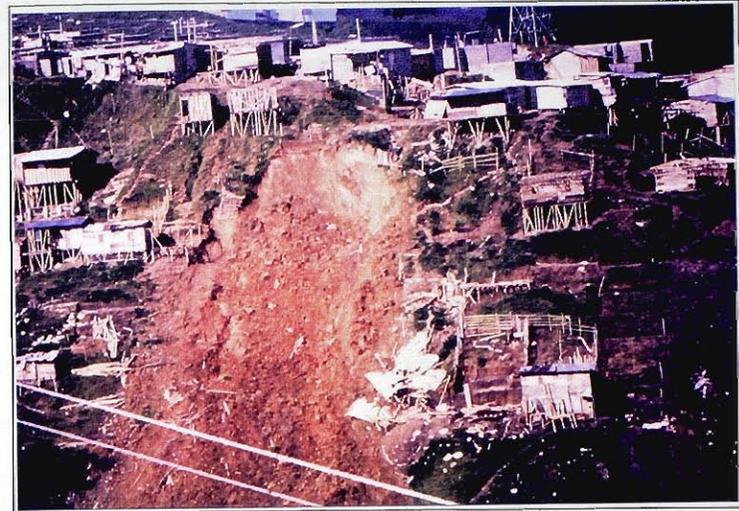
Figure 3.7: Landslide hazards in the Rio Chinchina catchment. Catastrophic rapid translational slide in a squatter area.
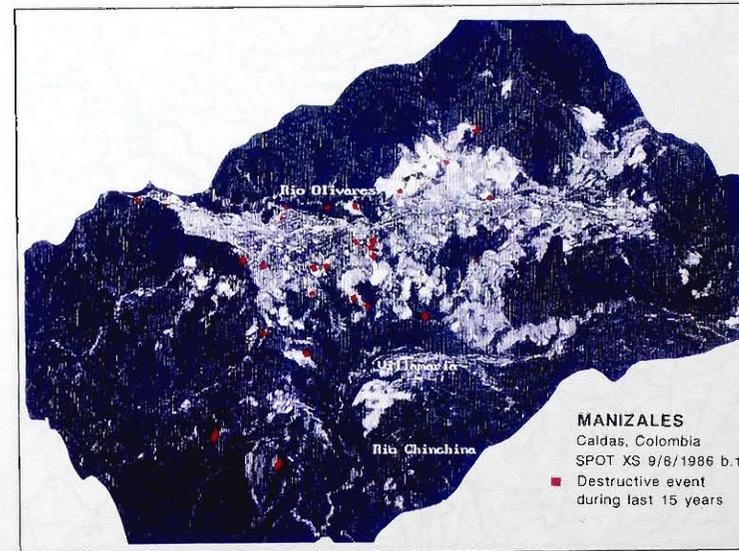
Figure 3.8: Three-dimensional view of Manizales, made by combination SPOT data with a digital terrain model.

3.1.3 The medium-scale study area

The medium-scale study area is located within the regional-scale area, between Manizales and Chinchina (see figure 3.9). This area was selected based on the following factors:

1. Its economic importance. The zone is used intensively for coffee cultivation. Chinchina is one of the major "coffee towns" in Colombia. Three important roads traverse the area: the main road from Cali and Pereira to Medellin in the west; the main road from Manizales to Medellin in the north; and the road connecting Pereira and Manizales with Bogotá in the south.

2. The high frequency of mass movements. Due to various factors which will be discussed later, the area is highly susceptible to rapid mass movements, which cause many casualties and considerable property damage.

Part of the data was collected for the entire 272-km^2 area. Due to the excessive effort necessary to collect and digitize all data for such a large area, however, only one-fourth of the area in the southwestern sector surrounding Chinchina was used in the analysis at the medium scale.

From west to east, three main terrain units can be distinguished in this sector: (1) the western part, with gentle slopes; (2) the terraces located in a graben structure in the central part of the sector; and (3) the eastern part, with steep slopes and fault-related valleys.
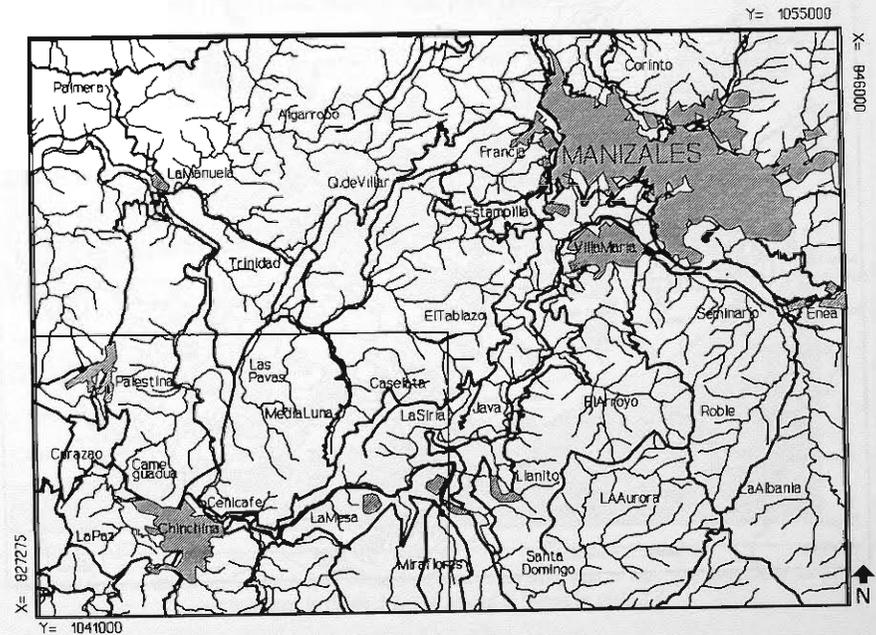
Figure 3.9: The medium scale study area.

3.1.4 The large-scale study area

The urban area of Manizales and its direct surroundings were selected as the study area for the large scale (see figure 3.10). The reasons to select this area were the following:

1. Manizales is a very rapidly growing city (see section 3.5.3) with an urgent demand for planning. In the plans for urban extension an analysis of natural risks has not usually been taken into account, resulting in slope failures within recently constructed parts of the town.
2. The city is located in a topographically unfavourable position: a gently sloping ridge with steep surrounding slopes. City extensions are often of an illegal type: squatter areas on dangerous slopes.
3. Manizales has suffered extensive damage in the past due to mass movements as well as earthquakes (see tables 3.1 and 3.2).

Two main types of mass movement hazard can be distinguished in the Manizales area:

1. Rapid debris or soil flows (indicated locally by the local term "derrumbe"), occurring on steep slopes and affecting the squatter areas as well as roads;
2. Reactivation of old landslides after earthwork and construction: extensions of the city have often been constructed in areas with a high density of old landslides.
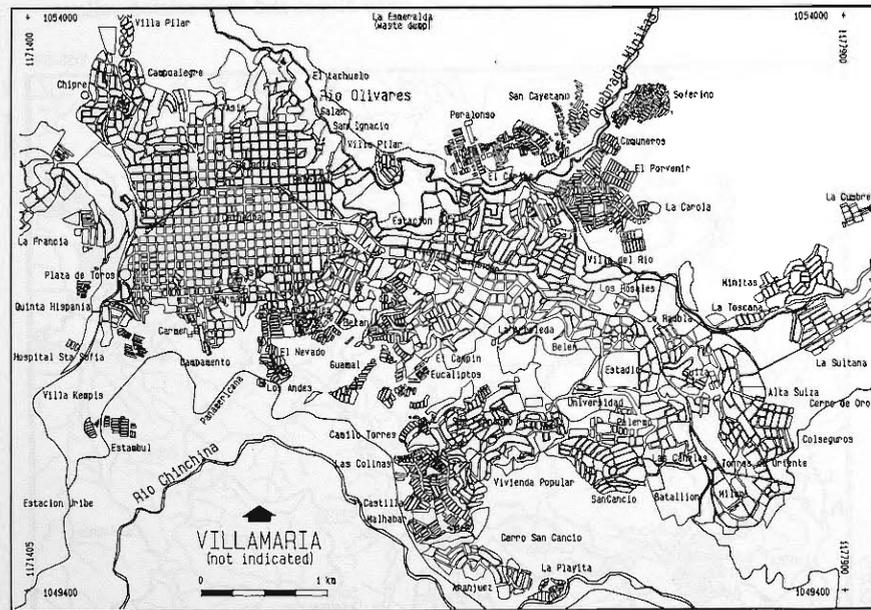
Figure 3.10: The large-scale study area.

3.2 Geological aspects

The geology of the area has been investigated quite extensively, and geological maps exist ranging in scale from 1:250,000 to 1:25,000 (Herd, 1974; Mosquera, 1978; IGAC, 1985, 1986; CHEC, 1985; James, 1986; INGEOMINAS, 1987; Navarro et al., 1988; Cortez, 1988; Florez, 1986; Chacon and Orozco, 1989; Handszer and Grand, 1989; Naranjo and Rios, 1989; Arcila, 1990; Vargas, 1990; Echavarria et al., 1991). An overview of the geological evolution of the area can be found in Navarro et al. (1988), Naranjo and Rios (1989), and Florez (1986).

3.2.1 Lithological units

Most of the lithological units have a marked north-south directionality, which is related to the Romeral fault pattern. Therefore, the geological situation can best be visualized in an east-west cross-section from the Nevado del Ruiz via Manizales to the Cauca valley (figure 3.11). A short description of the lithological units encountered in this cross-section is given in table 3.4, which is based on the geological reports cited above. The nomenclature is rather confusing. Most of the geological units were named unsystematically, and only a few of them are described as Groups or Formations. There is no uniform use of codes for the units in the map. Whenever information is available on radiometric ages, the age is given in absolute terms, otherwise only relative dates are given. Ages based on C-14 and K-Ar datings were presented by Thouret (1989a) and Naranjo and Rios (1989).
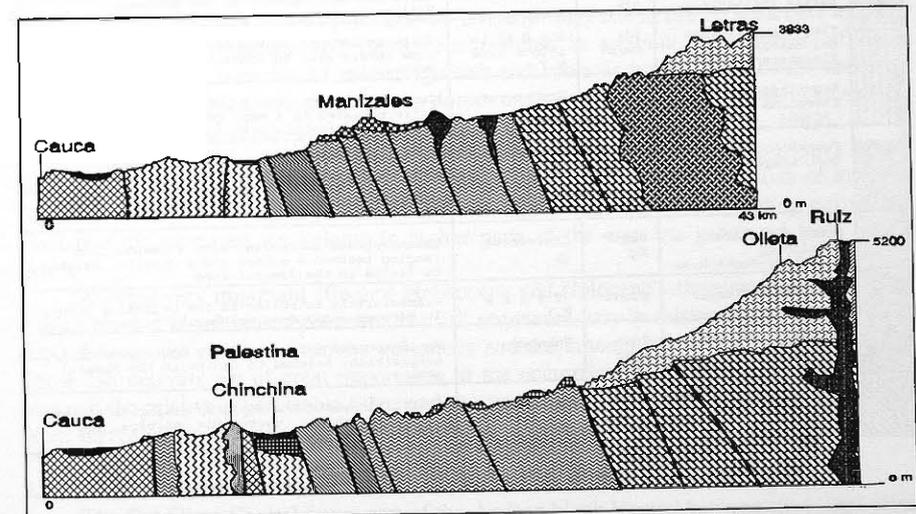
Figure 3.11: Generalized geological profile through the study area from west to east. The location of the profile is indicated in figure 3.2. The legend is shown in table 3.4.

Original Spanish Name	Codes Used	Age	Description
Depositos alluviales	Qal Qam	Holocene	Alluvial and torrential deposits within alluvial fans, low terraces, and floodplains
Cubertura de cenizas	Qto	Pleistocene Holocene	A sequence of fine, sandy, and gravelly layers with maximum thickness of about 15 m
Material de terrazas	Qfl Qfvl	Pleistocene 6,000 - 38,000 B.P.	A complex of alluvial, fluvio-volcanic, fluvio-glacial, and volcanic materials. The most abundant material is matrix-supported conglomerate
Ignimbritas del Rio Claro	Qrm	100,000 - 500,000 B.P.	A complex of pyroclastic flow deposits occurring in the valley of the Rio Claro, with a maximum thickness of 350 m
Sedimentos tertiarios de Chinchina	Toi	Late Pliocene	A complex of alluvial, fluvio-volcanic, and lacustrine sediments occurring west of the Romeral fault zone
Formación Casabianca	Tscb Tpvi	Late Pliocene	A complex of alluvial, fluvio-volcanic, and lacustrine sediments, located disconcordantly over the Manizales Formation, and characterized by a higher degree of weathering
Porfidos de Pereira y Chinchina	Tadp	Pliocene	Porphyritic intrusive of andesitic composition; occurs in isolated bodies west of Chinchina
Formación Manizales	Tsmz Tpvi	Late Miocene Early Pliocene	A complex of sedimentary and volcanic rocks derived from the Ruiz-Tolima volcanic complex, underlying the city of Manizales. Composed of matrix- and block-supported conglomerates, pyroclastic flow deposits, and alluvial sediments
Basaltos de San Cancio, Tesorito and Barrio Lusitania	Qdsc Qdt Qlb	1.2 ± 0.2 M.Y.	A series of lava flows, domes, and small volcanoes associated with the Manizales-Villamaria fault
Flujos andesiticos del Mioceno-Pleistoceno	TQs LR/LV	0 ± 0.05 to 1.05 ± 0.08 M.Y.	Volcanic complex of the Ruiz-Tolima. Different flow levels with an andesitic-dacitic composition
Esquistos de Lisboa-Palestina	Kclp Kap Kelp	Cretaceous	Consisting of two units that cannot be differentiated in a map: quartzitic, graphitic schists and amphibolitic schists
Formación Quebradagrande	Kis/Kd Kqd Kqc Kqal Kqlc	Cretaceous	Also indicated as "metasedimentary-volcanic" complex of Aranzazu-Manizales. Two members: one consisting of turbiditic sequences, and the other basaltic, occurring concordantly within the sedimentary member
Stock dioritico-gabrico de Chinchina-Santa Rosa	Kdg Kg	Cretaceous	Metamorphosed intrusive, with a composition ranging between a gabbro and a diorite. Related to faults in the Romeral zone
Stock de Manizales	KTcdm	62.4 ± 1.8 M.Y.	Granodioritic intrusion in the Cajamarca group. It becomes sandy upon weathering
Intrusivo neisico de Chinchina	Inch Kgar Pnch	Unknown	Metamorphosed intrusive; very heterogeneous in composition. Related to faults in the Romeral zone
Gruppo Cajamarca	es,pen q,Pes Pzc	Unknown (Paleozoic)	Quartzitic-sericitic schists, graphitic schist, chloritic schists, quartzites, marbles, and calcareous schists

Table 3.4: Geological units in the study area. Symbols are those used in figure 3.11.

The nucleus of the Cordillera Central is formed by Paleozoic rocks of the Cajamarca group, which were uplifted during the Upper Paleozoicum as result of Late Hercynian orogenesis (Irving, 1971). These rocks are intruded by a number of intermediate and acidic batholites, stocks, and dikes of Jurassic and Cretaceous age, such as the Manizales stock (Barrero et al., 1969; Irving, 1971). The rocks occurring in the central and western part of the

study area are mostly of Cretaceous age, formed in a geosynclinal basin. Deep sea sediments are found (Kclp/Kap), as well as Flysch-type materials (Kis) intercalated with submarine lavas (diabases and basalts). Near the Cauca river, oceanic basalts are found; these are related to the subduction zone that was situated in the Cauca depression during the Cretaceous. In later periods this subduction zone migrated westward.

Tectonic uplift of the area started near the end of the Cretaceous, and continued throughout the Tertiary into the Quaternary (Irving, 1971). The major tectonic uplift, in which the fault systems of Romeral and Palestina played an important role, took place during the Late Cretaceous and Early Tertiary. Most of the rocks experienced intensive metamorphism, and intrusives related to the Romeral fault zone (Inch, Kdg) occurred locally. Practically all rocks have faulted contacts.

The later stages of tectonic uplift were accompanied by important volcanic activity along the axis of the Cordillera Central (Herd, 1974). The Ruiz-Tolima complex was formed by repeated eruptions of andesitic and dacitic lavas. The flows unconformably overlie the Cajamarca group and the Manizales stock.

During the Late Miocene and Early Pliocene large volumes of sediments related to volcanic activity were deposited throughout the area. Most of these materials were later removed by subsequent erosion. In the graben structures between the Romeral fault zone and the Cauca fault system these deposits reached considerable thickness. Remnants of these materials are found in the Manizales area, where the Manizales and Casabianca formations, composed of debris flows, pyroclastic flows, and lacustrine and alluvial sediments, are preserved with thicknesses of up to 260 m (Naranjo and Rios, 1989). Renewed tectonic activity during the Pliocene and Pleistocene resulted in tectonic displacement of these materials as well as intrusion of several igneous and volcanic bodies, such as the andesitic intrusions west of Chinchina, and later the domes and lavas of San Cancio, Barrio Lusitania, and Tesorito, located along the Villamaria-Termales fault (Naranjo and Rios, 1989).

Volcanic activity continued during the Pleistocene, with the formation of lava flows, now mostly restricted to presently existing valleys. Below the maximum limits of the lava flows the valleys were filled with debris flows and pyroclastic flows. During periods of glaciation the increased ice volume in higher parts of the area has generated large debris flows.

Another very important effect of Pleistocene and Holocene vulcanism is deposition of a thick blanket of ash over the terrain. The ash sequences vary in thickness and composition, depending on the distance from the volcanoes and the amount of erosion since deposition. These ash deposits are of great importance in the occurrence of mass movements. Contact between the relatively permeable ashes and the underlying, less-permeable, weathering soils often serves as the failure surface for landslides.

3.2.2 Fault patterns

The Cordillera Central forms part of the Andean block located between the Nazca plate to the west, with an eastward subduction movement of about 6-8 cm/year, the South American plate to the east, moving west-southwest at a velocity of 1-3 cm/year, and the Caribbean plate to the north, with a southeasterly movement of 1-2 cm/year (Page, 1986). As a result, the Andean block is moving northeast with an average velocity of 1 cm/year. The Andean block is experiencing compression in an east-west direction and extension along a southwest-

northeast axis. This combined action results in sinistral and inverse displacement in the majority of the fault systems (James, 1986).

Three major fault systems can be differentiated in the area (James, 1986; Navarro et al., 1988; Salgado and Chacon, 1991):
1. The Cauca fault system occurs in the western part of the area and has a total length of 800 km. It forms the western margin of the Cordillera Central. It is also the western margin of a graben structure with the Romeral zone as eastern margin. The Cauca fault system is considered active.
2. The Romeral fault system is one of the most important fault zones of Colombia. It extends south-north from the Colombian-Ecuadorian border to Barranquilla, a length of more than 1200 km. It is assumed to be the remnant of a Jurassic-Lower Cretaceous subduction zone (Page, 1986). It forms the separation between the Paleozoic and Cretaceous rocks of the western slope of the Cordillera Central. The faults of this system show clear evidence of Quaternary activity. The system displays lateral right displacements of tens of kilometres. The Romeral fault zone consists of numerous sub-parallel anastomosing faults with individual lengths of up to 50 km. These individual faults have been mapped and named quite inconsistently in the literature. The faults can be observed clearly in the study area, visible in the form of fault scarps, linear valleys, and concentrations of landslides. In the study area the faults of this system dip generally eastward, with dip angles between 35 and 90 degrees (Navarro et al., 1988).
3. The Palestina fault system extends 410 km northeast-southwest (Page, 1986). The fault has displaced Paleozoic metamorphic rocks over a distance of 28 km in a right lateral movement together with vertical movement in the western part. The fault has been active during the Quaternary, as is evident from displacements within ash layers (Page, 1986). The volcanic activity in the region is assumed to be related to this fault. The Palestina fault can be observed very clearly in the upper catchment of the Rio Claro, where it forms steep cliffs and fault scarps (see figure 3.15). Several eruption points along this fault line can also be observed. No displacement of morainic walls has been observed, indicating that the fault system has not been active during the Holocene.

Other faults related to vulcanism and characterized by the occurrence of thermal springs lie in an east-west direction. These include the Santa Rosa fault, the Nereidas faults, and the Villamaria-Termales fault (CHEC, 1985).

Detailed information on faults and lineaments in the Manizales area is scarce, due to the limited number of exposures in fault zones (Naranjo and Rios, 1989; Salgado and Chacon, 1991). The most important fault directions in the Manizales area are:
1. North-south. An important north/south-directed fault (West Salamina fault) is found west of Manizales, bordering the neighbourhood of La Francia (see figure 3.10). Along this fault a series of large mass movement complexes is found. A large building located on this fault trace was destroyed during the 1979 earthquake. The steep cliffs west of Manizales are controlled by a number of small faults (oriented northwest-southeast), which terminate westward against the West Salamina fault. Between these faults, the Manizales Formation has been displaced vertically by about 200 m in a number of blocks, partly as a result of gravitational tectonism. Another north/south-oriented fault (Manizales-Aranzazu) runs through the centre of Manizales, and continues both in northward and southward direction in deep, V-shaped valleys. North of Manizales it

34

forms the contact between the gabbros of the Rio Olivares and the Quebradagrande Formation. A third north-south fault (El Perro) is found in the eastern part of Manizales.
2. Northwest-southeast faults. Several faults running in this direction and controlling drainage lines can be found, such as the "Cementerio" fault or the San Cancio fault.

At various locations throughout the area, displacement in ash sequences was observed, indicating Quaternary fault activity. The relationship between the faults and mass movements is, however, more due to their width and amount of mylonitization and deformation than due to their seismic activity. In the main Romeral fault an area up to 500 m wide is affected.

3.2.3 Seismic events

The study area is located in a zone of important seismic activity, in which earthquakes with a magnitude of 6 or larger on the Richter scale have occurred with an approximate return period of 15 years (James, 1986; Valencia, 1988). The area has been designated in the national study of the "Codigo Colombiano de Construcciones Sismo-Resistentes" as having high seismic hazard (AIS, 1984).

For an analysis of historical regional seismicity a record of 331 earthquakes occurring between 1595 and 1979 was collected from the literature (Ramirez, 1975; James, 1986; Valencia, 1988; Page, 1986). The earthquakes occurred within the area between 4.5-6.0° north latitude and 74.5-76.5° west longitude. The quality of the data improves considerably after the .1960s, when at least three seismic stations were in operation in Colombia. Three sources of earthquakes are recognized:
1. The subduction zone of the Nazca plate and the Andean block. Approximately 90% of the earthquakes occurring in the area at depths of 70-120 km in the Manizales area, and at reduced depth towards the west, are related to the subduction zone of the Nazca plate and the Andean block. One of the concentrations of these deep seismic events is in the area between Chinchina and Santa Rosa (James, 1986).
2. Surficial fault movements. Activity of faults near the study area, such as the Romeral, Palestina, Mistrato, and Cauca faults, and of more distant faults, such as the Santa Martha-Bucaramanga fault, account for 10% of the earthquakes occurring in the area.
3. Volcanic activity of the Nevado del Ruiz. Since the renewed volcanic activity of the Nevado del Ruiz volcano in 1984, a large number of surficial (<10 km) seismic tremors have been recorded by the Volcanological Observatory of Manizales (Muñoz and Nieto, 1988, 1989). From the installation of the seismic network on 19 July 1985 until 15 november 1986, 10,400 seismic events were recorded. All of these were of low magnitude (<2) and did not affect adjacent urban areas.

The seismic records were used by Valencia (1988) to calculate return periods. Because the seismic record is incomplete, three different relations were established for seismic events with magnitudes greater than 6.

35

For the period 1595-1979

$$M_s = 8.4 - 2.9\log(384/RY)$$ [3.1]

For the period 1922-1979

$$M_s = 8.2 - 2.9\log(57/RY)$$ [3.2]

For the period 1958-1979

$$M_s = 7.4 - 2.7\log(21/RY)$$ [3.3]

in which M_s = magnitude on the Richter scale and RY = return period in years.

Valencia (1988) presented a study on microseismicity in the study area, based on a record of 80 days between July and September 1987, during which 63 local seismic events with magnitudes less than 3 were recorded. The following relation was calculated:

$$M_s = 3.8 - 1.9\log(80/RD)$$ [3.4]

in which RD = return period in days. In that study, several zones with a concentration of microseismic activity were outlined. None of the cities or villages within the study area were located in such a zone. Three of the zones occur near, or in, the study area.

1. A zone of concentration some 15 km north of Manizales with seismic events with focal depths of 13 to 10 km and with an apparent relationship to the faults of the Romeral zone (faults: Filandia, la Merced, Romeral North, Neira Aranzazu and San Jeronimo).
2. A zone of concentration some 15 km west of Manizales. These earthquakes show no clear relationship with existing faults. Only one event with a focal depth of 37 km is related to the Filandia fault.
3. A zone of concentration between Chinchina and Pereira of seismic events with focal depths of 9-15 km, related to the Santa Rosa and Filandia faults.

From an analysis of the focal mechanisms it was concluded that the faults within the Romeral zone are of the normal fault type, and that the so-called Chinchina alignment is an inverse fault (Valencia, 1988). This is in accordance with the assumption that the terrace area of Chinchina, located between these two systems, is a graben in which extensive accumulation of material could take place.

Manizales has suffered great damage from earthquakes several times, of which those of 1878, 1938, 1962, and 1979 were the most severe and lead to the loss of lives. Detailed documentation of the observed damage exists for the earthquake that occurred on 23 November 1979 (Galvis et al., 1980). That earthquake, with a magnitude of 6.3 on the Richter scale, occurred at a depth of 106 km in the northern part of the Department of Valle del Cauca some 75 km southwest of Manizales. Six persons were killed in Manizales, and several parts of the city were damaged so severely that they had to be demolished and rebuilt. Total damage was estimated to be 1×10^9 Colombian pesos. Some 10 years after the earthquake an inquiry was held among the population of Manizales on the phenomena observed during this earthquake (Salgado and Hurtado, 1991). The data of the questionnaires were processed by computer and intensity values were obtained for about 500 locations. Contour lines of equal intensity were plotted and an isoseismic map constructed. Unfortunately, the isolines were drawn in a very confusing manner, and a new interpolation could not be executed because the original point data were unavailable. The isoseismic map of Salgado and Hurtado

(1991), and known sites of damage (Encizo, 1989) are shown in figure 3.12. Intensity values range from 4 to 8 in some small areas.

The isoseismic map does not always coincide with the known damage sites. After a comparison of this map with the fault map of Manizales (Salgado and Chacon, 1991), no marked relationship between high-intensity values and the location of faults was observed. Most of the earthquake damage was related to ground shaking. Evidence of liquefaction or earthquake-induced slope failure was scarce. Unfortunately, no inventory of landslides was made immediately after the earthquake, and detailed aerial photos from dates shortly before and after the 1979 earthquake were also not available. The intensity values recorded from the 1979 earthquake are influenced by different factors. On the one hand, morphological, geological, and geotechnical factors play a role in determining seismic acceleration during the earthquake. On the other hand factors related to the quality and type of buildings play a role in the amount of damage observed.
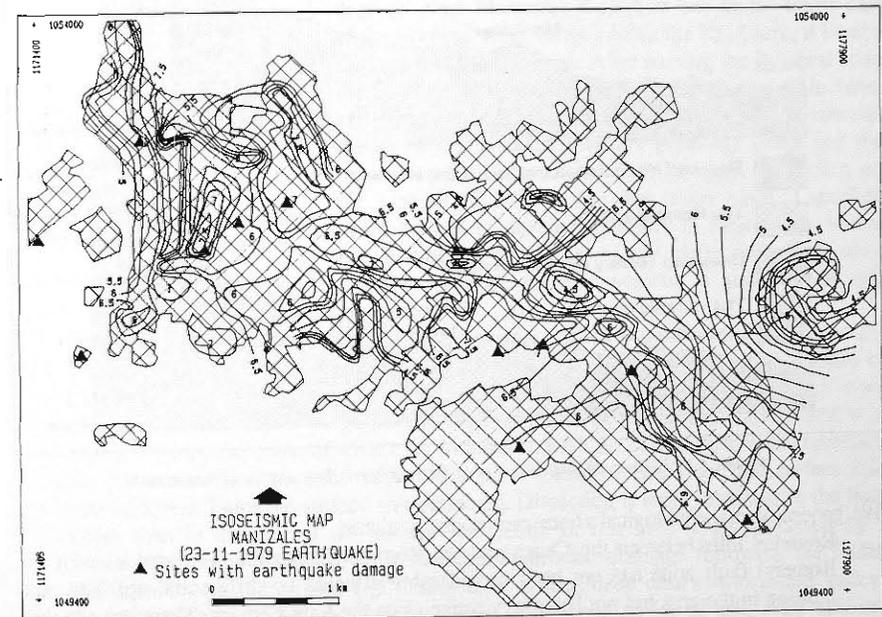
Figure 3.12: Isoseismic map made by interpolating point information obtained from questionnaires (after: Salgado and Hurtado, 1991). Areas with damage are also indicated (Encizo, 1989).

3.3 Geomorphological aspects

The Rio Chinchina area is a typical Andean environment: an active mountain chain in the wet equatorial zone, characterized by deep weathering, strong Plio-Pleistocene uplift and associated deep fluvial incision, mass movement problems, and active vulcanism at higher elevations interfering with Pleistocene glaciation (Florez, 1986).

3.3.1 Geomorphological zonation

With the exception of the terraces, the geomorphological zones in the area are oriented north-south as a consequence of the tectonic framework, lithology, and altitude. Therefore they can be explained most conveniently on the basis of the geomorphological cross-sections across the same transect used for the geological zonation (see figure 3.13).
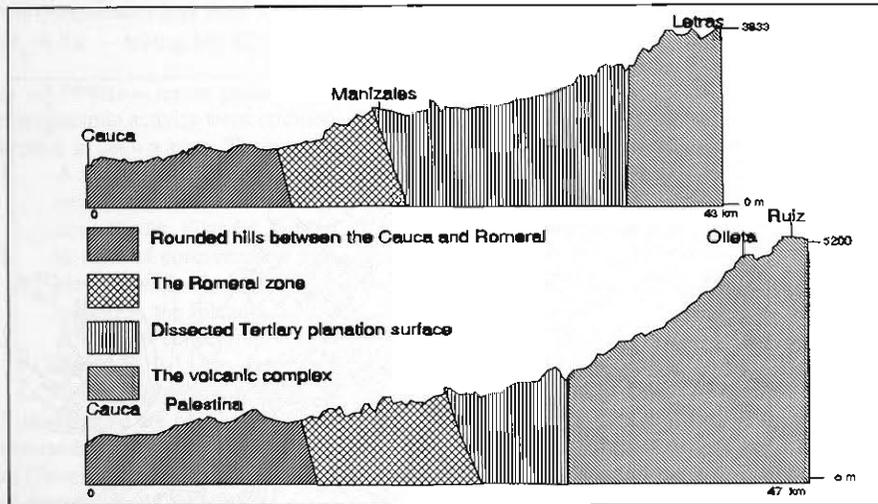
Figure 3.13: Geomorphological zones in the study area. See text for explanation.

Five general geomorphological zones can be distinguished:
1. Rounded hills between the Cauca and the Romeral fault zone. The area west of the Romeral fault zone has not been considerably affected by differential uplifting, and faulting in the area has not been very active since the Late Tertiary. Therefore, the area does not have large differences in altitude. The altitude ranges from approximately 830 m near the Cauca valley to 1400 m near Palestina. The elongated hill of Palestina, bordered by the Chinchina fault, with associated Tertiary intrusives, and marking the western margin of the local graben of Chinchina, reaches altitudes of approximately 1600 m. The gentle hills are of a denudational origin and are covered with a thick mantle of residual soil and weathered ash. Within this relatively flat area large volumes of fluvio-volcanic, alluvial, and lacustrine sediments have been deposited. Tertiary sediments of a molasse type are found in the northwestern part of the area and south

of Chinchina, where they even occur on water divides. Due to subsequent denudation, the original Tertiary accumulation surfaces are no longer recognizable. The Quaternary sediments in this area can be found at a number of different terrace levels, especially around Chinchina and Santagueda. Slopes in the area are generally gentle. Steep slopes (up to 45°) occur only along terrace scarps and on the eastern slope of the Palestina hill. Mass movement phenomena are not abundant in this region. Fossilized landslides are found along the terrace edges. Active landslides occur on the terrace slopes and the eastern slope of Palestina hill.

2. Romeral fault zone. The area between Chinchina and Manizales is characterized by a number of fault-related, north/south-oriented valleys and ridges with steep slopes. In cross-section the area has a stepped appearance, due to the differential uplift of the blocks separated by faults. The relationships between the faults and the drainage pattern is very clear. Figure 3.14 shows how the Rio Chinchina changes its course four times
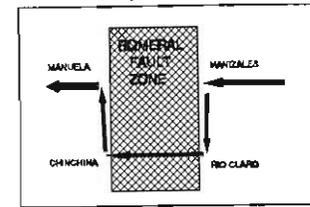
Figure 3.14: Schematic representation of the Chinchina river crossing the Romeral zone.

between Manizales and La Manuela, making turns of 90 degrees. Near Manizales it follows one of the faults east of the Romeral zone. After joining the Rio Claro, it breaks through the Romeral zone. After passing the Romeral zone the direction of flow changes to the north near Chinchina, and finally changes to the west again near La Manuela. Slopes in the Romeral zone are generally steep, and the thickness of the ash cover varies strongly, depending on the amount of erosion that has taken place. Landslide problems can be severe, especially in fault zones, where the bedrock material is highly deformed. The most common type of mass movement is soil slip or soil avalanche.

3. Dissected tertiary planation surface. The area east of the Romeral zone and west of the Tertiary lava deposits is characterized by remnants of a Tertiary planation surface of Late Eocene-Early Oligocene age (Florez, 1986). In this zone, the hilltops reach more or less equal altitudes. During Pliocene vulcanism, part of the surface was covered with fluvio-volcanic deposits, of which the Manizales and Casabianca formations represent the remnants. Pliocene uplift of the Cordillera Central has divided the surface into several levels. Later the surface was dissected. Dissection is more intensive in the fault zones than in the rest of the terrain. The centre of this area is characterized by a dendritic drainage pattern or by a north/south-directed drainage following the faults. The main rivers (Chinchina and Claro) have eroded deep east/west-oriented valleys through this zone. The area has an almost continuous cover of ash, with uniform sequences of silty sand and lapilli. The area is characterized by the occurrence of large flow slides, which have shown little differentiation in size or activity since the 1940's. The steep slopes of the major valleys, and the fault scarps, have by far the highest frequency of active surficial landslides.

4. Volcanic complex. The highest part of the study area consists of a series of lava flow levels, among which the upper part has been shaped by glacial erosion. The lowest lava flows, originating from the Ruiz-Tolima complex, are found at an altitude of 2300 m near Hacienda Laguna Baja. From this altitude to the maximum glacial limit, the terrain

is characterized by very steep slopes, covered by original Andean forest, with a high density of surficial debris avalanches. Individual flows cannot be recognized due to denudation, except for the younger flows found within the valleys of the Rio Claro and Rio Chinchina. In the glacially eroded upper part of the complex the slopes are much gentler and covered with thick mantles of morainic material and post-glacial ash sequences. On these slopes gulley erosion and solifluction are the most common denudational processes. The shield volcanoes of Nevado del Ruiz and Santa Isabel are glaciated above 5000 m.

5. Terraces. This geomorphological unit is not indicated in the cross-sections of figure 3.13, as it is unrelated to altitude. A large number of different terrace levels can be observed throughout the area. They are very difficult to correlate because they are generally quite homogeneous in composition and may occur at different levels due to differential uplift. Most terraces are composed of debris flow material and alluvial materials. They differ with respect to the degree of weathering and ash cover. The following terrace levels have been identified:

   i. The oldest terrace level occurs west of Chinchina, near the water divide with the Rio Campoallegre. It is slightly sloping to ENE, and has therefore not been deposited by the Rio Chinchina. It is considered a remnant of an accumulation level originating from the Rio San Eugenio and Rio Campoallegre.

   ii. The largest terrace level found is that of the town of Chinchina. It appears to be correlated downstream with several isolated terraces and with the large terrace of Santagueda. Correlated units upstream are much more difficult to identify due to differential uplift in the Romeral zone. The La Mesa level and some isolated levels along the Rio Chinchina are also thought to be of the same age. The terrace of Villamaria may also be of the same age. The thickness of the deposits ranges from 75 to 150 m. (Navarro et al., 1988). The Chinchina terrace level consists of various materials. Between debris flows a pyroclastic flow deposit about 20 m thick is found, which covers an old terrace landscape. Radiocarbon (C-14) dating of a tree trunk at the contact resulted in an age of >50,000 years. The pyroclastic flow deposits are correlated with the large deposits in the Rio Claro valley. The lowest occurrences of pyroclastic flow materials are found in La Manuela. The age of the pyroclastic flows of the Rio Claro valley is estimated to be between 500,000 and 100,000 years (Thouret, 1989a). The Chinchina terrace, which incorporates these pyroclastic flow deposits, should date from the same period.
   Lacustrine sediments occur on top of the pyroclastic flow deposits in some parts of the terrace of Chinchina. These may originate from local damming of the Chinchina river by a large landslide from the eastern slope of the Palestina hill. The abandoned meander located at the foot of the landslide may have been caused by the landslide event as well. The Rio Chinchina, after a short period of complete blockage, was forced to flow around the landslide until the river was able to cut through the foot of it.

   iii. A younger terrace level is found in the Chinchina valley east of Manizales, near the airport La Nubia. These terrace materials have a thickness of about 50 m and consist of debris flow and alluvial materials with intercalated volcanic ash.

Radiocarbon (C-14) dates ranged from 6000 to 38,000 B.P. (Naranjo and Rios, 1989).

   iv. A rather recent terrace deposit is located in the industrial area of Manizales (Maltería Licorera Caldas). An alluvial fan of the Quebrada Manizales points with its apex toward the northeast (see figure 3.28, section 3.6.4). The upper part of the catchment of the Quebrada Manizales consists of very steep slopes in the granodioritic material of the Manizales Stock. This terrain is characterized by the frequent occurrence of large debris avalanches, which have been deposited on the Maltería fan. In the lower part the fan consists of an intercalation of pyroclastic materials and debris flow materials. The fact that the highest part of this fan is free of ash indicates that the debris flow activity is very recent, and that future debris flows are possible.

3.3.2 Volcanic aspects

After the 1985 eruption of the Nevado del Ruiz a great amount of research was done to determine the volcanic history of the area, as a basis for a better volcanic hazard map. The first hazard map was completed some days before the catastrophic eruption in November 1985 (INGEOMINAS, 1985). This map predicted that during a large eruption there would be a high probability that lahars would seriously affect the city of Armero. A revised version of the map was published one year later (Parra et al., 1986). Historical eruptions are known from 1595, 1845 and 1985. For the period 1829 to 1833, some eruptions were mentioned in the literature for which no field evidence was found (Parra et al., 1986). On the basis of studies of stratigraphic columns and radiometric datings (Herd, 1974; Thouret et al., 1989a), a total of 24 important eruptions has been identified for the last 6247 years, of which 8 produced pyroclastic flows of considerable dimensions, 14 produced ash falls, and 2 produced lava flows. The average return period for a large eruption is considered to be on the order of 260 years. The following hazards are associated with volcanic eruptions:

- *Lava flows.* The area surrounding the Nevado del Ruiz is covered by a large number of lava flows, from different eruptions with different sources. The oldest are dated as Pliocene. One of the youngest flows was dated 4750 ± 11 B.P. (Thouret, 1989a). Some of the older and younger lava flows in the upper Rio Claro catchment are shown in figure 3.15. The direct risk from lava flows is considered minimal (Parra et al., 1986), as they are likely to affect only uninhabited areas above 4000 m. An indirect effect, however, could be the formation of lahars.

- *Pyroclastic flows.* On the basis of the known occurrence of pyroclastic flows in the area, three levels of hazard were defined (Parra et al., 1986), with probabilities of 0.57, 0.29, and 0.04 in the case of a new eruption. An area centred around the volcano with a diameter of 10 km was assigned the greatest hazard for pyroclastic flows, as were the valleys of the Claro and Molinos rivers up to a distance of 20 km from the crater, where flow heights of 100 m may occur.

- *Lateral blast.* The probability of partial destruction of the volcano due to a lateral blast (similar to the Mount Saint Helens eruption in 1980) is considered to be 0.08 in the case of a new eruption (Parra et al., 1986). This type of hazard exists only for the northeastern sector of the volcano.

LEGEND:

PRESENT GLACIER	MORAINE
BARE LAVAS WITH GLACIAL STRIATIONS	LAKE
YOUNG LAVA FLOWS FILLING LOCAL DEPRESSIONS	NEAR VERTICAL CLIFF IN LAVA
GLACIALLY ERODED YOUNG LAVAFLOWS WITH RUGGED MORPHOLOGY	ESCARPMENT
GLACIALLY ERODED OLD LAVA FLOWS WITH SMOOTH TOPOGRAPHY	EL RECODO FLOWSLIDE
FLOODPLAIN WITH ACCUMULATION OF SLOPE DEPOSITS	LANDSLIDE
C GLACIAL CIRQUE	SOLIFLUCTION
E ERUPTION POINT	STREAM
	MAIN FAULT

Figure 3.15: Geomorphological sketch map of the upper Rio Claro catchment, showing tectonic, volcanic, glacial, and denudational features. See text for explanations.

- *Pyroclastic falls*. Three different hazard areas were outlined for ash (particle size < 2 mm), lapilli (2-64 mm) and volcanic bombs (>64 mm) (Parra et al., 1986). The thickness of pyroclastic deposits did not exceed 30 cm for any single eruption during the last 15,000 years (Parra et al., 1986). Rojas et al. (1986) presented isopach maps for four pre-historic and historic events. From these maps it was concluded that the prevailing wind direction (northwest to northeast) had been the same for all four events. The eruption of 1985 resulted in a cover of pyroclastic material to depths of 70 mm or more up to 1 km from the crater, and 10 mm at a distance of 4 km. On the glacier near the crater the average thickness of the ash layer was recorded as 2 m. The maximum diameter of particles 10 km from the crater was 20 cm (Calvache, 1986a). However, damage related to ashfall was recorded throughout the study area (Arcila and Valencia, 1985).

A map showing total ash thickness for the entire study area at a scale of 1:200,000 was presented by Florez (1986). This map shows that most of the area has an ash cover of more than 5 m, except for the steep slopes in the Romeral fault zone, the eroded lava slopes, and the glacially eroded area.

Figure 3.16 displays three ash profiles, which are considered characteristic for three different regions in the study area.

A.   The post-glacial ash profile, occurring on the glacially eroded slopes in the highest part of the terrain. This sequence, including some buried soils, covers the topography as a continuous blanket with a constant thickness.

B.   A typical profile for the area between the Romeral fault zone in the west and the glacially eroded terrain in the east. It is characterized by sequences of silty sand, sand, and coarse sandy ashes with variable thicknesses.

C.   A characteristic profile for the area west of the Romeral fault zone. No individual layers can be observed within the ash profile. The ash is weathered, and the sandy and coarse sandy layers are lacking.
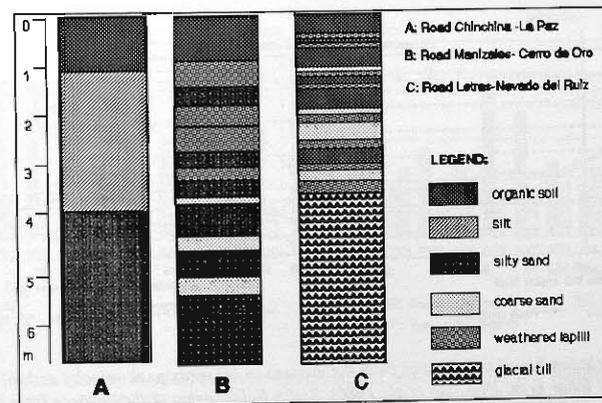
Figure 3.16: Typical ash profiles within the study area. See text for explanation.

- *Lahar*. The hazard for the occurrence of a lahar - a debris flow of pyroclastic materials, incorporating rock fragments, eroded alluvial deposits, trees, ice, and water, triggered by a volcanic eruption - is considered most important in the study area. The eruptions of 1595 and 1845 produced lahars which were larger in dimension than the lahar of 1985 (Mojica et al., 1985). The lahar of 1985 originated from the interaction of hot pyroclastic flows and surges with snow and firn of the summit ice cap of the Nevado del Ruiz. The lahars were formed by various processes described by Calvache (1986b) and Naranjo et al. (1986). The magnitude of a lahar depends on the type and magnitude of the volcanic eruption and on the availability of water and unconsolidated sediments in the summit area of the volcano as well as in the transportation zone. The surface area of the ice-cap is more critical than the total ice volume for the lahar potential. Prior to the 1985 eruption the glaciated area in the Chinchina and Claro catchments was 7.95 km^2, and the ice volume was 262 million m^3. The volume of ice which melted during the eruption was estimated at 6 million m^3 for the Chinchina-Claro catchments (Calvache, 1986b; Thouret et al., 1989a), which is only 2.3% of the total volume. Flow velocity and maximum discharge were calculated by Naranjo et al. (1986) on the basis of field evidence, such as the height of the deposit on an obstacle or the height difference between both sides of a curve. The left-hand part of figure 3.17 shows the effect of the distance from the crater on the mean peak velocity and peak discharge of the lahar. In the channel section upstream of the hamlet of Rio Claro, practically all unconsolidated material was eroded. Deposition in the downstream region was on the order of only 15-30 cm. Several attempts have been made to model potential lahar magnitudes (Amaya, 1986; Estudios y Asesorias, 1986). Figure 3.17 (right-hand side) presents the results of modelling the lahar height versus distance to the crater for three events: the 1985 event, a probable event similar to the ones from 1595 and 1845, and a maximum event in which all ice would melt (from Estudios y Asesorias, 1986). The results should be considered preliminary due to the large uncertainty of input factors, and need to be improved.
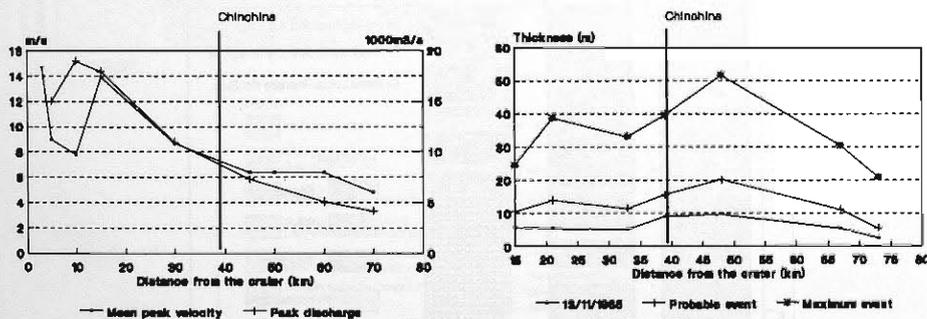
Figure 3.17: Left: Relationship of the distance from the volcano to (a) mean peak velocity and (b) maximum discharge for the 1985 lahar event (Naranjo et al., 1986). Right: Relationship of the distance from the crater to height of lahar for three events: 1985, probable event and maximum event (Estudios y asesorias, 1986).

3.3.3 Glacial aspects

Glacial aspects play a role not only in the formerly glaciated area (above 3000-3600 m), but also influence the rest of the study area, as volcanic eruptions during glacial periods resulted in lahars with magnitudes far greater than could develop presently. Some of the most important terrace levels discussed in section 3.3.1 are related to glacial periods. During the period of maximum glaciation, the glaciated area was 40 times larger than the present.

Herd (1974) correlated glacial stages in the Ruiz area with the stages in other areas in Colombia. Thouret in IGAC (1986) distinguished five different stages in the Ruiz-Tolima area. Within the study area it is difficult to identify these stages. In figure 3.15 all moraines visible on 1:60,000 scale aerial photos of the upper section of the Rio Claro catchment have been mapped. The extent of the "Ruiz" stage, dated as the "little" ice age, for the Santa Isabel glacier can be clearly recognized. Above a series of morainic walls the rocks are bare, without an ash cover, and show clear glacial striations. Instead of a few clearly defined limits of moraines, as in the map by IGAC (1986), a large number of terminal and lateral moraines are found, especially in the southern portion of the map. The two cirques in the western sector have clear moraines as well, indicating that they had active independent glaciers for some time. The valley glacier of the Rio Claro was at that time still present, indicated by a nick in the glacial valley floor where the moraines of the cirques are cut off. A very marked U-shaped valley is found in the bottom centre of the figure, lined by lateral moraines.

The present glacial equilibrium line lies at about 5100 m; the line of a mean annual temperature of 0° lies at 4900 m (Thouret et al., 1989a).

3.4 Climatic aspects

A large amount of climatic data is available for the study area, from different sources (HIMAT, 1990; CENICAFE, 1990; and CHEC, 1990). However, the observation intervals of the various stations differ strongly, so it is rather difficult to prepare climatic records for a longer period based on many stations. Some monthly statistics are given in figure 3.18.
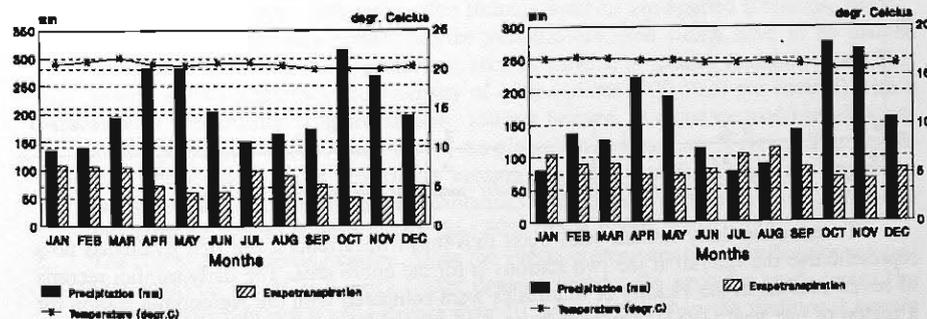
Figure 3.18: Mean monthly rainfall, evapotranspiration, and temperature for two stations in the area. Left: CENICAFE (Chinchina). Right: Facultad Agronomia (Manizales).

The rainfall distribution over the year is bimodal, with maximum precipitation in

The rainfall distribution over the year is bimodal, with maximum precipitation in April/May and in October/November. The vertical distribution of rainfall is believed to be bimodal as well (Vis, 1989): there is a rapid increase of rainfall with altitude at elevations between 1000 and 1400 m, followed by a decrease and a second maximum at 2800 m, above which the rainfall decreases rapidly. The accuracy of this information is questionable, however. The differences in rainfall amounts with altitude may be caused by local topographic differences, such as valleys extending into mountain ranges.

Return periods for 24-hour rainfall, based on a 20-year record (1970-1990), for two stations is given in figure 3.19.

Chinchina: Cenicafe
R24=75.2+34.6logRI
STD= 2.56

Manizales: Agronomia
R24=65.1+34.9logRI
STD= 3.06
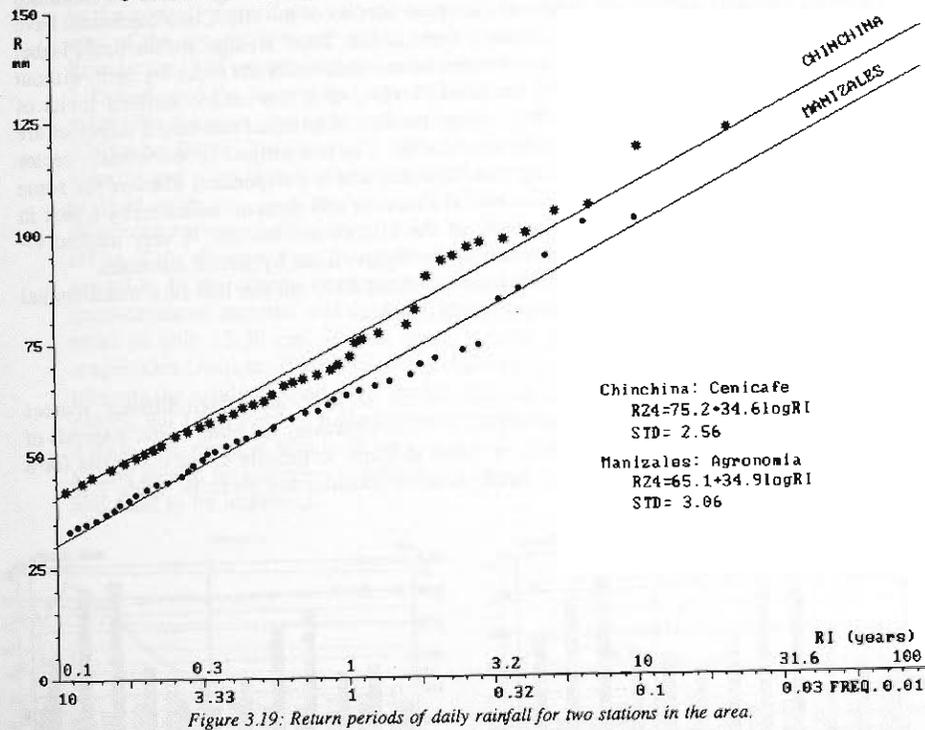
Figure 3.19: Return periods of daily rainfall for two stations in the area.

To correlate daily rainfall with mass movement occurrences, we first evaluated how representative the rainfall at the two stations is for the entire area. The daily rainfall records of seven stations in the vicinity of Manizales were compared with the Agronomia station for a period of one year (1982). The correlation proved to be rather poor. Even over a city such as Manizales it is not possible to extrapolate the rainfall of one station to the whole municipal area. Thus, it is not possible in this area to use only the rainfall data for a central climatic stations in evaluating the relationship between rainfall and landslide occurrences.

3.5 Land-use aspects

3.5.1 Deforestation

The study area has only a short history of economic development. Until the middle of the nineteenth century nearly all of the area was forested. First colonization of the area from the northern state of Antioquia started some 150 years ago. Manizales was founded in 1849. The main motives for colonization were (a) the search for gold, which is found in limited amounts in the granodioritic intrusion east of Manizales, and (b) population pressure and deterioration of agricultural land in Antioquia. The main activity in the area at that time was cattle raising, and for that reason the Andean forest was cut and transformed into grassland. After the beginning of the twentieth century, coffee cultivation developed to become the most important land use in the area below an elevation of 2000 m. Nowadays, practically all of the original forest has been cut, except on the very steep, inaccessible lateral slopes of the lava flows in the eastern part of the study area. There is little historical information on the effect of this deforestation on the occurrence of mass movements. Gomez reported as early as 1943 about large active mass movements in the area east of Manizales, and mentioned deforestation as the major cause. Due to a shorter response time of river discharge to rainfall after deforestation, river erosion has increased dramatically, leading to retrogressive landslide phenomena. According to Gomez (1943) most of the large landslides occurred during the first decades of this century, after deforestation. Unfortunately it is difficult to verify this statement, as the earliest available aerial photos of the region are from 1946. Since then the large mass movement phenomena have not undergone major changes, as verified by the author by sequential aerial photo interpretation.

3.5.2 Coffee cultivation

The part of the area situated roughly between elevations of 1000 and 2000 m is one of the most important coffee-producing regions in Colombia. The National Coffee Research Centre (CENICAFE), responsible for research on coffee and alternative crops, is located near Chinchina. In the area three different coffee farming systems are applied (Palacios, 1991):

1. *The traditional farming system*. Coffee varieties are used which have to be planted under trees providing shade protection, such as banana, or guadua (bamboo type). This system allows a relatively low density of coffee plants (900-1200 per hectare) with a shadow tree density of approximately 150 per hectare. The commercial harvest starts after 4 years and the probable life of the plantation is less than 30 years. The system usually does not require fertilizer or erosion-control measures. Around the beginning of the 1960s all Colombian coffee plantations were classified as "traditional". Presently this farming system is used in less than 50% of the coffee area.

2. *The "technified" farming system*. Since the 1950s, coffee varieties have been developed that could be grown at a much higher density, without the need for shade trees. The plant density can reach values more than 10 times higher than the traditional system (5000-10,000 per hectare), but the system requires abundant application of chemical fertilizers and intensive maintenance. Construction of soil conservation works is very important, as the soil is exposed to direct rain impact, which leads to soil erosion. Due to their high productivity the plants start to decline after 4 to 5 years, and have to be renewed more frequently than in the traditional system. After clearing and before new

plants have become productive, the plantations are very susceptible to soil erosion and mass movement, especially on steep slopes.

3. *The modern intermediate farming system.* The same coffee varieties are used as in the "technified" system, but with some shade trees, a lower density of plants per hectare (1500-5000), and relatively modest application of fertilizer. The relationship between coffee price and fertilizer costs determines whether a system with or without shade is chosen. Generally the higher susceptibility to mass movement and erosion of the "technified" system does not play an important role in the farmer's decision.

3.5.3 Urbanization

In the first decades after its foundation in 1849, Manizales did not experience significant growth. Economic development started with the cultivation of coffee in the beginning of the twentieth century. Manizales has always been the capital of the Caldas department, and therefore has a high density of services, government offices, etc. (Turkstra et al., 1991). The subdivision of the old Caldas department into three smaller departments (Risaralda, Quindio, and Caldas) in 1966 caused a stagnation in urban development.

The history of urban growth, both in number of inhabitants and in hectares of urbanized area, is represented in figure 3.20 (Universidad Nacional de Colombia, 1986). The map of historical development of Manizales is given in figure 3.21 (modified from Abramovsky, 1990). This map shows that until the 1960s, the rate of development was rather constant, and that the explosive growth occurred during the 1970s and 1980s. In the initial phases of development, urban growth took place on the relatively flat T-shaped hilltop on which Manizales was founded. However, after occupying all suitable land in the flatter top area, the city began to develop into the surrounding very steep slope ranges. Especially low-income groups were forced to live under dangerous conditions. One solution used to create more space for city extension is flattening the topography. One method applied often is the construction of "hydraulic fills", by damming a valley at its outlet and subsequently filling it with material washed down from the surrounding

Figure 3.20: Historical development of Manizales. Both the number of inhabitants and the size of the urbanized area (ha) are given.

ridges, which are being flattened. Once a reservoir has filled it is left to consolidate for a period of 1 to 10 years before houses are constructed (Ruiz, 1981; Angeles et al., 1989). The largest fills, in the townships of Palermo and Bajo Palermo, have a volume of approximately 1 million m^3. Most of the fills have been made by private companies, without geotechnical site investigations. The exact locations of the oldest fills in the town centre are not very well known. There have not been major stability problems associated with the hydraulic fills, although current research is being undertaken to investigate their behaviour during a strong earthquake.
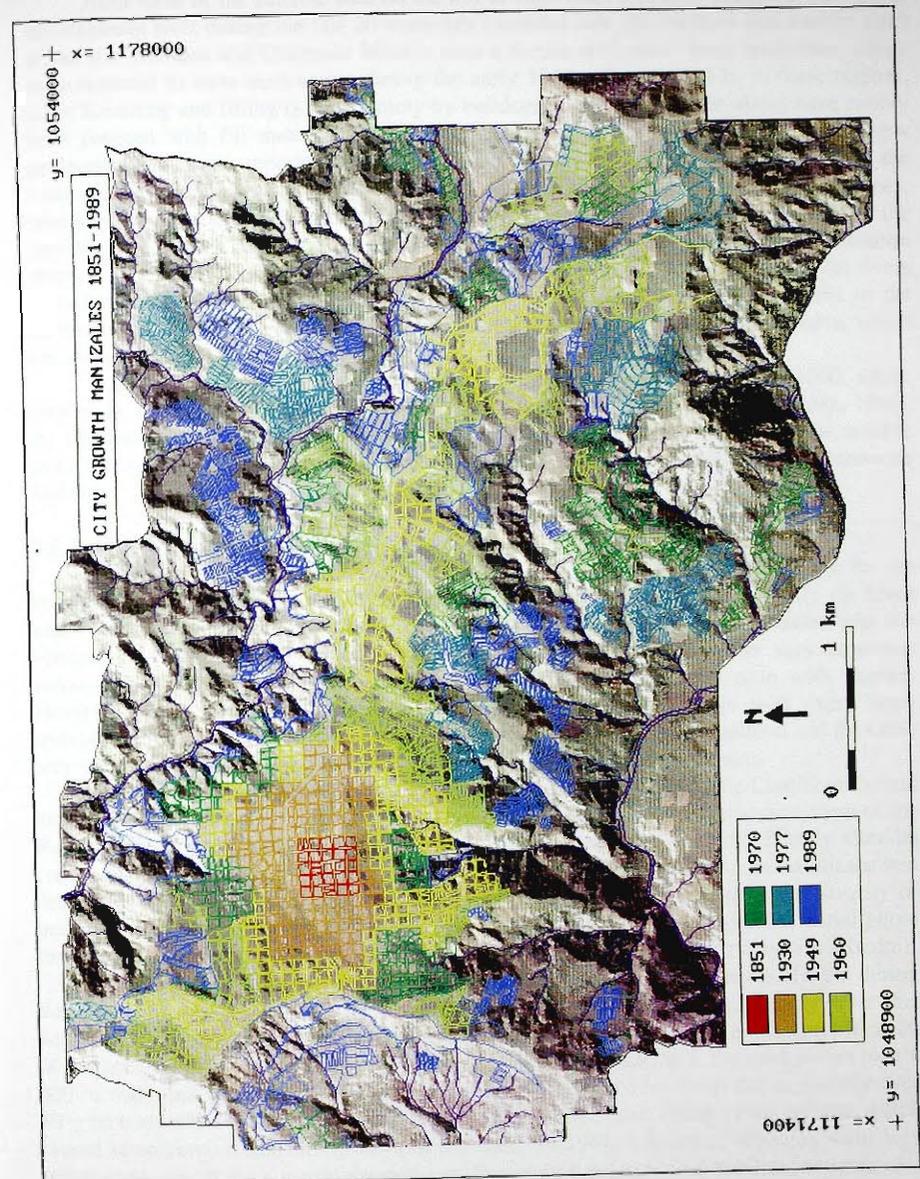
Figure 3.21: Historical development of Manizales.

After most of the suitable sites on the hill of Manizales had been occupied, new urban development built during the last 20 years has extended into the northern and eastern sides of the Rio Olivares and Quebrada Minitas over a terrain with many large landslides, which were reported to have been active during the early 1940s (Gomez, 1943). In these regions, slope flattening and filling is done mainly by bulldozers, and many of the slides have simply been covered with fill material. Several problems with reactivated landslides below new settlements have been reported (Barrio Peralonso, Barrio Villa Julia). During the 1980s the municipality executed programmes to relocate squatter areas situated on dangerous slopes, after a series of catastrophic landslide events on the northern and southern steep slopes of the city. Manizales has a large problem of soil and, especially, water pollution. Water purification plants do not exist, so all wastewater, as well as all the garbage, is disposed of into the rivers Chinchina and Olivares. A site for a large sanitary landfill was recently selected in the northern part of Manizales, but unfortunately the site lies on two dormant landslides, which are showing signs of reactivation.

The projected number of inhabitants in Manizales in the year 2000 is 370.000, which implies an urban extension after 1985 of 430 ha (Universidad Nacional de Colombia, 1986). As Manizales has only limited available and suitable land for future growth, a new satellite town (called "km 41") is being built some 40 km west of Manizales, along the Pan American highway.

3.5.4 Infrastructure

Due to its strategic location, Manizales has always been an important centre for the transport of goods over the Cordillera Central. Until 1918 this was possible only via horse trails. Between 1918 and 1922 a cableway was constructed to connect Manizales with the village of Mariquita along the Rio Magdalena. During the 1930s another very important infrastructural work was accomplished: connection of Manizales by train with Pereira. However, maintenance of this railroad through the very steep terrain with many slope instability problems became more and more problematic. Therefore the railroad and the cable way were demolished during the 1960s after the construction of new roads.

The first main road from Manizales eastward to the Letras pass in the Cordillera Central and on to Bogotá was constructed in the early 1940s, as were the hydroelectric system of the Rio Chinchina river, and the drinking water supply system for the city. Shortly after its completion a new, modern drinking water plant in the valley of the Quebrada Gallinazos was destroyed by a large debris flow and had to be rebuilt. Figure 3.22 shows the severity of landslide problems along the road to Letras, shortly after its construction. The aerial photo interpretation shows the section where the road crosses the granodioritic intrusive (Ktcdm).

The main road from Manizales to Chinchina and Pereira existed previously, but during the 1960s it was widened to cope with the increased traffic density. Shortly after this widening some severe mass movement problems occurred, due mainly to incorrect location of surface drainage. At the most problematic site, known as La Siria, the road passes over a 300-m wide and very steep, fault-related water divide, with very steep slopes (locally over 40°) on both sides. Due to inappropriate drainage from the road a deep gulley formed, which caused retrogressive landsliding towards the road. In 1967, a series of retaining walls was constructed, which did not stop the problem. Presently protection and stabilization works are still in progress (See figure 3.23 and figure 4.6).
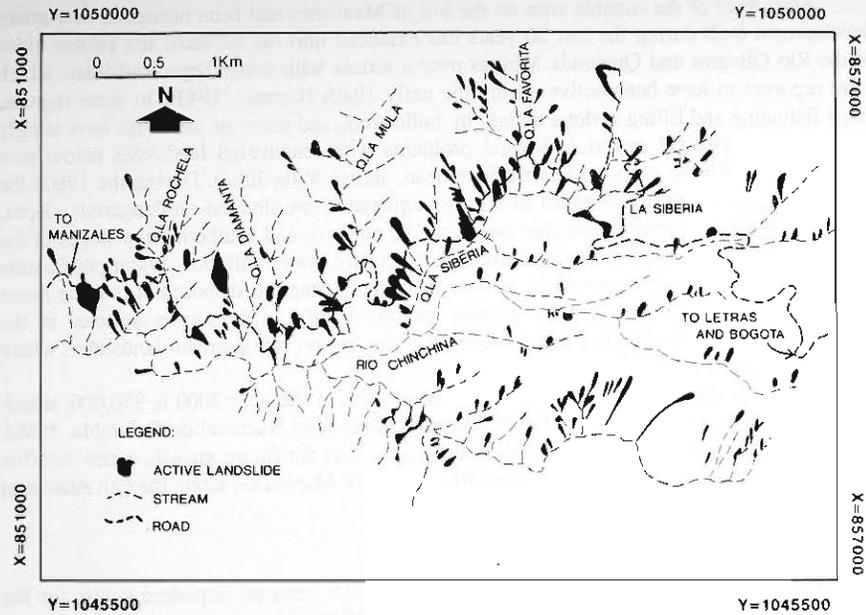
Figure 3.22: Severe slope instability problems along the road from Manizales to Letras shortly after its construction in the early 1940s. Only the active features are indicated in black.
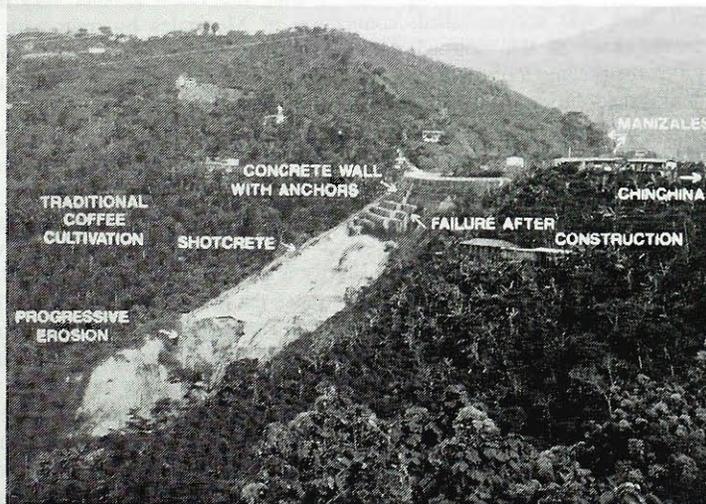
Figure 3.23: Overview of the La Siria landslide and erosion complex along the main road Chinchina-Manizales.

Due to the mass movement problems at La Siria, an alternative road was planned from Manizales to Chinchina. Since the 1960s this road, located further north via the hamlet of La Manuela, has been under construction. In the design of the road, only geometrical aspects played a role. Geotechnical characterization of potential landslide zones was not carried out. Shortly after the start of construction several large landslide problems occurred. One of these, of similar severity to La Siria, occurred less than 2 km from the start of the road, in a location called La Estampilla. At this location a trench-form cut 35 m deep was excavated in the slope. Soon after construction, the upslope part started to present great landslide problems. A fossil landslide complex was reactivated by the removal of its toe support, and successive movements mobilized the entire upslope area. Extensive stabilization works, such as a retaining wall, anchoring, and internal drainage, were executed. Most of these works were subsequently destroyed. An overview of the Estampilla landslide is given in figure 3.24.
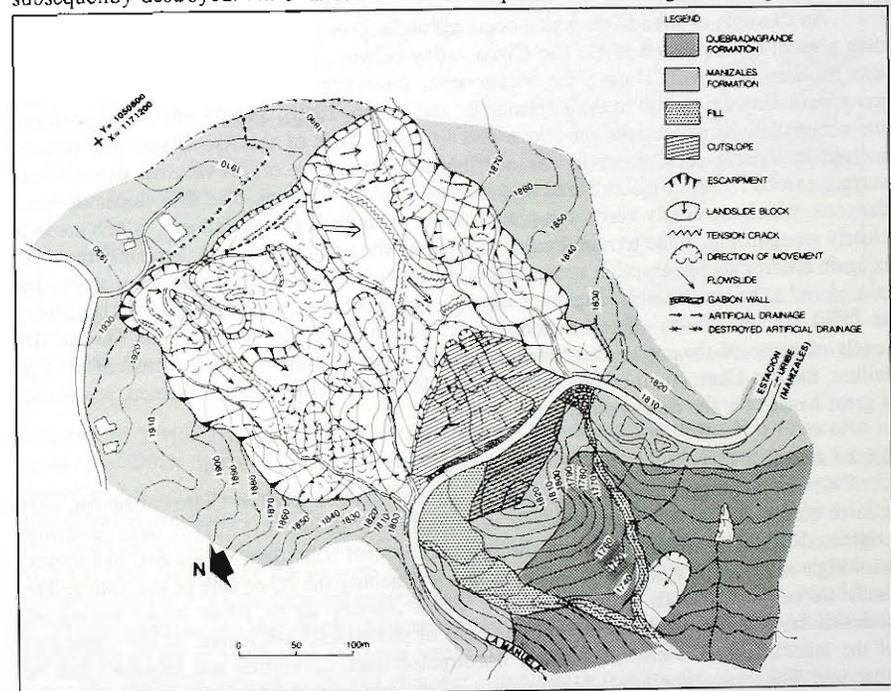
Figure 3.24: Overview of the Estampilla landslide.

Another severe landslide problem is found some 4.5 km further along the road from La Estampilla in the direction of La Manuela. At that location, known as Queibra de Villar, the road makes a sharp turn to the south parallel to the Rosario river, which for some length follows the continuation of the fault line which crosses La Siria. Due to undercutting of the river in the very weak fault material a large rockslide occurred, which destroyed the road over

a distance of some 200 m. The slope was stabilized by constructing rock terraces and deviating the drainage from the road to the other side of the hill. There it caused severe erosion and landsliding as well, so that now the hill is unstable on both sides, and a situation similar to that at La Siria is likely to occur.

3.6 Examples of mass movements

In this section some examples will be given of different types of mass movement occurring in the Manizales-Chinchina area, and some of the most important landslide-causing factors will be discussed. This discussion is presented in the form of a number of small case studies of individual landslides, each associated with a characteristic causal factor.

3.6.1 Landslides caused by river incision

An example of a landslide which occurred under geomorphological conditions different than present can be found in the Rio Claro valley between the hamlet of Rio Claro and the Rio Molinos waterfall. During the Pleistocene, this valley was filled with a very large pyroclastic flow up to 300 m thick (Handszer and Grand, 1989). Shortly after its deposition, the accumulation, which was far above the erosional basis of the Rio Claro, was rapidly incised in those places where it was not lithified. Remnants of the original depositional surface can be found as isolated mesas, separated by deep canyons. The side slopes of these canyons, which are nearly vertical in places, show a number of large failures, which are still clearly recognizable in the terrain. Part of this area is shown in figure 3.25. Presently the river is again eroding its pre-eruption streambed in metamorphic rocks, and the adjacent slopes are considered to be less instable. However, care should be taken in characterizing the landslides as fossil. The possibility of reactivation by an earthquake is not hypothetical. On the flat levels of some of the mesas clear tension cracks can be observed. In the case of a large failure, the Rio Claro could be blocked and a landslide reservoir could be formed, presenting a great hazard for the downstream area.

3.6.2 Landslide caused by glacial oversteepening

One of the largest landslides in the area is found in the upper Rio Claro catchment, near a farm called El Recodo (the landslide is indicated in figure 3.15). This huge landslide originated from the western slope of the glacially eroded Rio Claro valley and has moved with high velocity over the flat floodplain, nearly reaching the other side of the valley. The landslide originated from a thick morainic cover (locally up to 10 m thick) resting on andesitic lavas and overlaid by a clear sequence of post-glacial ash layers. At the upper part of the landslide, in the cuts of a newly constructed road, no regular ash sequence can be observed. The topsoil contains a high quantity of ash, but some boulders and cobbles are also found, which precludes the possibility of a normal ashfall deposit. Some wood fragments, located approximately 2.5 m below the terrain surface, were sampled for C-14 dating. The result of this dating was surprisingly recent: between 1667 and 1797 AD. The possibility that a fairly recent tree remnant had been sampled cannot be excluded with certainty, but the two facts together (no regular ash deposits and recent C-14 dating) can serve as evidence for a very young age of this apparently fossil landslide. The example illustrates how difficult it may be to characterize landslides as "fossil".

3.6.3 Reactivated landslides caused by the 1985 lahar event

Another example of a fossil landslide which has occurred under geomorphological conditions different from the present can be found close to a new highway bridge near Chinchina.

Figure 3.25: Geomorphological map of the pyroclastic flow levels of Conventos-Guamal in the Rio Claro valley with a number of fossil landslides.

Between the bridge and the city of Chinchina, an old meander curve of the Rio Chinchina is found (see sketch map of figure 4.3), which was produced when the river was not as deeply incised as it is presently. Due to the presence of a sequence of permeable ash and pyroclastic flow deposits overlying less permeable debris flow materials, some large rotational landslides developed, of which the backward-tilted blocks can still be recognized in the aerial photos. At the present location of the western end of the bridge another large landslide occurred, as can be concluded from the forward-bulging slope. The foot of this landslide was covered later by terrace materials, so that reactivation caused by river erosion is no longer expected. The western abutment of the bridge has been partly constructed in the landslide deposit.

The landslide located in the old meander curve which reaches the Rio Chinchina was reactivated after the 1985 Nevado del Ruiz eruption due to the severe toe erosion caused by the lahar. The remnants of the road and the houses, which were still present before 1985, can only be found with difficulty in the terrain. At present a retrogressive movement is taking place, involving more and more parts of the fossil landslide.

Some 8.5 km downstream, near La Manuela, another large mass movement occurs which was reactivated by the 1985 lahar. The strong lateral erosion of the river-bed reactivated a large landslide in a fault zone with highly disintegrated black schists. According to local farmers the landslide was already present before 1985, but movement was so limited

that an unpaved road which connected La Manuela with the village of Palestina, and which crossed the landslide at the downslope sector, could be used by cars. During the reactivation in 1985 this road moved downslope some 5 m horizontally and 2.5 m vertically. A new road was constructed some 300 m further upslope. Due to subsequent retrogressive failure the landslide is now endangering this new road as well. Drainage from this new road is one of the factors which has caused accelerated slope failure in the upper section. The central section of the flowslide is covered with relatively old coffee plants and some high trees, which have not been destroyed. Trees in the downslope section, where movement was greatest, have toppled or died because the roots were destroyed by the shear movement. The maximum thickness of the moving mass was estimated from field observations to be on the order of 10 m. Figure 3.26 shows a geomorphological sketch map of the La Manuela landslide.

3.6.4 Earthquake-related landslides

East of Manizales, between the margin of the city and the industrial centre of Maltería, the terrain is covered by a large number of very large mass movements, which are mainly of the flowslide or flow type. They occur in rounded hills with a very thick ash cover, which is locally up to 15 m thick (Mool, 1992). Most of the mass movements are very large: a few hundreds of meters in length and up to 100 m in width. Figure 3.27 shows some examples of flowslides occurring on the south slope of the Cerro de Oro ridge near the radio tower. The thickness of these moving masses is considered to be on the order of 10 to 20 m, involving mainly ash deposits and some underlying residual soils. The flowslide in the western part of the map is located on an active north-south fault, called El Perro (Naranjo and Rios, 1989). Along this fault line clear displacements of about 50 cm have been observed within ash layers. Considering the large dimensions of these flowslides and their geomorphological setting, they are most probably triggered by earthquakes. In the same map of figure 3.27 also a number of landslides are indicated which occur along the margins of deeply incised valleys. These are believed to have occurred as a result of renewed fluvial incision after deforestation. The flowslides mentioned earlier are not related to such valleys, however.

The ash profiles in this area show a relatively uniform sequence of sandy silt layers and coarse sandy/gravelly layers with individual thicknesses mostly no more than a few decimetres (see also figure 3.16). In the lower part of the profile, at an average depth of 5-7 m, a volcanic sand layer occurs with an average thickness of 10 cm. This "grey sand layer" is well sorted (C_c = 1.4, C_u = 3.8), equi-granular (D_{50} = 0.57 mm), and very loose, with a relative density of 5.94% (Koirala, 1992). The material is very permeable, with a saturated hydraulic conductivity of 106-121 cm/day (Mool, 1992). The "grey sand" layer is confined between two sandy silt layers which are fairly well graded (C_c = 0.7, C_u = 10.3), have a D_{50} of 0.16 mm, a higher density, and a lower permeability (10-100 cm/day). The grey sand layer, when saturated, can suffer vibratory compaction when subjected to seismic tremors. Under cyclic vibrations, pore pressure in the grey sand layer may increase until it leads to soil liquefaction. Koirala (1992) has studied the liquefaction potential of the "grey sand" layer and concluded that it is highly susceptible to liquefaction. Mass movement phenomena which show characteristics of liquefaction can be found in the area east of Manizales. Especially the Pleistocene terraces, composed of debris flow material with a relative thick cover of pyroclastic material, contain some flowslide and flow phenomena which can be explained adequately only as a result of liquefaction.
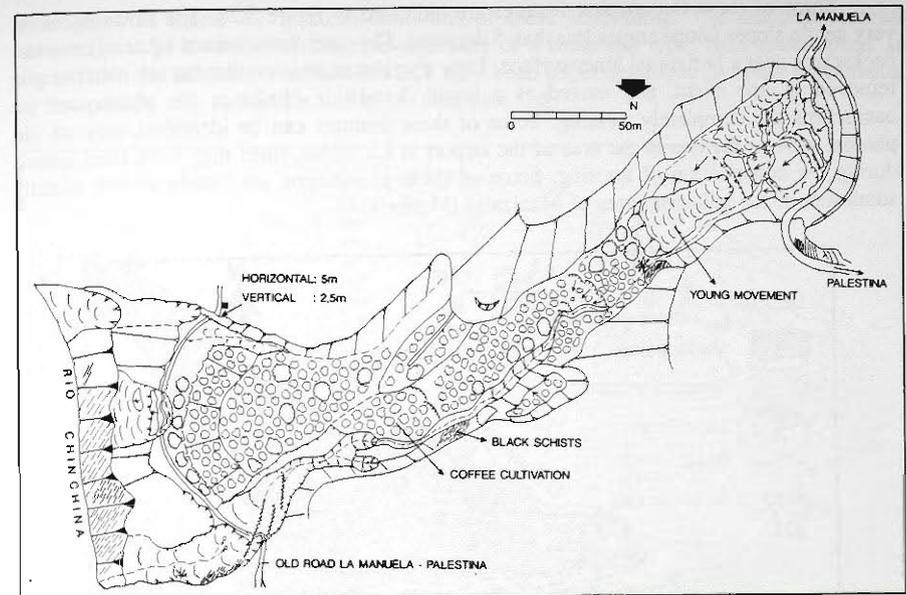
Figure 3.26: Geomorphological sketch map of the La Manuela landslide.
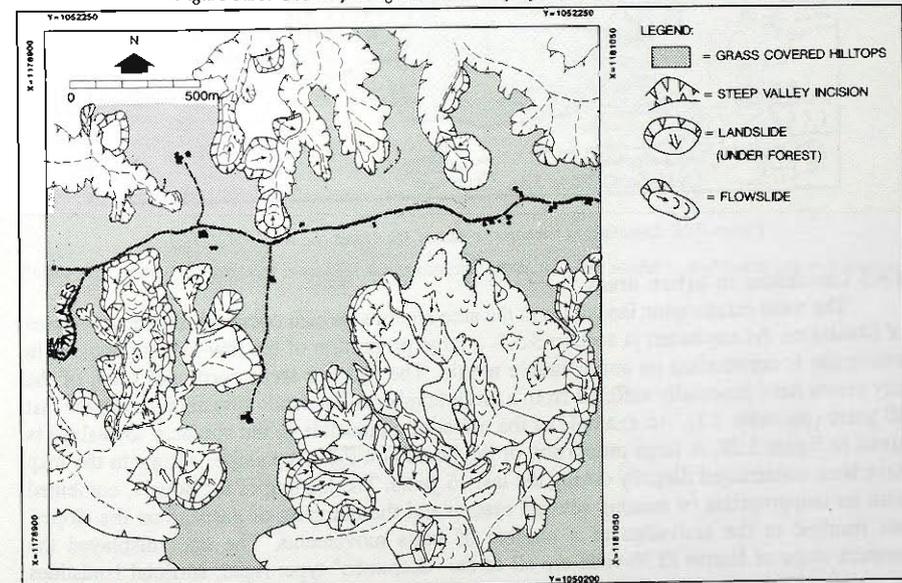
Figure 3.27: Landslides in the Cerro de Oro region east of Manizales.

Some of these liquefaction features are indicated in figure 3.28. The flows occur on very gentle slopes (slope angles less than 5 degrees). They are characterized by nearly vertical backscarps near a horizontal inner surface. They give the impression that the ash material was removed in one event, and moved as a liquid. Landslide blocks in the vicinity of the backscarps are completely missing. Some of these features can be identified only on old photos, such as the one in the area of the airport at La Nubia, since they have been altered during the construction of housing. Some of these phenomena are clearly visible directly southwest of the industrial area of Manizales (Maltería).
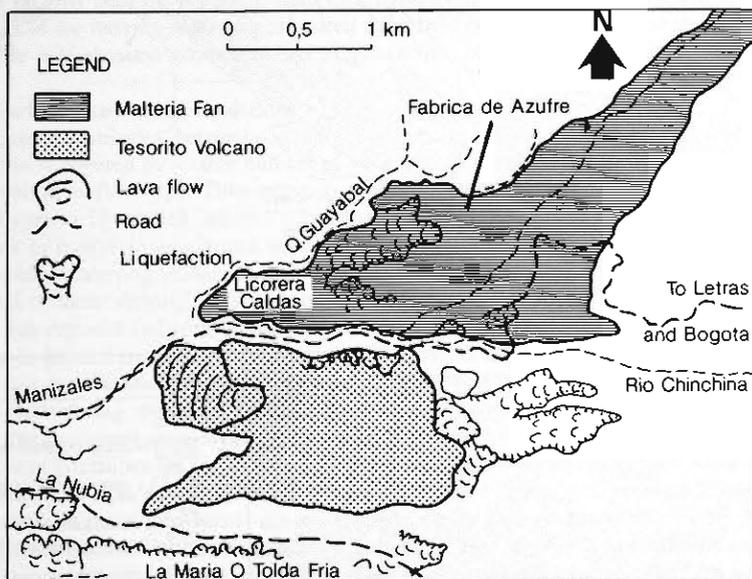
Figure 3.28: Liquefaction phenomena east of Manizales (La Nubia-Maltería).

3.6.5 Landslides in urban areas

The most catastrophic landslides in the area are those which occur within the urban area of Manizales. As explained in section 3.5.3, a large proportion of the low-income housing in Manizales is constructed on unfavourable terrain. The squatter areas north and south of the city centre have especially suffered from a large number of landslide disasters during the last 20 years (see table 3.1). An example of the effect of a landslide in the southern townships is given in figure 3.29. A large proportion of the houses on the steep slopes shown in the map have been constructed illegally during the last 15 years. The loading of the houses, combined with an inappropriate or missing sewage system and the dumping of garbage on the slopes, has resulted in the activation of a number of mass movements. The ones displayed the western slope of Barrio El Nevado are all of the "derrumbe" type: rapid, surficial landslides in the upper soil layer, in which the material is transported away from the source area. (The

photograph in figure 3.7 is taken from one of these landslides). The mass movements occurring in the township of Bajo Nevado were of a rotational type, with lower speed. In figure 3.29, the houses are indicated which have been either destroyed by mass movements, or removed by city authorities due to the landslide risk.
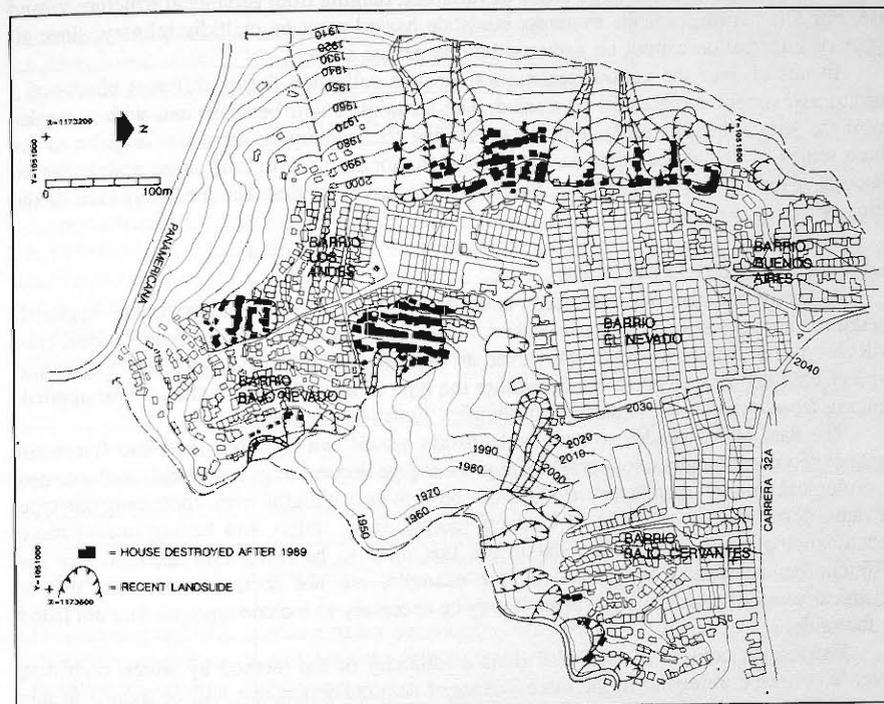
Figure 3.29: Houses destroyed or evacuated due to landslide problems in the southern neighbourhoods in Manizales.

CHAPTER 4. DATA COLLECTION

Slope instability phenomena are related to a large variety of factors, involving both the physical environment as well as human interaction. Assessment of landslide hazard therefore requires knowledge about a large series of variables, ranging from geological structure to land use. For this reason, projects to assess landslide hazard must be multidisciplinary, since all types of information cannot be gathered by one person alone.

In this chapter the various techniques for data collection during different phases of a hazard assessment project will be treated. The techniques will be illustrated with examples from the Rio Chinchina study area. In presenting the techniques, emphasis is given to the three scales of analysis defined in section 2.6 (regional, medium, and large scale). Before discussing the techniques, however, an overview is given of the data needed at each of the three scales.

4.1 Scale-related input data

A list of the various input data needed to assess landslide hazard at the regional, medium, and large scale is given in table 4.1. The list is extensive, and only in an ideal case will all types of data be available. However, as will be explained in chapter 6, the amount and type of data that can be collected determine the type of hazard analysis that can be applied, ranging from qualitative assessment to complex statistical methods.

The data layers needed to analyse landslide hazard can be subdivided into five main groups: geomorphological, topographic, engineering geological or geotechnical, land use, and hydrological data. A "data layer" in a GIS can be seen as one digital map, containing one type of data, composed of one type of element (points, lines, units), and having one or more accompanying tables. Of course, the layers that have to be taken into account vary for different environments. Tectonic data, for example, are not needed in an area that is seismically inactive, and in some areas it may be necessary to include types of data not listed in the table.

The second column of table 4.1 gives a summary of the method by which each data layer is collected, referring to the three phases of data collection that will be treated in this chapter (image interpretation, fieldwork, and laboratory analysis). The last three columns in table 4.1 give an indication of the relative feasibility (high, moderate, or low) of collecting a certain data type at each of the three scales under consideration.

Due to the large size of areas to be studied at the regional scale (on the order of 500-2000 km^2), and because of the objectives of hazard assessment at this scale (discussed in chapter 2), detailed data collection for individual variables is not a cost-effective approach. Data gathered at this scale is limited to the delineation of homogeneous terrain mapping units, and collection of regional seismic data. At the medium scale, nearly all of the data layers given in table 4.1 can be gathered for areas smaller than 200 km^2. The use of terrain mapping units at this scale is no longer important, for reasons that will be discussed in section 4.3.2.1. At the large scale, where the study area is generally smaller than 50 km^2, all of the proposed data layers can be collected.

Data types	Summary of data collection techniques	Feasibility of data collection		
		Regional scale	Medium scale	Large scale
GEOMORPHOLOGY				
1. Terrain mapping units (TMUs)	Satellite image interpretation + walk over study	High	Moderate	Low
2. Geomorphological units	Aerial photo interpretation + field check	Moderate	High	High
3. Geomorphological subunits	Aerial photo interpretation + field check	Low	High	High
4. Landslides (recent)	Aerial photo interpretation + field descriptions	Low	High	High
5. Landslides (older period)	Aerial photo interpretation + collection of landslide records from newspapers, fire brigades, or church archives	Low	High	High
TOPOGRAPHY				
6. Digital terrain model (DTM)	Collection of existing contour maps	Moderate	High	High
7. Slope map (degrees or %)	Made from a (DTM)	Moderate	High	High
8. Slope direction map	Made from a DTM, no extra data collection required	Moderate	High	High
9. Breaks of slope	Aerial photo interpretation	Low	Moderate	High
10. Concavities/convexities	Made from a DTM, or detailed photo interpretation	Low	Low	High
ENGINEERING GEOLOGY				
11. Lithologies	Checking of existing geological maps, or by mapping if no data is available	Moderate	High	High
12. Material sequences	Made by a combination of other maps (geomorphological, geology, slope and DTM). (See section 5.4.4.2	Low	Moderate	High
13. Sampling points	Field descriptions of soil and rock outcrops, and laboratory analysis of selected samples to characterize material types	Moderate	High	High
14. Faults & lineaments	Satellite image interpretation, aerial photo interpretation, and fieldwork	High	High	High
15. Seismic events	Collection of existing seismic records	High	High	High
16. Isolines of seismic intensity	Questionnaires on the observed damage from earthquake(s)	Low	Moderate	High
LAND USE				
17. Infrastructure (recent)	Aerial photo interpretation + topographic map	Moderate	High	High
18. Infrastructure (older)	Aerial photo interpretation + topographic map	High	High	High
19. Land-use map (recent)	Aerial photo interpretation + classification of satellite images + field check + field descriptions	Moderate	High	High
20. Land-use map (older)	Aerial photo interpretation	Moderate	High	High
21. Cadastral blocks	Collection of existing cadastral maps and data base	Low	Low	High
HYDROLOGY				
22. Drainage	Aerial photo interpretation + topographic map	High	High	High
23. Catchment areas	Aerial photo interpretation + topographic map or modelling from a DTM	Moderate	High	High
24. Meteorological stations	Collection of existing meteorological data	High	High	High
25. Water table	Field measurements of Ksat + modelling (See section 5.4.4.3)	Low	Low	Moderate

Table 4.1: Overview of input data needed for landslide hazard analysis. See text for explanation.

4.2 Collection of existing data

Gathering existing data related to input variables is the first important activity in a GIS-supported landslide hazard analysis. The amount, and the quality, of existing data determine to a large extent the timespan during which a project can be executed. The data listed in table

4.2 are considered crucial in the execution of a hazard study at the three scales mentioned. They can often be collected only at high cost due to the time-consuming methods needed. All other existing data related to one of the data layers mentioned in table 4.1 are also useful as reference. It is strongly advised never to use data obtained by others without thorough inspection and revision. One should never trust blindly the information presented in a map, but always check it with one's own experience. Such a low-quality map overlaid with related data may produce large errors and inconsistencies that are revealed after many hours of digitizing. An example is the use of a soil map, based on physiographic units, which may be quite different in legend structure and extent than a terrain mapping unit map produced by another person. Such error sources are discussed further in chapter 7. Those maps in which image interpretation plays an important role, and in which the quality of the product depends largely on the experience of the interpreter, will produce the greatest inconsistencies. These maps will be quite erroneous if not based on thorough field checks. Moreover, they are normally based on legends other than those that can be used in the analysis. It is therefore advisable to remake the maps, and base them on new image interpretation.

```
Regional scale (1:100,000)

Indispensable data: - 1:100,000-scale topographic maps
                    - 1:50,000 (or larger) panchromatic aerial photos

Desirable data:     - SPOT pan or XS stereo or LANDSAT TM or LANDSAT MSS
                    - Seismic records
                    - 1:100,000-scale geological map

Medium scale (1:25,000)

Indispensable data: - 1:25,000-scale topographic map, preferably with a contour interval of
                      25 m or less
                    - 1:25,000 (or larger) recent panchromatic aerial photos

Desirable data:     - 1:25,000 (or larger) panchromatic aerial photos from earlier dates
                    - 1:50,000- or 1:25,000-scale geological map
                    - 1:25,000 (or larger) land-use maps
                    - Seismic records
                    - Rainfall records

Large scale (1:10,000)

Indispensable data: - 1:10,000-scale topographic map with contour interval < 10 m
                    - 1:10,000 (or larger) recent panchromatic aerial photos

Desirable data:     - Landslide records (from newspaper, church, or fire-brigade records)
                    - Geotechnical reports with borehole and soil strength data
                    - Climatic data (daily rainfall, temperature, evaporation)
                    - Seismic records
```

Table 4.2: Indispensable and desirable input data for the three scales.

4.3 Image interpretation

Interpretation of remote sensing images, such as satellite images or aerial photos, is one of the most important phases in a landslide hazard assessment project. As can be seen from table 4.1, many of the data layers are obtained by image interpretation, combined with field checks. For this purpose a number of remote sensing tools are available. The most widely used are shown in table 4.3, together with some of their technical specifications (after Rengers et al., 1992).

Detection in table 4.3 means that it is possible to decide if an object of known spectral characteristics is present or absent at a specified geographical location. *Recognition* of an object means that it is possible to decide if an object of known form and spectral

characteristics is present in the image, and *identification* means that it is possible to identify objects of variable form and spectral characteristics on the basis of their form characteristics and context within the background.

		Type of imagery						
		LANDSAT MSS	LANDSAT TM	SPOT XS	SPOT PAN	Aerial photos 1:50,000	Aerial photos 1:25,000	Aerial photos 1:10,000
Ground resolution cell size		80	30	20	10	0.5	0.25	0.1
HIGH CONTRAST feature-background	Detection	320	120	80	40	2	1	0.4
	Recognition	560	210	140	70	3.5	1.8	0.7
	Identification	800	300	200	100	5	2.5	1
LOW CONTRAST feature-background	Detection	1600	600	400	200	10	5	2
	Recognition	2400	900	600	300	15	7.5	3
	Identification	3200	1200	800	400	20	10	4

Table 4.3: Table with the minimum sizes of objects to be detected, recognized, and identified for various conditions of contrast with their background in various types of imagery. Values should be used only as an indication of the order of magnitude. All units are in meters.

The use of stereoscopic imagery in slope stability studies is very important in view of the clear and diagnostic morphology, created by mass movements. Features such as scars, disrupted vegetation cover, and deviations in soil moisture or drainage conditions are generally used in conjunction with morphological features. Considering the size of most landslides, which is on the order of several tens to a few hundreds of metres, the most useful photographic scale is around 1:20,000. At this scale the phenomenon can not only be identified as a slope instability feature, but a preliminary analysis of the feature is also possible as the elements of the landslide can be recognized and analysed. Overviews on the recognition of landslides from imagery are given by Rib and Liang (1978) and Crozier (1984). It can be concluded from table 4.3 that the satellite imagery available today is not suitable for identifying mass movement phenomena, unless they are very large. Nevertheless, several authors have used LANDSAT or SPOT images for the identification of mass movements (Gagon, 1975; McDonald and Grubbs, 1975; Sauchyn and Trench, 1978; Stephens, 1988; Huang and Chen, 1991; Vargas, 1992). If landslides have to be identified the use of aerial photos is indispensable.

4.3.1 Image interpretation at the regional scale

As was seen in table 2.3, the number of aerial photos required and hence the time needed for interpreting very large areas at a regional scale will be too great in relation to the required degree of precision at this scale. Therefore it must be concluded that a detailed landslide occurrence map cannot be made practically at the regional scale. This has important consequences for the type of hazard analysis that can be applied at the regional scale, as will be explained in chapter 6.

Although satellite images cannot be used very well for the inventory of landslides, they do play an important role in regional-scale analysis, where the initial objective is to divide

the terrain into zones with homogeneous conditions of geology, soil, and geomorphological processes, i.e., to make a terrain classification. SPOT (panchromatic or multispectral) is particularly suited to this purpose due to its stereoscopic capabilities and its relatively good spatial resolution. The use of LANDSAT MSS or TM in geomorphological terrain classification is limited due to the lack of stereo-viewing capabilities and the poorer spatial resolution. The higher spectral resolution offered by LANDSAT is relatively unimportant in terrain classification.

In many regional-scale engineering or development projects, thematic maps of sufficient quality covering a large area are assumed to be unavailable during the initial stage. Instead of creating these maps one by one, followed by their combination, a more suitable approach to a small-scale framework (1:100,000 or smaller) for the storage of different kinds of geo-data may be terrain classification based on interpretation of stereo SPOT imagery or small-scale photography.

Many different classification systems have been developed over the years, which can be classified as geomorphological analytical, morphometric, physiographical, biogeographical, or lithological-geological (Aitchison and Grant, 1967; Brink et al., 1965). The most important systems were compared by Mitchell (1973) and van Zuidam (1986).

Most of these classifications have a tight hierarchical structure, which may hinder their flexible use, or they are based on a single parameter, or a limited set of parameters. To overcome these problems, the terrain classification system based on the delineation of terrain mapping units was developed (Meijerink, 1988). A *terrain mapping unit* is defined as a unit which groups zones of interrelated landform, lithology, and soil. It is a natural division of the terrain that can be distinguished on stereo SPOT imagery or small-scale aerial photographs, and verified on the ground. The units are differentiated on the basis of photomorphic properties in the stereo model. The system does not have a strict hierarchical structure. The user can construct the legend according to the important parameters encountered in the study area and the purpose of the study.

The terrain mapping unit approach has been used successfully in various geomorphological and engineering geological applications, such as highway planning (Akinyede, 1990) and erosion studies (Bocco, 1991). The TMU approach may not always be scientifically consistent, in the sense that classification parameters are not strictly applied at the same hierarchical level in different studies. Its application is directed instead to a more practical use: how to divide a terrain into homogeneous units for practical applications. The following satellite images were available for the Rio Chinchina study area:
* SPOT XS 9 August 1986, path/row 643/340, incidence angle 14.1° left, western part;
* SPOT XS 9 August 1986, path/row 644/340, incidence angle 18° left, eastern part;
* SPOT XS 5 September 1986, path/row 643/340, incidence angle 26.1° right, western part.

From these images a stereo pair covering half of the area could be made. Unfortunately, stereo images for the whole study area could not be obtained due to the high percentage of cloud cover in the eastern part of the September image (path/row 644/340). Various false-colour images were made using different image enhancement techniques. The best image was obtained using the histogram of the unclouded area in a linear stretching and an edge enhancement of bands 2 and 3. In this image, taken 9 months after the Nevado del Ruiz eruption of November 1985, the deposits of the lahar flow through the Rio Claro Valley and the ash covered areas around the volcano can be observed clearly.

The SPOT stereo pair images were used together with a geological map to delineate faults and prepare the TMU map. For the eastern part, where no stereo SPOT was available, small-scale aerial photos (1:60,000) from 1966 were used instead. Three levels of complexity were distinguished: complexes, units, and subunits (see table 4.4), based on a series of factors used to distinguished mapping areas.

Level of complexity	Distinguishing factors
Terrain mapping complexes (TMCs)	- Main origin (denudational, volcanic, etc) - Climatic zonation - Altitudinal zonation - Overall geological setting (without formation names)
Terrain mapping units (TMUs)	- Lithology (possible only if geological map is available) - Overall geomorphological setting
Terrain mapping subunits (TMSs)	- Drainage density - Relative relief - Detailed geomorphological setting

Table 4.4: Hierarchical structure of the TMU legend and the factors used for each level.

Terrain mapping complexes (TMCs) give the most general subdivision of the terrain based on the main origin of each complex (i.e., denudational, volcanic, etc.) and the general climatic, altitudinal, and geological setting. TMCs present an association of TMUs with different lithological and morphological features, but with the same morphogenetic setting. Using this method, nine TMCs could be identified (see table 4.5 for legend), which are almost all oriented north-south, due to the fact that both the main geological groups and the altitudinal zones follow that trend.

Each TMC is divided into a number of TMUs, based on lithology. Although the legend structure is hierarchical, the same parameter was not always used at the various levels. Complexes 600, 700, and 800 are all underlaid by andesitic lavas, so subdivision into TMUs on the basis of lithology would be inappropriate. These complexes were instead subdivided into TMUs using the geomorphological setting as a basis.

At the third level, terrain mapping subunits (TMSs) were subdivided on the basis of relative relief and drainage density, except in areas where this would not reveal much insight, such as the terrace levels.

The classification factors mentioned above resulted in a total of 9 TMCs, 37 TMUs, and 117 TMSs. The TMCs are listed in table 4.5. The complete legend used to delineate the subunits is given in appendix 1. The code numbers of the units consist of three digits. The first digit refers to the TMC, the second to the TMU, and the third to the TMS. Figure 4.1 gives an example of a map with TMSs coded according to the legend given in appendix 1. The image of figure 4.1 was obtained by overlaying the digitized boundaries of the TMSs on an ortho-image. This ortho-image was constructed within ILWIS, using about 30 control points throughout the area and a DTM. The DTM was made by interpolation of digitized contour lines with a contour interval of 50 m. A pixel size of 20 m, equal to the spatial resolution of the SPOT XS data was chosen, resulting in a file of about 8 Mb. Figure 4.1

shows the western part of the study area, including the cities of Manizales (upper right) and Chinchina (lower centre). The Rio Claro is clearly visible due to the high reflectance values of the unvegetated lahar deposits. Terrain mapping complexes 100 to 500 can also be observed.

Although the use of aerial photos for landslide inventory at the regional scale is very time- consuming and usually inappropriate for a reconnaissance survey, it was nevertheless applied in this area. This was done to compare the results of a hazard analysis using mass movement data with one in which these data are lacking, and to evaluate the feasibility of using large- scale aerial photo interpretation in small sample areas in TMUs and extrapolating the results over larger regions. For this purpose a large number of recent aerial photos covering the entire study area at a scale of approximately 1:30,000 were interpreted using a very simple legend (see section 6.1.1).

Code	Description
100	Units of fluvio-glacial and fluvio-volcanic origin occurring in the main valleys throughout the area.
200	Units of denudational origin with thick mantles of unlithified materials (ash and residual soils) with small signs of recent uplift occurring in the western portion of the area at altitudes of 900 – 1300 m
300	Units of denudational structural origin subjected to intense recent uplifting and consisting of north/south-oriented valleys and ridges occurring in the Romeral fault zone, at altitudes of 1300 – 2200 m
400	Units of denudational structural origin consisting of plateau remnants with clear signs of recent uplifting occurring in the surroundings of Manizales at altitudes of 1700 – 2300 m
500	Units of denudational origin consisting of a uniformly dissected planation surface occurring east of the Romeral fault zone at altitudes of 2200 – 3000 m
600	Units of denudational origin consisting of rugged topography in lava flows occurring in the eastern part of the area at altitudes of 3000 – 3600 m
700	Units of glacial origin consisting of glacially eroded older lava flows occurring in the eastern part of the area at altitudes of 3600 – 4200 m
800	Units of glacial and volcanic origin consisting of glacially eroded younger lava flows occurring at altitudes of 4200 – 4800 m
900	Units of glacial origin consisting of glaciers and very recently deglaciated lava flows

Table 4.5: Legend of terrain mapping complexes

4.3.2 Image interpretation at the medium scale

As can be seen in table 4.1, interpretation of aerial photos is one of the major input sources at the medium scale. Data layers such as the landslide inventory, geomorphological map, engineering geological map, fault map, land-use map, and infrastructure map are all based on photo-interpretation with additional field checks. In this section the important aspects of photo interpretation for the collection of these data layers will be discussed.

4.3.2.1 Geomorphological interpretation

The most complex, and the most subjective, type of thematic photo-interpretation at the medium scale is geomorphological interpretation. The geomorphological map, however, plays an important role in many of the analytical techniques that will be treated in chapter 6. It is therefore important that this map be as realistic as possible. Additional comments on the objectivity of geomorphological mapping will be given in the chapter 7.

Figure 4.1: Examples of the use of satellite imagery (SPOT XS) for regional scale analysis. Above: overlay of terrain mapping subunits on a false-colour composite of a part of the study area. The code legend is given in appendix 1. Below: three-dimensional view of the Chinchina-Manizales area. Made by combination of a DTM and a SPOT satellite false-colour image

Many different geomorphological mapping systems have been proposed either for universal application or for specific areas (usually mountainous terrain). Overviews of conventional geomorphological mapping systems at medium and large scales are presented by Demek and Embleton (1978) and van Zuidam (1986). In common practice many different systems are being used. The conclusion can be drawn that there is no universally accepted system that is adequate for mapping in different environments, as is the case in soil sciences.

Comparisons of different systems have been presented by Gilewska (1976), Klimazewski (1982), Van Dorsser and Salomé (1983), Salomé and Van Dorsser (1982,1985) and Sumbukeni (1991). In contrast to the systems applied on the regional scale, which almost all involve outlining homogeneous units, the conventional geomorphological mapping systems for scales of 1:25,000 and larger are based on individual representation of features such as morphometry, morphography, drainage, genesis, chronology, materials, or processes with different symbols, lines, colours, and hatchings. The various mapping systems differ in the importance assigned to each feature and in the method of representation. They all have in common, however, that different types of geomorphological data are combined on one map sheet.

One example of such a mapping system has been developed for mountainous areas in the Alps by the Alpine Geomorphology Research Group at the University of Amsterdam (Rupke et al., 1987). The legend, shown in figure 4.2, can be used like building blocks: all symbols and line elements can be combined to characterize the terrain. Part of the study area around Chinchina, which was mapped according to this legend system, is shown in figure 4.3A. Other examples of maps made according to this legend were presented in chapter 3. The legend of figure 4.2 could not be followed completely in figure 4.3A, because some of the features present in the area (pyroclastic flow material, for example), were not represented in the original legend.

Figure 4.2: An example of a symbol-based legend structure for medium- and large-scale geomorphological mapping: the system of the Alpine Geomorphology Research Group of the University of Amsterdam.

Geomorphological maps based on such detailed legends can serve as excellent "geomorphological data bases", from which an experienced geomorphologist can extract a large amount of information for applied mapping, such as geotechnical maps or hazard maps (Seijmonsbergen, 1992). However, such data bases should be consulted only through the eyes and with the expert knowledge of the geomorphologist, and cannot be formalized in decision

rules applicable in a GIS. Symbol-based geomorphological mapping systems are unsuitable for use in a GIS for the following reasons:

1. A GIS requires information for each pixel in a raster structure, or for each polygon in a vector structure. Information for all parts of the terrain is required to avoid problems in analysis. Many of the conventional geomorphological systems do not display information for the whole terrain, but only for geomorphologically "interesting" parts. Other systems apply full coverage, but are based on lines, and the area between the lines is not coded but is instead interpreted by the geomorphologist based on the information from surrounding lines and symbols. Whenever colouring or hatching of areas is used, it applies only to one feature, such as morphometry (slope classes), morphogenesis or chronology. Thus, in conclusion: most maps are not uniform polygon maps.

2. Most conventional systems store different types of information on a single sheet, using different signatures such as symbols, lines, letters, numbers, colours, and hatching. In a GIS, each pixel or polygon in one data layer can contain only one type of information.

These problems should be avoided in a geomorphological mapping system developed for medium- or large-scale analysis with a GIS. To overcome these problems the basic information of a geomorphological map should be expressed in polygons, as in the terrain mapping unit approach at the regional scale. The legend should contain a combination of the various features of a geomorphological map, with morphogenesis as the main factor.

There is, however, an essential difference between the TMU approach and the geomorphological approach at large scales. A TMU is a homogeneous unit defined on the basis of lithology, morphogenesis, processes, and soils. The legend unit "denudational slopes", for example, would have to be divided into the same number of TMUs as there are lithological units in an area. This would result in far too many legend units for a geomorphological map. Moreover, the objective on the medium scale is to make separate maps for each of the individual parameters, and to analyze the importance of each parameter, either individually or in a multivariate approach.

To overcome the problem of too complicated legends the construction of separate maps for different geomorphological features is recommended. The following subdivision of data layers for the geomorphological information is suggested:

• *Morphometry*. Morphometric information in a GIS is provided by a DTM, which displays the elevation at the centre of each pixel. From this DTM, morphometric maps can be made displaying slope angle, slope aspect, and slope concavity/convexity, when appropriate calculation programs are available;

• *Drainage*. Drainage can be digitized separately in the form of line symbols;

• *Materials*. Materials can be stored in a map displaying the spatial distribution of material sequences;

• *Mass movement and erosional features*. These can be mapped separately as isolated polygons (mass movements), points (mass movements that are too small to represent at scale), or lines (rill and gullies);

• *Morphogenesis and morphography*. These can be combined in legend units and mapped as polygons;

• *Chronology*. Chronological information can be included by adding an extra column to the table of the units of morphogenesis and morphography. However, for applied geomorphological mapping, this feature is generally less important.

Figure 4.3: Comparison of a conventional symbol-based geomorphological map (A) based on a free interpretation of the legend of figure 4.2, and three different data layers used to represent this information in a GIS: (B) geomorphological units (see table 4.7 for legend); (C) geomorphological subunits (see table 4.8); and (D) denudational features (the legend is the combination of the column "type" and "subtype" in table 4.9). Some of the polygons in maps B, C and D were too small to show their coding. The area shown is situated around Chinchina.

Some of these data layers, such as materials and morphogenesis, may partly share boundaries. In conclusion it can be stated that the geomorphological map in the strict sense should be based on morphogenetic and morphographical aspects. All other aspects are mapped separately and are called DTM, slope map, slope direction map, drainage map, lithological map, or process map. When the term *geomorphological map* is used in the following sections, the strict sense is meant.

In figure 4.3 (B,C, and D), the conventional geomorphological map of figure 4.3A is subdivided into three data layers: main geomorphological units, geomorphological subunits, and denudational features.

During photo-interpretation, a legend structure for the geomorphological map has to be defined. It is useful to define various levels within the geomorphological map, analogous to the approach at the regional scale. Three such geomorphological levels have been distinguished (see table 4.6). The relationship between units at the different geomorphological levels and the landslide occurrence can be evaluated during subsequent analysis.

Geomorphological levels	Parameters used in the interpretation
Geomorphological complexes (GC)	- Morphogenesis
Geomorphological units (GU)	- Morphogenesis - Main landforms
Geomorphological subunits (GS)	- Morphogenesis - Detailed landform - Morphography

Table 4.6: Structure of the Geomorphological legend and the parameters used for each level.

Geomorphological complexes (GCs) represent the most general subdivision of the terrain that can be made on the basis of aerial photo interpretation. They are associations of geomorphological units with the same morphogenesis, for example a terrace landscape or a fault related terrain. They are not necessarily uniform in lithology. They can be compared with the terrain mapping complexes identified from satellite images, although they are mostly smaller in size. Geomorphological units (GUs) are units characterized by the same morphogenesis and landform types. They can be compared with land facets in the TRRL/MEXE system, or Terrain Units in the CSIRO and ITC systems. The legend used in the study area is given in table 4.7. Geomorphological subunit (GSs) are the smallest sections of the terrain that can be presented on a 1:25,000-scale map. A GS consists of one landform, for which the genesis, together with morphographical characteristics is given. The legend used in the study area is presented in table 4.8.

In constructing the legends, more emphasis was placed on dividing the terrain into units with potentially different severity of slope processes than on the pure scientific logic in the subdivision. This is comparable to the TMU approach at the regional scale. Subdivision of the terrain was not begun at the lowest level at the regional scale (Terrain Mapping Subunits) for the following reasons:

- This would have produced far too complex a subdivision of the legend. The legend for the TMSs at the regional scale already contained 127 different units (see appendix 1). Dividing these further would be unworkable;
- The parameters used in delineating TMCs, TMUs and TMSs (see table 4.4) are different

from those used for geomorphological mapping at the medium scale (see table 4.6). Lithology, which forms an important parameter in the TMU map, is not considered in the medium-scale geomorphological map.

- The regional-scale and medium-scale analyses are two different procedures, which normally are not sequential. Either a regional study or a medium-scale study is performed, depending on the scope of the project.

The geomorphological aerial photo interpretation of the study area was performed using recent 1:10,000- and 1:30,000-scale aerial photos. First, the geomorphological subunits were outlined, which was a very lengthy process. The boundary lines of the geomorphological units and complexes were chosen in such a way that they mostly coincided with the limits of the geomorphological subunits.

Nevertheless, when the legends of the geomorphological units (table 4.7) and the geomorphological subunits (table 4.8) are compared, it can be seen that the two sets of codes do not correspond. For example, geomorphological units 20-27 are fluvio-glacial units, while the same numbers for the subunits correspond to denudational hilltops, ridges, and horizontal slope sections. The geomorphological units and geomorphological subunits form two individual layers which are not related directly via their codes. This was done to prevent the construction of a very complex legend system. This is illustrated in figure 4.4. Consider, for example, a geomorphological unit with the code 52 (denudational slope). Within this unit there may be various subunits, such as hilltops (21-23), fluvial valleys (51-54), slope deposits (38), large mass movement and erosional features (61-65), and denudational slopes (31-37). If all these subunits should have to be made by subdividing the code of the geomorphological units, practically every code in table 4.7 would have to be combined with each subunit code listed in table 4.8, leading to hundreds of legend units. Basically the problem is related to the "homogeneity" of terrain units. This homogeneity is related to the generalization which is applied. If larger units are defined, generalization is larger, and the units are not as homogeneous as when smaller units are defined.

10. ALLUVIAL UNITS	50 DENUDATIONAL UNITS
11 Alluvial valley floor 12 Alluvial terraces	51 Denudational hilltops and flat areas 52 Denudational slopes 53 Denudational niches
20. FLUVIOGLACIAL/FLUVIOVOLCANIC UNITS	54 Denudational hills 55 Colluvial slopes
21 Terrace level 1 22 Terrace level 2	56 Large landslide or erosional area
23 Terrace level 3 24 Terrace level 4	60 DENUDATIONAL STRUCTURAL UNITS
25 Terrace slope 26 Abandoned meander	61 Fault scarp 62 Fault related denudational slopes
27 Terrace covered by colluvial material	63 Fault related denudational niches 64 Fault related denudational hills
30. FLUVIO-VOLCANIC UNITS ON STRUCTURAL PLATEAU	65 Fault related large landslide 66 Lith. differences in denudational slopes
OF MANIZALES	67 Lith. differences in denudational niches
31 Plateau 32 Plateau remnants on lower altitudes	68 Lith. differences in denudational hills
	70 ANTHROPOGENIC UNITS
40. VOLCANIC UNITS	71 Levelled area
41 Pyroclastic flow terrace level 42 Pyroclastic flow terrace slope 43 Dome	72 Filled up area 73 Reservoir

Table 4.7: Legend used for the delineation of geomorphological units.

```
10 ALLUVIAL, FLUVIO-GLACIAL, AND FLUVIO-VOLCANIC
   UNITS
   Floodplain:
      11 Frequently inundated
      12 Not inundated
   Terrace level
      13 Flat
      14 Undulating
      15 Sloping
      16 With colluvial and or alluvial cover
   Alluvial fan
      17 Active
      18 Not active

20 DENUDATIONAL HILLTOPS, RIDGES, AND (SUB-)
   HORIZONTAL SLOPE SECTIONS
   Hilltops
      21 Wide and predominantly flat
      22 Moderately wide and rounded
      23 Narrow and sloping
   Ridges
      24 Wide and predominantly flat
      25 Moderately wide and rounded
      26 Narrow and sloping
   (Sub-) horizontal slope sections
      27 With colluvial cover
      28 Without colluvial cover

30 SLOPES WITH LESS ACTIVE DENUDATIONAL
   PROCESSES AND COLLUVIAL SLOPES
      31 Straight and short slopes
      32 Straight and long slopes
      33 Convex and short slopes
      34 Convex and long slopes
      35 Concave and short slopes
      36 Concave and long slopes
      37 Vertical slopes
      38 Footslopes with colluvial cover

40 DENUDATIONAL NICHES
      41 Length <= width with straight slope
      42 Length <= width with convex slopes
      43 Length <= width with concave slopes
      44 Length > width with straight slopes
      45 Lenght > width with convex slopes
      46 Lenght > width with concave slopes
```

```
50 MAINLY FLUVIAL VALLEYS
      51 Deep with V-shaped cross-section
      52 Deep with U-shaped cross-section
      53 Shallow with V-shaped cross-section
      54 Shallow with U-shaped cross-section

60 LARGE MASS MOVEMENT OR EROSIONAL AREAS
      61 Large backscarp
      62 Large landslide
      63 Large flow
      64 Large flowslide
      65 Large erosional area

70 DENUDATIONAL STRUCTURAL NICHES AND RIDGES
   Ridges
      71 Related to lithological changes
      72 Related to fault
   Niches
      74 Length <= width, lithologically rel.
      75 Length > width, lithologically rel.
      76 Irregular, lithologically related
      77 Length <= width, fault controlled
      78 Length > width, fault controlled
      79 Irregular, fault controlled

80 DENUDATIONAL STRUCTURAL SLOPES
      81 Dip slope
      82 Face slope
      83 Fault scarp
      84 Triangular facet

90 ANTHROPOGENIC LANDFORMS
      90 Levelled hilltops
      91 Levelled slopes
      92 Levelled ridges
      93 Levelled denudational niche
      94 In-filled valley
      95 Hydraulic fill
      96 Material dump on slope
      97 Cut slope
      98 Stabilized slope
      99 Quarry
```

Table 4.8: Legend for the geomorphological subunits.
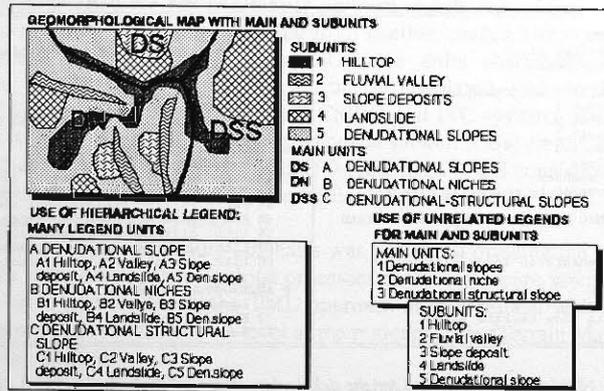
Figure 4.4: Example of geomorphological units, containing many different geomorphological subunits, with two different legend structures. Left: hierarchical structure, leading to a large number of legend codes. Right: individual legend codes for units and subunits, leading to less legend codes.

4.3.2.2 Mass movement inventory

The mass movement occurrence map is crucial in the analysis, since it is based on the assumption that the conditions under which failure took place in the recent past will be comparable to those that will cause landslides in the near future. Therefore, the accuracy of this map should be high, both in the correct location and correct classification of slope instability phenomena. Many different systems have been proposed for classifying slope movements, such as Sharpe (1938), Zarúba and Menčl (1969), Nemčok et al (1972), Crozier (1973), Coates (1977), Varnes (1978), and Hutchinson (1988). An overview is given by M.J. Hansen (1984). As shown in the literature (Fookes et al., 1991; Carrara et al., 1992), both the exact positioning and the classification of mass movements have a rather subjective element in photo-interpretation and they may vary considerably among interpreters. The errors occurring from this subjectivity will be evaluated in more detail in chapter 7.

Aerial photo interpretation of mass movements in tropical regions with intensive agricultural land use is faced with more difficulties, such as:

- Mass movements are masked very soon after their occurrence by the abundant growth of vegetation. After a few years it may be extremely difficult to identify mass movement, and even more difficult to describe the type and degree of activity.
- Mass movements which occur in agricultural and densely populated areas are immediately modified by man and become invisible.
- The major landscape-building process in a denudational area is mass movement, and thus the entire area is covered by vague scarps and slope convexities and concavities which are indications for old mass movements. However, "old" can mean hundreds or thousands of years, or it can mean years or decades. This illustrates the general difficulty in interpreting ages and activities of mass movements.

It should be stressed that for an accurate aerial photo inventory of landslides in tropical regions, a thorough understanding of the field conditions is indispensable.

In the process of photo-interpretation of mass movements, the use of a photo-checklist is highly recommended. It forces the interpreter to use clear guidelines for the identification and description of mass movements, resulting in a more objective map. It allows also for a posterior reclassification, based on the features included used in the check-list for each landslide. An example check-list is given in table 4.9. For each mass movement, the features from the list can be written in a table or directly on the transparent photo-interpretation sheet, together with a unique code for the landslide.

Originally a much more detailed checklist was used, including factors on dimensions, possible causes, observed damage, etc. However, using such an elaborate checklist proved to be impractical as it was too time-consuming to shift repeatedly from the stereoscope to a writing table for a detailed description of each mass movement, and because many of the features were difficult to determine from aerial photos.

In determining landslide type from aerial photo interpretation, we considered using a comprehensive classification system, such as that of Hutchinson (1988). The problem with complex systems is that they require data on many features that cannot be interpreted from aerial photos, such as the exact movement mechanism, the speed of the movement or the material in which the movement took place. It was decided instead to base the classification completely on the information that could be extracted from aerial photos. Therefore, a simplified version of the Varnes (1978) classification (shown in table 4.9) was used.

	TYPE	SUBTYPE	ACTIVITY	DEPTH	VEGETATION	SCARP-BODY
1	Slide	Rotational	Stable	Shallow	Bare	Scarp
2	Flowslide	Translational	Dormant	Deep	Low vegetation	Body
3	Flow	Complex	Active		High vegetation	
4	Derrumbe					
5	Creep					

Table 4.9: Example checklist used in photo-interpretation of mass movements. See text for explanation.

After this fieldsurvey the mass movement type *derrumbe* was included in the classification. Derrumbe is the local Spanish word for soil avalanches: a very fast, shallow, mostly translational failure, during which the material is transported to the nearest stream or blocking object. The material involved is mostly volcanic ash, but it can also be residual soil or terrace deposits.

The five types were defined on the basis of the following photomorphic properties:
1. *Slide*: scarp and more or less intact body;
2. *Flowslide*: scarp, and body with sliding blocks in the upper section, developing into a flow lobe in the lower part;
3. *Flow*: scarp may be unclear, and the body is completely in the form of a flow lobe;
4. *Derrumbe*: clearly definable source area on steep slopes and no body visible;
5. *Creep*: only detectable from terracettes in the slope produced by cattle in grassy vegetation.

The subtypes defined in table 4.9 can be differentiated as follows:
1. *Rotational*: circular source area with steplike morphology of the body;
2. *Translational*: straight source area;
3. *Complex*: combination of the two.

The degrees of activity given in table 4.9 represent more accurately degrees of "freshness" of the mass movement, as it is often very difficult to separate "activity" from "relative age". The following criteria were used:
1. *Stable*: the feature is recognizable as a mass movement, by its form, the presence of a scarp, hummocky terrain or deviation in the drainage pattern. The scarp is not clear and the mass movement is covered with high vegetation. Due to its geomorphological setting the movement is not expected to be reactivated by normal triggering events. It is difficult to evaluate what their behaviour will be under extreme earthquake accelerations, so this has not been taken into account.
2. *Dormant*: the feature is clearly recognizable, but covered with high vegetation. Due to its geomorphological setting a reactivation by triggering event cannot be excluded.
3. *Active*: the feature is clearly recognizable and shows clear signs of activity, mostly detectable by a lack of vegetation cover.

For the division of depth into superficial or deep, a "deep" mass movement was defined as one with a depth of more than 5 m. Three vegetation classes were used: bare, low vegetation without trees, and high vegetation including trees. Scarps and bodies were identified and mapped separately, as long as the size of the phenomenon in relation to the map scale permitted it. After describing a mass movement with the above mentioned features, a unique identifier was assigned to each outlined unit. The identifier consists of a sequential

number, followed by a six-digit code, composed of the values from the checklist. For example, 320-123111 represents mass movement number 320, which is a scarp of an active, shallow, translational slide without vegetation.

Evaluating landslide activity in more detail than can be done by interpreting photos from one point in time requires multitemporal aerial photo interpretation. Information on newly formed or reactivated mass movements can be obtained by interpreting photos from two, or more, different time periods. The time interval chosen depends to a large degree on the availability of aerial photos, on the available time for photo-interpretation and on the expected relationships between land-use changes and landslides. In this study, a timeperiod of two decades was used.

Multitemporal photo-interpretation should be done by the same person, starting with the most recent set of photos and proceeding with older sets. This way inconsistencies in interpretation between different maps can be avoided. However, the process is very time-consuming, and one often has to change from one set of photos to another to compare the different situations. The importance of this multitemporal interpretation is to identify those mass movements that have appeared anew or that have increased in activity between the two dates. Two important factors should be borne in mind, however:
1. If land-use changes have taken place between the two dates, it may be difficult to distinguish between new mass movements that have occurred and previously existing mass movements that are more easily detected due to a decrease in vegetation cover.
2. Differences in quality and scale between the photos from different years may cause errors when long existing mass movements visible on recent, large-scale photos, are not seen on old photos due to poor quality.

For the multitemporal photo-interpretation, three sets of photos with scales ranging from 1:10,000 to 1:30,000 with a time lapse of about 20 years were used; these will be referred to later as the 1940s, 1960s and 1980s photos.

Initially, a detailed inventory was made using the most recent, 1:10.000-scale photos. These allowed much better identification of the locations, types, and activities of mass movements than the recent 1:25,000-scale photos. The photos from the 1940s are of very poor quality. Nevertheless, they proved useful in identifying contemporary mass movements that were not interpreted even as "dormant" or "stable" from the newer sets. Two examples of the usefulness of multitemporal photo-interpretation are given in figure 4.6. These photos reveal considerable changes in mass movement activity and size between two times for both areas. The upper two aerial photos from 1940 and 1960 show the site called La Siria, along the main-road between Manizales and Chinchina. Here a large landslide/erosional area has occurred since the 1960s. This feature was caused by inadequate drainage of the road along a steep slope underlaid by disintegrated black shale in a fault zone. No landslide is visible at this location on the 1940s photo. However, a similar problem occurred further west in a zone where no activity is visible in later photos. The area displayed in the lower two photos of figure 4.6 is located several kilometres northeast of the former area in a steep, fault-related valley. Land-use changes during the last decades have caused enormously accelerated erosion, triggering landsliding on the upper parts of the slope.

4.3.2.3 Interpretation of drainage network

For a thorough analysis of the relationship between mass movements and drainage patterns, the drainage information displayed on a 1:25,000-scale topographic map is usually insufficient. Often additional photo-interpretation is required to obtain a consistent drainage network. Drainage lines in the study area were interpreted from 1:10,000-scale aerial photos and drawn on a transparent sheet overlying the topographic map and the geomorphological subunit map to ensure that the drainage lines coincided with the valleys interpreted in the geomorphological analysis. In this way an extra length of 169 km of drainage lines was recognized. Of the total length of drainage lines, 54% was not represented in the topographical map. Figure 4.5 displays the drainage network derived from the topographic map and from the additional photo-interpretation.
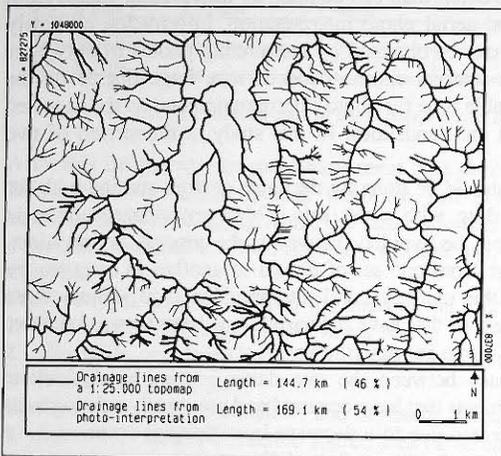
Figure 4.5: Importance of photo-interpretation for delineating the full drainage network.

4.3.2.4 Land-use interpretation

It is important that the mass movement activity analysis done by multitemporal aerial photo-interpretation is accompanied by a sequential interpretation of land use and infrastructure, in order evaluate the relationship between changes in mass movement activity and land-use changes. The legend used for land-use interpretation will obviously differ for each region, depending on the crops present in the area. Also during a prior field survey observations should be made to identify those land-use types most related to the occurrence of landslides. In photo-interpretation of infrastructure, a clear distinction should be made between major roads or railways where the construction required large cuts and fills, and those which did not influence the topography significantly.

For this study area, with about 80 percent of the area under coffee cultivation, it was important to monitor the changes in the different systems of coffee cultivation, since a introduction of the "technified coffee" farming system on steep slopes might be associated with an increase in mass movement activity.

The following main land-use types were delineated (v. Duren, 1992):

- Natural forest,
- Secondary forest,
- Mixed forest, shrubs, and grass,
- Traditional coffee cultivation, with shadow trees and low density of coffee plants,
- "Technified" coffee cultivation, with few shadow trees and high density of coffee plants,
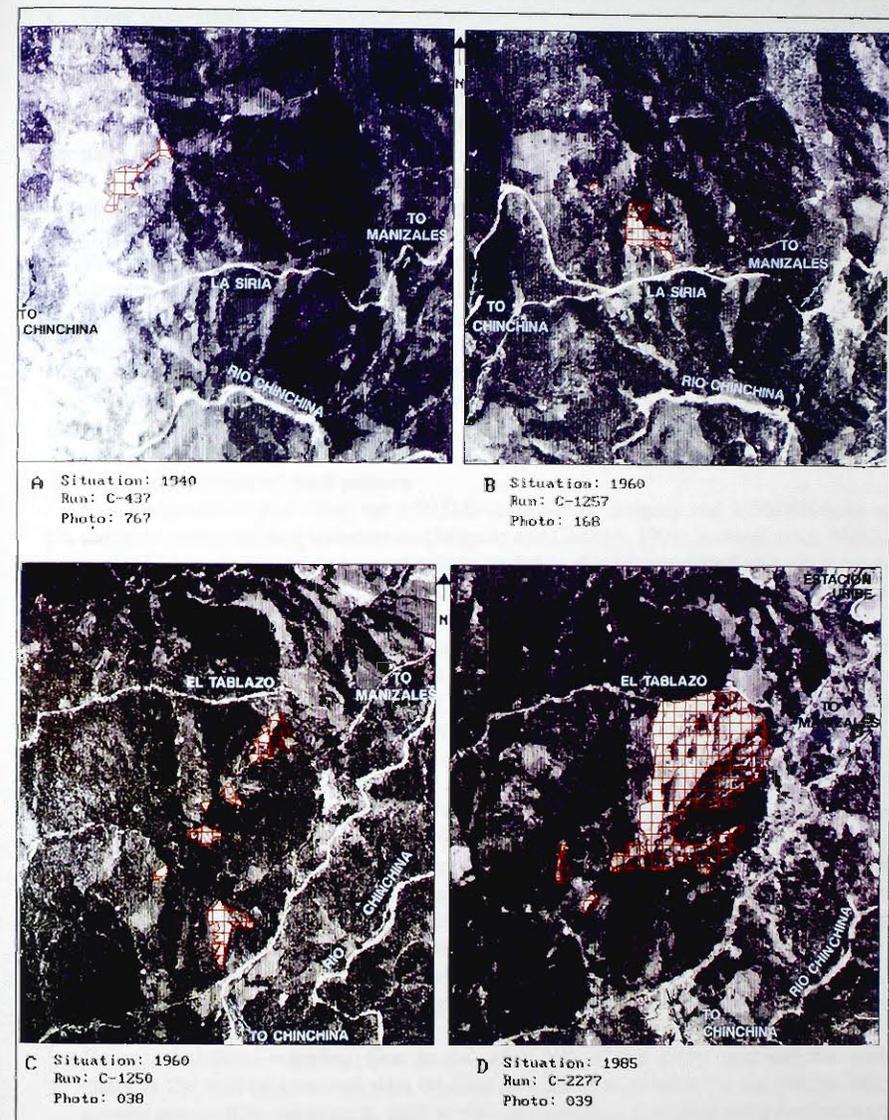
Figure 4.6: Two examples of multitemporal aerial photo-interpretation. The upper two show the area denoted as La Siria, on the Panamerican road between Manizales and Pereira. The lower ones show the area El Tablazo, southwest of Manizales.

- "Technified" coffee cultivation without shadow trees and with high coffee plant density,
- Other cultivation,
- Grassland,
- Bare land.

Excellent land-use information from the 1980s is available for the municipalities of Chinchina, Palestina, and Manizales on 1:10,000-scale maps, on which land use is indicated per parcel (Federación Nacional de Cafeteros de Colombia, 1985). The land use of part of the study area in the municipality of Villamaria was obtained by photo-interpretation.

In addition, land-use maps for the entire area for the 1960s and 1940s have been derived from aerial photos (van Duren, 1992).

The infrastructure also had to be mapped by photo-interpretation, because the most recent topographic map dates from 1970. Distinction was made between (a) main roads connecting municipalities, (b) secondary connecting roads (mostly non-paved), and (c) local roads to provide access to farms, (d) railway lines, (e) pipelines and channels for a hydroelectrical station, (f) poles of high-power electrical lines, and (g) town boundaries. Isolated farm houses were also mapped, although most of these were already present on the 1:10,000 scale land-use maps.

4.3.2.5 Interpretation of fault pattern

Faults were delineated using the 1:50,000-scale SPOT imagery and 1:30,000-scale aerial photographs, using existing information (Salgado and Chacon, 1991; Navarro et al, 1988). The stereo SPOT images proved to be particularly useful in this interpretation as a good overview could be obtained to interpret the continuous fault lines in the region. A distinction was made between *faults*, clearly recognizable on the imagery and mentioned in the existing maps and reports, and *lineaments*, that are not clear in the images. Unfortunately it was difficult to obtain field verification of the interpreted faults, since most of the outcrops where faults are suspected are difficult to check due to the almost continuous cover of volcanic ash, the thick weathering zone, and the dense vegetation cover.

4.3.3 Image interpretation at the large scale

Photo-interpretation at the large scale consumes less time than at the medium or regional scale (as shown previously in table 2.5) for the following reasons:

1. The area for large-scale studies is usually much smaller than for the other scales, and is often no more than some tens of square kilometres.
2. Collection of detailed borehole information and of geotechnical data is much more important aspect than image interpretation at this scale.

The photo-interpretation methods applied at the large scale are almost identical to those at the medium scale. The following paragraphs outline the minor deviations required for the large-scale analysis:

- *Geomorphological mapping*. Due to the small size of the study area and the types of analysis that will be executed with the data sets, there is no need for the interpretation of general geomorphological units, such as geomorphological complexes or geomorphological units. Interpretation is done only at the subunit level. These subunits are generally much smaller than those outlined in medium-scale mapping.
- *Mass movement inventory*. Interpretation of mass movements has to be executed with

more precision than at the medium scale. At the large scale (with map scales of 1:10,000 to 1:5,000), all mass movements can be outlined at scale, with clear differentiation of scarp and body area. At this scale it becomes important to map changes in the extent of landslides over time, which is not very possible at the medium scale.

- *Drainage.* For analysis of the drainage system in an urban area such as Manizales, the human impact on the drainage network is important. Many drainage lines have been trained, or even led underground into culverts. Therefore, photo-interpretation must be augmented by maps, for example, of the sewage system of the city.
- *Land use and infrastructure.* In an urban environment much emphasis should be given to the urban infrastructure. The detailed outlines of the city were therefore carefully mapped from aerial photos and existing maps.
- *Fault mapping.* Fault mapping from aerial photos in an urban environment proved to be very difficult, since almost all features are masked by the large man-made earth movements that have been carried out. For this purpose, old photos from the 1940s were used, when the city was much smaller.

4.4 Field techniques

Although fieldwork takes only a small portion of the total time needed for an assessment of landslide hazard (5 to 20% was shown in table 2.5), it is one of the most important phases. Only through thorough fieldwork can the researcher obtain an impression of the real- world situation, i.e., of the various factors that are really important in the analysis. It is therefore advisable to include more than one period of fieldwork. The first consists of a walk- over survey, during which decisions are made on the variables to be sampled and the legends to be used for the various maps. Also in the first phase collection of existing data should take place. The second field-visit should be used for data collection, and should be executed after image interpretation. The major part of data base design should be finished before the second field period so that the data obtained in the field can be entered quickly in the data base.

In this section the data to be collected during fieldstudies for each of the three scales will be discussed and examples of results will be given for the Chinchina study area.

4.4.1 Fieldwork at the regional scale

Since the area in a regional investigation is so large, it is not practicable to obtain a sufficient number of quantitative data for a detailed characterization of the various terrain units. Therefore, no systematic quantitative data collection is suggested for the regional scale, and fieldwork will serve merely as a walk-over survey to compare the interpreted terrain mapping units with the actual field situation.

In this study, I initially planned to use checklists to collect semi-quantitative data for each TMU, using variables such as the percentage of TMUs or TMSs covered by certain land-use, landslide, or soil types. During the initial field visit to the Rio Chinchina area, however, I decided not to use this method because it is very difficult to estimate in the field percentages of cover in large terrain units in a mountainous area with dense vegetation cover. No good overview of a TMU or TMS can be obtained from groundlevel. Any attempt to do so would result in pure guesswork, or at best be excessively time-consuming. One possible solution would be to use aerial photos or satellite imagery to select a number of sample areas in each TMU or TMS and make more detailed observations only in those areas. This method was not

workable either, since the area was too heterogeneous, with too many different TMSs, to allow sampling in all of them. For these reasons I decided not to collect any (semi)-quantitative field data. Instead, the area was traversed by car, or by foot in the higher regions, where no passable roads exist with the following objectives:
- To obtain photographs of characteristic areas to be used later in final production of the TMU map;
- To make simple field descriptions of the various TMUs and TMSs;
- To make a general mass movement inventory, with special attention given to the types and frequency of mass movements occurring in the various TMSs;
- To obtain information to be used in designing the various map legends for the medium scale analyses.

4.4.2 Fieldwork at the medium scale

Fieldwork at the medium scale is executed for the following two purposes:
- To field-check photo-interpretation maps;
- To collect (semi)-quantitative data.

Two methods of data collection can be applied:
1. Using hard-copy checklists for the various types of observations, which are designed in accordance with the data base structure, and entering data into the data base at the field residence using a laptop computer;
2. Entering data directly when collecting in the field using small, hand-held, inexpensive field computers. In the department of soil surveys at ITC this is already common practice, using a SHARP 1500A hand-held computer (Elbersen and Catalan, 1986).

Both methods allow the consistency of the collected data to be checked during the fieldwork period itself, and provide an opportunity to identify gaps in the data that still need to be filled. This allows observation points with abnormal, suspect or missing values to be revisited for verification. Both methods have advantages and disadvantages. The first method allows extra information, such as field sketches, to be added on the back of the checklist, but the disadvantage is that parts of the checklist can be overlooked or values outside of the possible range can be entered. In the second method, the computer program can check immediately whether all data have been entered correctly, and it can warn when values are added that are outside the possible range (for example, a total of grain-size estimations that exceed 100%). The disadvantage of the second method is that all data become "impersonal", just numbers in a data base, which may make it difficult during data analysis for the researcher to remember details of the field situation.

In the Chinchina area both methods of data collection were applied. Initially a hand-held computer was used (ATARI Portfolio), which employs 64-Kb memory cards and which has a built-in LOTUS-compatible spreadsheet. However, due to problems with the interface for sending data to a personal computer, this method had to be abandoned. Subsequent data were entered in field checklists. Unfortunately, no laptop computer was available in the field so the data could only be aggregated later.

An overview of the field techniques used in landslide hazard mapping is given by Sowers and Royster (1978), Selby (1982), and Dackombe and Gardiner (1983).

4.4.2.1 Geomorphological fieldwork

A simple checklist, prepared before commencing the fieldwork, can be used to check the geomorphological photo-interpretation. The list contains points of uncertainty arising during photo-interpretation that can be checked systematically in the field. Example formats for the sheet are given in appendix 2. The points entered in the list coincide with points marked on the photo-interpretation sheets. During geomorphological fieldwork, a second list (appendix 2) can be used to collect relevant morphographic point information, including factors such as slope length and concavity-convexity. This information may serve as a quantitative basis for the interpreted geomorphological subunits. It may also be useful to obtain more information on slope angle values at various locations in the terrain in order to check the digital slope map and, if necessary, update it.

4.4.2.2 Collection of mass movement data

In addition to checking photo-interpretation of mass movements, fieldwork was aimed at collection of more detailed data about mass movements. These data were collected using a checklist, designed in accordance with the data base structure. Nowadays the use of checklists in landslide analysis is quite common, especially for studies based on computer applications. Extensive landslide checklists were used by Carrara and Merenda (1974) and by Neuland (1976) for multivariate statistical analysis. Presently a very extensive checklist for landslide description is used by the Italian National Research Council (CNR). The French Geological Survey (BRGM) uses a landslide checklist for the development of a national landslide data base (Asté et al., 1990). Simple landslide checklists have even been used to create a global data base on landslides (Cruden and Brown, 1992). The National Landslide Information Center of the U.S. Geological Survey works at a national scale for the United States (Brown, 1992). Baez et al. (1988) used a checklist in a national investigation on landslides for the Colombian road network, and used descriptive statistics to analyze the important parameters involved. Simple checklists are also used in the direct geomorphological hazard mapping presented by Kienholz (1977, 1978).

In the ideal case, mass movements to be described should be selected during the photo-interpretation phase using a random sampling process, but in such a way that for each mass movement type a sufficient number is selected. Unfortunately, this procedure could not be followed since photo-interpretation was not yet completed at the time of the fieldwork.

The checklist designed for this study, and an accompanying explanation table are given in appendices 3 and 4. An overview of the most important variables is presented in table 4.10. Most of the variables selected for description are relatively simple to evaluate or measure, and were selected in order to minimize guesswork and reduce the time needed for filling in the list. Two variables, however, are difficult to assess: the landslide depth and the main cause of failure.

For each mass movement, one line in the landslide sheet should be filled in. For some variables, the value 0 may be entered, if the variable cannot be determined. When doubt exists about a value, the user may enter a question mark behind the code. For some variables (MAINCAUSE, STABIL, DAMAGE, VULNER, and LANDUSE) more than one answer is possible. In that case, the predominant class should be entered fist. If there is a soil outcrop visible in the landslide scarp, a soil profile should be taken using the method described in section 4.4.2.3.

The landslide checklists were used in the study area by different persons (Koopmanschap, 1992; Niehaus, 1992; Mool, 1992), leading to some problems in data consistency (see section 7.3.5).

SLOPE INFORMATION

SLOPEUP Slope length up	SLODOWN Slope length down	SLOPROF Slope in profile	SLOPLAN Slope in plan
1 0 - 50 m	1 0 - 50 m	1 Straight	1 Straight
2 50 - 100 m	2 50 - 100 m	2 Concave	2 Concave
3 100- 500 m	3 100- 500 m	3 Convex	3 Convex
4 >500 m	4 >500 m		

GENERAL LANDSLIDE INFORMATION

TYPE Landslide type	SUBTYPE Landslide subtype	MECHANIS Movement mechanism	ACTIVITY Activity	LSDEPTH, LSLENGTH, LSWIDTH Dimensions of the feature
1 Slide	1 Rotational	1 Fast/single	1 Stable	Landslide depth in m
2 Flowslide	2 Translational	2 Slow/single	2 Dormant	Landslide length in m
3 Flow	3 Complex	3 Fast/various	3 Active	Landslide width in m
4 "Derrumbe"		4 Slow/various		
5 Creep		5 Contin./slow		
		6 Discont./slow		

CAUSES

MAINCAUS (Inferred causes)

0 Unknown	6 Deforestation	12 Faultzone	
1 Stream erosion	7 Coffee change	13 Earthquake	
2 Road undercutting	8 Natural water entry	14 Slope	
3 Building undercutting	9 Artificial water entry	15 Rainfall	
4 Loading by fill	10 Permeability change		
5 Loading by construction	11 Slope // discontinuity		

DAMAGE, STABILIZATION, AND ELEMENTS AT RISK

DAMAGE Observed damage	STABIL Stabilization measures	VULNER Elements at risk	LAND USE Land use before failure	
0 No damage	0 No measures	0 Nothing	1 Bare	11 Residential
1 Main road	1 Artificial drainage	1 Main road	2 Grassland	12 Industrial
2 Local road	2 Retaining wall	2 Local road	3 Shrubs	13 Road
3 Crops	3 Terraced slope	3 Crops	4 Trees	
4 Grassland	4 Slope flattening	4 Grassland	5 Mix grass/shrubs/trees	
5 Forest/shrubs	5 Check-dams	5 Forest	6 Young coffee, no trees	
6 Farm area	6 Reforestation	6 Farm area	7 Old coffee, no trees	
7 Residential	7 Other measures	7 Residential	8 Young coffee with trees	
8 Industrial		8 Industrial	9 Old coffee with trees	
9 Stream		9 Stream	10 Farm area	

INFORMATION ON SCARP AREA

SCARPSTAT State of scarp	SCARPVEG Scarp vegetation	SCARPFORM	SCARPAREA (in m²)	WATEROUT Seepage
0 No scarp	0 No scarp	0 No scarp	0 No scarp	0 No seepage
1 Clear	1 Bare	1 Circular	1 Small (< 200m²)	1 Seepage
2 Vague	2 Low vegetation	2 Elongated	2 Medium (200 - 500)	
	3 High vegetation		3 Large (> 500)	

INFORMATION ON BODY AREA

BODYSTAT State of body	BODYFORM	BODYAREA (in m²)	BODYVEG Body vegetation	BODYHYD Water content
1 Intact	0 No body	0 No body	0 No body	0 No body
2 Disintegrated	1 Length=width	1 Small (< 500m²)	1 Bare	1 Dry
3 Flow lobes	2 Length>width	2 Medium (500 - 2500)	2 Low vegetation	2 Wet zones
4 Not present	3 Length<width	3 Large (> 2500)	3 High vegetation	3 Saturated

Table 4.10: Overview of variable classes for the landslide checklist.

4.4.2.3 Soil observation sheet

Besides geomorphological mapping and description of the mass movements, fieldwork at the medium scale is designed to collect data for the preparation of an engineering geological map. The map itself is made by combining several maps within the GIS (see section 5.4.4.2.) During fieldwork, data are collected to characterize various soil and rock materials outlined on the map.

Soil observations in the field focused on the following aspects:
- Collection of data on material sequences via profile descriptions,
- Description of the different material types with a number of simple variables.

The method for soil description is based on the procedures developed at ITC for large-scale engineering geological mapping (Rengers et al., 1990). Prior to the second fieldwork period, a list of all materials occurring in the Chinchina area was prepared. This list was based on geomorphological photo-interpretation, existing geological maps and reports, and the general overview of the area obtained during the first walk-over field survey. The list is given in table 4.11. In the medium-scale study area, all of the material types are not equally important. This is reflected in the number of observation points visited for each material type.

The list in table 4.11 contains all material types, including rocks and soils. The different rock types are grouped according to their origin (sedimentary, metamorphic, etc.) and classified as residual soil, weathered rock, and fresh rock. The base of weathering grade IV (above which more than 50% of the rock is decomposed and/or disintegrated into soil) is taken as the limit between soil and rock (Anonymous, 1990). The transported soils were divided into anthropogenic soils, fluvio-volcanic soils, debris flow materials, pyroclastic soils (ash) and a miscellaneous group including alluvial, fluvio-glacial, and glacial materials. The pyroclastic soils are divided into fine grained, sandy, and coarse sandy. For the transported soils, a subdivision between weathered and unweathered was defined initially, but this was abandoned later due to the lack of clear differentiating criteria both in the field and in the laboratory.

For the soil observations, a checklist was designed in accordance with the data base structure. An overview of the variables is given in table 4.12, and an explanation of the classes is presented in table 4.13. The checklist itself is given in appendix 5. The variables for field description of soils are described in Anonymous (1990), Selby (1982), Dackombe and Gardiner (1983), Cooke and Doornkamp (1990). Most of these data are obtained by direct measurement or observation. Others, such as permeability or grain size percentage were obtained by estimation. These field estimations proved to be very difficult, and differed greatly from the values measured in the laboratory (see also section 7.3.5). In the checklist proposed here not all the parameters suggested previously (Anonymous, 1990), were used, because some were too detailed for general characterization or too difficult to estimate in the field. Some of the parameters, such as bulk density, plasticity, porosity, grain-size distribution, and mineralogy, were therefore tested in the laboratory on a limited number of samples (see section 4.5).

For each soil outcrop, a separate soil observation sheet was filled in. The first step in soil description is to divide the soil outcrop into a number of different layers. Each layer is assigned a unique identifier, entered as LN (layer number) in the checklist, starting from the top of the profile. For each layer, the depth (in cm) below the terrain surface of the top and the bottom of the layer were entered into the columns TOP and BOTTOM, and the

descriptive parameters were filled in. Pocket penetrometer and shear vane test results were made if the soil material allowed it. In outcrops with coarse materials, grain-size estimations of the coarser fraction were performed by line counting, on which the percentage cobbles and boulders on a scanline of 10 m was measured.

CODE	MATERIAL TYPE	CODE	MATERIAL TYPE
100	PYROCLASTIC MATERIALS	700	INTRUSIVE ROCKS
110	FINE GRAINED	710	PORPHYRITIC ANDESITE (Tadp)
111	- Unweathered	711	- Residual soil
112	- Weathered	712	- Weathered rock
120	SANDY	713	- Fresh rock
121	- Unweathered	720	QUARTZDIORITE/GABBRO (Ktcdm)
122	- Weathered	721	- Residual soil
130	COARSE SAND/FINE GRAVEL	722	- Weathered rock
131	- Unweathered	723	- Fresh rock
132	- Weathered	730	METAMORPHIC GABRO (Kdg)
		731	- Residual soil
		732	- Weathered rock
		733	- Fresh rock
200	ALLUVIAL/FLUVIOGLACIAL/GLACIAL/ MISCELLANEOUS	800	METAMORPHIC ROCKS
210	RECENT ALLUVIAL MATERIAL	810	METAMORPHIC INTRUSIVE (Inch)
220	Alluvial terrace material	811	- Residual soil
221	- Unweathered	812	- Weathered rock
222	- Weathered	813	- Fresh rock
230	TILL	820	PALEOZOIC SCHIST (Pe)
231	- Unweathered	821	- Residual soil
232	- Weathered	822	- Weathered rock
240	BURIED SOILS	823	- Fresh rock
250	LACUSTRINE SEDIMENTS	830	CRETACEOUS SCHIST (Kclp-Kap)
		831	- Residual soil
		832	- Weathered rock
		833	- Fresh rock
300	FLUVIO-VOLCANIC	900	META-SEDIMENTARY ROCKS WITH VOLCANIC INCLUSIONS
310	DEBRIS FLOW MATERIAL		
311	- Unweathered	910	BLACK SHALES AND SCHISTS
312	- Weathered	911	- Residual soil
313	- Cemented	912	- Weathered rock
314	- Recent lahar material	913	- Fresh rock
320	PYROCLASTIC FLOW MATERIAL	920	CHERTS, GRAUWACKES, SANDSTONES, CONGLOMERATES, etc. (Kis)
321	- Unweathered		
322	- Weathered	921	- Residual soil
323	- Cemented	922	- Weathered rock
400	SLOPE DEPOSITS	923	- Fresh rock
410	PREDOMINANTLY FINE GRAINED	930	LAVA INCLUSIONS (Kd)
420	PREDOMINANTLY SANDY	931	- Residual soil
430	PREDOMINANTLY COARSE	932	- Weathered rock
		933	- Fresh rock
500	ANTHROPOGENIC SOILS	1000	SEDIMENTARY ROCKS
510	ROAD FILL	1010	TERTIARY SEDIMENTS IN WEST (Toi)
520	URBAN LAND FILL	1011	- Residual soil
530	SANITARY FILL	1012	- Weathered rock
600	EXTRUSIVE ROCKS	1013	- Fresh rock
610	ANDESITIC LAVAS	1020	FLUVIO-VOLCANIC/VOLC/ALLUVIAL: MANIZALES FORMATION (Tm)
611	- Residual soil		
612	- Weathered rock	1021	- Residual soil
613	- Fresh rock	1022	- Weathered rock
620	BLOCK LAVA	1023	- Fresh rock
621	- Residual soil	1030	FLUVIO-VOLCANIC/VOLC/ALLUVIAL: CASABIANCA FORMATION (TCB)
622	- Weathered rock		
623	- Fresh rock	1031	- Residual soil
		1032	- Weathered rock
		1033	- Fresh rock

Table 4.11: List of materials occurring in the study area, along with the corresponding material codes.

From the results an average layer thickness of the various soil material types can be calculated. Figure 4.7 shows the frequency distribution of ash thickness calculated from the soil profile data. It can be concluded from this that in general the measured ash thickness is between 2 and 5 m. This distribution may deviate from reality because the correct measurement of ash thickness in the field is met with several difficulties (section 5.4.4.1.).

Variable	Class	Explanation	Variable	Class	Explanation
Observer	name	Name of observer	Permea	5	Estimated permeability class
Project	name	Project name	Sorting	4	Code for sorting
OP	OP:	Observation point	Consist	7	Code for consistency
Run	-	Photo run (F.e. C-2275)	Redens	5	Code for relative density
Photo	nr	Photo number	PerB	%	Estimated weight % boulders (fraction >20 cm)
Day/Month	dd/mm	Date of observation	PerC	%	Estimated weight % cobbles (fraction 7.5 - 20 cm)
Location	name	Location description	PerG	%	Estimated weight % gravel (fraction 0.475 - 7.5 cm)
Sector	-	Map sector	PerS	%	Estimated weight % sand (fraction 0.075 - 4.75 mm)
Altitude	m	Altitude in metres	PerF	%	Estimated weight % fines (fraction < 0.075 mm)
Sdir	degree	Slope direction			
Sdip	degree	Slope angle			
Sheight	m	Height of outcrop			
LN	nr	Layer number, starting from 1 at the surface	PPMIN	kgf/cm2	Min. pocket penetrometer value
Top	cm	Depth from surface to the top of layer	PPAVG	kgf/cm2	Avg. pocket penetrometer value
Bottom	cm	Depth from surface to the bottom of layer	PPMAX	kgf/cm2	Max. pocket penetrometer value
			Vavalue	ton/m2	Shear vane result
Material	code	Code of material type	Dummy	ton/m2	Shear vane dummy value
Color		Color using Munsell	Varesi	ton/m2	Residual shear strength
Layering	3	Code for layering	Sample	OP/S/..	Code for soil-sample taken
Cement	5	Code for cementation	Sdepth	cm	Sampling depth
Moist	4	Code for soil humidity	Labtest	-	Laboratory test to be executed

Table 4.12: Overview of variables used on the soil observation sheet.

LAYERING	SOIL HUMIDITY	SORTING	
1 Absent 2 Irregular 3 Regular	1 Dry 2 Moist 3 Wet 4 Saturated	1 Poor 2 Moderate 3 Good 4 Very good	
CEMENTATION	**PERMEABILITY**	**CONSISTENCY**	**RELATIVE DENSITY**
1 Uncemented 2 Very weak 3 Weak 4 Strong	1 Very low 2 Low 3 Moderate 4 High 5 Very high	1 Very soft 2 Soft 3 Moderately firm 4 Firm 5 Very firm 6 Hard	1 Very loose 2 Loose 3 Moderate 4 Compact 5 Very compact

Table 4.13: Variable classes for soil observations.
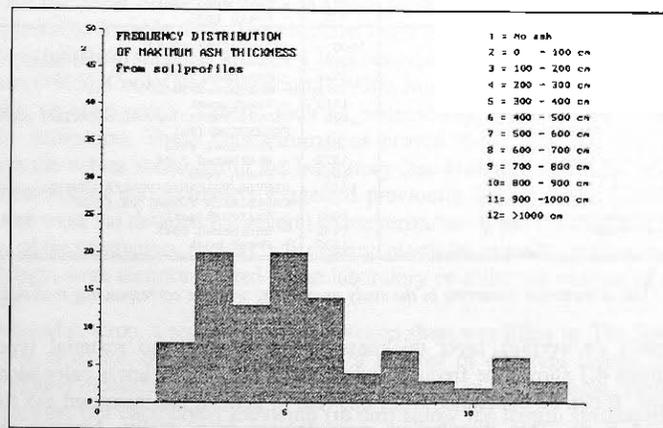
Figure 4.7: Frequency distribution of ash thickness as calculated from observation point data (n = 143).

Analogous thickness distributions could be calculated for each material type existing in the medium-scale study area (see appendix 6), resulting in a general description of the weathering profiles for the different lithological types. Average residual soil depth ranges between 2 and 4.5 m. Maximum thickness can be as high as 20 m. The values from this table can be used as indicative values for residual soils and weathered rock in the engineering geological maps (see section 5.4.4.2), which are used in the large scale hazard analysis.

The values given in appendix 6 should be evaluated with care, especially for residual soil thickness, as it is very rare to encounter an outcrop in which the entire weathering profile can be observed. The low values for the weathered rock are therefore explained largely by the fact that usually only a part of the total profile could be seen. Comparing the values derived from the data base and qualitative data from the same area (Cortez, 1988) confirms the fact that the outcrops measured seldom permitted the complete weathering profile to be measured.

In addition to the material sequences that were described, a qualitative characterization of the various materials was made with the soil checklist. The resulting tables are given in appendices 7 and 8. The usefulness of these descriptive parameters can be discussed. They are very subjective, and large variations arise in observations made by different individuals. A number of these variables could even be assessed after fieldwork, once a good understanding of the grain-size distributions is obtained. Probably the most useful data in the soil observation sheet are the weight percentages of boulders, cobbles, gravel, sand, and fines. These estimates allow the user to draw general conclusions on the susceptibility of the material to mass movement. The grain-size estimates for the various observation points were aggregated per material type and frequency distributions were calculated and plotted in histograms (see appendix 9).

4.4.2.4 Rock observation sheet

The third type of information that is collected in a medium-scale analysis using field checklists is rock characteristics. The objective is to gather information on the following features:
- Lithological variability of the various rock units,
- The importance of weathering in the various rock units,
- Rock mass characterization using rock material strength indices and fracture spacing.

Many different classification systems exist for geotechnical rock mass classification (Deere and Deere, 1988; Wickham et al., 1972; Bieniawski, 1973; Barton et al., 1974). Most of these systems were developed for mining or tunnelling projects and involve factors that are relatively unimportant for slope instability analysis.

The format for the rock mass description used in this study is a fairly simple one, developed for use in engineering geological fieldwork at ITC (Rengers et al., 1990). As the description method is applied here to characterize mapping units and not specific sites, detailed information on discontinuity orientation is omitted. In the structurally heterogeneous study area, with highly fractured and folded meta-sedimentary and metamorphic rocks, discontinuity patterns cannot be extrapolated over large areas. Identification of the weathering intensity zones, using the classification of Dearman (1976), is important in tropical environments. Collection of descriptive rock data in the tropical Rio Chinchina basin was hindered by extensive weathering and the limited number of good rock outcrops due to vegetation and ash cover.

The first step in describing the rock mass in an outcrop is to a divide it into homogeneous zones, called "lithological groups" (LG). A lithological group is defined as a homogeneous zone in the outcrop with a uniform degree of weathering, lithological composition, and/or discontinuity pattern. The LGs are not necessarily positioned in a vertical sequence. Therefore no measurements of depth are given, but instead the area percentages of the various LGs within the rock outcrop are measured/estimated.

The elements used in the rock observation sheet are given in table 4.14. The checklist used and an explanation of the classes are given in appendix 10. For the material codes the same table as for the soil classification was used (table 4.11). However, since many of the mapped rock units were very heterogeneous with respect to their lithological composition, a separate parameter was added for lithology. During the fieldwork, executed by Colombian geologists (Echavarria et al., 1991), a table containing the lithologies encountered in the area was constructed. This allowed the percentage occupied by various lithologies in each rock material type (see table 4.11) to be calculated. For this purpose the summed area of outcrops with a certain lithology was divided by the total area of all outcrops in a material type. The results of this calculation are given in appendix 11. Most of the material units occurring in the area are relatively homogeneous in lithological composition. The most heterogeneous rock material in the area is unit 920 (meta-sedimentary rock of the Quebradagrande formation). Separate mapping of these lithologies in the engineering geological map proved to be impossible because of their strong lateral variation and the difficulty in interpolating between different rock outcrops.

An analogous procedure can be done for weathering zones (appendix 12) or combinations of lithologies and weathering. The percentage of different weathering zones for each material type gives an impression of the rock mass strength. Material types with a high percentage of schists (820, 830, and 910) also have a high percentage of highly and completely weathered zones.

Variable	Class/ format	Explanation	Variable	Class/ format	Explanation
Observer	name	Name of observer	SH	-	Schmidt hammer rebound value
Project	name	Project name	Angle	degree	Angle of Schmidt hammer test
OP	-	Observation point.	PLmax	Bar	Point load oil pressure at failure
Run	-	Photo run (F.e. C-2275)			
Photo	nr	Photo number	SL	mm	Distance between cones
Day/Month	dd/mm	Date of observation	Dir1	degree	Discontinuity set 1: direction
Location	name	Location description	Dip1	degree	Discontinuity set 1: dip
Sector		Map sector	Type1	1-6	Discontinuity set 1: type
Altitude	m	Altitude in metres	Spac1	1-5	Discontinuity set 1: spacing
Sdir	degree	Outcrop direction	Dir2	degree	Discontinuity set 2: direction
Sdip	degree	Outcrop angle	Dip2	degree	Discontinuity set 2: dip
Sheight	m	Height of outcrop	Type2	1-6	Discontinuity set 2: type
LG	nr	Lithological group	Spac2	1-5	Discontinuity set 2: spacing
LGPERC	%	Percentage in outcrop occupied by LG	Dir3	degree	Discontinuity set 3: direction
			Dip3	degree	Discontinuity set 3: dip
LITHO	nr	Detailed lithological characterization	Type3	1-6	Discontinuity set 3: type
			Spac3	1-5	Discontinuity set 3: spacing
Material		Code of material type	Sample	-	Sample code
WS	1-6	Weathering zone	Test	-	Proposed rock test
Wdepth	cm	Vertical depth of weathering			

Table 4.14: Overview of variables used for rock mass description. See also appendix 10.

One of the simplest methods for obtaining general information on rock material strength is the Schmidt hammer rebound test (Selby, 1982). The rebound values of this spring-loaded

hammer give an index value for the compressive strength of rock materials. Values below the minimum sensitivity of the Schmidt hammer were recorded as zero. For each material type, Schmidt hammer values were divided into those higher than 10 and those lower than 10, including the zero readings. Average and standard deviations were calculated and frequency distributions were made. Example frequency distributions of the Schmidt hammer values within the main rock materials in the study area are given in appendix 14. The corresponding statistics are given in appendix 13. Andesitic lavas of material type 610 have the highest material strength, and the Paleozoic schists of the Cajamarca formation as well as the graphitic schists within the Quebradagrande formation have the lowest rock material strength, with more than 25% of the readings below the sensitivity limit. The other rock materials can all be classified as moderately strong with predominant Schmidt hammer values between 25 and 50. The Schmidt hammer results were used in the characterization of engineering geological units. When a sufficient number of measurements are available, the distribution of Schmidt hammer values for the various lithologies within a material unit can also be calculated.

Rock discontinuity measurements were collected systematically on the rock observation sheet. In general only the three most important discontinuity sets were described, for which the type, orientation and spacing class were measured. The discontinuity spacing measurements were aggregated per material type (see appendix 15). Most of the rocks have close extremely close spacing.

4.4.3 Fieldwork at the large scale

Due to the limited size of the study area at the large scale (see figure 3.10) and the proposed deterministic analysis techniques to be used (see section 2.5.8), the necessary input data must be more quantitative than the data at smaller scales. At the large scale, collection of specific hydrological and geotechnical data needed in hydrological and slope stability models is important. Therefore the fieldwork should focus on the following objectives:

- Detailed description of soil profiles,
- Collection of hydrological parameters,
- Determination of groundwater levels,
- Determination of soil strength characteristics.

The spatial variability of geotechnical and hydrological variables, such as cohesion, internal friction angle, bulk density, water content, saturated conductivity, and water retention, should be given careful attention during field data collection. Temporal variability of factors such as water content and groundwater level is important, but the determination is costly and very time-consuming. The temporal variability of these factors should instead be obtained using simple hydrological models. Because the large-scale analysis is intended for areas of tens of square kilometres and not for single landslides, the use of complex field-instrumentation methods is not feasible. Strong emphasis should also be given to the collection of existing geotechnical reports, to obtain maximum available information on soil profiles and geotechnical characterizations.

Laboratory analysis of geotechnical parameters plays a very important role at the large scale. During fieldwork, analyses such as saturated conductivity tests and detailed surface profiling of landslides for back-analysis were conducted.

4.4.3.1 Soil profile descriptions

The same checklists can be used for soil description at the large scale as at the medium scale, but the sampling density should be higher and the observations should be much more detailed. Collection of semi-quantitative data from the soil observation sheet is no longer recommended, since the information they provide is too general. The soil sheets are used mainly to describe the various material sequences in detail.

Soil observations at this scale are preferentially made from boreholes, as this reduces errors in soil thickness measurements, which occur when describing outcrops along roads or in valleys. For the Manizales area the majority of the soil observations was derived from existing geotechnical reports made by local consulting firms or by the Corporación Regional Autonoma de Manizales, Salamina y Aranzazu (CRAMSA, 1990). Most of the profile information (90%) for the inhabited parts of the area where no soil outcrops exist was also derived from boreholes. The main problem with these data arose in translating soil descriptions made by the engineers, which was often very brief and inadequate, into the material codes used in this study (table 4.11). The borehole descriptions usually did not specify whether the soil was pyroclastic material, residual soil, or fluvio-volcanic material. Therefore, additional soil observations were made in the field, close to existing boreholes described in those reports, where the soil types were checked. This helped to reduce errors in translating soil types, but, nevertheless, many of the soil descriptions proved to be useless.

4.4.3.2 Detailed landslide descriptions

Collecting descriptive data on landslides using field checklists is less important at this scale, since statistical analysis methods are no longer applied, and the data to be collected may be of a different nature than those for a larger area. In a large-scale study area only one or two rock types may be outcropping, so that this factor becomes less important in differentiating zones with different landslide activity. The landslide checklists developed for the medium scale can be used to obtain general insight into the different landslide types and the soil and topographical conditions under which they occur.

In addition to the landslide checklists, more detailed landslide descriptions were made, including detailed geomorphological mapping of individual landslides and slope profiling. To perform a back-analysis to determine values for cohesion and angle of internal friction, at least three landslides of the same type and in the same material should be described in detail.

Several techniques can be used to produce detailed slope profiles (Dackombe and Gardiner, 1983). One of the most rapid methods is the use of a pantometer: a parallelogram with known base length which is moved along the slope profile. At every point along the profile the angle between the vertical pole and the sloping pole is measured. The end point of every observation is used as the starting point for the next one. For each profile the altitude of the highest observation point is determined from the detailed topographic map and noted on the observation sheet. Along the profile, important features are noted next to the slope angle readings. The pantometer angles are recalculated to x and z data using a conversion program (Mählmann, 1991). The program allows the data to be converted into input formats for a GIS (ILWIS), a hydrological program (SLOHYD), slope stability programs (SLIDE and SLAN), and a backanalysis program (CASA).

In the study area a total of 50 landslide profiles occurring in three sets were measured. The first set consists of landslides in sandy ash sequences, 3 to 7 m thick overlying residual

soils of the Quebradagrande formation. The second set occurred in fine volcanic ash overlying residual soil from the Manizales and Casabianca formations, all in the vicinity of Manizales. A third set of measurements was taken in landslides in fine-grained ash overlying weathered schists in the vicinity of Chinchina. From each set a limited number of landslides occurring under the same conditions were selected.

The profiles were treated in a back-analysis program called CASA (Kuiper, 1990), based on a circular failure model. First the sliding surface and the original pre-failure profile are constructed. Several profiles can then be combined to calculate cohesion (c) and angle of internal friction (φ) (Van Asch, 1986). The crucial factor in the back-analysis is the location of the water table in metres below the surface at the time of failure. Because this factor is unknown, several water table depths were used and the results were compared. Normally two extreme situations were taken: one with a groundwater table at the surface, and one with a water table at 8 meters below the surface (i.e. below the failure surface of all slides). The first option resulted in unacceptable values. Moreover, water-table depths less then 4 m showed φ values that were far too low compared to laboratory results. The results of the backanalyses for the three sets of landslide situations are given table 4.15.

Set	Number of slides	Material in which slide took place	Modelled groundwater situations			
			Without groundwater		Groundwater at surface	
1	8	Sandy ash (code 120) on residual soils of the Quebradagrande formation	c´= 3.01	φ´= 30.6	c´= 12.7	φ´= 32
2	7	Fine ash (code 110) on residual soil from the Manizales and Casabianca formation	c´= 3	φ´= 29	c´= 6.9	φ´= 30
3	9	Fine ash (code 110) on residual soils from schists	c´= 0.5	φ´= 32	c´= 0.8	φ´= 34

Tables 4.15: Back-analysis results for different soil types and groundwater conditions (cohesion is in KPa).

The back-analysis method applied has a number of serious drawbacks:
1. The back-analysis program assumes the presence of a circular failure surface, which was not the case in most of the landslides.
2. The landslides may each have occurred under different groundwater situations. The program requires one absolute value for the depth of groundwater below the surface, which is applied for all landslides. When groundwater values of several metres are used, some of the landslides in the group may have their failure surfaces below the groundwater level and others above it. In future it would be better to adapt the program so that it is possible to use relative groundwater depth (height of the groundwater level above the failure surface/depth of the failure surface), but even then the assumption that all landslides occurred with the same relative groundwater depth is questionable.
3. Since the groundwater depth is unknown the user can manipulate the result to obtain satisfactory results by changing the groundwater value and/or deleting landslides that affect the expected result negatively.

The results from the back-analyses are to be used in the infinite slope modelling, presented in section 6.5. However, due to the drawbacks given above, these results can only be used in combination with existing laboratory data, and even then the results are only

indicative. To improve the value of the results, more attention should be paid to possible groundwater conditions. On the other hand, the method can also be used to check extreme groundwater conditions: at the surface, or below the failure surface.

4.4.3.3 Hydrological measurements

One of the most important elements in the application of slope stability models is groundwater level. In order to obtain more insight into groundwater fluctuations over time, a hydrological model was to be used, since field monitoring with piezometers or tensiometers was not feasible due to time constraints, and due to the heterogeneity and size of the study area. The hydrological modelling will be discussed in section 5.4.4.3.

One of the most important parameters in such a model is saturated hydraulic conductivity (Ksat). This was determined in the field using the inverse borehole test, described by Kessler and Oosterbaan (1974). Around 100 tests were performed, predominantly in the area surrounding Manizales. Most of the tests were conducted in volcanic ash. It was rather difficult to find suitable sites where measurements in residual soils could be performed, due both to the covering ash mantle and to the fact that material exposed to the surface, was often dry and cracked and not representative of the situation below the ash layer.

Results of the saturated conductivity tests are presented in figure 4.8. Results were divided into three groups: silty and fine sandy ash, with a K-sat range of about 10-70 cm/day; coarse sandy and gravelly pyroclastics, with a range of 90-200 cm/day or even higher; and residual soils, with values less than 20 cm/day. Variations in the distributions are caused by differences in grain-size distributions, weathering grades, and presence of macropores. Values in the lapilli (coarse sandy and gravelly pyroclastics) were very high, which sometimes made measurement impossible, since the borehole could not be filled before starting the measurement. The presence of these lapilli layers in the ash profiles is of large importance for the hydrological situation. Problems may arise when lapilli layers are discontinuous, and especially when they wedge out in the down slope direction.
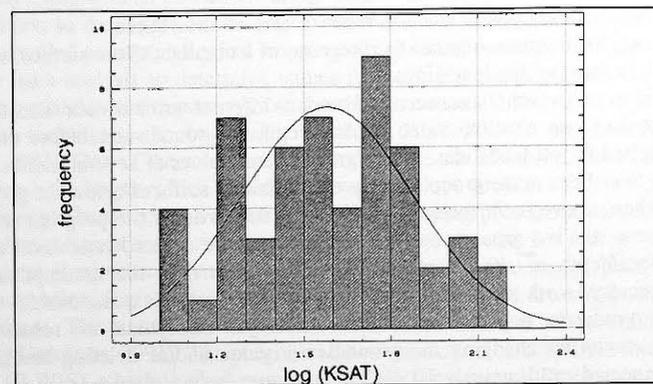
Figure 4.8: Frequency distribution of the log of saturated conductivity values determined with the inverse borehole method in volcanic ashes.

Detailed soil observations in the area east of Manizales revealed that the lapilli layers were usually continuous. In the area directly surrounding Manizales, however, ash profiles are much less homogeneous; moreover, lapilli layers are very discontinuous and tend to thicken in the down slope direction, due to slope movements shortly after their deposition.

4.5 Laboratory analyses

In addition to the field techniques laboratory analyses on soil samples were performed at both the medium and the large scales. Laboratory tests were conducted for the determination of grain-size distribution, Atterberg limits, water retention characteristics, bulk-density, soil strength, and clay mineralogy.

Most of these data are collected to obtain insight into the geotechnical characteristics of the various soil types occurring in the area. The water retention data were used in hydrological modelling, as discussed in section 5.4.4.3. Density and soil strength data were used in the slope stability model, which will be treated in section 6.5.

4.5.1 Grain-size distribution

To characterize the soil material types with respect to their grain-size distribution, about 200 samples were collected from the various soil material types shown in table 4.11. They were dry-sieved in the soil laboratory of the National University in Manizales, using standard American Society for Testing Materials (ASTM) sieves (ASTM, 1989). The grain-size curves were· grouped by material type, after which the average and standard deviation for each fraction could be calculated. Subsequently, all curves for one soil type were plotted together. Figure 4.9 shows examples of the grain-size distribution from pyroclastic materials. The results for all material types are given in appendix 16. The results for the pyroclastic materials a showed a relatively high content of fine sand. Even the soil characterized as fine-grained ash contained 20 to 50% sand.

4.5.2 Soil classification

For the purpose of soil classification some 200 samples were collected. Additional information was obtained from literature (CRAMSA, 1990). The Universal Soil Classification System (USCS) method for classification of soils for engineering purposes (ASTM, 1989) was used. The data were rearranged according to soil type, and the classification was done automatically up to the group name, using a treelike batch file structure. The results for the soil types in the area are given in appendix 17. In addition a batch file was written to plot the results for each soil type automatically in a plasticity chart. Figure 4.10 gives an example of the plotted plasticity values for fine grained ash.

4.5.3 Water retention

Samples for soil retention analyses were taken at a limited number of points, covering the most important soil types. They were tested using a standardized method at the soil laboratory of IGAC. Unfortunately PF0 was not determined. The results for the pyroclastic materials are displayed in figure 4.11.

4.5.4 Bulk-density

Soil density was measured in a limited number of undisturbed samples to obtain a general idea on the dry density, and the range of in situ densities. Samples for in situ density analyses were taken during both dry and wet seasons, to obtain a reasonable range of values throughout the year. Saturated densities were not defined. Statistics were calculated for the different soil material types. The results are displayed in appendix 18. Soil density values for the pyroclastic materials (material codes 110, 120, and 130) are quite low. Average dry density value for the ashes ranges from 1.02 to 1.15 g/cm^3. Average in situ densities for these materials ranged from 1.38 to 1.45 g/cm^3. The low density of the ashes can be explained by their mechanism of deposition. Deposition from the air usually results in a loose soil structure. In particular, the lapilli layers, composed of fragments of pumice, may have densities as low as 0.6 g/cm^3. Similar results for ash soil are reported by Vis (1989). Densities were also determined for a number of rock samples in the various rock material types (appendix 19).
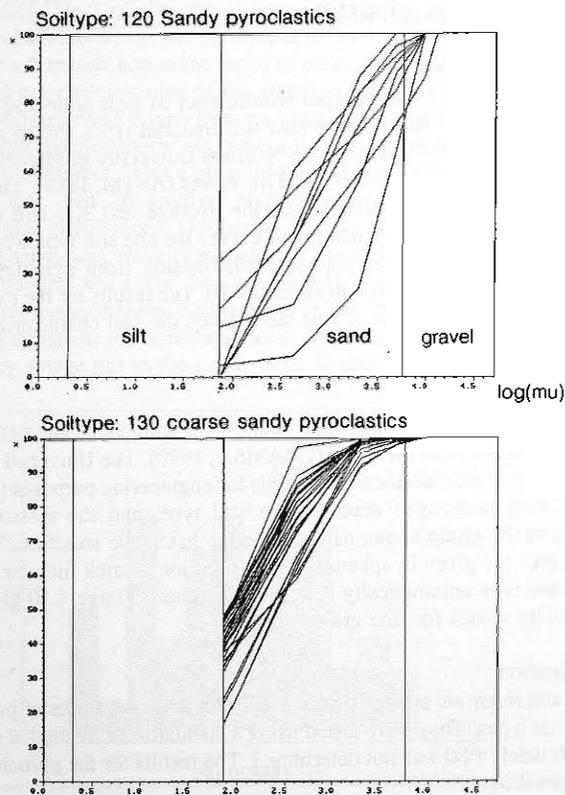
Figure 4.9: Grain-size distribution curves for pyroclastic materials within the study area. (Above) Sandy pyroclastics (material code: 120); (Below) coarse sandy pyroclastics (material code: 130).
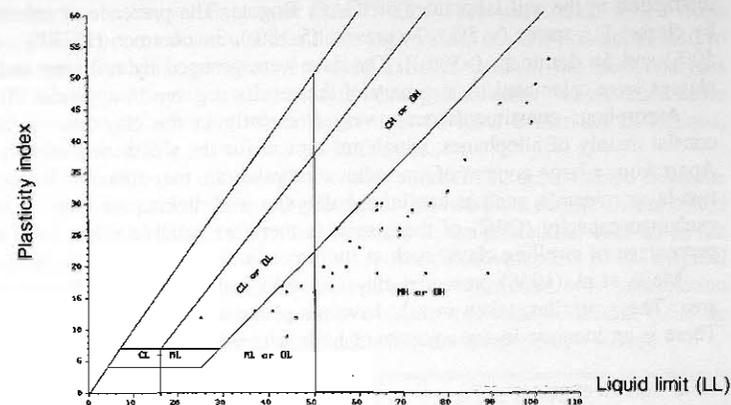
Figure 4.10: Example of a plasticity chart showing the data points for fine grained ash (material code: 110).
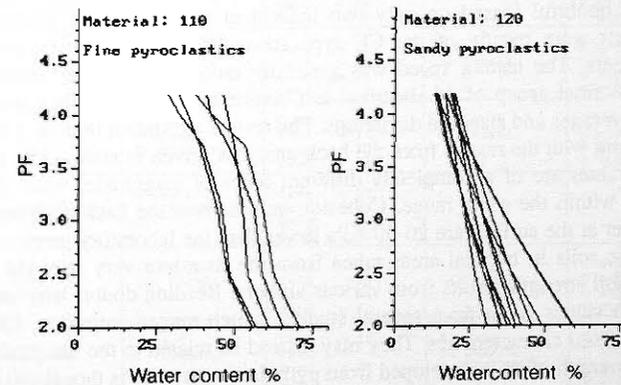
Figure 4.11: Water retention curves for samples of pyroclastic materials. (Left) Fine pyroclastic (material code 110); (Right): Sandy pyroclastics (material code 120).

4.5.5 Clay mineralogy

For a small number of samples clay mineralogy analyses were performed using X-ray diffraction in the soil laboratory of IGAC, Bogota. The presence of minerals was indicated by classes [1= traces (< 5%), 2= present (5-15%), 3= common (15-30%), 4= abundant (30-50%) and 5= dominant (>50%)]. The data were grouped by soil type and the predominant classes were calculated. A summary of the results is given in appendix 20.

Amorphous constituents occur very frequently in the clay fraction. In ash soils they consist mainly of allophanes, which are typical for the weathering of this type of material. Apart from a large content of amorphous material, the clay minerals belonging to the 1:1 or two-layer minerals, such as kaolinite, halloysite, and dickite, are most abundant. The cation exchange capacity (CEC) of these soils is therefore relatively low (<30 mEq/100 g). The percentage of swelling clays, such as montmorillonite or vermiculite, is very low.

Mejia et al. (1968) presented clay mineralogical results from four profiles in the study area. These profiles, taken in ash, have allophane as the major constituent in all horizons. There is an increase in the amounts of halloysite and some montmorillonite with depth.

4.5.6 Soil strength

Due to financial and time constraints only a very small number of samples could be tested for soil strength characteristics. This type of data was obtained almost completely from existing geotechnical reports, mainly from CRAMSA (1990) and some from the work of the Ministerio de Obras Publicas and the Universidad Nacional (MOPT-UN, 1990). The problems described in section 4.4.3.1 of recoding the soil material types caused difficulties in assigning the test results to the different soil materials types in table 4.11.

Both shearbox test and triaxial test results were extracted from the reports. Results that were very doubtful (based on only two individual tests, for example) were omitted. The triaxial tests were mostly of the CU type (consolidated, undrained), with pore pressure measurements. The testing speed was generally quite high, on the order of 0.08 to 0.25 mm/min. A final group of 46 shearbox test results and 28 triaxial test results was used to calculate averages and standard deviations. The results are shown in table 4.16. If these values are compared with the results from the back-analyses (given in table 4.15), it is clear that the cohesion values are of a completely different order of magnitude, while the friction angle values are within the same range. Cohesion values from the back-analyses calculated with groundwater at the surface are 20-30 KPa lower than the laboratory results. Cohesion values for volcanic soils in tropical areas taken from the literature vary strongly. Reading (1991) presented soil strength results from various authors. Reading doubts whether the wide range in cohesion values taken from several studies, which ranged from 0 to 156 KPa, is a true reflection of soil characteristics. They may instead be related to the test procedures followed. The field strength of soils developed from pyroclastic material is thought to depend upon the soils' microstructure. Halloysite and allophane give these materials their special properties: high water content and water retention capability, high void ratio, low density, high permeability, and potentially high cohesion values (Belloni and Morris, 1991). The strength of the material is due to an open skeleton of minerals, surrounded by clay particles and a viscous gel. The porous texture seems to be associated with the presence of sequioxides, coating the surface of the clay minerals, binding them together and providing a component of their apparent shear strength and the "bonding" mentioned by many researchers (Belloni

and Morris, 1991). These bonding effects may account for the high cohesion values. From table 4.16 it can be concluded that high cohesion values do not occur only for the ash soils; practically all soils have cohesion values greater than 15 KPa. Tests were made with a slope instability program (SLIDE) to evaluate whether these high values of cohesion could lead to slope failures. The same landslide profiles were used as were used in the back-analyses (section 4.4.3.2). Practically all landslides were stable when groundwater was assumed to be at the surface and cohesion values were taken larger than 10 KPa. Under dry conditions, cohesion values greater than 4 KPa never resulted in failures.

Apart from the possible effect of "bonding", the high cohesion values obtained from the literature are considered to be related to the test procedure followed. All samples were tested in the same laboratory of CRAMSA, and systematic errors in the procedure, such as in the measurement of pore pressures, could have occurred. As we did have access to the original test results these errors are no longer traceable. Here it can be concluded only that caution should be taken with the use of these data in slope stability analysis. In section 6.5.3 an evaluation will be given of possible failure conditions using an infinite slope model.

MATERIAL TYPES	Shear box tests		Triaxial tests	
	NUMBER OF TESTS, AND SOURCE	TOTAL STRESSES C in KPa, φ in degrees	NUMBER OF TESTS, AND SOURCE	EFFECTIVE STRESSES C in KPa, φ in degrees
110. Fine ash	10 tests 6: CRAMSA 4: EEC/UNESCO	Cavg = 41 Cstd = 11 φavg = 30 φstd = 6	5 tests 5: CRAMSA	C'avg = 38 C'std = 6 φ'avg = 29 φ'std = 3
120 Sandy ash	2 tests 2: CRAMSA	Cavg = 21 Cstd = 7 φavg = 29 φstd = 2	4 tests 4: CRAMSA	C'avg = 10 C'std = 6 φ'avg = 33 φ'std = 5
310 Debris flow material	6 tests 6: CRAMSA	Cavg = 45 Cstd = 22 φavg = 22 φstd = 7	3 tests 3: CRAMSA	C'avg = 33 C'std = 5 φ'avg = 22 φ'std = 3
520 Urban landfill	8 tests 6: CRAMSA 2: MOPT-UN	Cavg = 35 Cstd = 17 φavg = 35 φstd = 4	4 tests 4: CRAMSA	C'avg = 15 C'std = 9 φ'avg = 32 φ'std = 1
830 Residual soil from schists	3 tests 3: EEC/UNESCO	Cavg = 52 Cstd = 22 φavg = 30 φstd = 12	-	-
920 Residual soil from meta-sedimentary rocks	10 tests 10: CRAMSA	Cavg = 53 Cstd = 19 φavg = 26 φstd = 7	4 tests 4: CRAMSA	C'avg = 26 C'std = 8 φ'avg = 29 φ'std = 4
1020 Residual soil from fluvio-volcanic material (Manizales Formation)	1 test 1: CRAMSA	Cavg = 12 Cstd = - φavg = 35 φstd = -	5 tests 4: CRAMSA 1: EEC/UNESCO	C'avg = 14 C'std = 11 φ'avg = 30 φ'std = 2
1030 Residual soil from fluvio-volcanic material (Casabianca Formation)	6 tests 4: CRAMSA 2: EEC/UNESCO	Cavg = 28 Cstd = 19 φavg = 26 φstd = 6	3 tests 3: CRAMSA	C'avg = 29 C'std = 9 φ'avg = 28 φ'std = 2

Table 4.16: Peak soil strength values for some soils. Data derived from CRAMSA (1990), MOPT-UN (1990) and from the present research project (EEC/UNESCO).

CHAPTER 5: DATA ENTRY

This chapter deals with the specific issues involved in data entry for a landslide hazard assessment project using a geographic information system. Data entry is undoubtedly the most cumbersome aspect of working with a GIS. As explained in section 2.7, the use of GIS increases considerably the time needed for pre-analysis activities. This is due mainly to time-consuming data entry. The extra time needed during this phase is more than compensated, however, by the flexibility and speed of analysis techniques, as will be demonstrated in chapter 6. From table 2.5 it can be observed that the use of GIS requires the following phases related to data entry:

- Data entry (digitizing),
- Data base design,
- Data validation,
- Pre-analysis data manipulation.

These four phases will be explained in the following sections, with major emphasis on applications at the medium and large scale. Illustrations of the data base prepared for the Chinchina area will be given. Owing to the general lack of knowledge about data entry in connection with GIS, among earth scientists working on landslide hazard assessment, I feel obliged to treat this subject rather elaborately.

5.1 Digitizing of data

5.1.1 Digitizing of maps

Manual digitizing remains the principal method to convert analogue map data into a digital format. The amount of work spent on digitizing maps can be very large, especially when many different input maps are to be used in the analysis. Constructing digital terrain models for the Chinchina area, for example, required digitization of 52 topographic sheets: 4 sheets at 1:100,000 scale with 50-m contour interval, 12 sheets at 1:25,000 scale with 50-m contour interval, 4 sheets at 1:5,000 scale with 10-m contour interval, and 32 sheets at 1:2,000 scale with 10-m contour interval. Another example is the large-scale geomorphological map of the Manizales area, presented in figure 5.1. Digitizing this map, with about 8000 segments and 2800 polygons, took about three weeks. Combined, geomorphological photo-interpretation and photo-to-map conversion took approximately 6 weeks.

Manual digitizing was performed on CALCOMP 9100 A0-size, and on CALCOMP 23240 A2-size, digitizers with resolution set at 10 lines/mm. The digitizing process for polygon maps includes definition of control points on the map used to convert the digitizer coordinates to map coordinates; digitizing line elements, that form the boundaries of mapping units; checking these line elements (segments); and coding of polygons. Although it is routine work, manual digitizing has to be done very precisely, to prevent errors such as shifts in control points, errors in the correct following of lines, overlooking of small segments during digitizing, and mistakes in the coding of line segments (for contour maps, for example) or polygons.

Figure 5.1: Polygon map of geomorphological subunits for the Manizales area, digitized at a scale of 1:10,000. Only the vectors are shown to illustrate the complexity of digitizing the map.

To reduce errors in digitizing photo-interpreted maps, special care should be taken in preparing the hand-drawn original. For detailed maps, such as the map shown in figure 5.1, this proved to be very difficult. One must overcome the inclination to proceed with digitizing before examining the map polygon by polygon and verifying that all are coded and enclosed by vectors. For this reason, constructing maps to be digitized, is much more time-consuming than producing conventional maps. In the latter case, it is possible to omit codes in areas where data are unknown or missing, whereas each polygon must be coded in maps that are to be digitized.

An important factor that should be taken into account during digitizing is the fit of different digitized maps. Digitizing maps containing related information separately invariably produces errors when these maps are combined. For example, when drainage lines and contour lines are digitized separately, the drainage lines will most probably fall outside of the contour lines. This type of problem occurred in the this study: backward recession points of the contours, when overlaid with strongly related data such as drainage lines and roads, were displaced considerably. The landslides were therefore redigitized, but in a file already containing data on drainage, roads, and contour information. For this reason, digitizing related information in one file using different codes for different types of information is recommended.

One of the most time-consuming and error-producing steps in preparing photo-interpretation maps is converting data from the photo to a base map. These errors can be reduced by first digitizing the photo-interpretation without conversion, and then recalculating the interpretation to the map coordinates by an ortho-photo program within the GIS (Bargagli, 1991). This program calculates the relief displacement on the basis of a digital terrain model and a data file containing control points with photo-coordinates and corresponding map coordinates. However, this method produces difficulties in matching the interpretations from neighbouring photos. Unfortunately, this program became available within ILWIS too late to be used extensively in this study.

Some data were entered automatically using scanners. Scanners can be used to enter both maps and images. A HPScanjet was used to scan (aerial)photos. The scanner allowed the use of 256-grey levels, full tones, half-tones, and line drawings. The resulting files in TIF format were converted to ILWIS format. Further enhancement of the scanned photos was done in ILWIS. Unfortunately, the maximum size of images that could be scanned was 21 x 29.7 cm, so that aerial photos (usually 23 * 23 cm) could not be scanned completely. This deficiency leads to problems in the subsequent ortho-image calculation, since not all of the fiducial marks on the photo are scanned.

The use of a line scanner was tested for scanning contour maps. The scanned map (bit map) was vectorized and heights were assigned to the various contour lines using the SYSCAN system. This proved to be rather time-consuming, especially since most of the available contour maps contained ancillary information that would have to be deleted later. The time needed for scanning and editing was as large as, or even larger than, for hand digitizing, so this method was abandoned.

5.1.2 Data conversion

Some of the existing data were already available in digital format. The most important sources of digital data were satellite images (SPOT images). The data were read from computer compatible tapes (CCT) using a tape-drive connected to an ERDAS system, or to a VAX-based image-processing system. A window covering the study area was selected and the data were converted to the ILWIS format. ILWIS was used for all image enhancement as well as for the creation of an ortho-image. The resulting false-colour composites were printed as positives on an OPTRONIX film writer. From these positives, normal prints could be made, which were used for the visual stereoscopic interpretation.

Map data for Manizales was available in USEMAP format (Turkstra et al., 1991). These data could be easily converted to the ILWIS format. However, due to the specific data structure of the USEMAP files, some files contained a large number of double segments, which had to be deleted individually. Some contour information for the western part of the area was available in SYSCAN format (Valencia, 1990). These data turned out to be incompatible with the digitized contour information due to a change in coordinate system, which could not be adjusted satisfactorily by coordinate transformation within ILWIS. The same was true for a large number of maps for the whole catchment, digitized at 1:100,000 (Lozano, 1989). Some of the drainage and contour maps digitized by La Rotta (1991) at scales of 1:100,000 and 1:25,000 could be used without problems of coordinate mismatch. In summary, the use of existing digital data is quite limited, as one is faced with the problems of different coordinate systems, resulting in imperfectly overlapping data.

5.1.3 Attribute data entry

Attribute data were simply typed into the ILWIS tabular data base after defining the columns. Data can also be entered into a word processor if the resulting ASCII file is converted to ILWIS format. In some cases data were entered in LOTUS and converted to ILWIS. In earlier work another data base system (ORACLE) was used, but data entry, updating, and querying proved to be much more time-consuming than in ILWIS, even when input screens were designed with the interactive application facility (IAF) (ORACLE, 1988). A large attribute data base related to land use from the coffee region was available in DBASE format (Federación Nacional de Cafeteros de Colombia, 1985). Problems were encountered during conversion to ILWIS, however, because the large number of records exceeded the capacity of ILWIS (16,000). For the urban sector of Manizales a cadastral data base was available (Turkstra et al., 1991), which was aggregated from the parcel level to the block level, and which was converted from DBASE to ILWIS format.

5.2 Data base design

Data base design needs to be initiated at the beginning of a project, before data collection, takes place, because the way the data will be stored in the data base determines the form in which data will be collected during aerial photo interpretation and fieldwork. The checklists discussed in chapter 4, and presented in the appendices, were prepared only after the structure of the data base was defined.

A GIS data base design is needed for both graphical data (maps) and for attribute data (tables). Graphical data can be stored as points (observation points, rainfall stations, etc.), lines (drainage lines, roads, contours, etc.), polygon maps (geomorphological, geological units,

etc.), or pixel maps (DTMs, satellite images, etc.). Attention should be paid to the connection between maps and tables. Tables and maps are linked such that the record number in the table corresponds to the pixel value of the map. Polygon data can be connected to tabular information either for each polygon separately (such as landslides) or for each mapping unit (such as geomorphological units), which may contain several polygons.

5.2.1 Graphical data base

The design of a graphical data base depends strongly on the specific requirements of the GIS which is used (e.g., vector or raster data structure, or a combination of these). The combination of raster and vector structure gives the highest flexibility, because some analytical techniques can be best performed in vector and others in raster mode (Aronoff, 1989). The ILWIS system used in this work is such a combined vector- and raster-based GIS. Vector storage is used for digitizing, network and linear analysis, and plotting, and raster data structure is used for analysis and image processing. The user can convert data, within certain limits, between these two data structures. Various types of maps are stored in the data base:

1. Digitized maps containing points, lines, or polygons. These maps contain both vector as well as raster files, and usually have accompanying tables in the attribute data base;
2. Digital images, such as satellite images or aerial photos, which consist only of raster files, mostly without accompanying tables;
3. Raster maps, which result from pre-analysis data manipulation, such as the engineering geological maps which are formed by a combination of different input maps. They usually have accompanying tables;
4. Final result maps with accompanying legend and annotation files, which are used for display and printing.

In the design of a graphical data base the following factors should be taken into account:

1. The inventory of available data types. A list of the available input data should be made, similar to the one displayed in table 4.1.;
2. Division of these data into "data layers". A "data layer" in a GIS can be seen as one digital map, containing one type of information and composed of one type of element (points, lines, or polygons related to one feature). Data from the same source, such as geological data, often have to be stored in different data layers: lithological units as polygons in one, and faults as lines in another. It is important to split the data layers such that data which are not directly related are stored in different layers.

The methods for mountain hazard analysis described in this study are intended for geographic information systems based on PCs. The use of a PC implies limitations with respect to data storage capacity. Uncompressed raster images are particularly voluminous. During the pre-analysis data manipulation and the data analysis phase, many intermediate and final result maps have to be stored. For the medium- and large- scale study, the total volume of data may be on the order of several hundreds of megabytes for an area of 250 km². In order to maintain sufficient working space on the hard disk, files should be compressed using run-length coding or quadtrees (Aronoff, 1989).

In the next three sections (5.2.1.1-5.2.1.3) the most important maps stored for the Rio Chinchina study area are discussed for each of the three scales under consideration. In the course of pre-analysis data manipulation and data analysis, many more maps were prepared from this basic data set.

5.2.1.1 Regional scale

The regional scale data were digitized mainly from 1:100,000-scale maps, covering an area of 722 km². The study area is located between the following x and y coordinates: x = 819,000 to 862,000, y = 1,024,000 to 1,060,000 (using the Colombian coordinate system with Bogotá as reference). The maps were rasterized with a pixel size of 65 m. The following data layers were prepared:

FCC: False-colour composites created from SPOT XS images. Source: SPOT (1986)

TMU: Terrain mapping units, digitized from a 1:100,000-scale image-interpreted map. Sources of lithological information: Herd (1974), Mosquera (1978), CHEC (1985), IGAC (1985, 1986), James (1986), INGEOMINAS (1987), Navarro et al. (1988), Cortez (1988), Florez (1986), Chacon and Orozco (1989), Handszer and Grand (1989), Naranjo and Rios (1989), Arcila (1990), Vargas (1990) and Echavarria et al. (1991).

CON100: Contour lines with contour interval of 100 m digitized from 12 map sheets at 1:25,000 scale. Source: IGAC (1967), La Rotta (1991).

DRAIN100: Drainage lines, digitized from 12 map sheets of 1:25,000 scale, and ordered with the Strahler order. Source: IGAC (1967), La Rotta (1991).

FAULT100: Faults and photogeological lineaments, digitized from 1:100.000 scale image interpretation map. Source: James (1986), Navarro et al. (1988), and Salgado and Chacon (1991).

PROCESS: Generalized process map digitized from 1:100.000 image interpretation map. Source: Florez (1986), IGAC (1985, 1986), SODEIC (1987), and Cortez (1988).

VOLCAN: Volcanic hazard map, digitized from a 1:100,000 map. Source: INGEOMINAS (1985), Parra et al. (1986), Thouret et al. (1989a).

GLACIER: Changes in the Ruiz glacier after the 1985 eruption. Source: Thouret et al. (1989a), Thouret (1989a), Calvache (1986a,b).

LANDUSE: Generalized land-use map, digitized from 1:100,000-scale map. Source: IGAC (1985, 1986)

SOILS: Generalized soil map, digitized from 1:50,000 soil map. Source: Federación Nacional de Cafeteros de Colombia (1982), IGAC (1979).

METEO: Meteorological stations. Source: HIMAT (1990), CHEC (1990), CENICAFE (1990), SODEIC (1987).

SISHIST: Table containing earthquake record for central Colombia. Source: Ramirez (1975), Page (1986), James (1986) and Valencia (1988).

ROADS: Road map, digitized from 1:25,000-scale topographic maps. Source: IGAC (1967).

CITY: City extensions, digitized from 1:25,000-scale maps. Source: IGAC (1967).

5.2.1.2 Medium scale

Information at the medium scale was digitized from 1:25,000-scale maps, with the exception of land-use data and contour lines, for which larger scale maps were used. Because of the very time-consuming process of map creation and digitizing, only a quarter of the originally planned area (262km²) at the medium was used. The data for this area, bordered in the lower left and upper right corners by the coordinates x = 827275, y = 1041000, x = 837000 and y = 1048000, respectively (using the Colombian coordinate system with Bogotá as reference), were rasterized with a pixel size of 12.5 m.

The following maps were stored in the data base for the medium scale:

BASE: Base map with 1-km² quadrangles digitized from 1:25,000 topographical maps. Source: IGAC (1967).

CONTOUR: Contour lines digitized from 1:25,000 scale topographic maps with contour interval of 50 m. Source: IGAC (1967).

CONCHIN: Contour lines digitized from 1:5,000-scale topographic maps with contour interval of 10 m. Source: IGAC (1987).

DRAINAGE: Drainage network, with indication of drainage lines derived from 1:25,000-scale topographic map. Source: IGAC (1967, 1987).

DRAINNEW: Drainage network, reordered from DRAINAGE by the Strahler method. Source: IGAC (1967).

DTM25: Digital terrain model, derived from CONTOUR and CONCHIN.

SLOPE: Slope angle map, in degrees, derived from DTM.
ASPECT: Slope aspect map, in degrees, derived from DTM.
ROAD60:   Road network, derived from 1960s aerial photos.
ROAD80:   Road network derived from 1980s aerial photos.
CITY60:   City extensions, derived from 1960s aerial photos.
CITY80:   City extensions, derived from 1980s aerial photos.
GEOL25N: Lithological units. Sources: Mosquera (1978), INGEOMINAS (1987), Navarro et al. (1988), Cortez (1988), Naranjo and Rios (1989), Arcila (1990), Vargas (1990) and Echavarria et al. (1991).
FAULT25:   Faults and lineaments. Sources: Navarro et al. (1988), Arcila (1990).
GEOM25C: Geomorphological complexes, derived from photo-interpretation. Source: Cortez (1988).
GEOM25M: Geomorphological main units, derived from photo-interpretation. Source: Cortez (1988).
GEOM25E: Geomorphological subunits, derived from photo-interpretation and fieldwork. Source: Cortez (1988).
SLIDE40:   Slope instability features, derived from interpretation of 1940s aerial photos.
SLIDE60:   Slope instability features, derived from interpretation of 1960s aerial photos.
SLIDE80:   Slope instability features, derived from interpretation of 1980s aerial photos and from fieldwork.
LUSE60:   Land use, derived by interpretation of 1960s aerial photos. Source: Van Duren (1992).
LU80CHIN: Land-use parcels of Chinchina municipality. Source: Federación Nacional de Cafeteros de Colombia (1985).
LU80PAL: Land-use parcels of Palestina municipality. Source: Federación Nacional de Cafeteros de Colombia (1985).
LU80MAN: Landuse parcels of Manizales municipality. Source: Federación Nacional de Cafeteros de Colombia (1985).
LUSE80:   Land-use, derived from interpretation of 1980s aerial photos and by combining the maps LU80CHIN, LU80PAL, and LU80MAN.
LUSEDIF: Land-use changes, derived by combining LUSE60 and LUSE80.

5.2.1.3 Large scale

The large-scale data set was digitized mainly from 1:10,000 scale maps. Raster maps were made, with a pixel size of 8.5 m, covering the area between the coordinates x = 1171400 to 1178000 and y = 1048900 to 1054000 (using the Colombian coordinate system with Medellin as reference). The size of the area was determined by the availability of detailed topographic data, the availability of large-scale aerial photos, and by total volume of data involved. Based on these factors, the entire urban area of Manizales was not mapped: the extreme eastern (La Nubia and Malteria) and western neighbourhoods (La Francia, Sacatin) were not included. The graphical data base for the large scale contains the following data layers:

CON49:   Contours, digitized from 13 1:2,000-scale maps with contour interval of 10 m. Source: IGAC (1949).
BOUND49:   Boundary of the area for which topographic data are available from 1949, screen digitized from CON49.
DTM49:   Digital terrain model, prepared from CON49.
CON89:   Contours, digitized from 19 1:2,000-scale maps with contour interval of 10 m. Source: IGAC (1989).
BOUND89:   Boundary of the area for which topographic data are available from 1989, screen digitized from CON89.
DTM89:   Digital terrain model, derived from CON89.
SLOPE89:   Slope map, in degrees, derived from DTM89.
ASPECT89:   Slope aspect map, in degrees, derived from DTM89.
DIF8949:   Elevation difference between the DTMs of 1949 and 1989.
MZGEOL: Lithological units, digitized from a 1:10,000-scale map. Sources: Naranjo and Rios (1989), Chacon and Orozco (1989), Vargas (1990) and Echavarria et al. (1991).
MZFAULT: Faults and alignments, digitized from a 1:10,000-scale map. Sources: Salgado and Chacon (1991), Navarro et al. (1988), Naranjo and Rios (1989).
ISOLINE: Isoseismic map, derived from questionnaires related to damage from the earthquake which occurred

on 23 November 1979. Source: Salgado and Hurtado (1991).
GEOM10:   Geomorphological subunits, derived from interpretation of 1980s aerial photos and fieldwork, and digitized from a 1:10,000-scale map.
SLIDE4010:   Slope instability features, derived from interpretation of 1940s aerial photos, digitized from a 1:10,000 scale-map.
SLIDE6010:   Slope instability features, derived from interpretation of 1960s aerial photos, digitized from a 1:10,000 scale-map.
SLIDE8010:   Slope instability features, derived from interpretation of 1980s aerial photos and detailed fieldwork, digitized from a 1:10,000-scale-map.
MZDRAIN: Drainage lines, digitized from a 1:10,000-scale map. Source: IGAC (1990).
MZLUSE: Urban land use, digitized from a 1:10,000 scale map. Source: Turkstra et al. (1991).
GROWTH: City extensions from 1851, 1930, 1949, 1960, 1970, 1977, and 1989, digitized from a 1:10,000-scale map. Source: Abramovsky (1990).
MZBLOCK: Cadastral city blocks, digitized from a 1:10,000-scale map. Source: IGAC (1990), Turkstra et al. (1991).
MZROAD: Road map, digitized from a 1:10,000-scale map. Source: IGAC (1990), Turkstra et al. (1991).
NETWORKS: Major electrical, telephone, water supply, and sewage networks, digitized from 1:10,000- and 1:2000-scale maps. Source: IGAC (1989, 1990), Innocenti (1992).

5.2.1.4 Summary of graphical data base

Table 5.1 lists all of the files in the graphical data base, indicating for each file the scale on which it was used, the data type, a relative indication of the amount of work required for preparation of the file (not including the work needed to prepare the map before digitizing), and the GIS table(s) connected to the map. The amount of work required to digitize the map is related to the complexity of the map (number of segments to be digitized), and the need to construct polygons. Digitizing detailed contour lines is less time-consuming than digitizing complex unit maps, such as geomorphological or landslide maps.

Table 5.1 and the preceding sections include only those input maps used for analysis at one of the three scales. Listing intermediate and final result maps would make the tables too large. One of the maps that is not listed is the engineering geological map, which is made by combining several input maps, in a procedure described in section 5.4.4.2. The engineering geological map is accompanied by many tables, containing field descriptions of soil outcrops, results of laboratory analyses, and the recalculated values of the data for each soil unit, which were described in chapter 4.

5.2.2 Attribute data base

Practically all data base systems used today for storage and analysis of attribute data (such as ORACLE, INGRES, INFORMIX, DBASE) in connection with geographic information systems are of the relational type. A relational data base is perceived by the user as a collection of tables, called *relations*. Relationships between data from various tables are assessed by matching columns (*key columns*) in two or more tables (Date, 1986). The attribute data base of ILWIS, called TABCALC, is a simple relational data base. Only two tables can be joined at the same time, and the result is written as a new column in the table. All tables are in ASCII format and can be exchanged easily with other software packages.

The attribute data base, described in the following sections, was designed for the ILWIS software package, but can be implemented without major changes in other data base systems. All data were entered in ILWIS for the following reasons:

MAP	SCALE	TYPE	WORK	TABLE
FCC	REG	PIXEL	VS	-
TMU	REG	UNIT	L	MANY[1]
CON100	REG	LINE	VL	-
DRAIN100	REG	LINE	M	-
FAULT100	REG	LINE	S	-
PROCESS	REG	POINT	L	PROCESS
VOLCAN	REG	UNIT	S	VOLCAN
GLACIER	REG	UNIT	S	GLACIER
LANDUSE	REG	UNIT	M	LANDUSE
SOILS	REG	UNIT	L	SOILS
METEO	ALL	POINT	VS	MANY[2]
SISHIST	REG	POINT	VS	EARTHQUAKE
ROADS	REG	LINE	S	-
CITY	MED	UNIT	VS	-
BASE	MED	UNIT	S	-
CONTOUR	MED	LINE	M	-
CONCHIN	MED	LINE	M	-
DRAINAGE	MED	LINE	S	-
DRAINNEW	MED	LINE	S	-
DTM25	MED	PIXEL	S	-
SLOPE	MED	PIXEL	S	-
ASPECT	MED	PIXEL	S	-
ROAD60	MED	LINE	S	-
ROAD80	MED	LINE	S	-
CITY60	MED	UNIT	S	-
CITY80	MED	UNIT	S	-
GEOL25N	MED	UNIT	L	MANY[3]
FAULT25	MED	LINE	M	FAULTS
GEOM25C	MED	UNIT	S	COMPLEXES
GEOM25M	MED	UNIT	L	MAINUNITS
GEOM25E	MED	UNIT	VL	SUBUNITS
SLIDE40	MED	UNIT	VL	SLIDE40
SLIDE60	MED	UNIT	VL	SLIDE60
SLIDE80	MED	UNIT	VL	MANY[4]
LUSE60	MED	UNIT	VL	LUSE60
LU80CHI	MED	UNIT	VL	MANY[5]
LU80PAL	MED	UNIT	VL	MANY[5]
LU80MAN	MED	UNIT	VL	MANY[5]
LUSE80	MED	UNIT	VL	LUSE80
CON49	LAR	LINE	VS	-
DTM49	LAR	PIXEL	M	-
CON89	LAR	LINE	VL	-
BOUND89	LAR	UNIT	VS	-
DTM89	LAR	PIXEL	M	-
SLOPE89	LAR	PIXEL	S	-
ASPECT89	LAR	PIXEL	S	-
DIF8949	LAR	PIXEL	S	-
MZGEOL	LAR	UNIT	M	MZGEOL
MZFAULT	LAR	LINE	S	MZFAULT
ISOLINE	LAR	PIXEL	S	-
GEOM10SLI	LAR	UNIT	VL	GEOM10
DE4010	LAR	UNIT	VL	SLIDE4010
SLIDE6010	LAR	UNIT	VL	SLIDE6010
SLIDE8010	LAR	UNIT	VL	SLIDE8010
MAPSLIDE	LAR	UNIT	VL	SLIDE87
MZDRAIN	LAR	LINE	S	-
M2LUSE	LAR	UNIT	L	MZLUSE
GROWTH	LAR	UNIT	L	-
MZBLOCK	LAR	UNIT	VL	MANY[6]
MZROAD	LAR	LINE	L	-
NETWORKS	LAR	LINE	VL	MANY[6]

[1] The TMU map is the central map for the analysis at the regional scale. Therefore, the information of the other maps is sampled for each TMU and stored in various tables related to the TMU map.

[2] This is one of the data layers used at all scales without change. The map contains the meteorological stations in the area, and is accompanied by a number of tables in which the predominantly daily, meteorological data are stored.

[3] At the medium scale, various maps are accompanied by a separate attribute data base. One of these is the geological map, which is accompanied by tables containing rock description data, taken in the field, and tables in which these data are recalculated for each rock unit.

[4] The landslide map prepared by photo-interpretation of recent aerial photos and fieldwork, is connected to a few tables in which the field description of landslides is stored.

[5] The land-parcel maps from the Federación Nacional de Cafeteros de Colombia (1985) are accompanied by an extensive attribute data base, in which data for the rural area is stored.

[6] The largest data base used in this analysis is the cadastral data base of Manizales, which has been aggregated to the city-block level and is connected to the map MZBLOCK. These data are only sparingly used in the hazard analysis, and are intended mainly for subsequent vulnerability and risk analysis (Innocienti, 1992).

Table 5.1: Overview of the map files present in the data bases for the three different scales. Indicated are the name of the file, the scale, the file type, the relative amount of work required to create the map (VS = very small, S= small, M = moderate, L = large, VL = very large), and the name(s) of the table(s) connected to it. Some maps are connected to many different tables.

1. To reduce the time needed to convert data between ILWIS and other data base systems.
2. To allow rapid connections between the tabular data and graphical data.
3. All data base queries required for this study could be handled satisfactorily within ILWIS, although extra steps were often required since more than two tables could not be combined simultaneously.
4. Many of the analysis techniques required both data base manipulation and plotting of results in graphs, or maps.

In designing the data base, the concept of normalization, or successive refinement (Howe, 1982), was followed as much as possible. Complete normalization was not always achieved, as this would result in too many small tables.

The attribute data base for different types of input data used in this study are presented in the following sections. The more important data base structures are given in the text, whereas relatively minor important ones can be found in appendices 21 to 23. It is beyond the scope of this discussion to explain the contents of each field separately. Instead, the figures containing the various data base structures indicate only the key columns with shading. The most important key columns have dark shading, while those that are used only in connection with descriptive tables are shown in lighter tones. The column names are always followed by a symbol to indicate the data type ($ = string, # = Byte, % = integer, & = real).

5.2.2.1 TMU data base

Hazard analysis at the regional scale is based predominantly on the use of attribute data connected to the TMU map. In general, the different maps used for the analysis, such as land-use or soil maps, are not of sufficient detail that the analysis can be executed on a pixel basis. The units in the TMU map define the polygons for which a hazard score will be given. It is therefore necessary to input all data into tables, related to this TMU map. This is done by map overlay of the TMU map and different input maps.

The data base, presented schematically in figure 5.2, consists of a central table (TMU.INF), which is connected directly to the map, a table (TMUDESC.TBL) with descriptions of terrain mapping complexes, units and subunits, and a table (TMUCROS.TBL) containing the predominant values of a number of variables occurring per Subunit. The individual variables are shown in the lower part of the scheme. These are produced by overlaying with the TMU map. The column Code% is the principal key column, containing the code for the terrain mapping subunits.

5.2.2.2 Meteorological data base

The structure of the meteorological data base is relatively simple (see appendix 21). A table (STATIONS.TBL) contains the locations, in x- and y-coordinates, of the available meteorological stations in the area. Average monthly and yearly rainfall, temperature and evapotranspiration data, are stored in three separate tables (RAINAVG.TBL, TEMPAVG.TBL and ETPAVG.TBL). The table RAINCOMP.TBL contains daily rainfall values for a selected number of days for all stations, to allow evaluation of spatial variability in rainfall. Daily rainfall values for the period 1971-1990 for two central stations in the area (Agronomia in Manizales and CENICAFE in Chinchina) are stored in the table DAYRAIN.TBL, which is very large. The table ANTERAIN.TBL is used to store antecedent rainfall values using windows of 5, 15, and 30 days. The method will be described in section 6.6.

5.2.2.3 Geological data base

Data related to the engineering geological descriptions of the lithological units are stored in the geological data base. The data base structure is shown in figure 5.3, which also indicates the relationship between the various tables and accompanying spatial data. The main table for geotechnical characterization is called ROCKDESC.TBL, which describes for each observation point the lithological group (homogeneous part of an outcrop), lithology, and geological formation. The tables LOCATION.TBL and PROJECT.TBL contain information on the location of the observation points both on the map as well as in the aerial photos, and a general description of the outcrop. The table containing the Schmidt hammer rebound values

(SCHMIDTH.TBL) is combined with the table containing the rock discontinuity descriptions (ROCKDISC.TBL), in order to classify the various rock units with respect to rock mass strength. The table POINTLOA.TBL contains the results of point-load testing on rock samples, and the table ROCKDENS.TBL contains results from laboratory density tests.

The tables mentioned above are combined, using a concatenated key of the observation point code (OP) and the lithological group code (LG) and all data are recalculated per material type (MAT) and stored in the result table ROCKRES.TBL. This table can be used in connection with the engineering geological map (see section 5.4.4.2) to characterize the units displayed in the map with respect to their engineering geological characteristics.
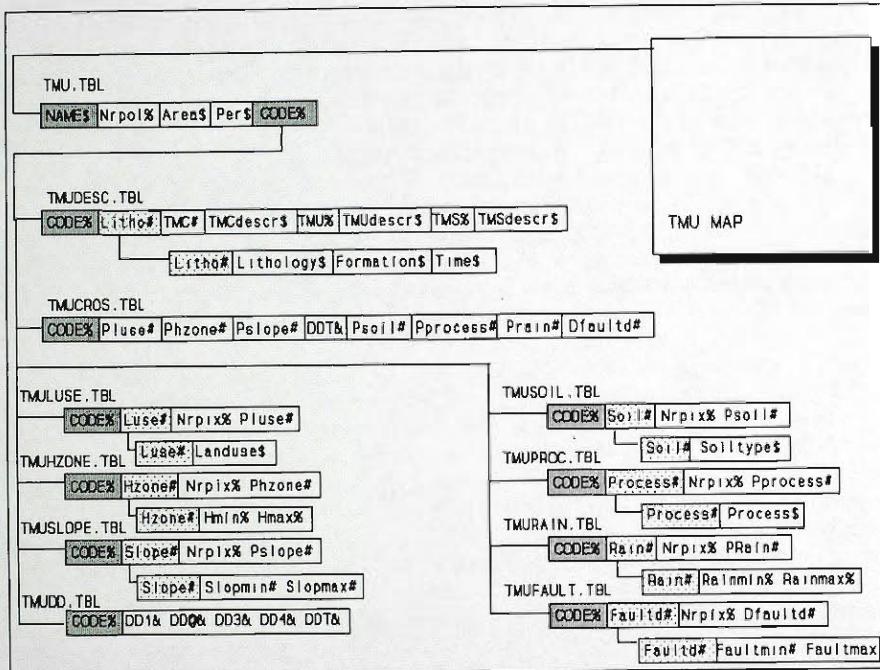
Figure 5.2: Structure of the TMU data base.

5.2.2.4 Landslide data base

Various issues related to the construction of the landslide data base were discussed in section 4.3.2.2, dealing with photo-interpretation of landslides, and in section 4.4.2.2, in which field description techniques were described. Both of these elements are clearly recognizable in the landslide data base (figure 5.4). The table PHOTOSL.TBL, contains basic information on type, subtype, activity, depth, vegetation, and division of scarp and body. In this table all mapped polygons receive a unique code (Slidenr%). A small percentage of all landslides were investigated in the field. Therefore, a connection is made between Slidenr%, which is present

for all landslides, and Mapnr%, which corresponds to the number given in the field. The field data consist of a large number of variables, listed in appendix 4, which have been stored in four different tables (FIELDSL1.TBL, FIELDSL2.TBL, FIELDSL3.TBL, and FIELDSL4.TBL). Description tables are also provided for those variables described by class codes.
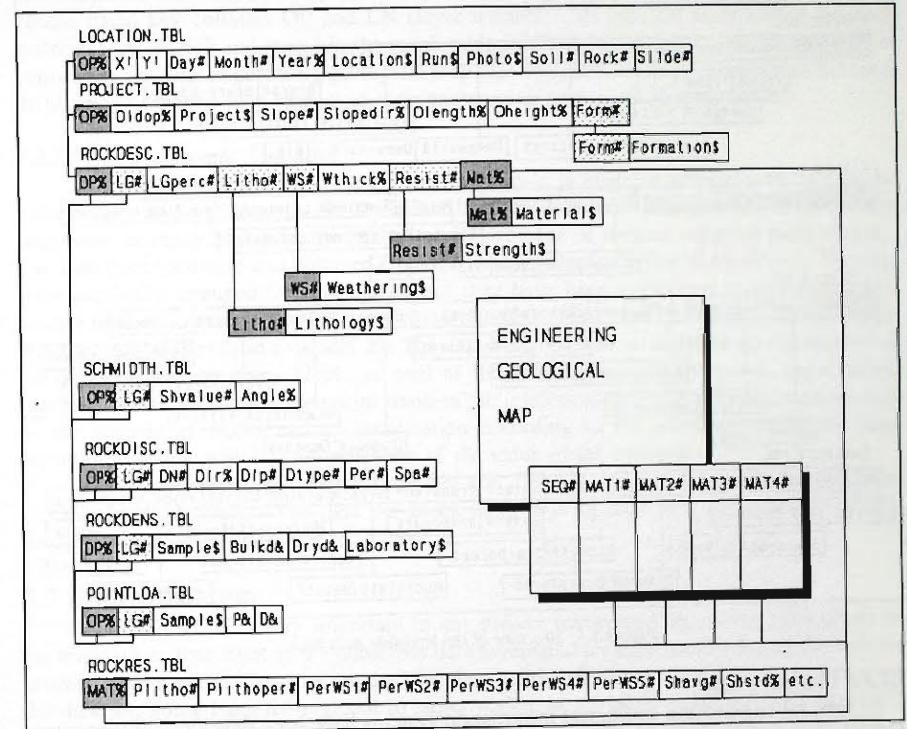
Figure 5.3: Structure of the geological data base.

5.2.2.5 Land-use data base

The land-use data base available for this area was prepared by the Federación Nacional de Cafeteros de Colombia (1985) through elaborate photo-interpretation and field visits using checklists and interviews with farmers. The data base is used mainly for land-use planning. It is, however, also useful for assessing landslide hazard, and even more useful for vulnerability and risk analysis. The data base (appendix 22) contains three different levels of spatial data. The tables FARMS.TBL, PERSONS.TBL, WORKERS.TBL, and MACHINES.TBL are connected to a map with digitized farm boundaries (with key column Farm%), and are in fact only useful for vulnerability and risk studies. The table

PARCELS.TBL is connected to digitized land parcel boundaries within the farm limits, and contains detailed information on the dominant and secondary land use within each parcel. A last table, called HOUSES is connected to a point file, listing all buildings within the rural area and indicating the type of building and the method of construction.
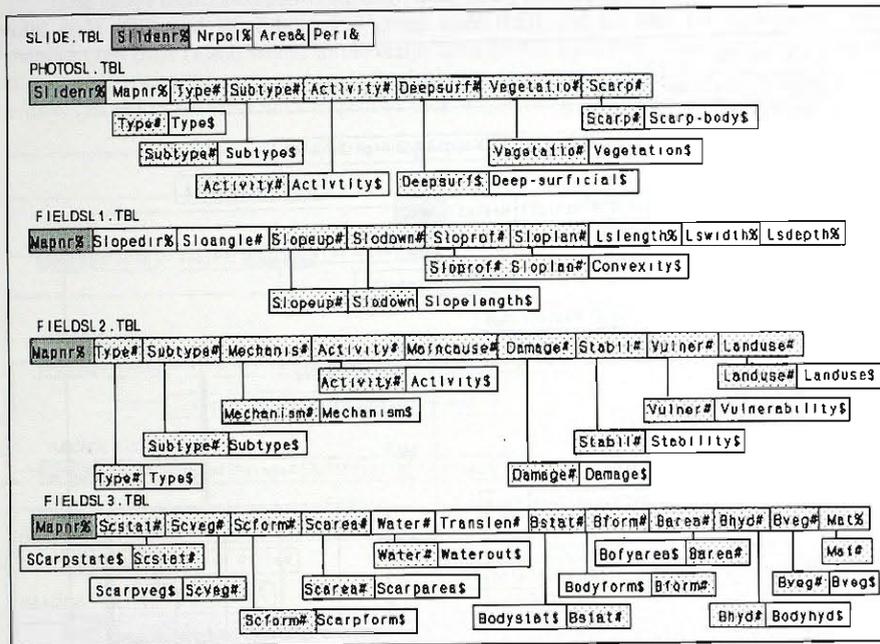
Figure 5.4: Structure of the landslide data base.

5.2.2.6 Soil data base

Several engineering geological information systems have been developed (Rosenbaum and Warren, 1986; McMillan et al., 1987; Raper and Wainwright, 1987; Chaplow, 1986). Most of these systems were developed for specific applications, such as borehole storage. Kooter (1988) presents a fully designed data base structure for an engineering geological information system (EGIS), which, to date, has not been implemented. Although the engineering geological data base designed in the present study is developed primarily for application in slope instability assessment, it can also be used for other applications, such as road planning or construction material analysis. Of course additional data would be included in those cases, but the relationships between the tables could remain the same. The structure of the soil data base is shown schematically in figure 5.5. The principal table in the soil data base is PROFILE.TBL, which contains the relationship between observation points, the number of layers and their thicknesses, and the types of materials (see also table 4.11). This table can be connected to a table containing the location and general information on the

observation points (LOCATION.TBL), via the key columns OP. The data base contains a number of tables with test results, such as soil classifications (SOILCLAS.TBL), grain-size distribution (SOILGRAI.TBL), saturated conductivity (KSATFIEL.TBL and KSATLAB.TBL), water retention (SOILPF.TBL), soil strength (SOILSHEA.TBL), clay mineralogy (CLAYMIN.TBL), and density (SOILDENS.TBL). All field and laboratory test results for the soil materials are stored in separate tables, which are linked to PROFILE.TBL via the concatenated key columns OP and LN (layer number). All data are recalculated for each material type (MAT) and stored in the result table SOILRES.TBL. This table can be used in connection with the engineering geological map (see section 5.4.4.2) to characterize the units displayed in the map with respect to their engineering geological characteristics.

5.2.2.7 Socioeconomic data base

The socioeconomic data base for the large scale is intended primarily for use in the vulnerability and risk analysis. In the hazard analysis only the indication of social class is important, as many landslides are related to the presence of squatter areas on steep slopes. The data base used here was obtained from the land registration office of Manizales. The data were originally arranged by land parcel, but they have been aggregated to the block level (with a total of approximately 2900 records) by Turkstra et al. (1991). The data base structure is shown schematically in appendix 23. The data base contains information on the number of buildings present on every block, as well as the building type (institutional, commercial, industrial, and residential). The social status of the residential houses can be retrieved, as well as the number of floors and a classification according to the point system of the land registration office, which is an indication of the value of the building.

The basic table in this data base is BLOCK.TBL. It is connected to the digitized city block map of Manizales. The data per block have been divided over five different tables, because of the large number of records.

5.3 Data validation

Data validation is very important in any project involving GIS, owing particularly to the tendency to lose sight of the numerous data layers and the data quality during the tedious process of data entry. The time required for data validation increases with the complexity of the data set, going from the regional to larger scales, as is visible in table 2.5. In chapter 7 the various sources and magnitudes of errors introduced will be discussed in detail. Data validation of both spatial and attribute data is achieved by performing cross-checks in the data base. For maps this can be done simply by overlaying different maps to evaluate the possibility of mismatches or incorrectly coded polygons. For attribute data, cross-checks are performed by making various connections between tables. Random checks of records and polygons can also be made. In practice data validation is not performed at a single stage of the process, but is done continuously throughout the project. Inconsistencies in the data are usually detected during data manipulation and data analysis, when strange results occur.
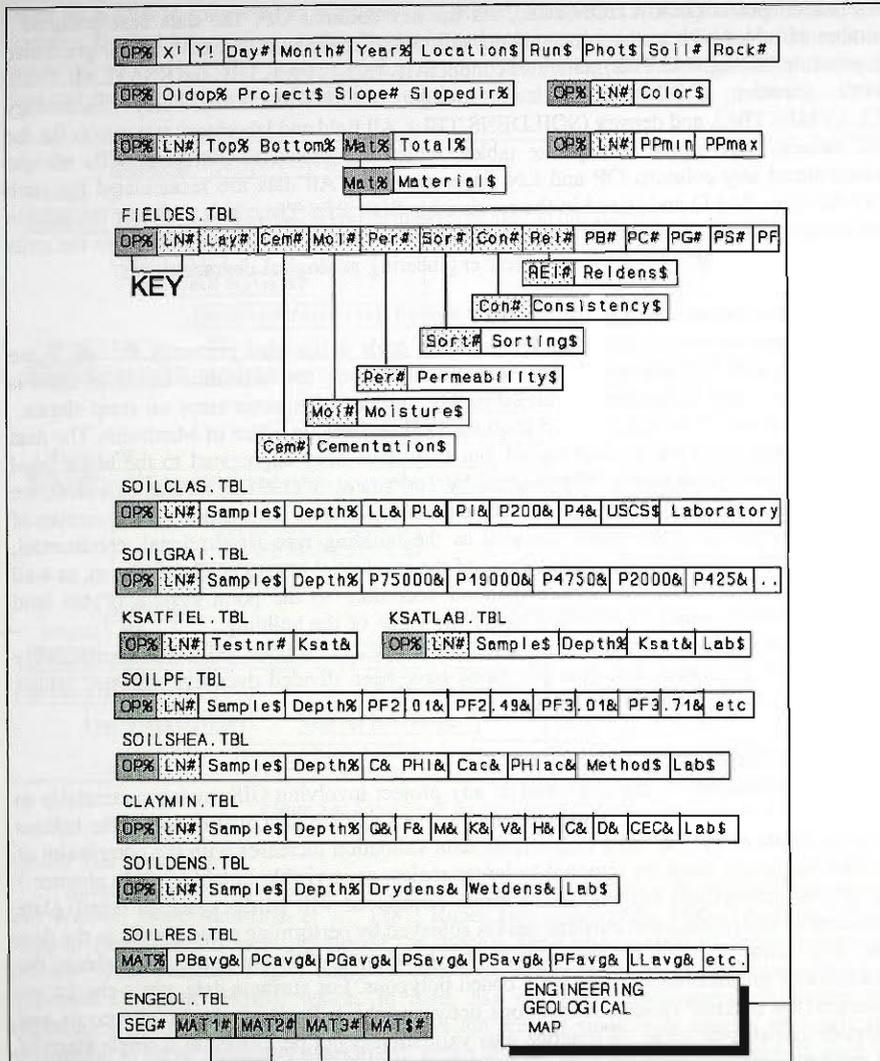
Figure 5.5: Structure of the soil data base.

5.4 Data manipulation

Once map and attribute data have been entered into the GIS data base, they generally cannot be used directly in analysis. Pre-analysis data manipulation must often be executed in order to re-arrange and combine the raw data in such a way that they can be used in the main analysis. Standard data manipulation procedures include construction of raster maps with identical coordinate systems and pixel sizes, construction of DTMs and their derivative maps, and preparation of different input maps for data analysis. In the following sections examples will be given of some specific data manipulation techniques at each of the three scales. Before treating these examples, a short introduction is given on the use of batch and response files, since these files are thought to be indispensable for well-structured data manipulation and analysis.

5.4.1 Batch files

The use of batch files in connection with a GIS is considered essential for a user-friendly analysis. A *batch file* is a file containing commands that are executed one at a time. These commands can be DOS commands, or specific instructions for the various subprograms within the GIS (ITC, 1992). The batch files can be considered "application programs", which allow the GIS to be used for a specific application. The advantages of using batch files are:

- "Decision rules" and sequences of commands are saved. The results of the application of a batch file can be checked, and if necessary the batch file can be modified and executed again.
- The ability to run a batch file with the use of variables allows execution of a similar sequence of commands with different data during each execution. Many GIS analyses require the execution of the same procedure, such as map crossing, for many different sets of input data.

In this research, batch and response files were written for practically all data manipulation and analysis techniques presented in chapters 2, 5, 6, and 7.

5.4.2 Sampling of variables at the regional scale.

Prior to qualitative analysis at the regional scale (section 6.2), which is basically a subjective weighting of the variable classes belonging to the TMU map, it is important to calculate the important factors per TMU. This "sampling" can be done in several ways:

1. By recoding TMUs. Lithology, one of the parameters included in the TMU legend (appendix 1), can be obtained simply by recoding each TMU on the basis of its lithology.
2. By describing factors in sample areas (see section 4.4.1).
3. By crossing with factor maps. For data such as land use, separate maps have to be made; these can later be crossed with the TMU map to determine the dominant land use type per TMU.
4. By sampling variables using counting circles. Topographic variables, such as internal relief, can be sampled from a DTM.

In this section an example will be given of the fourth method, which is quite similar to the use of filters in image enhancement. In this case, however, the filters are very large, and are of a circular form. In order to obtain a value for the internal relief (altitude difference in metres per square kilometre of area) the area of the circles should be approximately 1 km^2.

To do this, a batch file was made in which the following parameters should be entered:
- Name of the map from which sampling would take place,
- Number of lines and columns and pixel size,
- Radius of the counting circles in pixels,
- Minimum X-value and maximum Y-value in the map.

The counting circles are defined by the batch file in the ILWIS table manipulation program, and plotted on the screen using the annotation program. Each circle receives a unique identifier, and the X and Y locations are stored in a table. After crossing the counting circles with the DTM the minimum and maximum heights contained in every circle are calculated and stored in a table. A new set of circles is then made with their centres shifted half the radius of the counting circle away from the first set. In this way four different sets of counting circles are obtained. The internal relief for points in the map, separated from each other by a distance of one-half the radius size, is calculated and plotted as points. Linear interpolation between the points results in a map displaying internal relief. This map is crossed with the TMU map, and average, minimum, and maximum relief intensity per TMU is calculated. This method is preferred to direct crossing of the TMU with the DTM, because TMUs with an elongated form may have a relatively large difference in altitude, although on the whole the internal relief is low.

5.4.3 Preparation of input maps at the medium scale

Most of the analysis methods to be applied at the medium scale require the preparation of a large number of input maps which are not made by digitizing hard-copy maps, but by combining various data layers in the GIS.

Considerable attention was devoted to construction of land-use maps dating from different times, in order to test the hypothesis that land-use change is one of the major triggering factors for landslides in the Chinchina area. The change in farming systems from traditional to "technified" coffee cultivation (see section 3.5.2) is thought to be especially important (Palacios, 1991). As mentioned in section 4.3.2.4, detailed 1:10,000-scale land-use maps at the parcel level exist for a major part of the area. The maps were digitized and polygonized using a complex code, which included the farm number, the parcel number, and the land-use code. The maps for the different municipalities were rasterized, renumbered according to the land-use code, and combined with the photo-interpreted section of Villamaria, for which no map data were available. The photo-interpreted land-use map of the 1960s was also digitized and rasterized, and the maps of the different times were crossed to form a third map, called LUSEDIF, used in the calculation of land-use changes.

A matrix comparing land use in the 1960s and 1980s is given in table 5.2 The rows represent the permillage (‰) land area in a given land use in the 1980s, broken down by the permillage land use of the corresponding area in the 1960s. For example, in the 1980s, 1.9% (19‰) was bare; reading across the top row of table 5.2, it can be seen that in the 1960s, the same land was represented by 4‰ bare, 5‰ grassland, 1, 2, and 4‰ in the three coffee cultivation methods, and 3‰ in other crops. Analogous information for 1960s and the fate of the corresponding land area in the 1980s can be obtained by reading down the columns. The diagonal intersect represents the land area with the same land use in the 1960s and the 1980s. The original land-use classes have been classified into nine main units in table 5.2 so that the result can be more easily evaluated.

LANDUSE IN THE 1980s	LANDUSE IN THE 1960s									TOTAL in 1980s
	1	2	3	4	5	6	7	8	9	
1 = Bare	4	5	0	1	2	4	3	0	0	19
2 = Grassland	1	44	0	8	21	13	3	0	1	91
3 = Shrubs	0	4	0	2	3	9	0	0	0	18
4 = Technified coffee without shade trees	2	115	4	77	114	166	16	4	2	500
5 = Technified coffee with shade trees	1	17	1	16	75	27	5	3	1	146
6 = Traditional coffee	0	0	0	0	0	115	0	0	0	115
7 = Other crops	0	16	0	7	13	9	10	0	0	55
8 = Forest	0	1	0	0	1	2	0	3	0	7
9 = Constructed area	0	26	0	3	4	4	0	0	12	49
Total land use in the 1960s:	8	228	5	114	233	349	37	10	16	1000

Table 5.2: Land-use changes since the 1960s, given in permillages of the total area. The rows show the land use in the 1980s and the columns the land-use in the 1960s.

From the table it can be concluded that land use is very dynamic over time. Only 34% (sum of the diagonal intersect values) of the area has remained unchanged over a period of 30 years. The largest changes are related to the extension of the area for coffee cultivation. Although only 6.5% of the area was changed from another land use to coffee, there was a very important change in farming systems for coffee cultivation. By the 1980s "technified" coffee cultivation without the use of shade trees was practised in half of the study area. The percentage occupied by traditional coffee decreased from 35 to 11.5%. Most of the newly acquired area for coffee cultivation were formerly under grass. The percentage of grassland decreased strongly from 23 to 9%. Another remarkable change is the increase in bare soil which is partly a result of mass movements and soil erosion, but is mainly due to the devastating lahar, which occurred in 1985, and which stripped all vegetation and soil cover in a large part of the Rio Chinchina valley. Between the 1960s and the 1980s the city of Chinchina grew considerably (from 1.6 to 4.9%).

It is important to keep in mind that land use is very dynamic in this area, and that these changes will have an important influence on the occurrence of mass movements, and the production of landslide hazard maps. As the land-use situation changes constantly, a hazard map should in fact also be adjusted constantly.

5.4.4 Preparation of input maps at the large scale

Deterministic modelling to assess landslide hazard, which is one of the techniques proposed for the large scale, requires preparation of a number of variable maps. One of the most important maps which has to be prepared via data combination is the engineering geological map. This map displays for each pixel the vertical material sequence, including both soil and rock types, that can be expected at that point. In an accompanying data base each material sequence is characterized by the variables presented in chapter 4.

It was decided not to construct this map directly from aerial photo interpretation and/or fieldwork for the following reasons:
- Correctly interpreting material sequences from aerial photos is difficult or impossible. Attempts to do this failed.
- Many of the factors used to determine material sequences are present in other maps, such as the slope map, the geomorphological map, and the geological map.

5.4.4.1 Ash thickness map

Preparation of an ash thickness map was based on the following considerations:

- Lithological information can be taken from the geological map, and the various rock units can be regrouped with respect to their rock mass strength.
- Information on soil types can be derived from the geological map for residual soils, and from the geomorphological map for transported soils.
- The presence of volcanic ash has created a special situation in the Rio Chinchina area. This material has blanketed the terrain, and then been partly removed by denudation.

In order to model ash thickness in the area, a model had to be made, explaining the variation in thickness based on other mappable phenomena. The thickness was considered to be related to the following parameters:

1. Distance from the volcano. The x-coordinate can be used to estimate this distance, because the ash sources (the Nevado del Ruiz and the Cerro Bravo volcanos) are both located in the far eastern portion of the area. Over the entire area this distance is of great influence, as discussed in section 3.3.2. But over relatively small areas the effect can be neglected.
2. Slope direction. During ash deposition the exposure of the slope with respect to the wind direction is an important consideration. On the leeward side of a hill ash accumulation was greater than on the windward side.
3. Local topography. In describing the soil profiles, it was found that the topography preceding ash deposition is a very important factor. However, this information can be obtained only by detailed drilling or geophysical measurements, which have to be restricted to small areas. For this reason it was not used in the analysis.
4. Denudational slopes. Ash thickness is believed to be much less on those slope sections where denudation has been considerable. Locations of such sections can be obtained partly from the geomorphological maps. This information is, however, difficult to use in practice, as most of the terrain has a denudational origin. Patterns of landslides and erosion change over time and may have affected areas that seem quite stable nowadays.
5. Slope angle. There should be a relationship between the slope angle and the ash thickness; thick ash will be expected mainly on flat or gently dipping slopes, while steep slopes are expected to have lost their ash cover by denudation.

For the entire Chinchina area a very general 1:100,000-scale map depicting ash thickness exists (Florez, 1986), but this map was not useful for work at the large scale.

Material sequences and layer thickness were measured for a large number of points throughout the area, and stored in the table PROFILE.TBL in the soil data base (see figure 5.5). From this table, ash thickness was calculated for each soil observation point. These points were plotted on a map, which was crossed with the slope map to compare ash thickness with the average slope angle in the area surrounding the point. The resulting plot of slope angle against ash thickness is given in figure 5.6. The graph shows a weaker relationship than expected. Low slope angles often also have thin ash covers. There is however an apparent upper limit in the graph, shown by the line, C, with the following equation: $T_{ash} = 1500 - 25A$ (where T_{ash} is the ash thickness in cm, and A is slope angle in degrees). This can be considered to yield the maximum ash thickness that could be expected at a certain slope angle. In practice, ash thickness varies between this maximum and a total absence of ashes, due to post-depositional erosion. A second line, D, in figure 5.6,

by the function $T_{ash} = 1100 - 25A$, is considered to be the "common" relationship between ash thickness and slope. It is merely an indication of a general trend, and actual values may deviate strongly from this. In section 6.5.3 the relation is evaluated critically using an infinite slope model.
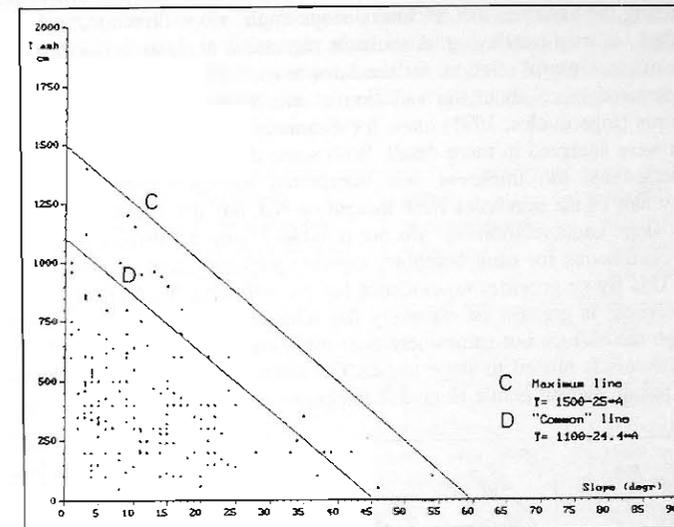
Figure 5.6: Relationship between slope angle and ash thickness for the soil observation points investigated in the field.

The weak relationship is caused by the following factors:

- Most of the soil descriptions were made in soil outcrops near human activity, such as along roads, houses etc. At these locations the ash may have been partly removed, or the thickness may have been under- or overestimated due to the slope angle of the cut slope, which is often not vertical. In the ideal case only observations from boreholes should be used, but this would result in a data set with too few observations.
- Some of the observation points taken from existing reports do not describe the entire profile, but only the upper section. If these points are used, ash thickness is underestimated. These points should be omitted.
- All observation points were considered, even those in areas which have been partly eroded, notwithstanding the relatively low slope angles at those locations. Transported ash soils in landslides were not described as ash, but as colluvial soil. This results in the absence of ash in some areas with low slope angles. Points measured in alluvial deposits in valley floors also result in the absence of ash in areas with low slope angles.
- The slope map used to determine the relationship between ash thickness and slope angle is of rather poor quality. This will be demonstrated in section 7.2.2.

- The points displayed in the graph are derived from all over the study area, with greatest density in the area between Manizales and Chinchina. The observation points all come from different geomorphological units, and are all a different distance from the volcano, which also influences the thickness of the ash cover.

To investigate the relationship between ash thickness and variables other than slope, a matrix containing the variables ash thickness, slope angle, slope direction, and x-coordinate was constructed via map overlaying. A multiple regression analysis performed on this data set did not result in a useful relation, for the same reasons discussed above.

To understand more about the variation of ash thickness within a small region, 97 borehole records (Ingeosuelos, 1991) made for a sanitary landfill project in the northern part of Manizales were analyzed in more detail. With some difficulty, due to the poor quality of the soil descriptions, ash thickness was interpreted for each borehole. Unfortunately, approximately half of the boreholes were located on old, but still active, landslides, so their ash thickness-slope angle relationship was not reliable. Figure 5.7 displays the measured ash thickness in centimetres for each borehole, together with elevation contours and landslide information. This figure provides no evidence for the following hypotheses:

- Ash thickness is greatest on relatively flat hilltops. The thickest ash profiles are not found on the hilltops but somewhere near mid-slope.
- Ash thickness is related to slope angles. On steep slope sections, ash thickness up to 9 m is found, and on gentle slope ash thickness less than 1 m occurs.
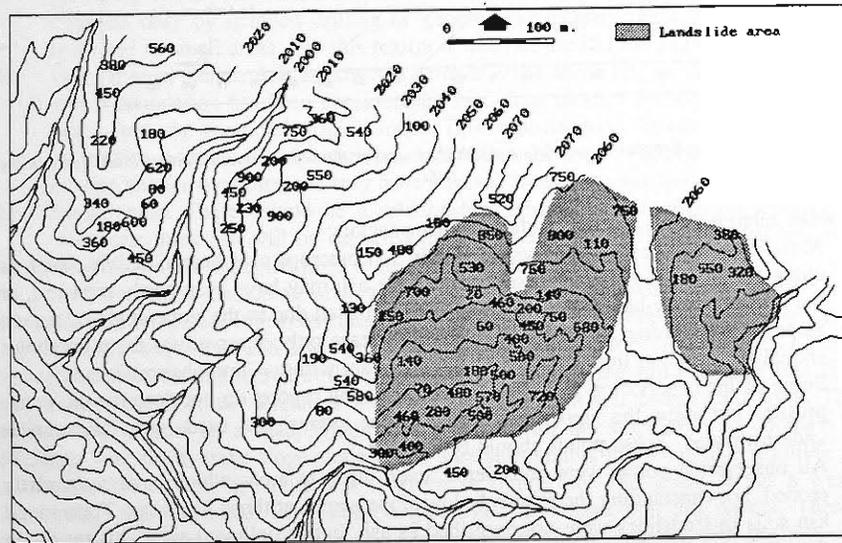
Figure 5.7: Ash thickness (in centimetres) for drillholes in a small area north of Manizales (sanitary landfill area). Elevation contours are in metres. Areas of active landslide are shaded.

This data set for a relatively small area failed to yield a useful model to estimate ash thickness. In conclusion, no clear relationship between ash thickness and one, or more, mappable phenomena was found. Since ash plays a very important role in slope stability analysis, as was concluded from field descriptions of landslides, more detailed investigation on this aspect will be required.

In subsequent analyses the "common relation" between ash thickness and slope angle (shown in figure 5.6) is used as a general estimation of ash thickness. The quality of the ash thickness map can be improved by using other data, such as a geomorphological map, a landslide map, and DTMs from different times. The method for using all of these data to estimate ash thickness is given in figure 5.8.
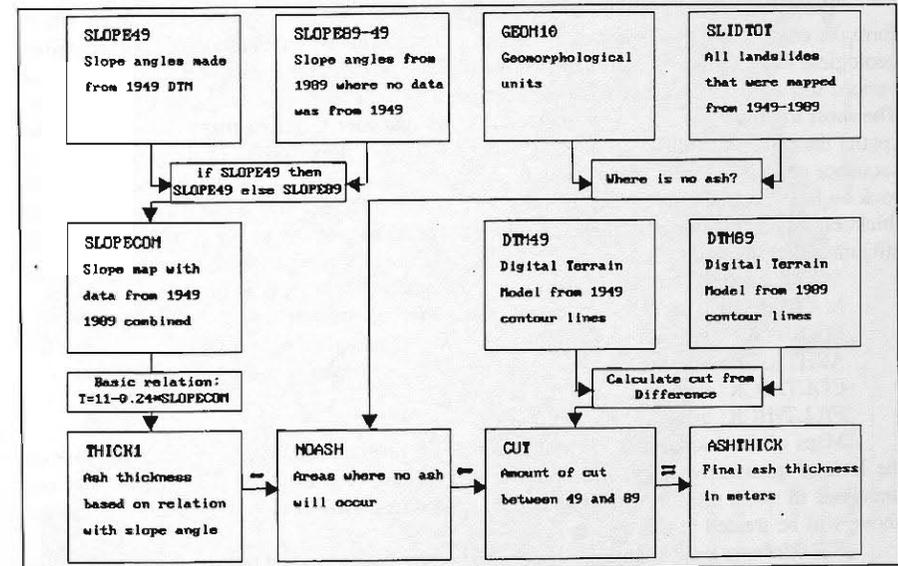
Figure 5.8: Working method for preparation of an ash thickness map of the Manizales area.

In the large-scale study area terrain movements related to the construction of new townships are many and very important. The amount of cut and fill can be calculated by comparing the DTMs from two different times (see section 5.4.4.2). The slope angles used in the relationship for ash thickness should be the original ones, before earth movement took place. Therefore the slope angles from the 1949 data were used when available, and for the rest of the area, where no 1949 data were available, the 1989 data were used. These slope angles were combined in the map SLOPECOM. Ash thickness was then calculated from this map using the "common" formula given in figure 5.6. Areas where no ash is expected, even though the slope angle may be low, can be obtained from the geomorphological and landslide maps. From these two maps a bit map was made (NOASH), indicating where no ash cover is expected. In the next step, ash thickness was reduced by the amount of cut which had taken

place. This amount of cut was calculated from the elevation differences between the 1989 and 1949 DTMs. By subtracting the amount of cut from the calculated ash thickness the final ash thickness map was made (See figure 5.9).

It is important to mention that areas where urban fill is found are not omitted from the ash thickness map. This was done considering the fact that urban fill is usually deposited over the original terrain, which may have an ash cover. Another remark related to the ash thickness map is that areas where landslides occur are considered to have no ash cover, because either the ash was removed by the landslide, or the ash was redeposited, and is now classified as slope deposits. This will be worked out in further detail in section 5.4.4.2.

5.4.4.2 Engineering geological map

The ash thickness map, treated in the preceding section, is only one of the maps which form the engineering geological data base. The method for the preparation of an engineering geological data base, presented here, allows storage of the three-dimensional distribution of various soil and rock layers without the need for a truly three-dimensional data base structure. The most important aspect of the methodology is that four different maps are made for the spatial distribution of different material types in the four upper layers of the profile. So if a sequence of four different materials is found, for example ash on residual soil on weathered rock on fresh rock, these four layers are stored in four different maps. The distribution of the thickness of each material is stored in different maps, to prevent overly complicated legend structures. For the Manizales area the following engineering geological data layers were made:
- MAT1: spatial distribution of the various materials occurring at the surface;
- MAT2, MAT3, and MAT4: spatial distribution of the materials in layers 2, 3 and 4;
- SEQUENCE: spatial distribution of the various material sequences;
- ASHTHICK: ash thickness map presented in the former section;
- COLTHICK: slope deposits thickness map;
- FILLTHICK: urban fill thickness map.

Maps of the thickness of alluvial material and residual soils were not made because of the lack of quantitative data, and because their thickness is usually so great that it is not important in slope stability calculation. The procedures used to create the maps mentioned above will be treated in this section.

Fill thickness map. Manizales is constructed over very rugged terrain, and construction of most parts of the city required large volumes of material to be moved to create smooth topography on which housing construction could take place (see section 3.5.3). Evaluating the volume of earth moved is important in preparing the engineering geological map. In areas from which material has been removed, it is important to know the total thickness of soil material excavated, in order to predict which material is exposed after cutting. When the total thickness of moved material was low, ash may still be present. Otherwise, residual soil underlying the ash will be exposed. For the areas where material was deposited it is important to know the thickness of fill. In this evaluation, DTMs from different years can play an important role. Two DTMs (one of 1949 and one of 1989) were subtracted yielding the change in topography for each pixel. Differences smaller than 3 m were not taken into account, as they are within the accuracy of the procedure followed. Figure 5.10 displays the classified cut and fill thicknesses for the Manizales area. The amount of cut or fill for those parts of the city which already existed in 1949 is not correct.
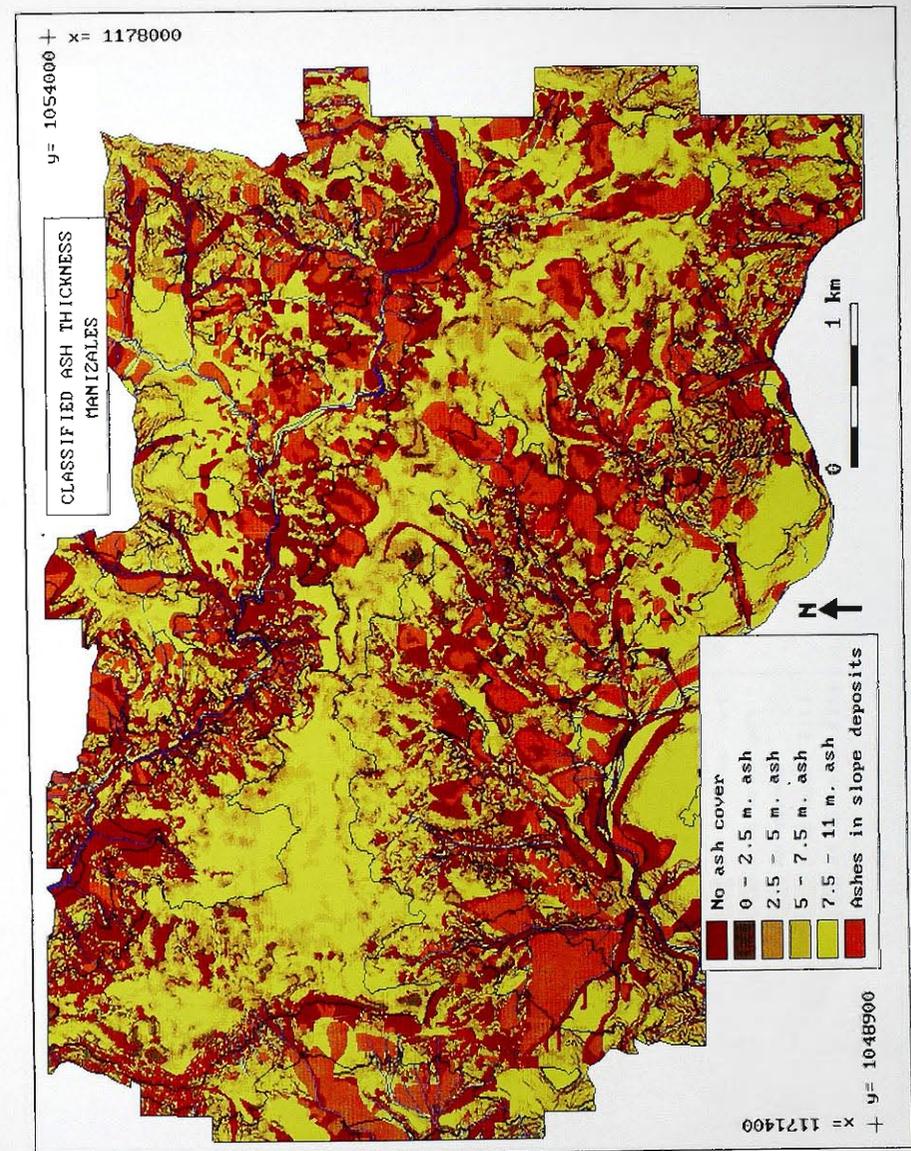
Figure 5.9: Classified ash thickness map of Manizales.
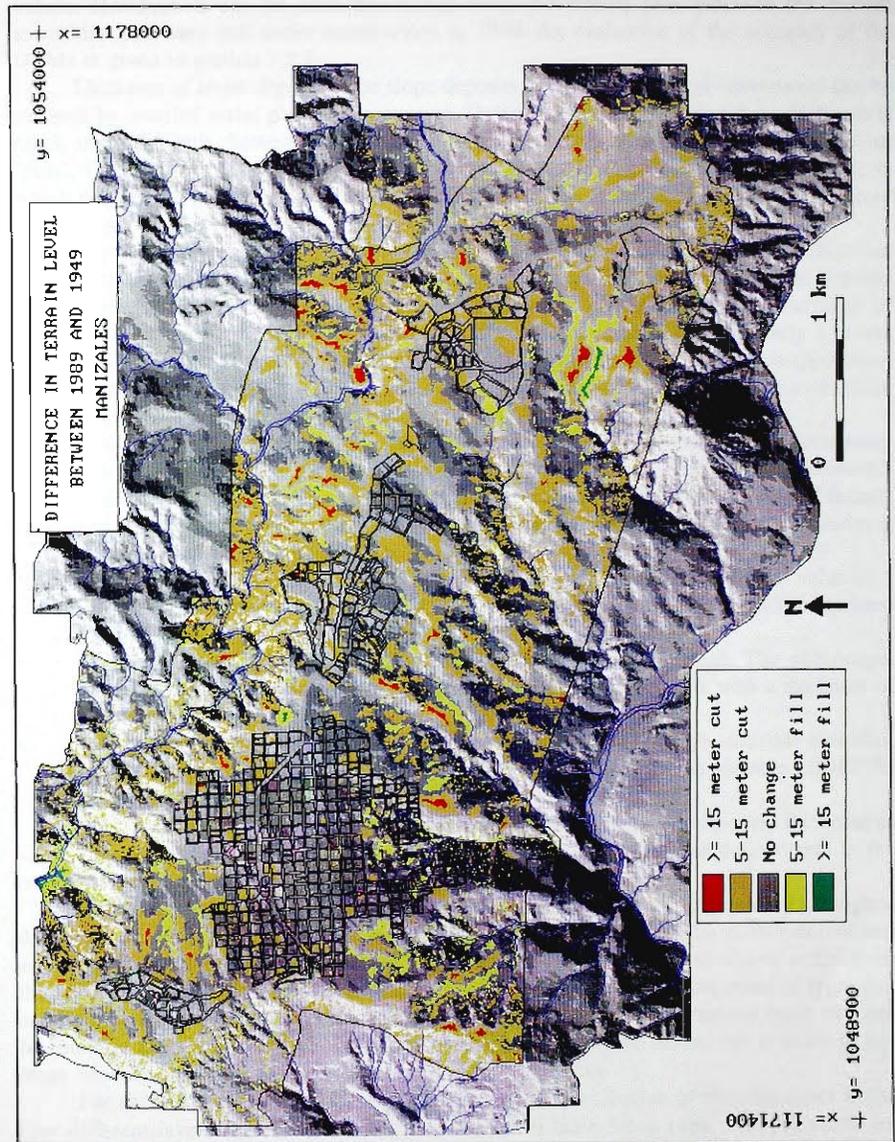
Figure 5.10: *Classified cut and fill thicknesses in the urban area of Manizales in the period 1949-1989.*

Therefore, the area covered by the city in 1949 is displayed in figure 5.10 to mask off the values. However, it can be seen that minor earth movements took place in the eastern townships that were still under construction in 1949. An evaluation of the accuracy of the DTMs is given in section 7.2.3.

Thickness of slope deposits. The slope deposits resulting from mass movements can be mapped by detailed aerial photo interpretation. Determining and presenting their thickness is much more difficult, however. This can be done only in qualitative classes of "thick" or "thin". Delineation of slope deposits can be obtained from the geomorphological map, in which the very large landslides are indicated, and from the landslide occurrence maps from different periods.

The mass movement complexes in the geomorphological map (GEO10) were classified as being thick (> 5 m). From the landslide occurrence maps, the thickness of slope deposits can be obtained in three different classes: absent, small, and great. In the description of landslides a parameter DEEPSURF is included, for which a limit of approximately 5 m was used to differentiate between deep and surficial mass movements. All landslides mapped from aerial photos from the 1940s, 1960s, and 1980s were taken into account for the evaluation. Mass movements were classified as follows:

- Landslide type 4: "Derrumbes" are failures resulting in the transport of material away from the source area towards a stream or a road. The occurrence of "derrumbes" therefore does not result in an accumulation of slope deposits at the location of failure. The affected materials (often ash) are removed from the slope and the underlying material (usually residual soil) is exposed.
- Landslide types 1 (slide), 2 (flowslide), and 3 (flow), with a DEEPSURF value of 1 (surficial). The mass movements fulfilling these requirements were considered to have a thickness of slope deposits of 5 m or less.
- Landslide types 1, 2 and 3, with a DEEPSURF value of 2 (deep). The phenomena fulfilling these requirements are considered to have slope deposits with a thickness of 5 or more.
- Mass movements of types 1, 2 and 3, which were described using a landslide checklist, can be displayed with their actual depth, by renumbering with the variable LSDEPTH from the FIELDSL2 table (figure 5.4).

This method produces a map that gives a good indication of the expected thickness of slope deposits. When more field measurements of landslide depth become available in the course of a landslide hazard project, the map can be updated easily.

Modelling material sequences. The last step in constructing the engineering geological data base is creation of material sequence maps, in which both the spatial distribution of soil and rock types can be presented, as well as the vertical sequence, without adding actual layer thickness values. The first step in the analysis is determination of the main material types that can be found, either at or below the surface. Table 5.3 lists the main material types that can be found in the Manizales area. For these eight material types no distinction is made at this stage between materials from different geological formations.

For each of the four maps that display the spatial distribution of material types in the four different layers (MAT1 to MAT4), the legend of table 5.3 is used. The procedure for creating the MAT1 to MAT4 maps is given schematically in figure 5.11. The maps displaying the thickness distribution of ash, slope deposits, and fill are used, as well as the slope map

117

and the geomorphological map. The surface material map (MAT1) is given in figure 5.12.
The surface material map (MAT1) is made using the following steps:

MATNR	MATERIAL
1	Ashes
2	Residual soil
3	Weathered rock
4	Fresh rock
5	Slope deposits
6	Alluvial deposits
7	Urban land fill
8	Hydraulic fill

Table 5.3: Main material types that occur in the Manizales area.

• An extra column called MATNR is created in the table connected to the geomorphological map.
• Those pixels in the map FILLT which have a (non-zero) value for fill are classified as urban land fill (code number 7 in table 5.3), or hydraulic fill (number 8), based on the information from the column MATNR in the geomorphological table.
• Those pixels in the map COLMAP which have a (non-zero) value for slope deposits are classified as slope deposits (number 5), if they were not yet classified in the first step.
• Those pixels with values for alluvial sediments at the surface (information derived from the geomorphological map) are classified as alluvial deposits (number 6), if they have not yet been classified in the previous steps.
• Those pixels in the map ASHT which have a (non-zero) value for ash thickness are classified as ash (number 1), if they were not yet classified in earlier steps.
• The remaining unclassified pixels are classified as residual soil (number 2) when the slope angle is less than 60°, and as weathered rock (number 3) when the slope angle is equal or greater than 60°.

Figure 5.11: Procedure for the construction of the material maps MAT1-MAT4.

Figure 5.12: Surface material map of Manizales.

The map displaying the material types occurring in the first layer below the surface (MAT2) is made using the following steps:

- Those pixels that have been classified in MAT1 as urban fill or hydraulic fill and have underlying slope deposits are classified as material number 5. If they do not have slope deposits but ashes underlying the fill, they are classified as material number 1, and otherwise as number 2.
- Those pixels classified as 5 (slope deposits) in MAT1 are classified as residual soil (number 2).
- Pixels classified as alluvial material in map MAT1 are classified as weathered rock (3).
- Ash in MAT1 is assumed to be underlain by residual soil in MAT2.
- Residual soil in MAT1 is assumed to be underlain by weathered rock in MAT2.
- Weathered rock in MAT1 is assumed to be underlain by unweathered ("fresh") rock in MAT2.
- Unweathered rock in MAT1 is also classified as such in MAT2.

Analogous steps are followed for the construction of maps MAT3 and MAT4. The last map consists almost completely of fresh rock.

The engineering geological maps presented so far cannot be connected directly to the geotechnical attribute data base discussed in chapter 4 and in section 5.2.2.6. In order to make this possible, the material types should be subdivided on the basis of geology, so that the material codes of table 4.11 can be used. In order to do this the four maps MAT1-MAT4 are combined with a geological map using a two-dimensional table (see table 5.4). Using this table the residual soil, weathered rocks, and fresh rocks can be subdivided in units related to lithology. For each combination shown in table 5.4 the material code of table 4.11 can be added as an extra column (shown in parentheses in table 5.4). All relevant geotechnical data can be retrieved from the tables containing the recalculated point observation data (section 5.2.2.6) through table joining.

Lithological units occurring in the Manizales area	MATERIAL TYPES (from table 5.3)							
	1	2	3	4	5	6	7	8
Debris flow materials (300)	10 (100)	21 (312)	31 (311)	41 (311)	50 (400)	60 (210)	70 (520)	80 (520)
Lavas (610)	10 (100)	22 (611)	32 (612)	42 (613)	50 (400)	60 (210)	70 (520)	80 (520)
Gabbros (730)	10 (100)	23 (731)	33 (732)	43 (733)	50 (400)	60 (210)	70 (520)	80 (520)
Metasedimentary rocks (920)	10 (100)	24 (921)	34 (922)	44 (923)	50 (400)	60 (210)	70 (520)	80 (520)
Manizales formation (1020)	10 (100)	25 (1021)	35 (1022)	45 (1023)	50 (400)	60 (210)	70 (520)	80 (520)
Casabianca formation (1030)	10 (100)	26 (1031)	36 (1032)	46 (1033)	50 (400)	60 (210)	70 (520)	80 (520)

Table 5.4: Matrix for subdividing the material types from table 5.3 (shown in column header) for the different geological units (shown in row header) resulting in a new two-digit numbering. The numbers in parentheses refer to the material code of table 4.11.

119

At this stage, engineering geological information can all be read all simultaneously using the RDPIX (read pixel) program in ILWIS, which allows values to be read for each pixel from various maps together with related information from tables. The types and spatial distribution of the material sequences are read from the maps MAT1-MAT4, the thickness of ash from the map ASHTHICK, the thickness of fill from the map FILLTHICK, the thickness of slope deposits from the map COLTHICK and the geotechnical data from tables linked to the MAT1-MAT4 maps, which all have the codes of table 5.4 attached as key column in accompanying tables. Figure 5.13 shows schematically how information on layer sequences as well as depths is obtained for each pixel.
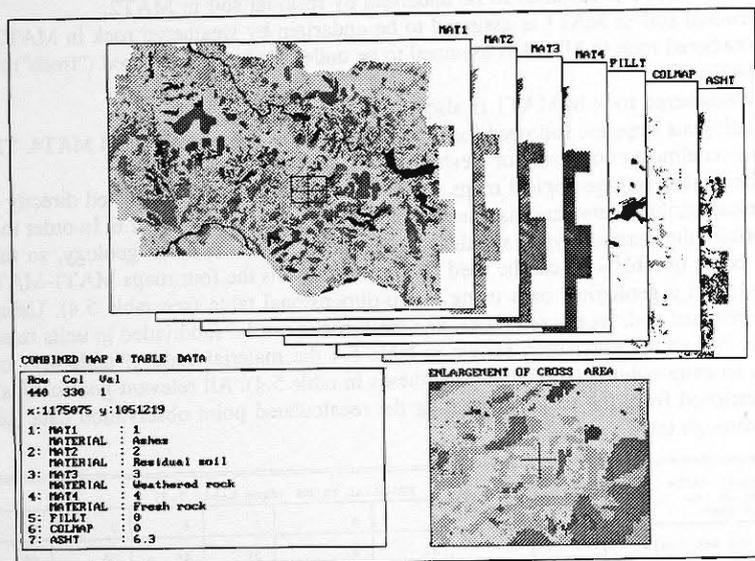
Figure 5.13: Schematic representation of how the engineering geological information is read from various maps and tables using the RDPIX program in ILWIS.

The method presented here is, however, based on several assumptions that are not always realistic:

- Ash thickness is related to slope angle as discussed in section 5.4.4.1.
- Slope deposits are underlaid by residual soils, due to removal of the ash cover.
- Alluvial deposits are underlaid by weathered rock.
- Urban fills may be underlaid by slope deposits, ash or residual soil, depending on the conditions in 1949.

The method is based primarily on the use of geomorphological information in the delineation of material types, and not on existing borehole data. The information on the spatial distribution of material types is more reliable than the thickness information, as this distribution can be obtained from detailed geomorphological maps. The fact that the maps are

made for relatively large areas implies that considerable generalization has taken place. When the method is used by a local agency over a longer period, new field observations can be added at any time, and the whole procedure is repeated, using batch files, leading to a successive improvement of the quality of the maps.

5.4.4.3 Groundwater simulations

One of the main factors which should be dealt with before executing a deterministic landslide hazard assessment at the large scale is the role of water in slope instability phenomena. Slope stability analysis of a number of the measured landslide profiles in ash overlying residual soils suggested the necessity to introduce positive pore water pressures into the calculations. Groundwater information from previous studies in the area proved to be very scarce. Groundwater levels are occasionally recorded in the borehole records (CRAMSA, 1990, Geotecnia, 1980; Ingeosuelos, 1991). Most of the borehole descriptions did not contain information on phreatic levels. This does not necessarily indicate that no groundwater was encountered. Usually it was simply not noted.

In order to obtain better insight into possible groundwater levels in the ash-covered slopes, a simulation model was used to assess ground water fluctuations in relation to precipitation. The best groundwater models are of a three-dimensional nature. To execute such models in a GIS, extensive neighbourhood operations should be performed. Unfortunately, the neighbourhood options in the latest version of ILWIS became available only after most of the present analyses had been completed. Therefore, analysis was based on a two-dimensional model, SLOHYD, developed at the University of Utrecht (Van Asch et al., 1992). This computer model calculates ground water fluctuations in layers with different hydrological constants (maximum five layers are allowed). A topographic slope can be subdivided into a number of vertical slices (maximum 30). In each slice, vertical unsaturated flow is assumed, while saturated flow can also occur horizontally. The model also allows for infiltration, evapotranspiration, and capillary rise of water (Van Asch et al., 1992). For each soil layer the saturated conductivity (K-sat), the volumetric pore space, the initial water content at field capacity, the Rijtema *nu* constant (Rijtema, 1969) and the Irmay n constant (Irmay, 1954) for the calculation of unsaturated hydrological conductivity, are entered. The last two values were obtained from tables relating these constants to soil texture. Profile boundary conditions, such as the groundwater height at the top and bottom of the profile, the amount of subsurface inflow from upslope, and the initial soil water condition of the soil layers, also have to be specified. The following daily climatic data are entered: Temperature (degrees Celcius), rainfall (mm), and potential evapotranspiration (mm). If values for rainfall intensity (mm/hour), available water (mm), and maximum evapotranspiration (mm) are not entered, the program estimates these using the data for temperature, rainfall, and PET.

The program allows groundwater levels during successive years to be calculated by taking the groundwater value for the last day of a previous year as the initial value for the next. The groundwater simulation models can be used in connection with a GIS in two ways:

1. Profiles, automatically sampled from a DTM, are read in the program together with soil information from the engineering geological map, and groundwater levels for a certain period of time are calculated.

2.   Standard slope profiles, with given slope length, angles, and soil profile, are calculated and the result is connected to similar slopes in the terrain.

Although the first method is much more precise, because it works on actual profiles taken from the terrain, it is far too time-consuming to apply over a large area. Therefore, the second method was used here, which necessarily leads to a simplification of the terrain. Standard profiles were selected with a combination of the following input data:

- Slope length: 50, 100, and 200 m;
- Slope angle: 15, 25, and 35 degrees;
- Ash thickness: 2, 6, and 10 m;
- K-sat of ash: 0.2, 0.4 and 0.8 m/day;
- K-sat of residual soil: 0.005, 0.01 and 0.1 m/day.

Initially a two layer model was used with different K-sat values for the ash and the underlying residual soil. A certain infiltration value was assumed for the weathered rock below the residual soil. No data were available on the saturated conductivity of the weathered rock. A value of 0.005 m/day was assumed. This two layer model yielded erroneous results, as the groundwater level increased above the contact of the two layers, without lowering in drier periods, due to errors in the program. For this reason the model was simplified to a one-layer model of ash over residual soil.

The method is presented schematically in figure 5.14.
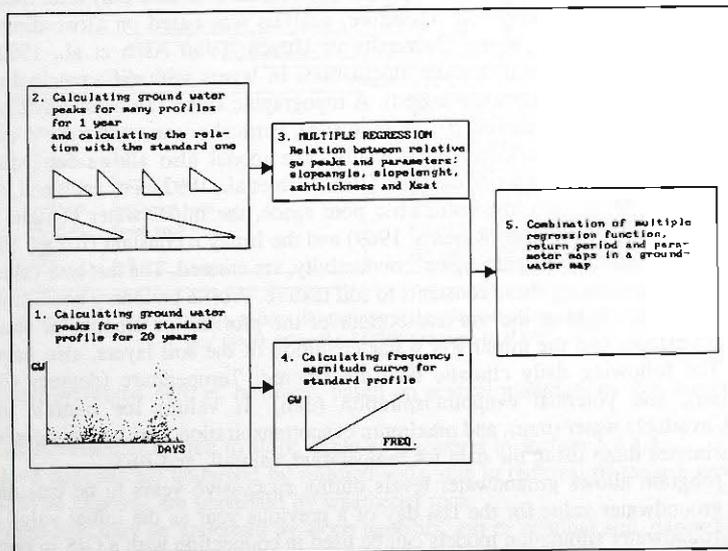
Figure 5.14: Working method for groundwater modelling.

The following steps were used to simulate groundwater levels in the Manizales area:
1.   Calculation of ground water fluctuations for a 20-year period on one standard slope.
2.   Calculation of groundwater fluctuations for one year in slopes with different slope angles, lengths etc., and comparison of the results with the values for the standard slope for the same year.
3.   Calculation of the relationship between the variables evaluated (slope angle, slope length, K-sat etc.) and the groundwater fluctuations for one year.
4.   Prediction of peak levels for all profiles by combining the results of steps 1, 2 and 3.
     5.   Calculation of groundwater maps based on the result of 4 with input maps for slope angle, K-sat, slope length etc. in GIS.
Each of the steps is presented in greater detail in the following paragraphs.

1. *Calculation of groundwater fluctuations for a 20-year period on one standard slope.* A representative profile was selected, with a slope length of 100 m, a slope angle of 25°, an ash thickness of 6 m and saturated conductivity of ash and residual soil of 0.4 and 0.01 m/day, respectively. Groundwater levels were calculated over a 20-year period using SLOHYD (1971-1990). Figure 5.15 shows the groundwater level peaks for the 20-year period plotted in one graph with the days of the year as x-axis. Two concentrations of peak levels can be seen, corresponding to the two yearly maxima in rainfall, of which the second achieves higher values. The highest peak within this 20-year period is 150 cm above the ash-residual soil contact.
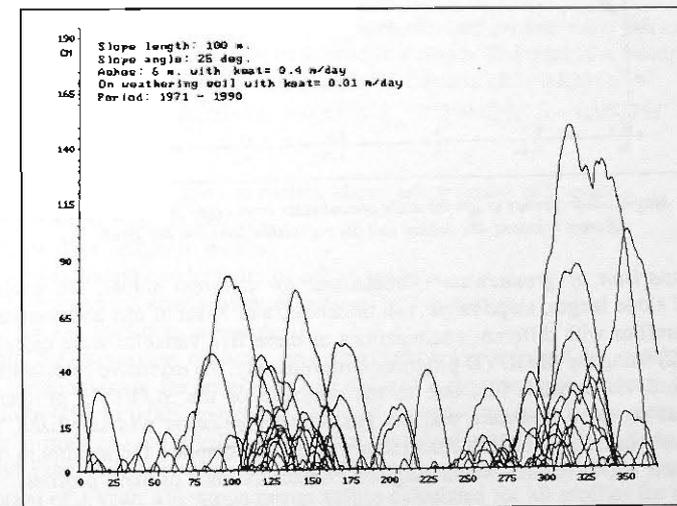
Figure 5.15: Groundwater peaks for the standard profile (in cm above the ash-residual soil contact) for the period 1971-1990. The values on the x-axis represent the days of one year.

Recurrence intervals (RI) for the daily groundwater values in the standard profile for the 1971-1990 period were calculated using a semi-logarithmic function. The resulting graph is shown in figure 5.16. When all values are used, the relationship is rather weak. If the data set is divided into two subsets (groundwater levels <125 cm and >125 cm), however, the relationship becomes much stronger. It can be concluded that high groundwater level peaks tend to flatten, and approach almost an absolute maximum value of approximately 175 cm. This may be caused by the fact that lateral flow increases considerably when the groundwater level is higher, due to the higher saturated permeability in comparison with the unsaturated permeability.
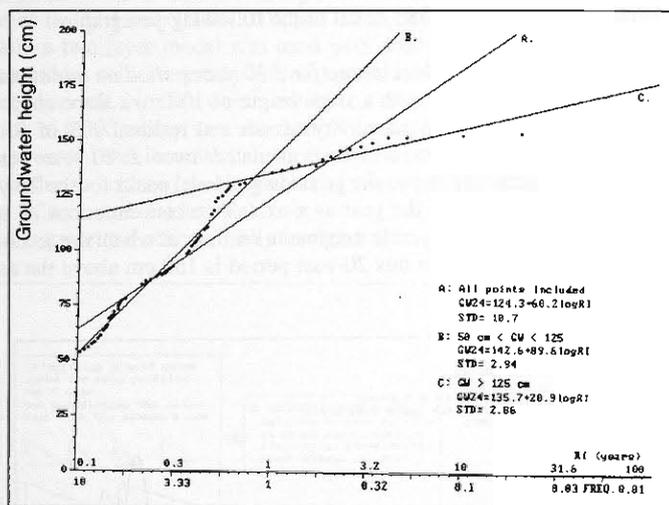
Figure 5.16: Magnitude-frequency graph for daily groundwater level peaks in the standard profile. Three different relations are drawn, and the regression formulas are given.

2. *Comparison of groundwater fluctuations for different slopes*. To evaluate the importance of slope length, slope angle, ash thickness, and K-sat of ash and residual soil, a total of 162 profiles with different combinations of these five variables were calculated for one year (1972) using the SLOHYD program. Unfortunately, the extensive calculations could not be executed via a batch file, due to the structure of the SLOHYD program. Each calculation was repeated to ensure that the groundwater situation was stabilized, and that fluctuations were caused by rainfall fluctuations. Table 5.5 displays the maximum height of the ground water above the ash-weathering soil contact for each of these profiles.

Standard profiles	L:50 A:15	L:100 A:15	L:200 A:15	L:50 A:25	L:100 A:25	L:200 A:25	L:50 A:35	L:100 A:35	L:200 A:35
K:0.4/0.01									
T: 2	0.84	0.85	0.84	0.84	0.84	0.84	0.82	0.84	0.84
T: 6	0.47	0.48	0.47	0.46	0.46	0.47	0.45	0.47	0.47
T: 10	0.31	0.32	0.31	0.30	0.30	0.31	0.30	0.31	0.31
K:0.8/0.01									
T: 2	0.86	0.87	0.86	0.86	0.86	0.86	0.83	0.86	0.86
T: 6	0.48	0.52	0.47	0.48	0.48	0.50	0.47	0.48	0.49
T: 10	0.36	0.38	0.36	0.33	0.34	0.37	0.32	0.35	0.36
K:0.2/0.01									
T: 2	0.87	0.87	0.87	0.87	0.87	0.87	0.84	0.87	0.87
T: 6	0.44	0.45	0.44	0.44	0.44	0.44	0.42	0.44	0.44
T: 10	0.25	0.26	0.25	0.25	0.25	0.25	0.24	0.25	0.25
K:0.4/0.005									
T: 2	1.67	2.00	2.00	1.47	1.66	2.00	1.38	1.20	2.00
T: 6	1.58	1.89	1.84	0.99	1.44	2.15	0.88	1.20	1.98
T: 10	1.44	1.73	2.05	0.83	1.36	1.81	0.76	1.02	1.83
K:0.8/0.005									
T: 2	1.25	1.71	2.00	1.21	1.45	2.00	1.13	1.56	1.30
T: 6	1.06	1.30	1.84	0.78	0.97	1.61	0.69	0.96	1.26
T: 10	0.76	1.22	2.07	0.63	0.85	1.48	0.54	0.71	1.17
K:0.2/0.005									
T: 2	2.00	2.00	2.00	1.93	2.00	2.00	1.61	2.00	2.00
T: 6	2.22	2.34	2.90	1.39	2.03	2.64	1.15	1.80	2.27
T: 10	1.97	2.18	2.69	1.29	1.84	2.46	1.02	1.57	2.09

Table 5.5: Resulting maximum groundwater peaks (in m above the ash-residual soil contact) for profiles with different combinations of slope length (indicated by L in metres), slope angle (indicated by A in degrees), ash thickness (indicated by T in metres), K-sat of ash and k-sat of residual soil (indicated by K in m/day).

3. *Calculating the relationship between variables and ground water fluctuation for one year*. The results from table 5.5 were reordered in a matrix and used in a multiple regression analysis. This resulted in the following regression formula (R^2= 0.8059):

$$GW = 3.234 - 0.012A + 0.00242L - 0.55957K_A - 210.627K_W - 0.05179T \qquad [5.1]$$

in which:

GW = groundwater level in metres above ash-residual soil contact;
A = slope angle in degrees;
L = slope length in metres;
K_A = saturated conductivity of ash in m/day;
K_W = saturated conductivity of residual soil in m/day;
T = ash thickness in metres.

From the regression analysis, and from table 5.5, it could be concluded that the saturated conductivity of the underlying residual soil is the most crucial factor. Reducing this variable from 0.01 to 0.005 resulted in a rise of groundwater by a factor greater than 2.

The formula as such is valid only for the calculated year 1972. To include a time aspect in the model the various profiles in table 5.5 should be compared with the standard profile, over a period of 1 year. The groundwater values calculated for all profiles for the year 1972 were represented as a percentage of the value of the standard profile. Again a multiple regression analysis was executed with this percentage value as the dependent variable. The resulting formula is as follows (R^2= 0.81):

$$DIF = 698.5 - 2.587A + 0.524L - 120.857K_A - 45490K_W - 11.186T \qquad [5.2]$$

in which DIF = deviation (in percent) of groundwater level from the value of the standard profile.

To test whether the calculated relationships between ground water level peaks of all profiles and the standard profile for the year 1972, were constant for other years, two additional profiles were calculated over a 20-year time period. The following two profiles were used:

- *Standard 2*: slope angle 35°, slope length 200 m, ash thickness 10 m, and saturated conductivities for ash and residual soil of 0.8 and 0.01 m/day, respectively.
- *Standard 3*: slope angle 15°, slope length 50 m, ash thickness 2 m and saturated conductivities for ash and residual soil of 0.8 and 0.005 m/day, respectively.

The groundwater level peaks of these two profiles exceeding the peaks of standard profile 1 were calculated, for the 20-year period. The results are shown in table 5.6.

Profile	Groundwater: % of standard 1 in 1972	Average deviation of peaks >20 cm 1971-1990	Average deviation of peaks >50 cm 1971-1990
Standard 2	-6.67 %	-5.19 %	-4.5 %
Standard 3	270.12 %	-22.25 %	70.33 %

Table 5.6: Calculated average difference for groundwater level peaks for the period 1971-1990 in relation to the standard profile 1.

From this table it can be seen that there is a large difference in results between standard profiles 2 and 3, which have different saturated conductivities for the residual soils. The groundwater level peaks for standard profile 2 calculated for the 20-year period are equally related to the values for standard profile 1 as for the one year calculation. Standard profile 3, with a lower saturated conductivity for residual soils, shows large deviations between the one-year and 20-year calculations. It was concluded that the standard profiles with K-sat values for residual soils of 0.01 m/day can be correlated over larger periods with the ratios calculated for the year 1972. Groundwater level peaks for the profiles with K-sat values of 0.005 should be correlated with their deviation from standard profile 3.

The matrix for multiple regression analysis was therefore divided into two groups: one with K-sat values of 0.01 and one with values of 0.005. A new regression analysis using K-sat values of 0.01 resulted in the following equation ($R^2 = 0.94$):

$$DIF = 199.477 - 0.128A + 0.013L + 16.444K_A - 14.836T \qquad [5.3]$$

The influence of the slope angle and slope length in this formula is very low. Simple regression of the ash thickness against the deviation from standard profile 1 resulted in a correlation coefficient of -0.96. thus ash thickness is very crucial in the analysis. In fact, calculation of groundwater level peaks in the area (using K-sat values of 0.4 m/day for ash and 0.01 m/day for residual soil) could be executed by using only the ash thickness map as input, using the formula:

$$DIF = 204.4 - 14.84T \qquad [5.4]$$

4. *Calculation of ground water maps with parameter maps in GIS.* An example groundwater map with a recurrence interval of 25 years is displayed in figure 5.17.
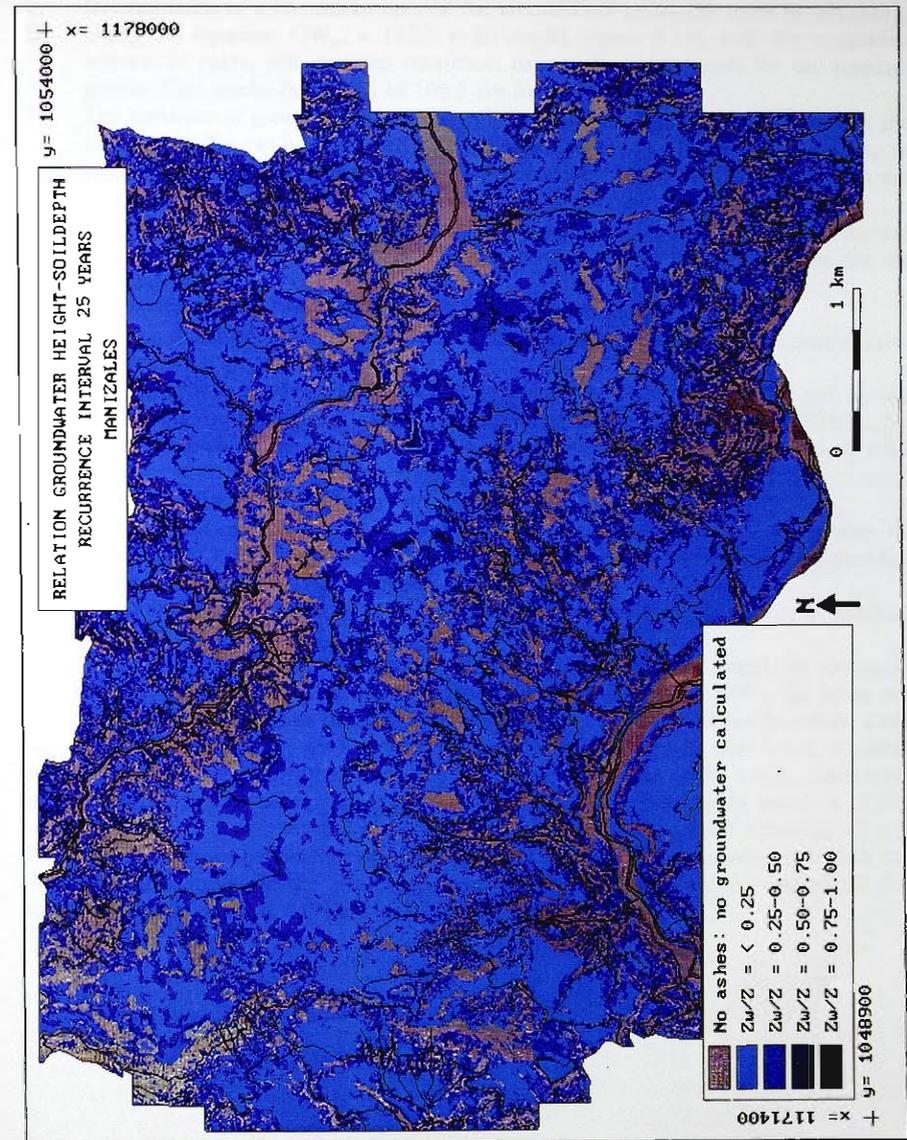
Figure 5.17: Simulation results for the Manizales area of maximum daily groundwater levels above the base of the ash with a recurrence interval of 25 years.

This map was made in the following steps:
1. Determination of a recurrence interval for groundwater peaks (25 years in this case);
2. Using the equation: $GW_{24} = 135.7 + 20.9logRI$ (figure 5.16), with the recurrence interval in years, will give the maximum daily groundwater peak for the standard profile. This results in a GW_{24} of 106.5 cm for this example.
3. The variation in groundwater levels for different conditions in relation to that of the standard profile can be calculated with equation [5.4], using the ash thickness map as input map. Final groundwater levels are obtained by multiplying the result with the maximum daily groundwater peak of the standard profile.

The resulting maps will be used later as one of the input maps in deterministic modelling (see section 6.5). The results should be treated only as indicative values, for the following reasons:
- The model used is very simple, based on a one-layer model.
- The two-dimensional model used cannot take into account the effects of concavities in the terrain on groundwater levels.
- The distribution of saturated conductivity values of the underlying residual soil are not sufficiently well known. Measuring these values in the field is rather difficult for reasons explained in section 4.4.3.3. As could be seen from the simulations with different K-sat values for the residual soils (table 5.5), these values have a very important effect on the resulting groundwater levels.
- The ash thickness map, which was used to calculate the spatial distribution of groundwater levels, was very difficult to produce as there was no clear relationship between ash thickness and mappable phenomena.
- It was impossible to calibrate the results with groundwater measurements in standard profiles.

When the values for the groundwater levels calculated using the model are compared with the sparse groundwater data found in the literature (Ingeosuelos, 1991), the levels are of more or less the same order of magnitude: between 50 and 150 cm above the ash-residual soil contact. Of course there are a number of cases where other results were found. In some of these, such as in barrio Milan, barrio Peralonso, or in the area of the newly constructed sanitary landfill in Manizales, higher groundwater levels are related to the presence of old landslides. It is clear that more detailed data are required on the spatial variability of ash thickness, K-sat measurements for residual soils, groundwater-level monitoring over time for some standard profiles in the area. Moreover, for modelling groundwater using GIS the application of neighbourhood operations should be further developed.

CHAPTER 6: ANALYSIS

In this chapter the various methods for landslide hazard analysis using PC-based geographic information systems (summarized in chapter 2) will be presented in more detail, and illustrated with data from the Rio Chinchina study area. The methods are presented in increasing complexity, from landslide distribution analysis to statistical and deterministic modelling. Each method will be demonstrated at the appropriate working scale(s) described in section 2.6 (regional, medium, and large). For each method an introduction is given to the calculation method, followed by a listing of the required input data and a presentation and discussion of the results.

Preliminary results of data analysis using the data set of Chinchina can be found in Rengers (1992), Rengers et al. (1992), Soeters et al. (1991), Alzate ans Escobar (1992), Van Westen (1989, 1992a, 1992b), Van Westen and Alzate (1990a,b), Van Asch et al. (1992), Sabto (1991), Koirala (1992), Mool (1992), Niehaus (1992) and Innocenti (1992).

The primary objective of this chapter is to illustrate the potential of each of the methods, rather than to present a final hazard map of the study area. Since a hazard analysis includes elaboration of each mass movement type separately, as discussed in chapter 2, presentation of five or more different hazard maps for each method and at each scale would lead too far. Therefore, a single mass movement type, "derrumbe" (presented in section 4.3.2.2), is selected for most of the analyses.

6.1 Landslide distribution analysis

The simplest type of landslide hazard map only outlines those areas where landslides have already occurred. Such a map provides very useful information on the frequency, types, and variations in time of mass movement phenomena. It does not provide direct information on the possible causes of slope failure.

In regions which are more or less stable in terms of their physical and human environment, i.e. factors contributing to mass movement do not change considerably within a time-span of a hundred years or so, a landslide distribution map may almost completely answer questions about where slope instability features are to be expected. The landslide distribution maps provide only a partial answer to the question of landslide hazard, however. Nevertheless, they are extremely important as input for most of the other analysis techniques, as they provide the information where, and how severely, mass movements occur. A number of different types of mass movement distribution maps will be treated in the following sections.

6.1.1 Simple landslide distribution analysis

The input data required for this type of map are the location and outline of mass movements as interpreted from aerial photos. For the *regional scale* the data are very difficult to obtain, as was discussed in section 4.3.1. The landslides displayed on such a map are not represented at scale, and therefore cannot be used as input for methods based on crossing mass movement maps with other input maps. The map is important, however, even though it is general in content, as it gives information on the frequency of mass movements within different terrain mapping units. The digitized mass movement distribution maps together with

their attribute tables are extremely useful in analysing the relationship between the different attributes, such as landslide type, area, depth, and activity. These tables were exported to an external statistical package and used for descriptive statistics. Some examples of these are shown in figures 6.1, 6.2, and 6.3. The map for the regional-scale data set is presented in figure 6.4. This map includes features related to the volcanic eruption of the Nevado del Ruiz on 13 November 1985, as well as erosional features. A clear zonation of geodynamic processes can be seen:

- Few mass movements occur in the western part of the area.
- The main mass movement type in the Romeral fault zone is "derrumbe".
- Different types of mass movements occur around the city of Manizales.
- Slides and flowslides occur mainly in the dissected terrain east of the Romeral zone.
- Rockfalls, combined with derrumbes, occur on the steep frontal parts of lava flows.
- Soil erosion and flows occur in the high Paramo region.

At the *medium and large scales* the individual mass movement phenomena on the input maps are assigned a six-digit code for mass movement type, mechanism, activity, depth, vegetation, and scarp (see sections 4.3.2.2, 4.4.2.2, and 5.2.2.4). The GIS techniques for this analysis method are extremely simple. The mass movement map is recoded with one of the six codes for the variables stored in the connecting table, or with a combination of these. The method was displayed schematically in figure 2.1. The six variables in the table can also be combined such that, for example, only the bare scarps of active, shallow, translational slides are shown. Figures 6.5 and 6.6 display the mass movement types for the study areas at the medium and large scales.

The mass movement distribution map of the medium-scale area (figure 6.5) leads to the following conclusions:

- Large slides can be found in the terraces, but most of them are fossil.
- Many derrumbes are related to the main Chinchina-Manizales road.
- Many mass movements are related to valley heads.

In the landslide distribution map for the large-scale area (figure 6.6), the present boundary of urbanized Manizales is indicated. Landslides that have occurred within this urban area are mostly masked by the urbanization, or they have been obliterated during earthworks that preceded construction. This map leads to the following conclusions:

- Relatively large slides and flowslides occur at the northern side of the Rio Olivares.
- Many small slides and derrumbes occur on the steep slopes near the city centre.
- Many mass movements of different types and sizes are related to the Pan American Highway on the southern slope of the city.

Figure 6.1 gives an overview of the relative area occupied by different mass movement types at the three different scales. The regional-scale information is only indicative, since the features are not represented to scale on the regional-scale map. The differences between the three diagrams are not related so much to the working scale, but to the fact that the medium- and large-scale maps occupy a smaller area than the regional-scale map. The differences are caused mainly by the large areal extent on the regional scale of cliffs in lava flows, where rock fall tends to occur, and by the area occupied by the volcanic debris flow from the Nevado del Ruiz volcano. The percentage of 2.9 for erosion on the regional scale is caused by extensive gullying in the Paramo area (Florez, 1986).
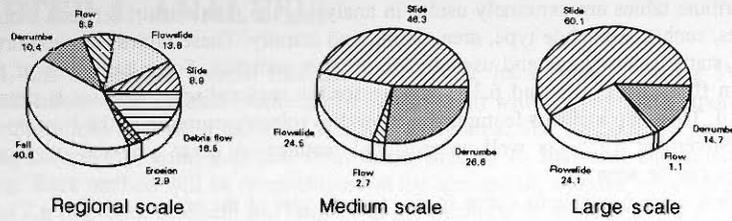
Figure 6.1: Denudational types indicated as the percentage value of the total area of denudational features of the study areas at the regional, medium, and large scale.
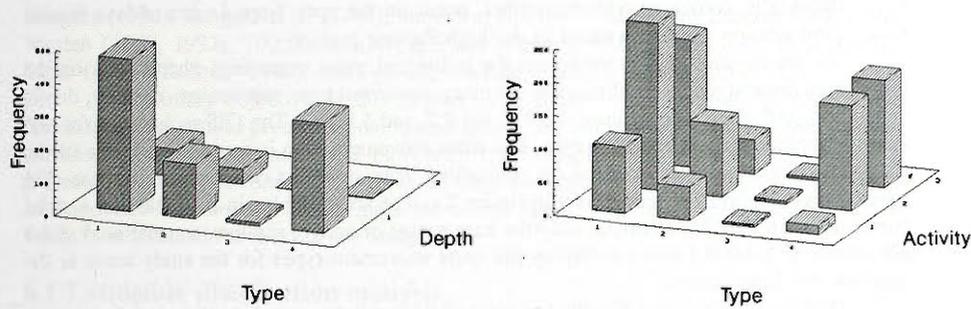
Figure 6.2: Frequency distributions of mass movement attributes at the medium scale. Left: Relationship between mass movement type (1 = slide, 2 = flowslide, 3 = flow, and 4 = derrumbe) and mass movement depth (1 = surficial, 2 = deep). Right: Relationship between mass movement type and activity classes (1 = Stable, 2 = Dormant, 3 = Active).
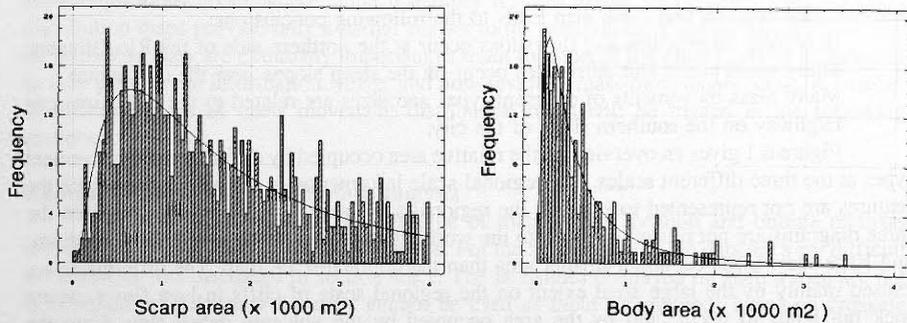
Figure 6.3: Frequency distributions of the surface area of mass movement scarps (left) and mass movement bodies (right). Y-axis displays frequency in number of features and X-axis surface area in 1000 m2.
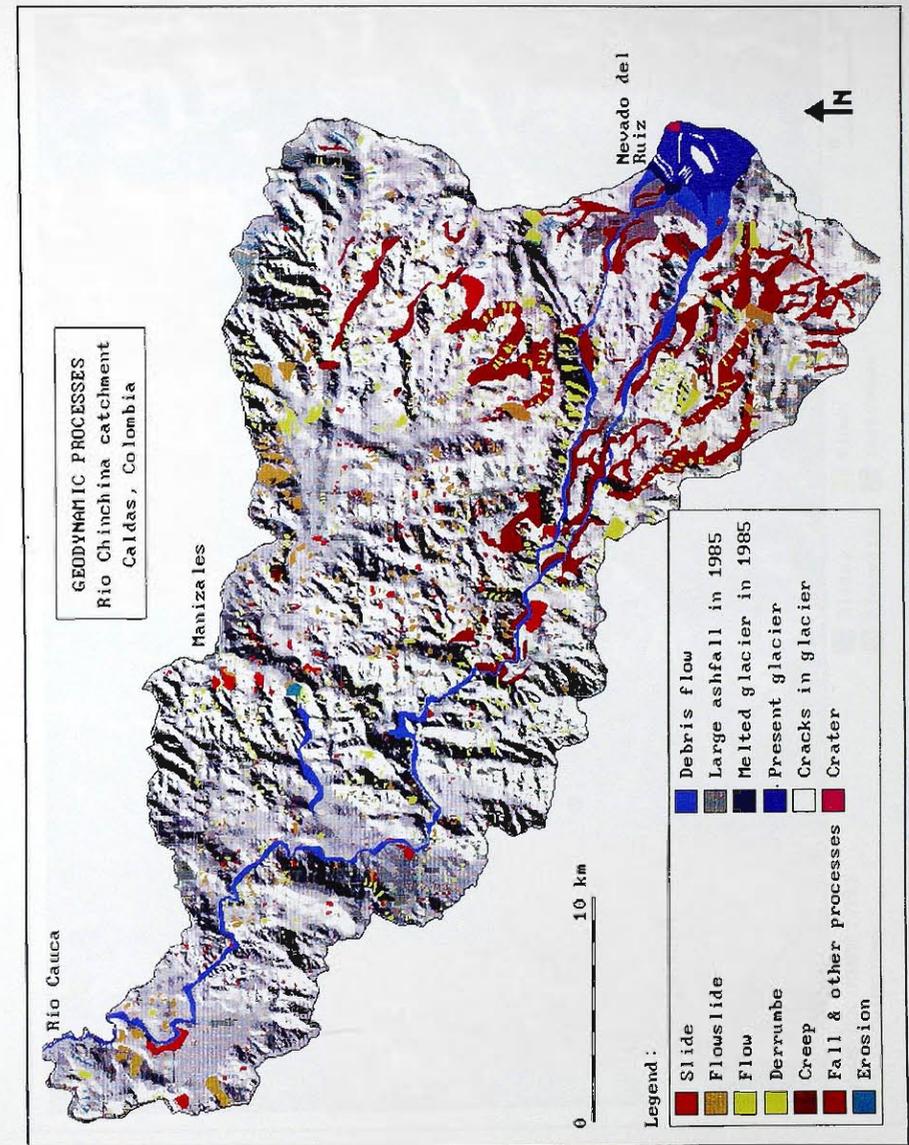
Figure 6.4: Geodynamic processes of the study area at the regional scale. Mass movement types, erosion phenomena, and features related to the 1985 Nevado del Ruiz eruption are indicated.
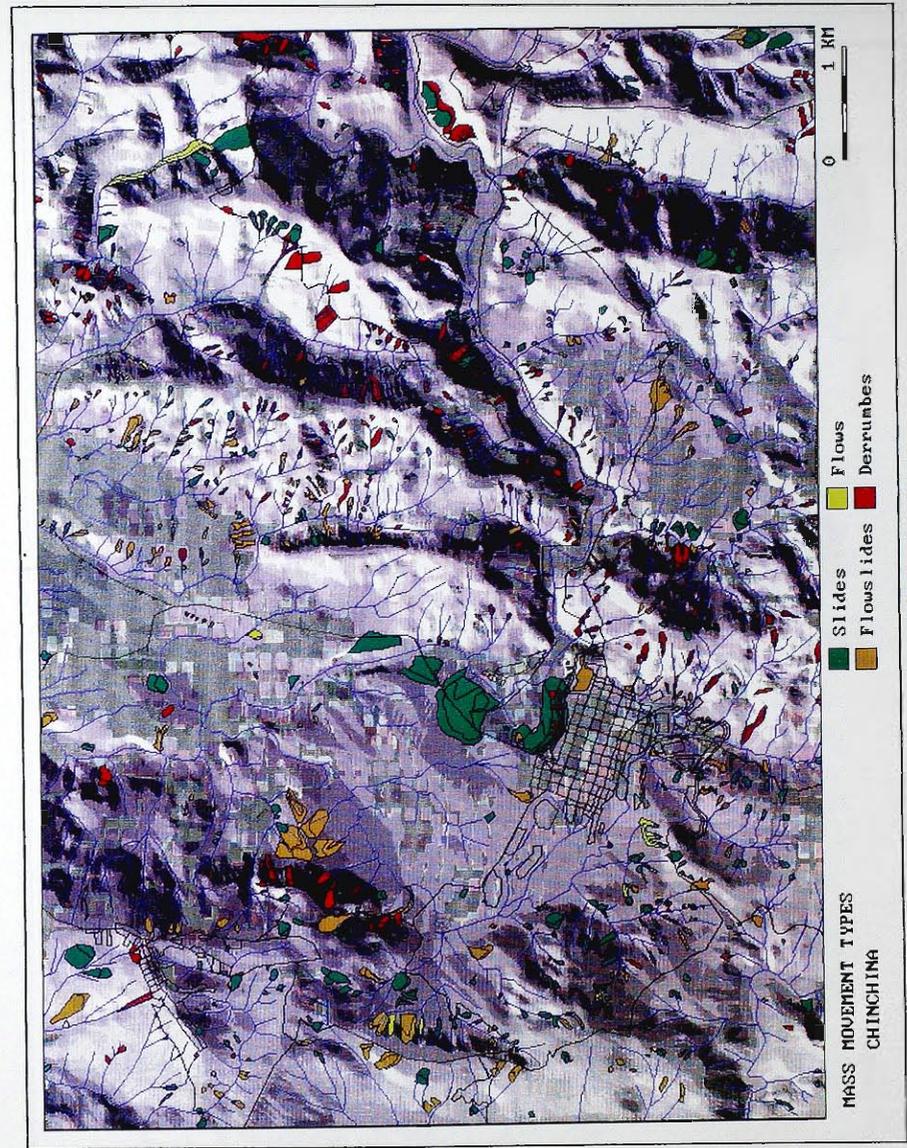
Figure 6.5: Mass movement types for the medium-scale study area.

130b
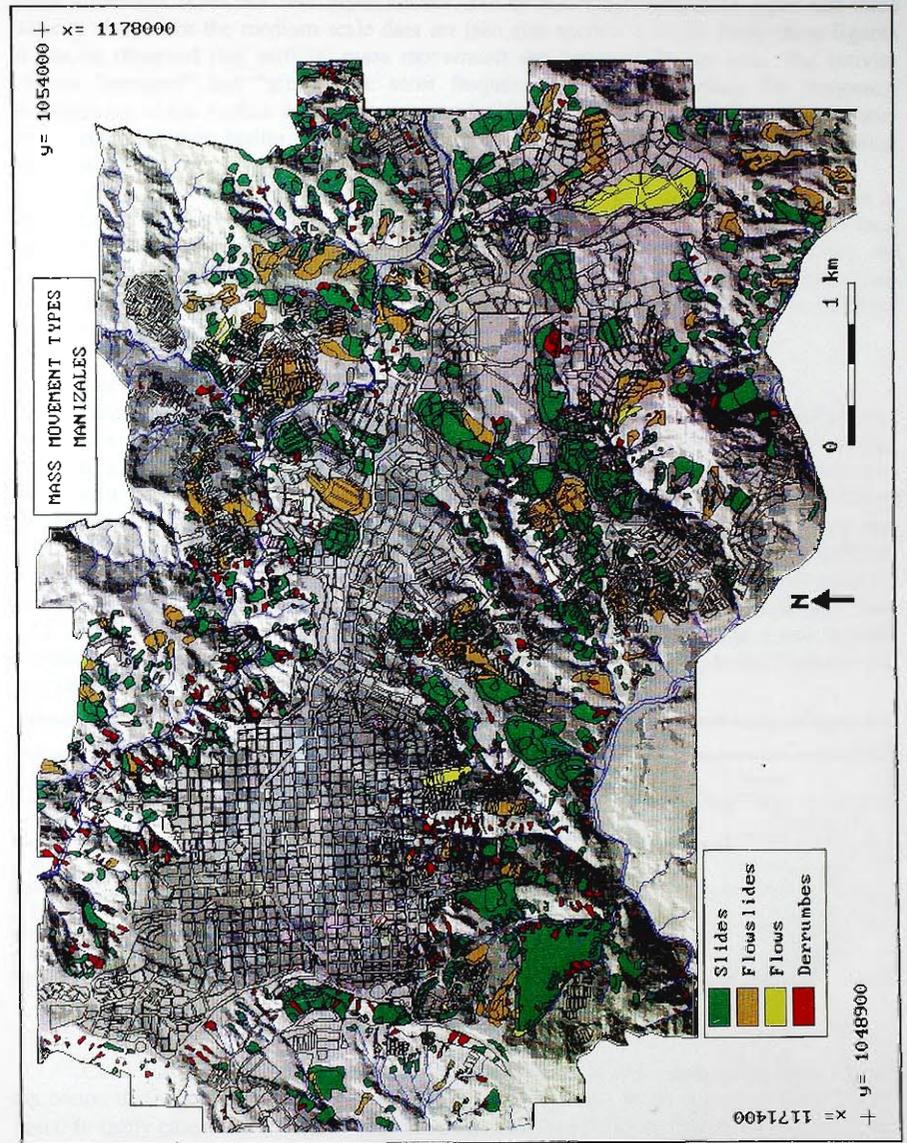
Figure 6.6: Mass movement types for the large-scale study area.

Figure 6.2 gives two examples of frequency distributions for the combination of four mass movement types and two depth classes, and of four mass movement types and three activity classes for the medium-scale data set (see also section 4.3.2.2). From these figures it can be observed that surficial mass movements are dominant in the area. The activity classes "dormant" and "active" are most frequent. Figure 6.3 displays the frequency distributions of the surface area of scarps and bodies for the medium_scale data set. There are more scarps than bodies in the area, due partly to the presence of derrumbes, of which the material has been transported away from the source area.

A number of descriptive landslide statistics for the medium-scale data set is given in appendix 24. This table contains information on the total area occupied by landslides, the total number of landslides, the landslide density based on pixels, the number of landslides per square kilometre, and the average surface area of landslides. These statistics can be calculated for all mass movements together, for the different types separately, and for the different activity classes separately.

6.1.2 Landslide activity analysis

The legend for the mass movement map, made by interpretation of aerial photos, includes a code for "mass movement activity". Three relative classes are used: stable, dormant, and active. However, as was mentioned in section 4.3.2.2, correct classification may be difficult. The use of multitemporal photo-interpretation provides more precise information on the activity of mass movements. Mass movements that have occurred in between two photo dates, as well as mass movements reactivated during the same period, can be detected by overlaying mass movement maps from the two dates. The method is shown schematically in figure 2.2. This can be done in a GIS with the use of a two-dimensional table (see table 6.1). The activity classes from two maps of different times are combined in a new legend, containing 16 classes. The development of each mass movement in the period between the two photo dates can be obtained from this legend.

Activity in younger photo	Activity in older photo			
	Not present	Stable	Dormant	Active
Not present	0: Not observed in both photos	1: Stable has become invisible	2: Dormant has become invisible	3: Active has become invisible
Stable	4: New but apparently stable	5: No change, still stable	6: Stabilized dormant slide	7: Stabilized active slide
Dormant	8: New but apparently dormant	9: Slightly reactivated to dormant	10: No change, still dormant	11: Slightly stabilized
Active	12: New and active slide	13: Reactivated stable slide	14: Reactivated dormant slide	15: No change, still active

Table 6.1: Two-dimensional table used to analyse landslide activity.

Code numbers 1 to 3 in table 6.1 may be considered to represent errors, according to the notion that whenever a mass movement occurs, it will also be present as a relict in later years. In many cases, however, the form becomes unrecognizable in recent photos, due to the effect of vegetation or human activity, such as land-use change, slope flattening, etc.

131

This method was used to assess landslide activity using the data sets for the medium and large scale. Results are shown in table 6.2 as percentage values of the total area of landslides observed.

Activity in photos from 1981-1987	Activity in photos from 1965-1969			
	Not present	Stable	Dormant	Active
Not present	–	6.0 11.0	6.3 38.3	6.3 20.6
Stable	10.5 3.9	14.2 3.0	4.1 2.3	1.7 1.8
Dormant	14.0 5.2	0.7 0.5	8.9 4.6	4.9 3.3
Active	15.4 2.4	0.7 0.2	1.6 1.6	4.7 1.4

Table 6.2: Changes in degree of activity for mass movements interpreted from recent (1981-1987) and old (1965-1969) aerial photos. The numbers represent for each combination of old and new activity the percentages of all mass movement types. The upper numbers refer to the medium-scale data set, and the lower to the large-scale data set.

The mass movement activity map for the large-scale area is given in figure 6.7. From the map and table 6.2 the following conclusions can be drawn:

- The large-scale area is strongly dominated by large, fossil, mass movements. The large percentage of landslides present in older photos which are not recognizable on more recent photos is due to the growth of the city (see figure 3.21), during which large areas were levelled, and existing mass movements were covered by fill material. These areas may experience stability problems, especially when the mass movement material was not removed before filling; loading of the fill may cause reactivation of the movements, as was the case in the townships of Villa Julia and Peralonso. These buried mass movement phenomena may also be reactivated during earthquakes. This has not occurred to date, since most of the new townships were only constructed during the last 20 years.
- Presently active mass movements in the large-scale study area occupy only a small percentage of the total area covered by slope instability phenomena. This is due to the fact that most of the active landslides are of the "derrumbe" type, which are usually small in size. The scarps produced by these movements rapidly become unrecognizable due to stabilization and growth of vegetation. The presence of artificial drainage works on a slope may be the only indication that there has been a stability problem in the last 30 years.

In the medium scale study area a much larger percentage (22.4%) of the total number of mass movements is active. The largest part of these (15.4%) has occurred at new locations. The increase in slope instability during the last 30 years has the following causes:

- Widening of the main road from Manizales to Chinchina resulted in a large number of new landslide problems (see section 3.5.4).
- In the steep areas northeast of Chinchina many new mass movements have occurred, which may have been caused by a change in coffee farming system.
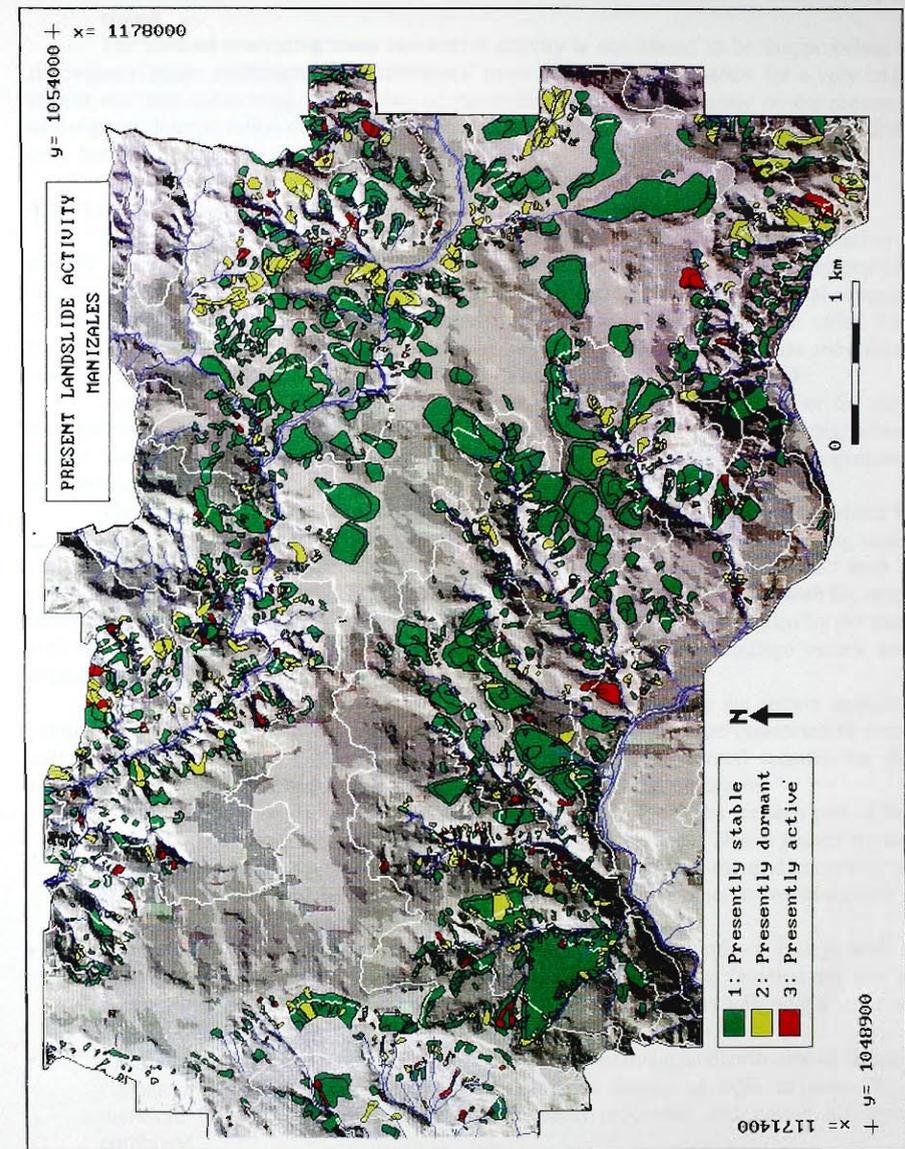
Figure 6.7: Mass movement activity map for the large scale area. See text for explanation.

- The lahar of 13 November 1985 triggered several landslides due to undercutting of slopes.

The method evaluating mass movement activity is considered to be inappropriate at the regional scale; collection of multitemporal mass movement information for a very large area is too time-consuming. The quality of the method depends completely on the accuracy of the photo-interpretation of landslides (see also section 7.3.1). Field verification is possible only for very recent photos.

6.1.3 Landslide density analysis

Instead of displaying mass movements individually, they can also be presented as a density value within mapping units. These units should be mapped by image interpretation, such as terrain mapping subunits (TMSs) at the regional scale, or geomorphological subunits (GSs) at the medium scale. Catchment areas may also be used as the basic units. The resulting map can be considered a very simple hazard map. When many mass movement types occur within a unit, it may be considered to have a high degree of hazard.

Such density maps can be made for all mass movement types together, or for each type individually. The latter type is more useful as it can be used in risk analysis, where certain mass movement types will cause different types and degrees of damage to population and physical infrastructure.

The required input data at the regional scale consist of the TMU map, which is rasterized in such a way that each polygon has a different record in the accompanying table, and the process map. At the medium and large scales, the geomorphological subunit map is used. The basic GIS technique is map crossing. The terrain unit map is crossed with the mass movement map and the area covered by landslides within a terrain unit is divided by the total area of the unit. The terrain unit map is then renumbered with the permillage values, and classified into a number of meaningful classes (see also figure 2.3).

This method is particularly useful at the regional scale, where the terrain mapping subunits (TMSs) form the basic units in the analysis. Hazard scores are connected to these units. Figure 6.8 gives the classified densities for various denudational features for the regional-scale area. From this figure a number of conclusions can be drawn:

- The maps for slide, flowslide, and flow show high density in the western part of the area, although there are hardly any active features in this area. This is caused by the fact that the mass movements recognized in the area were not mapped according to activity, which would be very difficult at the regional scale since it would require a more detailed photo-interpretation.
- The map for debris flow processes displays one polygon outside of valleys with a class 2 (frequency 0-5‰) for debris flows. This is caused by the fact that this unit is crossed in one small section by a valley with a debris flow, thus assigning a value to all of the unit.
- The map showing all denudational processes shows nearly equal distribution of density classes. Practically all of the area has a landslide density of 10‰ or more. It is therefore important to make maps of individual processes, and not of all types combined.

For the mapping of density the following aspects are very important:

- Correct delineation of "homogeneous" units. How homogenous are the units at the

133

TMC, TMU, or TMS, or individual polygon level? These considerations will be treated further in section 7.3.4. "Homogeneous" units should not be too large; otherwise there will be inhomogeneity in mass movement density within the unit.
- Correct delineation and classification of geodynamic processes (see also section 7.3.1).

The procedure for creating mass movement density maps for the medium and large scale is similar to that at the regional scale, with the exception that the geomorphological subunits map is used as the "homogeneous units map", and only active mass movement map used. The resulting maps for these scales are not displayed here.

6.1.4 Landslide isopleth analysis

Landslide density calculated using the method described above does not display density per unit area. For some applications, such as testing the homogeneity of the outlined TMUs, it may be useful to represent the density per square kilometre, or per hectare. Preparing such a map using conventional techniques is cumbersome. The number of mass movements, or the area occupied by mass movements, has to be counted inside circular areas, which partly overlap. With a GIS, this task can be automated. For this purpose a batch file was written, with more or less the same structure as the one used for sampling of internal relief (see section 5.4.2). A set of counting circles is made in such a way that the whole map is covered by circles. Each circle has a different code number, and the x- and y-coordinates are stored in a table. A bit map is made for each of the mass movement types, and the circle map is crossed with each of these bit maps. For each circle, the mass movement density is calculated. After that a continuous density surface is created by linear interpolation between the centres of the circle. From this map isolines are extracted via reclassification and raster-to-vector conversion. An example of an isopleth map for the density of "derrumbes" at the regional scale is given in figure 6.9. At the regional scale, sampling circles with radii of 20 pixels were used, resulting in an area of 4.8 km². For the medium-scale data set, counting circles with radii of 30 pixels were used (2.8 ha). The use of 1-km² circles at the regional scale and 1-ha circles at the medium scale was not possible as the maximum number of counting circles that can be used (255) would have been exceeded.

The quality of the isopleth map depends strongly on the circle size that is used. The larger the circle size, the greater the generalization becomes. With a slight modification, a similar calculation can be done to construct isopleth maps based on the number of mass movements per unit area. The method is applicable at all three scales, if landslide maps are available, but is most useful at the regional scale, where it is more important to know the concentration of mass movements than their exact locations.
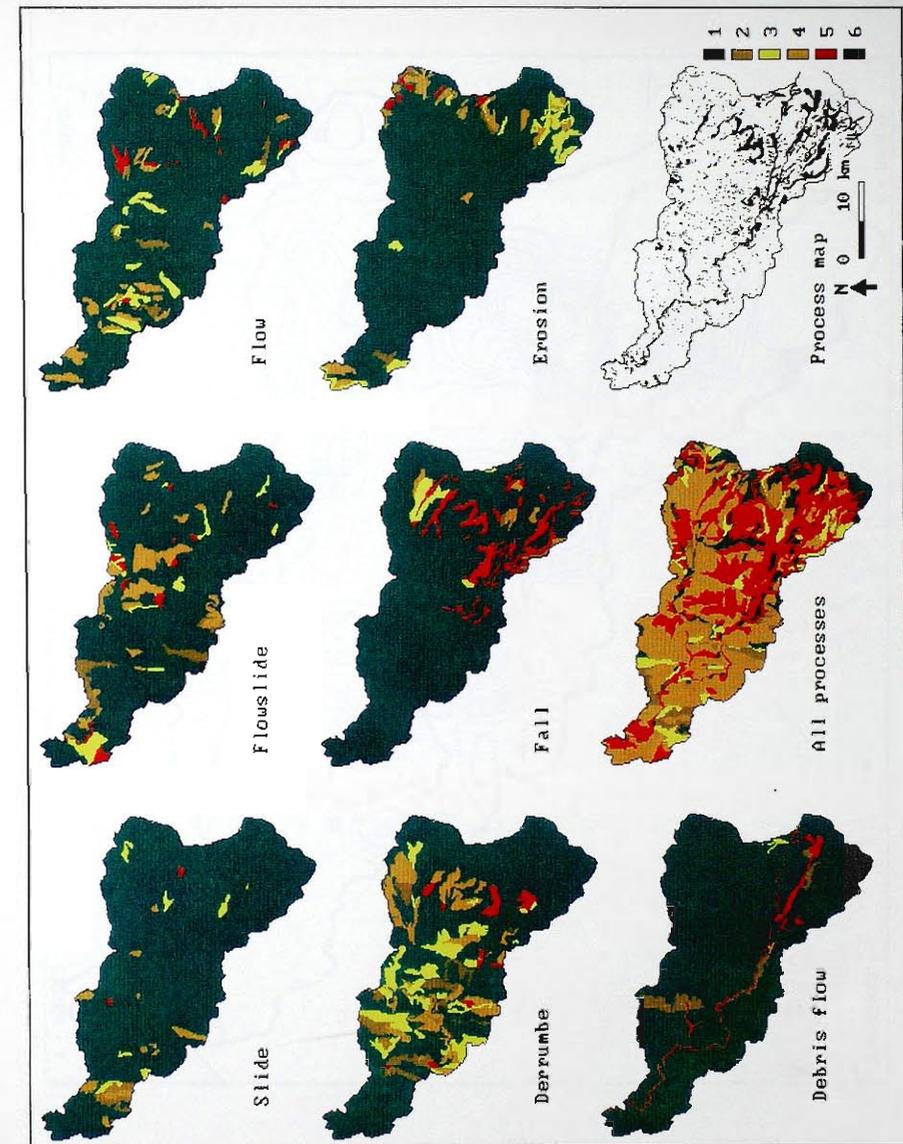
Figure 6.8: *Classified density values for several denudational processes calculated per terrain mapping subunit (regional-scale area). Legend: 1 = 0‰, 2 = 0 - 5‰, 3 = 5 - 10‰, 4 = 10 - 50‰, 5 = > 50‰.*
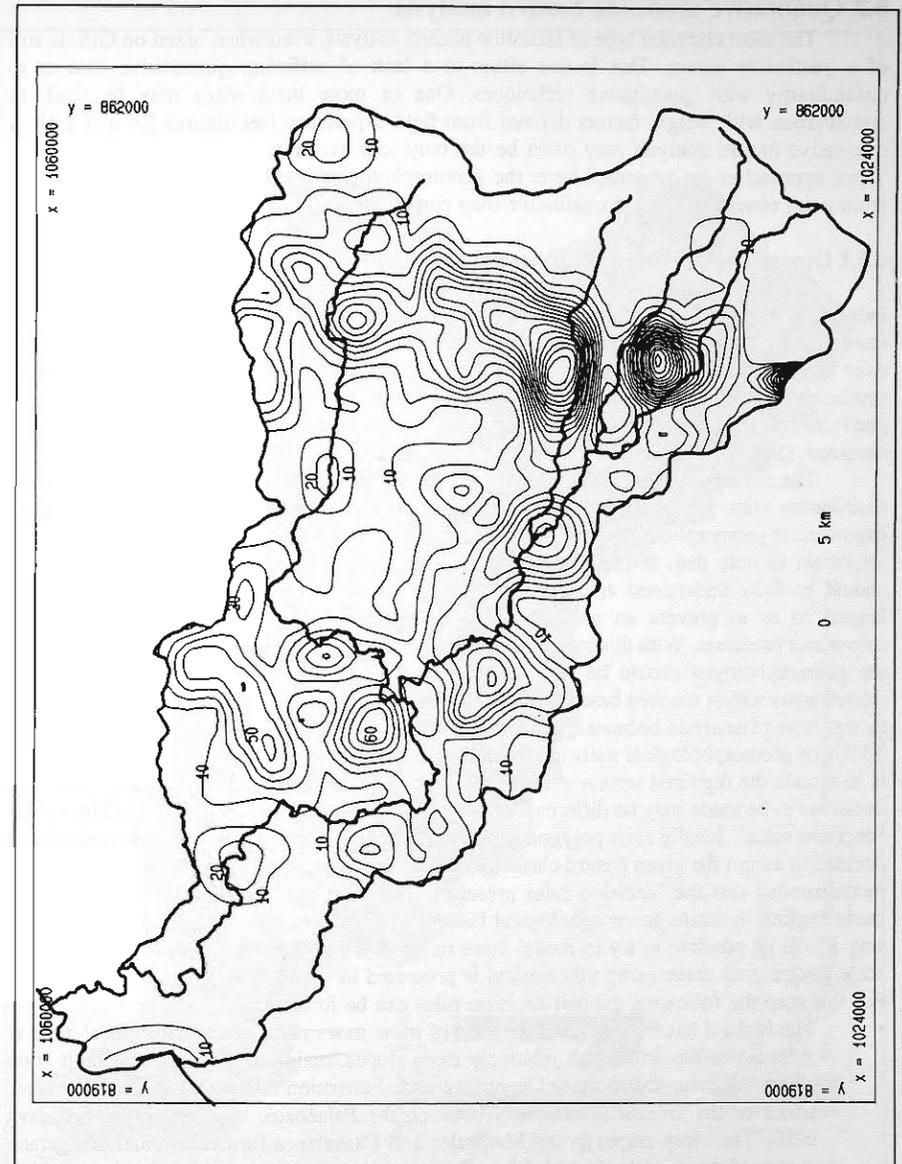
Figure 6.9: Landslide isopleth map for the density of "derrumbes" at the regional scale. Contours of equal density classes of 10‰ are displayed.

6.2 Qualitative landslide hazard analysis

The most common type of landslide hazard analysis, even when based on GIS, is still of a qualitative nature. This is due either to a lack of sufficient quantitative data or to unfamiliarity with quantitative techniques. One or more input maps may be used, in combination with weight factors derived from field experience (see figures 2.4 and 2.5). A qualitative hazard analysis may often be the only tool available in areas with scarce data. Three approaches are presented here: the geomorphological method, the analysis of factors from point observations, and qualitative map combination.

6.2.1 Geomorphological landslide hazard analysis

In some hazard mapping projects the time and money available are so limited that individual maps of the factors which are important in the occurrence of mass movements cannot be made. In regional-scale analysis, it is usually impossible to obtain sufficient data over large areas. At the other scales this may be impossible when a hazard map has to be produced in a very short time period. In other cases the hazard map is one of many end products of a geomorphological survey, during which considerable field experience is obtained. (Seijmonsbergen et al., 1989; Seijmonsbergen, 1992).

The most important map in a landslide hazard assessment project, besides the landslide distribution map, is a geomorphological map. Such a map, provided that it is made by an experienced geomorphologist, will provide a maximum of information in a short time. It is important to note that, in order to arrive at a reliable hazard map, the area under survey should be fully understood and worked out on the basis of a complete geomorphological legend so as to prevent an unbalanced result showing all "anomalies" as due to mass movement processes. With this information, obtained from photo-interpretation and fieldwork, the geomorphologist should be able to formulate his field knowledge about the potential hazard areas within the area based on a series of decision rules. The GIS is not very important in this type of analysis because the main task of the geomorphologist will be to recode the TMUs or geomorphological units into hazard classes. The easiest way to create a hazard map is to recode the digitized terrain units with relative hazard scores (high, medium, low). The decisions to be made may be different for every polygon and cannot be formalized into strict "decision rules". Ideally each polygon should have an explanation why the geomorphologist decided to assign the given hazard class. In practice this is usually not executed. It is strongly recommended that the "decision rules present in the mind of the geomorphologist" will be made explicit in future geomorphological landslide hazard assessment research. Only in this way it will be possible to try to model these rules within a GIS. An example of a regional-scale hazard map made using this method is presented in figure 6.10.

For this map the following general decision rules can be formulated:

- The highest hazard for the occurrence of mass movements of the "derrumbe" type is assigned to the areas with relatively steep slopes, mainly in the Romeral fault zone where the meta-sedimentary Quebradagrande Formation is exposed, and in the higher zones of the area at the contacts between the Palaeozoic methamorphics and lava cliffs. The steep slopes in the Manizales and Casabianca formations, and the terrace slopes of the pyroclastic and debris flow deposits, are also considered to have a high hazard for rapid movements.

Qualitative hazard map
(combination of all processes)
Rio Chinchina, Colombia

Low hazard
Medium hazard
High hazard
Very high hazard

Percentage of total
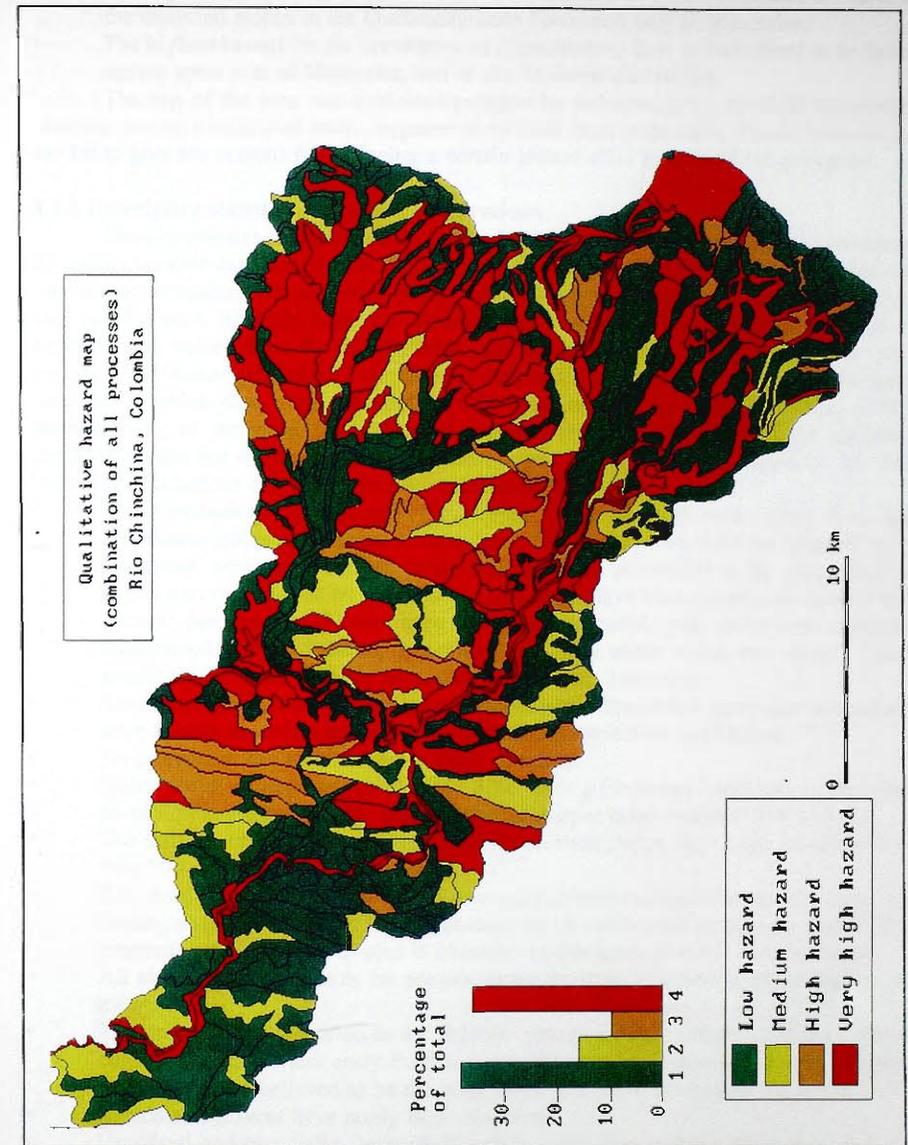
Figure 6.10: Hazard map of the regional-scale area, made by recoding individual terrain mapping subunit polygons.

- The highest hazard for the occurrence of rotational slides and flowslides is found in the dissected slopes in the Quebradagrande Formation east of Manizales.
- The highest hazard for the occurrence of (liquefaction) flow is considered to be in the terrace areas east of Manizales, and in the Malteria alluvial fan.

The rest of the area was evaluated polygon by polygon, using the field knowledge obtained during a walk-over study, augmented by field descriptions and photos. It would go too far to give the reasons for assigning a certain hazard class to each of the polygons.

6.2.2 Descriptive statistics from field observations

Field knowledge on the important factors leading to mass movements can be enhanced by using checklist data (see section 4.4.2.2). The data obtained from landslide observations can be used to evaluate the important causal factors, such as material type, topography, land-use, etc. for each landslide type. For this purpose a series of batch files was written to aggregate the values from the SLIDE table (see section 5.2.2.4) for each landslide type-subtype combination. Figure 6.11 displays the results for all landslides in the medium-scale data set, in which data were collected for 211 mass movements (Koopmanschap, 1992), predominantly of the slide, flowslide, and derrumbe types. A summary of the landslide checklist results for different mass movement types can be found in appendix 25. The following conclusions can be drawn from the checklist:

- The distribution of mass movement types based on field data differs from the distribution obtained by photo-interpretation (figure 6.1). The different types of mass movement were not described in the field in equal proportion to the percentage in which they occur in the area. Slides and flowslides have been sampled at more or less correct percentages. Flows have been oversampled and derrumbes strongly undersampled, due to the topographical conditions under which they occur. Flows usually occur in more easily accessible terrain than derrumbes.
- Rotational slide movements are most frequently described. Flow type mass movements were always described as having a translational movement mechanism.
- No preference can be observed in slope direction.
- Slides occur on slope angles of 40 to 80%, with a frequency maximum in the class 55-65%. Flowslides and derrumbes occur at steeper slope angles (75 to 110 %).
- The majority of the mass movements occurs on short slopes, with slope lengths of less than 100 meters.
- The distribution for the downslope convexity (slope convexity in profile) does not display a clear peak. There is a slight majority of movements on straight slopes. The predominant slope form in plan is concave, as this leads to water concentration.
- All movement mechanisms are present, however, there is a clear peak for fast single events.
- The major causes identified in the field are stream erosion, undercutting due to road construction, and water entry from upslope. Permeability contrasts between ash and residual soil are believed to be the most important cause of shallow landslides.
- Remedial measures have rarely been observed.
- Grassland and especially "technified" coffee cultivation without shade trees are the predominant land-use types where mass movements occur.

137
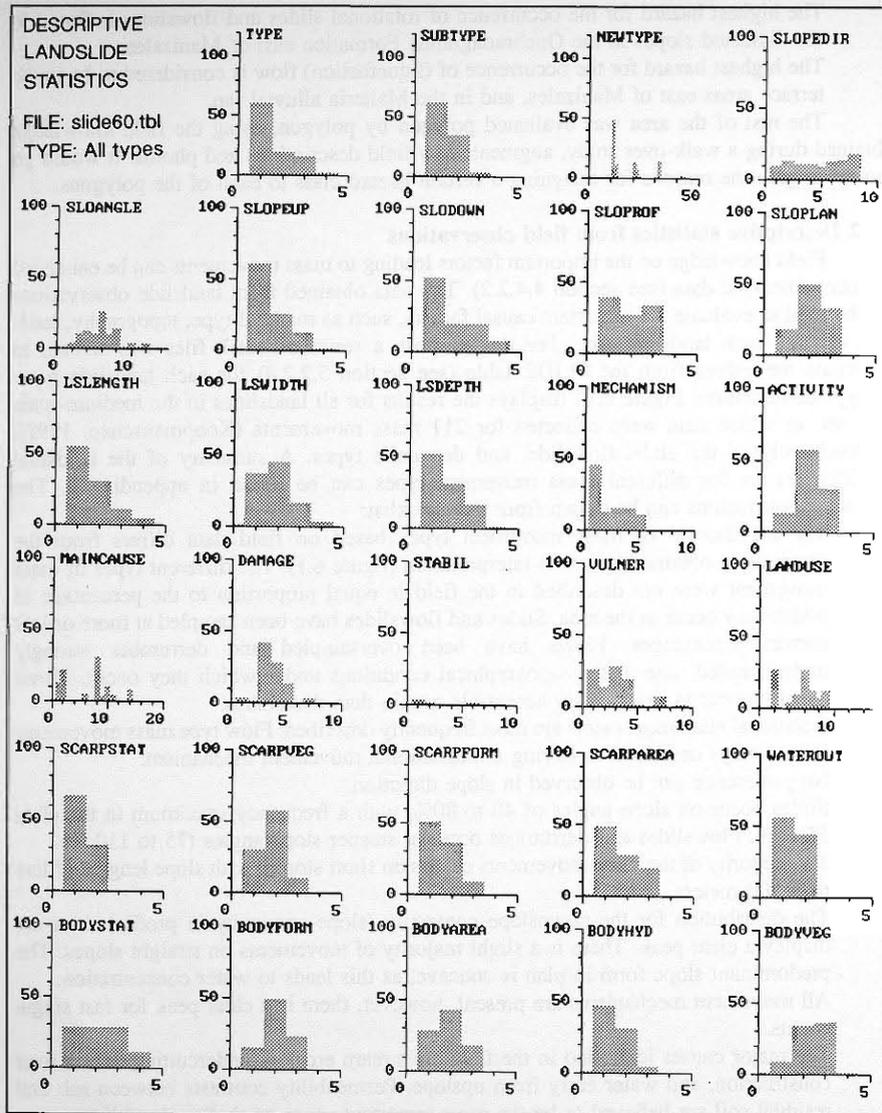
Figure 6.11: Frequency distributions (in percentages) of landslide characteristics aggregated for all 211 mass movements described in the medium-scale study. The explanation of the variable classes is given in table 4.10. The legend of the material codes can be found in table 4.11. Slope direction is in classes of 45°, and slope angle is given in classes of 10%.

To improve the quality of this method the mass movements to be described should be selected randomly from the mass movement distribution map. Unfortunately, this was not possible in the present study for the reasons explained in section 4.4.2.2. Moreover, landslide descriptions should be made by the same observer, as different observers will describe the same phenomena differently. Completing the checklist (appendix 4) for one mass movement requires a considerable amount of time. Depending on the size and complexity of the landslide, this may be on the order of 0.5 to 2.5 hours. In many cases it will not be feasible to fill in the entire list, and only a subset of the most relevant attributes should be selected.

6.2.3 Qualitative map combination

In this method it is assumed that assignment of weights is not supported by quantitative evidence. It is done by the earth scientist who is engaged in the analysis, and depends on his or her understanding of the interrelationships between factors which are important in the occurrence of mass movements. The method can be applied at all three scales. The number of input maps which are used depends on the opinion of the researcher, who decides beforehand which factors are important, and are therefore to be mapped and digitized. An important aspect in the choice of the data to be collected is the cost/benefit evaluation. Two questions have to be answered for each variable to be collected:

- Does it provide relevant information at the detail of the output product?
- Is the investment in time and money to collect the data justifiable in relation to the expected information that can be produced?

The most important factors for slope stability assessment are geotechnical characteristics, slope angle and groundwater level. However, groundwater level information is not relevant on the regional scale, as its spatial variation, causing some parts of a slope to be stable and others unstable, are not mappable at a regional scale. Moreover, the data cannot be obtained without excessive costs. The following factors are considered to be important at each of the three scales in the preparation of hazard maps using qualitative map combination:

- *Regional scale*: geomorphological origin, lithology, drainage density, and internal relief.
- *Medium scale*: slope angle, lithology, geomorphological complex, geomorphological main and subunit, land use, distance to valley heads, distance to roads, and distance to active faults.
- *Large scale*: slope angle, downslope curvature, cross-slope curvature, slope length, thickness of pyroclastic cover, lithology, and distance to roads and houses.

Several methods can be used to determine weighting values for the input maps:

- Walk-over studies: during a walk over study information is collected about the important factors related to the occurrence of mass movements, without actually mapping the phenomena over the entire area. This is useful only at the regional scale.
- Landslide descriptions: the use of landslide description checklists, as described in section 4.4.2.2, allows for a better understanding of the important factors. This method is most suitable at the medium and large scale.
- Overlaying of landslide information with input maps: when a landslide map is available, it can be overlaid on various input maps, and the important classes can be identified visually.

In these methods the GIS is not used to calculate quantitative weights. The analysis

with GIS includes the following steps (see also figure 2.5):
•   Entering weight values in tables connected with the input maps;
•   Recoding the input maps with these weight values;
•   Summing the individual weight maps into a hazard map;
•   Classifying this map into a limited number of classes.

The weight values assigned to each of the variable classes may be on the order of 0-10, indicating an increasing importance for landslide occurrence. Often the input maps themselves also receive weighting values, so that, for example, slope angle is considered twice as important as land use. A GIS can be helpful in assigning higher weighting values to specific combinations of factors, which one knows are associated with a higher probability of landslides than the combined sum of each factor alone. An example of this is the combination of recently planted "technified" coffee plantations without shade trees occurring with steep slopes. This is a relatively rare combination, as most "technified" coffee cultivation is restricted to flatter areas, due to its vulnerability to erosion and mass movements on steep slopes. If the two factors are treated individually, it would be impossible to give their combination a higher score. "Technified" coffee cultivation by itself should receive a relatively low score, as it is confined mostly to flatter areas. Steep slopes may receive a high score, but for all land uses and not just "technified" coffee cultivation.

This problem can be solved if combination rules are used. These are mostly Boolean (IF..THEN) statements, in which certain combinations of variables can be selected for a higher score. The major problem with this method, however, is that a large number of "decision rules" have to be formulated, taking into account all possible combinations of factors. Some important combinations may be "overlooked". To achieve all possible combinations of variable classes the resulting weight values for combinations of two input maps could be stored in a matrix, where the x- and y-axis values are the variable classes. In practice a combination of the three methods (recoding from tables, Boolean statements and two-dimensional tables) will give the best results.

In this study, limited attention has been given to this method of analysis as GIS does not play an important role in the analysis for the evaluation of critical conditions. Weight values are not obtained quantitatively, and the method is also referred to as the "blind weighting" method (Gee, 1992). The use of the method is justifiable only when no landslide map is available, so that quantitative weights cannot be determined.

Results maps produced using this technique are not presented in this study to avoid bias that may result from the author's knowledge from quantitative analysis. Another researcher, who does not have this a priori knowledge, might decide upon very different weight values. In this case, comparison with maps obtained via other methods would be incorrect, since the maps were not produced independently.

6.3 Univariate statistical analysis

In this section several methods for univariate statistical analysis will be presented. Univariate statistical analysis deals with one dependent variable (in this case the occurrence of mass movements) and one independent variable. The importance of each factor is analyzed separately. Specific combinations of variables can also be tested by treating the combination map as a new variable. The methods are based on the assumption that the important factors leading to mass movements can be quantified by calculating the density of mass movements for each variable class. Map crossing and landslide density calculation form the core of the analysis. In this section, several methods are worked out in detail: susceptibility mapping, information value method, and weights of evidence modelling (see also section 2.5.6). Before that the basic approaches in the use of GIS for statistical analysis and the selection of variables will be treated.

6.3.1 Basic approaches

Before a statistical analysis is performed it is important to define the units which will be used as the basis for sampling of variables. Basically two different approaches can be followed, which have important implications for the use of GIS (see figure 6.12):

1. *Aggregation of values for terrain units*. The important aspect in this method is the selection of relevant, homogeneous terrain units which are used as the basis for the calculation. The relevant input variables, such as lithology, slope angle and soil type are sampled for each terrain unit and the result is stored in a table. The percentage of the unit occupied by landslides, or the number of landslides within the unit, is also calculated and stored in a table. GIS is used basically for the sampling procedure. The analysis itself is done on the tabular data, and can be executed in an external statistical package or spreadsheet. The final hazard map is made by assigning the resulting hazard scores from the statistical analysis for each terrain unit to the original terrain map. The method is shown schematically in figure 6.12 (top). The method is mostly applied using a vector-based GIS in which the repeated crossing of many input maps, required in the other method of analysis described below, is very time-consuming.

The terrain units which can be selected are the following:

a.   *Large cells*. The first examples of multivariate analysis for landslide hazard assessment (Carrara et al., 1978) were based on large quadrangles, or cells, with sizes of 100 x 100 m or more. A problem with such cells is that they do not represent natural boundaries in the terrain. A cell may be located in two terrain units with very different relationships to the occurrence of mass movement. This method has been abandoned in the literature.

b.   *Geomorphological units*. A more appropriate division of the terrain is obtained by using geomorphological units. They are based on natural boundaries, but may be rather irregular in form, which can be a disadvantage in some methods. Delineation of geomorphological units depends on the skill of the geomorphologist, and is therefore subjective (see section 7.3.2).

c.   *Catchments or slope sections*. Another possibility is division based on catchments or homogeneous slope sections. A major advantage is that these can be derived (semi-) automatically from a detailed DTM. Carrara et al. (1990, 1991) have used this method successfully. The units may be located, however, within geomorphologically different

zones.

In this study a catchment map was used which was derived semi-automatically from a DTM, using neighbourhood operations. This method has some serious limitations:

- The resulting hazard map will give hazard scores for each terrain unit. Within a terrain unit no differentiation is made. Therefore the resulting map is rather general and does not fulfill requirements at the medium scale and large scale (see section 2.6).

- The aggregation of data per terrain unit will cause a generalization of the input variables which may affect the results of statistical analysis. It is always a problem how the data should be aggregated. Results will be different when the average, predominant, minimum, or maximum value of a variable is used.

- The relationship between mass movements and other variables is not evaluated at the location of the phenomena themselves. When a unit has steep slopes, for example, they may occur in different locations then the landslides present in the unit.
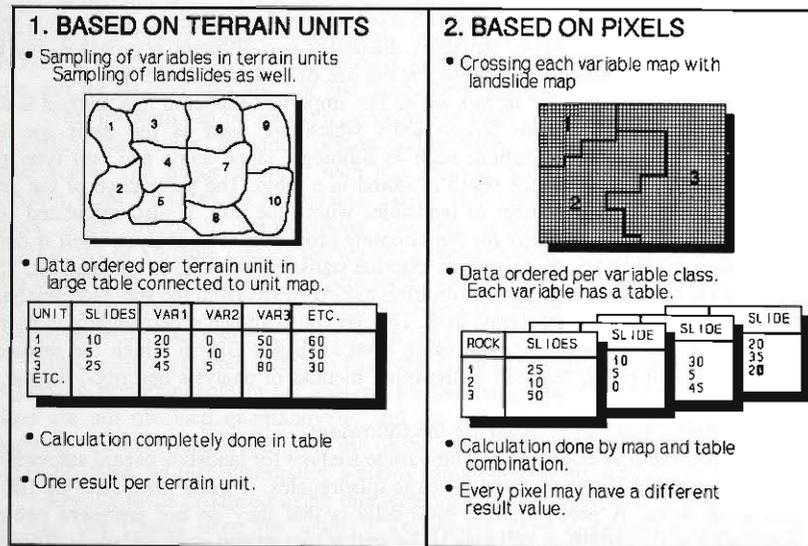
Figure 6.12: Two basic approaches in statistical analysis. Above: Aggregation of variables for terrain units. Below: Pixel based calculations.

2. *Pixel based calculations.* This method does not require aggregation of input variables over larger units in the terrain. In a raster-based GIS, the terrain is divided into a very large number of cells, also called pixels, which are generally smaller than the smallest unit in any one of the input maps. The relationship between mass movements and variable classes is established by crossing each input map with the landslide distribution map, and the subsequent calculation of mass movement densities per variable class. The results are stored

in a table related to the input maps. Final calculation of hazard maps is made by combining the weight values of the individual input maps. In contrast to the other method, the analysis is done basically on maps, and not on tables. Many separate map crossings and combinations are required. The method is shown schematically in figure 6.12.(bottom). The use of individual pixels as a basis for statistical analysis has a number of important advantages compared to the other method:

- The variables do not have to be generalized or aggregated for a terrain unit, so that generalizations are not needed.

- The relationship between the occurrence of mass movements and input maps can be evaluated at the same location.

- The resulting maps will give hazard information at the pixel level, resulting in a more detailed map.

- The analysis can be performed within the GIS and without the need for an external statistical package.

6.3.2 Variable selection

For a successful application of statistical methods, selection of the most important variables is of crucial importance. Based on knowledge about the field conditions or by use of descriptive statistics of data collected at observation points it is possible to obtain a general idea of those variables that play a role in the occurrence of mass movements. Selection of relevant variables for statistical analysis contains an important subjective element. It is generally useful to start the analysis with a large set of variables and to eliminate those which prove to be unrelated to the occurrence of mass movements. Field knowledge is very important in this respect, so the scientist can select those factors known to be important, thus avoiding waste of time and expense in the collection of irrelevant data. The list of variables used in the statistical analysis for the medium scale is given in table 6.3. A description of each of the 178 variable classes is given in appendix 26. As can be seen from this table, some of the input variables have been divided into several maps. Maps with classified distance to drainage lines were made for different stream orders. Classified distance to valley heads and classified distance to faults have been separated for the different geomorphological complexes. Based on field observations, the relationship between landslides and geomorphological complexes was expected to be much stronger in the Romeral fault zone than in the map as a whole. The road from Manizales to Chinchina was treated as a separate variable since it was expected to have a much higher influence on the occurrence of landslides. It crosses the Romeral zone in an east to west direction and important cuts and fills have been made during its construction. Two different classifications of slope angle were used: one of 10 classes, which represent equal percentage cover in the map (equal number of pixels in each class), and one classified in ranges of 10°.

To test the importance of combinations of variables, cross-maps were made of the most important input maps (See table 6.4). An attempt was also made to combine the most important variables in a single map. This was done using two general approaches:

1. *Direct crossing of input maps, without a simplification or recoding.* Four maps (slope class, geology, land use, and geomorphological complex) were crossed pairwise. The combination of slope classes (SLOC2 with nine classes) and geology (GEOL with 14 classes) resulted in a map with 99 combinations. The combination of the land-use (LUSE with nine

classes) and the geomorphological complexes (GEOC with three classes) maps resulted in a map with 27 classes. These two intermediate maps were crossed and a final map with 689 different class combinations was the result.

Map code	Number of classes	Description	Map code	Number of classes	Description
DR1	3	Distance from 1st order streams	DR2	3	Distance from 2nd order streams
DR3	3	Distance from 3rd order streams	DR4	3	Distance from 4th order streams
DR5	3	Distance from 5th order streams	DRT	3	Distance from all streams
DR12	3	Distance from 1st and 2nd order streams	DR13	3	Distance from 1st, 2nd, and 3rd order streams
DR14	3	Distance from 1st, 2nd, 3rd, and 4th order streams	DRS1	3	Distance from valley heads in the western hills
DRS2	3	Distance from valley heads in the Romeral zone	DRS3	3	Distance from valley heads in the terrace areas
DRS	3	Distance from valley heads in the whole area	GEOC	3	Geomorphological complexes
R	3	Distance from all roads	R1	3	Distance from the main road from Manizales to Chinchina
R2	3	Distance from main and secondary roads except (R1)	R3	3	Distance from all roads
PLANC	4	Classified cross-slope convexity	PROFC	4	Classified downslope convexity
F	5	Distance from all faults	F1	5	Distance from faults in the Romeral zone
F2	5	Distance from faults in the western hills	CATS	5	Classified catchment size
F3	5	Distance from lineaments	CITY	5	Distance from city
SLLC	7	Classified distance from ridges	ASPCL	8	Classified slope direction
DTMC	9	Classified altitude in classes of 100 m	SLOC	10	Classified slope map with 10 intervals containing equal number of pixels
SLOC2	9	Classified slope map in groups with of 10°	LUSE	9	Land-use classes
GEOM	11	Geomorphological main units	GEOS	9	Geomorphological subunits
GEOL	14	Geological units			

Table 6.3: Summary of the input maps used in the statistical analysis at the medium scale. The number of classes, the code of the file, and a description are given. See appendix 26 for an explanation of the classes.

2. *Crossing of simplified input maps*. Direct crossing of many different input maps will result in a very large number of combinations, of which most will have a very low number of pixels. A test of direct crossing of the maps DRT, DRS, GEOL, GEOC, GEOS, SLOC2, F, and R resulted in 3848 different class combinations, of which 67% was smaller than 50 pixels. Therefore the original input maps were reclassified into a smaller number of classes. The classes with very low landslide densities were grouped together, and the remaining were ranked according to increasing densities. Variables that appear in different maps, such as

drainage (in DRT, DRS, and GEOS) or recent alluvial and lahar deposits (GEOL, GEOS, and LUSE) were reclassified as well, to ensure they had the same areal extent in the different maps. The following maps were crossed, after recoding (see figure 6.13):

File code	Number of Classes	Variables	File code	Number of Classes	Variables	File code	Number of Classes	Variable
C1	25	GEOC * SLOC2	C9	9	GEOC * DR1	C17	40	SLOC2 * F
C2	25	GEOC * GEOL	C10	99	SLOC2 * GEOL	C18	26	SLOC2 * R
C3	25	GEOC * GEOM	C11	81	SLOC2 * GEOM	C19	25	SLOC2 * DRS
C4	27	GEOC * GEOS	C12	67	SLOC2 * GEOS	C20	26	SLOC2 * DR1
C5	27	GEOC * LUSE	C13	75	SLOC2 * LUSE	C21	101	GEOL * GEOS
C6	23	GEOC * SLLC	C14	58	SLOC2 * SLLC	C22	67	GEOL * GEOM
C7	12	GEOC * PLANC	C15	36	SLOC2 * PROFC	C23	112	GEOL * LUSE
C8	12	GEOC * PROFC	C16	36	SLOC2 * PLANC			

Table 6.4: Summary of the cross-maps with the number of classes and the code of the file.
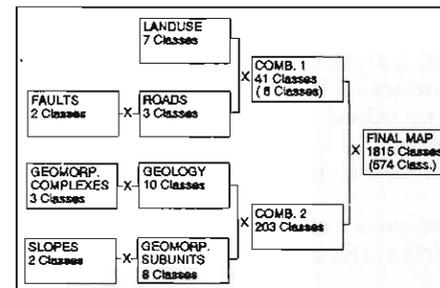
Figure 6.13: Creation of a combination map by crossing several reclassified input maps.

- LAND USE = Reclassified land-use map with seven classes (coffee without trees, coffee with trees, other crops, shrubs and trees, grass, bare, and built-up area).
- FAULTS = Reclassified distance to faults with two classes (distance < 150 m to a fault, and the rest).
- ROADS = Reclassified distance to roads, with three classes (distance < 50 m to main Chinchina to Manizales road; distance < 50 m to other main and secondary roads; distance >= 50 m to all roads)
- GEOMORPHOLOGICAL COMPLEXES = Not reclassified (western hills, Romeral zone, and terraces);
- GEOLOGY = Reclassified geological map with 10 units;
- SLOPE = Reclassified slope map with two units (slopes angles < 30 ° and >= 30 °).
- GEOMORPHOLOGICAL SUBUNITS = Reclassified geomorphological subunits with eight classes (alluvial, hilltops, denudational slopes, denudational niches, valleys, large landslides, slope deposits, and valley heads).

Two combination maps were made (final map in figure 6.13):
1. Including the land-use map, resulting in 1815 classes,
2. Excluding the land-use map, resulting in 574 classes.

Table 6.5 gives a frequency table of the number of variable combination classes occupying different surface areas for each of the two maps. From this table it can be concluded that the use of the land-use map, which does not show a very strong relationship to occurrence of landslides (as will be explained later), results in a very large number of

combinations. This large number of combinations will cause problems in computer memory storage in many of the calculation procedures explained later in this chapter. An evaluation of the effect of a large number of variable classes will be given in section 7.4.

EXCLUDING THE LAND-USE MAP				
Size of combination class in number of pixels	Number of combination classes	Percentage of total combinations	Total number of pixels per combination class	Percentage of total area in the map
< 50	208	36	3902	1
50 - 100	61	11	4470	1
100 - 500	154	27	35761	8
> 500	151	26	391400	90
INCLUDING THE LAND-USE MAP				
< 50	1042	57	15790	4
50 - 100	230	13	16848	4
100 - 500	356	20	76993	18
> 500	187	10	325900	75

Table 6.5: Class sizes of combinations resulting from crossing input maps.

6.3.3 Landslide susceptibility analysis

6.3.3.1 Introduction

A simple and useful method in statistical analysis to determine the importance of different variables for the occurrence of mass movements is the use of pairwise map crossing. In order to evaluate the importance of each of the individual maps, a cross between these maps and a landslide occurrence map is performed. The landslide densities can be easily calculated from the resulting cross-table. For each variable class and landslide type two types of densities can be calculated:

1. *Area density* = density expressed as the number of pixels with landslides divided by the total number of pixels within the variable class. This can be displayed as a percentage or permillage contents.

$$D_{area} = 1000 \frac{\text{Npix}(SX_i)}{\text{Npix}(X_i)} \qquad [6.1]$$

in which:
D_{area} = Areal density in permillage,
$\text{Npix}(SX_i)$ = number of pixels with mass movements within variable class X_i,
$\text{Npix}(X_i)$ = number of pixels within variable class X_i.

2. *Number density* = density expressed as the number of landslide occurrences per square kilometre of area of the variable class.

$$D_{number} = \frac{1 \cdot 10^6}{\text{Area}(X_i)} \text{Number}(SX_i) \qquad [6.2]$$

in which:

D_{number} = Number density (number/km^2),
$\text{Area}(X_i)$ = Area in square meters of variable class X_i,
$\text{Number}(SX_i)$ = Number of mass movements within variable class X_i,
The value of $1 \cdot 10^6$ is used to convert the area from square metres to square kilometres. Calculating area density is simple, since it is possible to use bit maps for mass movement occurrence (presence or absence). To calculate the number density, it is necessary to cross the input maps with a mass movement distribution map in which each mass movement feature has a unique code. The number of features per variable class can then be calculated by summing the number of different codes per variable class.

The individual input maps were crossed with the mass movement map SLIDE, in which each polygon was given a unique code. This way, one map crossing is sufficient to produce both the area and number density for the different mass movement types and activities.

A problem arises when a mass movement phenomenon crosses a class boundary. Should a landslide be counted only once, or should it be counted twice when it occurs in two areas? The second option was chosen, with the restriction that the scarp area should be present in each of the classes, since that is the area where the landslide originated.

Figure 6.14: Schematic representation of problems encountered in density calculations based on numbers. See text for explanation.

The problem is displayed schematically in figure 6.14. The map is the result of crossing a landslide map containing five (A to E) landslides with an input map containing two classes. Two of the landslides occur in both units. In the table a distinction is made between the scarps and bodies of a slide. The scarps and bodies have been coded separately (polygon numbers in table and map). Three phenomena have both a scarp (1) and a body (2). In calculating densities based on number, the slides which have both a scarp and a body are counted first, to prevent double counting of slides. This is done in the batch file by calculating the minimum value for SCARP/BODY when the column LANDSLIDE is used as a key. Then those units in which the MIN(SCARP) is not equal to SCARP are deleted. In this case the cross-unit numbers 3, 5, 7, 10 and 11 are deleted. Then the number of slides per unit can be calculated by counting the remaining number of cross-unit numbers within a class. This would result in a value of 3 for class 1 and a value of 3 for class 2. Note that landslide

C is counted twice, due to the presence of the scarp area in both classes, and that landslide E is counted only once.

When the relationship between the density per class and the density for the whole map is determined the overlapping phenomena should not be calculated more than once for the whole map. The number of landslides in the whole map is five. Assuming the areas of both classes are equal to 1 ha, than the number densities will be:

- Number density in class 1: 3/1 = 3 slides/ha,
- Number density in class 2: 3/1 = 3 slides/ha,
- Number density in whole area: 5/2 = 2.5 slides/ha.

Calculation of the area and number densities was limited to 12 different combinations of mass movement type and activity. They were calculated for 31 of the variables listed in table 6.3. Batch files were written in which the entire process of map crossing and density calculation was performed automatically from an input table containing the names of the input maps. This input table included a CALL command invoking the main calculation batch file. The average calculation time for determining both the area and number density for 12 different combinations of type and activity, and using one input map, was approximately 20 minutes on a 386 computer.

The output of the batch file consists of two files per variable (one for permillage area and one for number/km²). The results can be presented in the form of histograms. Figure 6.15 shows an example of such a graph for the variable SLOC2.
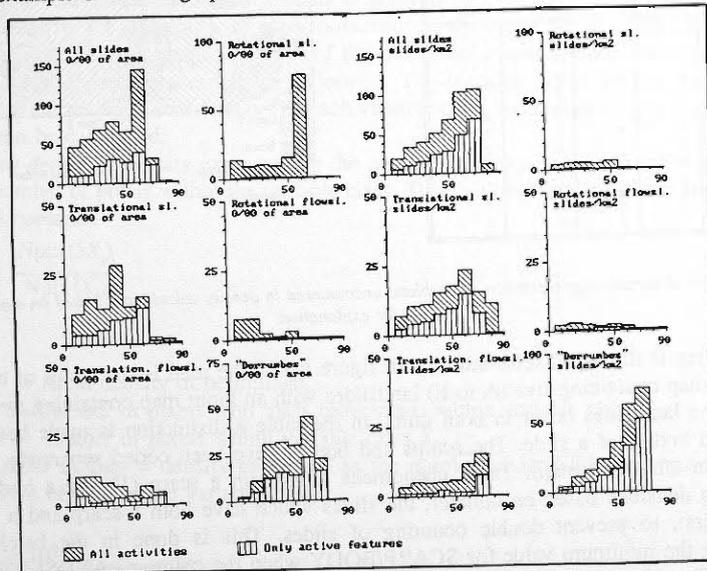
Figure 6.15: Example of results for the density calculation of slope classes (variable SLOC). The figure displays two blocks of six histograms. The left block is for density expressed in permillage of the total area per slope class. The right block expresses density as number of slides/square kilometre. In each graph there are two histograms: one representing all stable, dormant, and active features together and one representing the active features only. The x-axis displays slope angles.

The six graphs in the left half indicate the density in permillage area and the six on the right half in number/km². The histograms for all stages of activity and those for only the active features follow more or less the same trend. This means that, at least for this area, there will not be much difference in the result if all features are used, versus just the active ones. The only clear difference occurs for rotational slides, where from the comparison of the two histograms for permillage area it can be seen that the stable slides appear in lower slope intervals. Comparing the histograms for the area and number density in figure 6.15, reveals large differences. The importance of the few, but very large, stable rotational mass movements can be observed very clearly. The high densities in the steeper slope ranges are explained by the many "derrumbes", which are mostly relatively small in size, and by the fact that these slope ranges occupy a smaller area, so even with a few landslides, the density will increase rapidly.

To evaluate the influence of each variable, weighting factors were introduced, which compare the calculated density with the overall density in the area. The formula for the density based on area is:

$$W_{area} = 1000 \frac{\text{Npix}(SX_i)}{\text{Npix}(X_i)} - 1000 \frac{\sum \text{Npix}(SX_i)}{\sum \text{Npix}(X_i)} \qquad [6.3]$$

And for the density based on number/km²:

$$W_{number} = \frac{1 \cdot 10^6}{\text{Area}(X_i)} \text{Number}(SX_i) - \frac{1 \cdot 10^6}{\sum \text{Area}(X_i)} \sum \text{Number}(SX_i) \qquad [6.4]$$

The weighting values are a measure of the amount by which mass movements within a class are over- or under-represented. For example, if within a variable class there is a density of active translational slides of 35/km², and the density of active translational slides in the whole area is 2.36/km², the weighting value will be 32.64. In this way either a positive or a negative weight may result for a variable, and the influence of different variables on the occurrence of mass movements can be compared.

6.3.3.2 Evaluation of variables

In figure 6.16 the weight values for the area density versus the number density of derrumbes are compared.
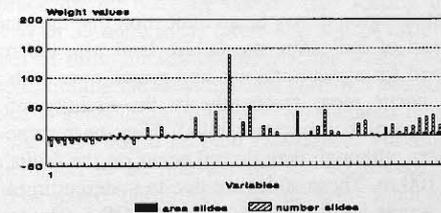
Figure 6.16: Comparison between weight values based on area and on number for a third of the 178 variable classes.

This figure shows that the weight values based on density per area have a much smaller variation than those based on number of slides/km². This is caused by the fact that most derrumbes cover only a small area. For rotational slides or flowslides with much larger areas the area density is a better indicator (Mool, 1992).

The highest weight values of variable classes are given for different mass movement types in appendix 27. The calculations were based on number density (nr/km²) and only active phenomena were used. An explanation of the variable classes is given in appendix 26. From appendix 27 the following conclusions can be made:

- The magnitude of the weighting values for the different types of mass movement reflects the relative occurrence of this type in the area. Types that occur more frequently will have higher density values, and also higher weight values, than less frequently occurring phenomena. The values for derrumbes are the highest, and the values for active rotational slides the lowest.
- Variable classes with a small areal extent are clearly overrepresented in the list of high- scoring variable classes. Classes based on distance from objects such as roads, rivers, valley heads, and faults generally occupy small areas. The occurrence of a few mass movements within these areas will result in high weighting values. Classes with large areas will generally have lower absolute weighting values. The geomorphological complexes, for example, are not present in the list for any of the mass movement types, although derrumbes are almost completely confined to geomorphological complex 2, the Romeral zone (see figure 6.5).
- The distance from valley heads (DRS, DRS1, DRS2, DRS3) are important variables for practically all mass movement types. The distance to valley heads class of less than 25 m in geomorphological complex 2 (DRS2-1) is listed among the five highest scoring classes for all processes. Striking in this respect is that the variables classes of down- and cross-slope convexity are completely missing in the list, although they are related to the presence of valley heads. This is probably caused by the poor detail of the DTM (see also section 7.2) used to calculate convexity classes, whereas the valley heads were interpreted from aerial photos, which have much greater accuracy.
- The slope angle classes (SLOC and SLOC2) do not show a clear picture for the weighting values. The high slope angle classes (> 50°) have high values, and the lower classes do not appear in the list. This is due to the small areas occupied by the higher slope ranges, and the poor quality of the DTM, so that slope angles given in the map may differ considerably from the real values (see section 7.2).
- The land-use class for shrubs (LUSE-3) occurs in nearly all of the lists. In this intensively cultivated region it may be an indication that the land-use map is probably too detailed. Instead of indicating pre-failure land use, the map shows that active slides are abandoned for agricultural use and grown over with shrubs.
- Rotational slides occur more frequently in the vicinity of valley heads within geomorphological complex 1 (western hills). They bear some relationship to faults occurring in the area, although they do not occur on the faults, but within a distance of approximately 100 m. These slides are due to undercutting by roads and drainage, as proven by the scores for R-1, DR4-1, and GEOS-5 (fluvial valleys). They occur usually at medium altitudes (DTMC-5) between 1500 and 1600 m.
- Translational slides are strongly related to valley heads, roads, and faults. They occur

on long slopes (SLLC-7) as well as in valleys (GEOS-5). The weathered debris flow materials occurring in the western hills have a relatively high number of translational slides.
- Rotational flowslides are less related to valley heads, and not at all to roads, but distance to drainage lines and faults both appear several times in the list of high-scoring variable classes. Two types of lithologies seem to be more susceptible to this type of mass movement: tertiary sediments (GEOL-14) and residual soil from dioritic gabbro (GEOL-4).
- Translational flowslides have a high occurrence on colluvial slopes (GEOM-8) with longer slope lengths (SLLC-7 and 6). A relationship to valley heads and faults is also present.

Only the 33 highest positive weighting values are given in appendix 27. It is, however, also important to examine those classes which have a distinctively lower density of mass movements than is normal in an area. As an example, the weighting values of all variable classes for active derrumbes are given in appendix 28. The following conclusions can be drawn from this table:

- Derrumbes do not occur in the lower or the highest slope ranges.
- Derrumbes occur less frequently in tertiary and quaternary sediments and more in the lithologies which are exposed in the Romeral zone. The geological unit Tadp however, which occurs only in the western part of the area, and which has an important cluster of derrumbes occurring on the steep slopes between Chinchina and Palestina, has a negative weight due to the fact that most of the material is exposed in rounded hills, with low slope ranges.
- The geomorphological units related to the terraces as well as the denudational hills receive negative weights.
- Geomorphological complex 2 (Romeral zone) has a much higher weight value than the other two complexes, which both have negative values.
- The highest scoring variable class is the distance of less than 50 m from the main road from Manizales to Chinchina, where a number of steep cutslopes occur.
- Among the highly scoring variables classes is a distance of less than 25 m from valley heads in the Romeral zone, and a distance of less than 100 m from faults in the Romeral zone.

6.3.3.3 Production of the susceptibility map

The weight values for the variable classes (see section 6.3.3.2) can be added to produce a hazard map. With 35 input maps (table 6.3) and 24 different combinations of type and activity, the number of different susceptibility maps which can be made is impressive. A small set of maps incorporating the most relevant variables should be selected. The optimal combination of variables is generally a problem. Two methods have been applied:

1. *Selection of the maps based on field experience.* Variable that are considered, on the basis of field experience, to be relevant for the occurrence of mass movements are selected and summed. For active "derrumbes" the following input maps were selected: slope class (SLOC2), geology (GEOL), land use (LUSE), geomorphological complexes (GEOC), distance to valley heads (DRS1 and DRS2), distance to roads (R1 and R2), and distance to faults (F1 and F2). The resulting map was crossed with a bit-map for active derrumbes, and

the percentage of derrumbes with a total score higher than 0 was calculated, which was 82 percent. The map was classified into four classes, after observing the changes in the curve of cumulative percentages of weighting scores for the pixels with active derrumbes. The resulting map is shown in figure 6.17. It shows a strong effect of valley heads, faults, and main road. Highest scores are found at those locations where a fault crosses a road, and valley heads are present on both sides of the road, which is the case, for example, at la Siria.

2. *Stepwise map combination*. The various input maps are added one by one. After addition of another map, the resulting scores are analyzed by crossing with the map showing active derrumbes. The percentage of pixels with derrumbes and a total score larger than zero is calculated (correctly classified pixels). If this percentage decreases after the addition of another map, such a map is rejected. If the percentage increases, the map is included.

The map addition sequence is given in table 6.6 with the resulting percentages of correctly classified derrumbes. The addition of the land-use map resulted in a considerable drop in correctly classified pixels with derrumbes. Adding the distance to roads map (R1) and the distance to faults map (F1) also lowered the percentage, which is rather strange as both maps have very high weighting values (see appendix 28) for the classes indicating a distance of less than 50 m. The highest class (distance > 50 m), however, has negative values, which causes the total of added weighting values to drop below zero in some areas in the map, which causes the percentage of pixels with derrumbes and total scores smaller than zero to increase. The resulting, classified map, is shown in figure 6.18. In this map the effects of faults and roads are not dominant. Results of the step-wise selection method depend on the sequence of map addition. Using a different order than the one given in table 6.6, other maps may be rejected or accepted.

Variable MAPS								% Correct classified	Added/ Rejected
SLOC2								64	Added
SLOC2	GEOL							91	Added
SLOC2	GEOL	LUSE						84	Rejected
SLOC2	GEOL	-	GEOC					92	Added
SLOC2	GEOL	-	GEOC	DRS2				92	Added
SLOC2	GEOL	-	GEOC	DRS2	R1			85	Rejected
SLOC2	GEOL	-	GEOC	DRS2	-	F1		84	Rejected
SLOC2	GEOL	-	GEOC	DRS2	-	-	GEOM	92	Added
SLOC2	GEOL	-	GEOC	DRS2	-	-	GEOM GEOS	93	Added

Table 6.6: *Step-wise selection of input maps. Whenever the percentage of correctly classified landslide pixels decreases, the input map that was added is rejected.*

6.3.3.4 Use of combined input maps

Selecting the proper variables in the analysis is of great importance. Weight values can also be calculated for one map containing combinations of variable classes. An example map is given in figure 6.19. An illustration of the effect of variable selection is given in figure 6.20, in which weight values for six different types of mass movement are given for two different subsets of distance to roads.
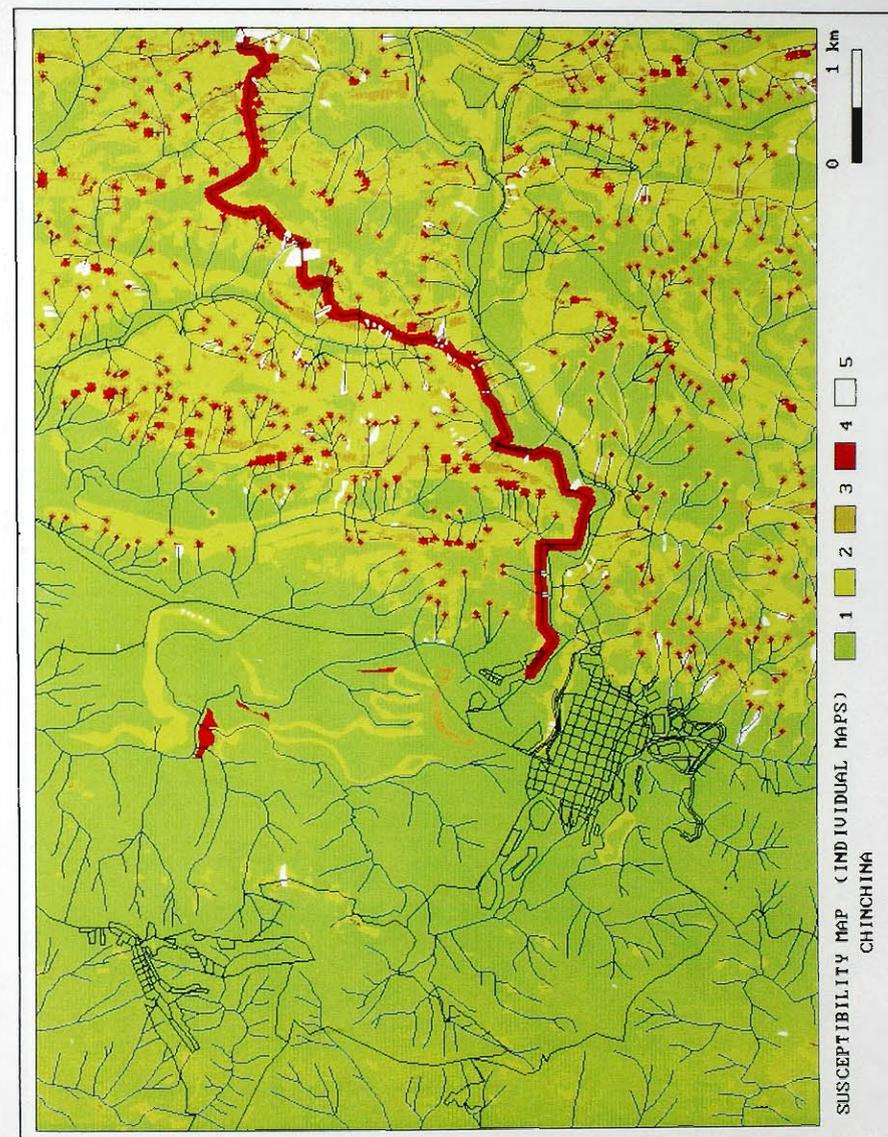
Figure 6.17: *Susceptibility map for active derrumbes for the medium-scale study area. The map is made for active derrumbes, by summing weight values for slope class, geology, land use, geomorphological complexes, and distance to valley heads, roads and faults. Legend: 1 = Very low, 2 = Moderately low, 3 = Moderately high, 4 = High, 5 = Location of derrumbes.*
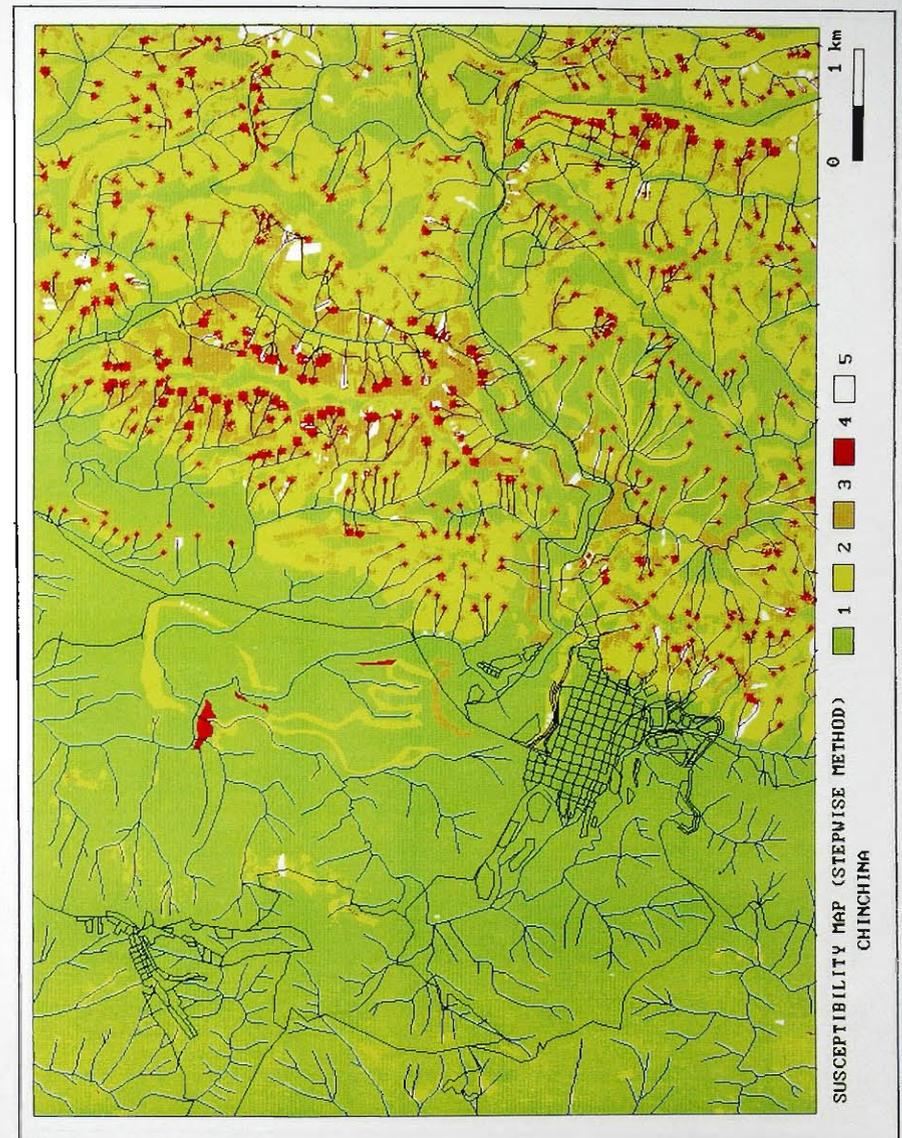
Figure 6.18: Susceptibility map for active derrumbes, made by step-wise addition of weight values from different input maps. Legend: 1 = Very low, 2 = Moderately low, 3 = Moderately high, 4 = High, 5 = Location of derrumbes.
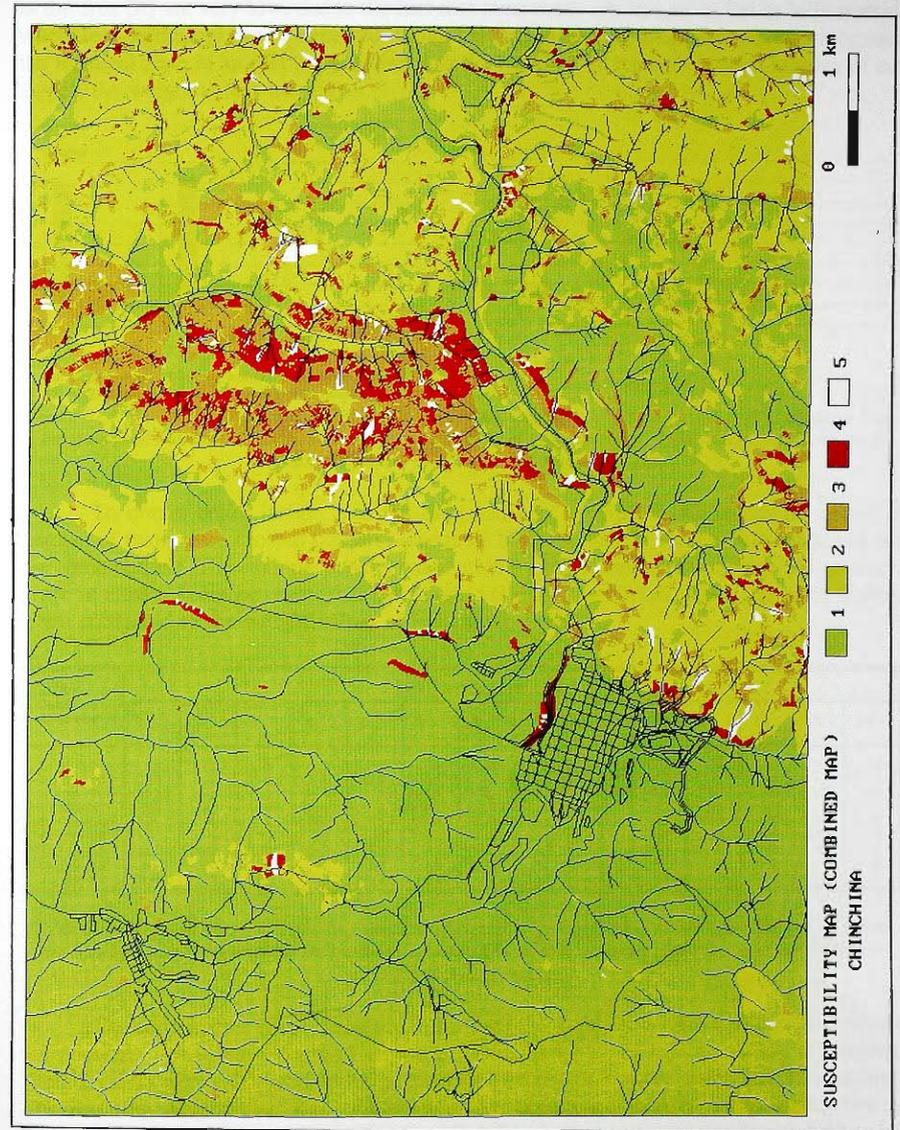
Figure 6.19: Susceptibility map for the occurrence of derrumbes made by calculation of the weight values for specific combinations of slope angle, geological unit, land-use class, and geomorphological complex. Legend: 1 = Very low, 2 = Moderately low, 3 = Moderately high, 4 = High, 5 = Location of derrumbes.

152c

From the figure it can be seen that the weight values for the subset of distance to all roads in the area (R) are very low, due to the fact that most roads are located in flat or hilly terrain, where few derrumbes can be expected. When only the main road is considered, which crosses the Romeral zone in an east to west direction (R1) and which contains a large number of cut slopes, the weight values are higher.
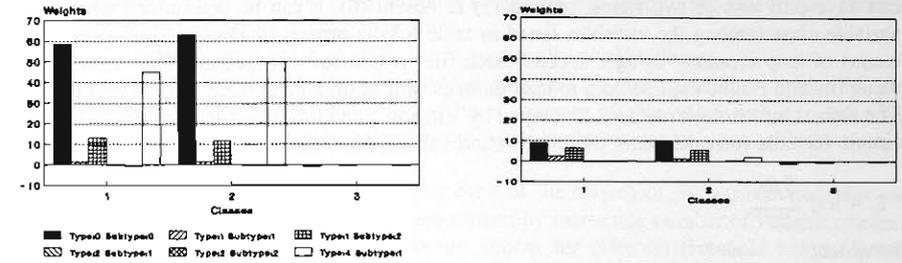
Figure 6.20: Weight values for two different subsets of roads. Left: weight values for 3 classes of distances from the main road Manizales-Chinchina (1 = <25 m., 2 = 25-50 m. and 3 = >50m.). Right: weight values for the 3 classes of distances to all main and secondary roads.

To obtain better insight into the importance of specific combinations of factors, a number of maps were crossed pairwise (see table 6.4), and weight values were calculated for the combinations. The example density calculation for the combination of slope and geology, given in table 6.7, demonstrates that the weight values for combined classes are much higher, when compared to the weight values of individual classes

SLOPE CLASSES degrees	GEOLOGICAL UNITS													
	1	2	3	4	5	6	7	8	9	10	11	12	13	14
1: 0-10°	2	-2	-2	3	5	-2	-2	-2	-2	-1	0	-2	-2	-2
2: 10-20	13	-2	-1	4	12	3	-1	-2	-2	-2	1	-2	-2	-2
3: 20-30	15	-2	1	6	5	12	-1	-2	-2	-2	16	-2	0	-2
4: 30-40	27	-2	2	15	5	-2	13	-2	-2	-2	-2	-2	4	-2
5: 40-50	25	-2	8	21	7	-2	2	-2	-2	-2	40	27	42	-2
6: 50-60	60	-2	37	39	3	-2	6	-2	-2	-2	50	-2	154	-2
7: 60-70	180	-2	162	-2	43	-2	-2	-2	-2	-2	-2	-2	-2	-2
8: 70-80	-2	-2	-2	2	-2	-2	-2	-2	-2	-2	-2	-2	-2	-2
9: 80-90	-2	-2	-2	-2	-2	-2	-2	-2	-2	-2	-2	-2	-2	-2

Table 6.7: Weight values for specific combinations of classes of geology and of slope angle. The weight values are based on number density (nr/km^2) and are calculated for active derrumbes. Description of the geological units is found in appendix 26.

The combination maps discussed in section 6.3.2 (table 6.4) were also used to evaluate the possibility of using a combination of variables as input for the calculation of weights. Weight values were calculated for the occurrence of active derrumbes, using number densities. The resulting weight map was crossed with the occurrence map of active derrumbes to determine the percentage of correctly classified features (i.e., features with a weight value higher than zero). The combination map resulted in 97% of derrumbes with a score above zero, indicating that the prediction was very good.

153

6.3.4 Information value method

6.3.4.1 Introduction

The use of a combination of numerical variables (such as slope angle values) and alpha-numerical variables (such as lithological units) in a statistical analysis is generally problematic. This can be solved by treating each variable class as a separate variable, which can have only one of two states: present (1) or absent (0). It can be determined whether a variable class (among the variables listed in table 6.3) is present or absent. This is done by means of map crossing, using a special batch file written for this method. The information value method can be applied both to land units as well as on a pixel basis (see section 6.3.1). The hazard information method, developed by Yin and Yan (1988), is based on the following simple formula for calculating the information value I_i for variable X_i :

$$I_i = \log \frac{S_i/N_i}{S/N}$$
[6.5]

In which:

S_i = the number of land units or pixels with mass movements and the presence of variable X_i,

N_i = the number of land units or pixels with variable X_i,

S = the total number of land units or pixels with mass movements,

N = the total number of land units or pixels.

The degree of hazard for a land unit or pixel j is calculated by the total information value I_j:

$$I_j = \sum_{i=0}^{m} X_{ij} I_i$$
[6.6]

in which:

m = number of variables,

X_{ij} = 0 if the variable X_i is not present in the land unit or pixel j and 1 if the variable is present.

6.3.4.2 Calculation based on terrain units

Calculating the information value based on terrain units requires the following steps:

1. Crossing of a land-unit map with the mass movement occurrence map, and calculation of both the area and number density for different types of mass movements.

2. Crossing of each input map with the land unit map, and calculation for each polygon of the percentage covered by each variable class.

3. Definition of the presence or absence of each variable class using a threshold value for the percentage, which has to be specified separately for each variable.

4. Combining the density values for the mass movement type selected with the presence/absence values of the variable classes, for each polygon.

5. Calculation of the terms N, S, N_i, and S_i (equation [6.5]) and combination of these into an information value I_i.

6. Evaluation of the information values of all variable classes, and combination into a

final information value I_j.

The input maps listed in table 6.3 were used to calculate the information values. Catchment areas were used as the basic terrain units for the calculation. Different tests were carried out with variations of threshold values (step 3), mass movement type and variable classes used in the final combination (step 6). Three different threshold values were used:

1. For the actual presence or absence of a variable class a threshold value of 1% (of the pixels with the variable class within a land unit) was used to account for the "noise" produced by errors in map matching.

2. A relatively high value of 20% was used for all variable classes.

3. A variable threshold value which was determined for each variable individually, and which can range from 1 to 99%. The magnitude of this value was decided after comparing the percentage values of the variable classes per polygon with the overall density.

The resulting information values for each of the classes of the various variables are given in appendix 29. The variable maps are ranked by increasing number of variable classes. For most variable classes various results are shown for different threshold values. Some conclusions from appendix 29 are given below:

1. Varying the threshold values produces in different effects on the information values for the various maps. The information values for the catchment size map (CATS) obviously do not change when the threshold is raised from 1 to 99%, as the catchment areas were used as the terrain units in the calculation.

2. Most maps show an increase in positive information values, or a decrease in negative information values, when the threshold values are increased (i.e., when the rule for determination of the presence/absence of a variable class is applied more strictly). In that case most of the polygons where the variable class is of only minor importance are eliminated, thus lowering the factor N_i in equation [6.5]. If there is a positive relationship between the occurrence of derrumbes and the presence of a particular variable class, elimination of those polygons where the variable class is only marginally present will lead to proportionally lower decrease of the factor S_i and hence to an increase in the information value. In the case of a negative relationship the decrease in S_i will cause some polygons, where an occasional combination of derrumbes and variable classes occurs, to be no longer counted. The decrease will be proportionally higher than that for N_i, leading to a decrease of the information value.

3. Some variable maps deviate from this general trend. Maps such as DRS2 (distance to valley heads in the Romeral fault zone), DR2, and DR5 (distance to second- and fifth-order streams, respectively) show a decrease in positive information values when the threshold is increased. This can be explained by the fact that the relationship between mass movements and the variable class is important, even if the variable class occupies only a small part of the catchment. For DRS2 this is obvious; the valley head will not occupy a large area in the catchment, but is nevertheless important in relation to derrumbes.

A general conclusion is that it is important to evaluate the importance of setting specific threshold values for each variable separately. Considering the magnitude of the information values for the variable classes, the following conclusions can be drawn:

1. The highest information values occur for certain slope ranges (SLOC), geological units

(GEOL), and maximum height zones (DTMC).

2. Other high information values occur for classes of the distance to valley heads in the Romeral fault zone (DRS2), the geomorphological complex of the Romeral fault zone (GEOC), the distance to the main Manizales-Chinchina road (R1), and the distance to faults in the Romeral fault zone (F1).

3. Strongly negative information values occur for some geological units (GEOL), some slope ranges (SLOC), and the geomorphological complex of terraces and western hills (GEOC).

4. Most of the variable classes show rather low information values, indicating that they are not very significant for the occurrence of derrumbes. One of the most striking variables which does not display a clear relationship is land use (LUSE). "Technified" coffee cultivation without trees (class 4 in LUSE) does not seem to have any relationship with derrumbes, contrary to what is observed in practice. Many areas where new coffee is introduced are highly susceptible to mass movements. The explanation for this is related to the selection of the variable classes. "Technified" coffee cultivation without shade trees occurs quite extensively throughout the area, mostly on gentle slopes. Problems with mass movements in this type of cultivation occur only on steeper slopes. When slope steepness is not separated from land use in the input data, the average value for the whole land-use class is calculated, and the characteristics of steep slopes are masked. Traditional coffee cultivation, on the other hand (class 6 in LUSE), is found almost exclusively in the steeper areas, which explains the higher information value. Another reason for the low values for "technified" coffee cultivation is that this farming system is susceptible to mass movements only during the first few years after planting. Since the landslide distribution map and the land-use map are not based on the same year, and the legend unit for "technified" coffee cultivation makes no distinction according to the year of planting, the resulting relationship is not obvious. An evaluation of the dependence of variables with respect to the occurrence of mass movements will be given in section 6.3.5.3.

5. The importance of creating relevant variable classes based on field knowledge is also clearly illustrated by the variable DRS (distance from valley heads). The information values for the entire area are slightly positive, and not as high as for the pairwise crossing of variable maps, discussed in section 6.3.3. When this map is divided into three maps for the three geomorphological complexes in the area, much higher positive values can be observed for geomorphological complex 2 (DRS2) than for the other two, whose values are either zero or negative. The same can be said for the variables R (distance to roads), F (distance to faults) and DR1 to DRT (distance to streams). This again stresses the importance of separation or combination of variables into groups, for which the user, based on field experience, expects stronger relationship than from individual variables.

From the matrix containing the information values for all variable classes a total information value was calculated for each catchment. The resulting information values were classified into classes of 0.5 each and frequency distributions were calculated in which the units with and without derrumbes are separated. Two threshold values, 1 and 20%, were used. The classification of the units is given in table 6.8 and the frequency distributions in figure

6.21. From the table it can be observed that there is a strong difference between the classified stable and unstable groups. The error in the unstable observed group is rather low (22 to 24 units were observed as unstable and predicted as stable), caused by some isolated derrumbes in the terrace scarp of Chinchina and some in the western hills. The error in the observed stable units, however, is very large (168 to 196 units were observed as stable and predicted as unstable). The units which have been classified as unstable on the basis of their information values are practically all located in the geomorphological complex of the Romeral fault zone, where the majority of derrumbes is located. The large difference between the two errors may indicate that the large number of units without active derrumbes which were predicted to be instable may be considered potentially hazardous areas.

Observed		Predicted		
		Stable	Unstable	Total observed
Stable	Threshold: 1 %	201	196	397
	Threshold: 20%	229	168	397
Unstable	Threshold: 1 %	24	131	155
	Threshold: 20%	22	133	155
Total predicted	Threshold: 1%	225	327	552
	Threshold: 20%	251	301	552

Table 6.8: Classification of stable and unstable groups.
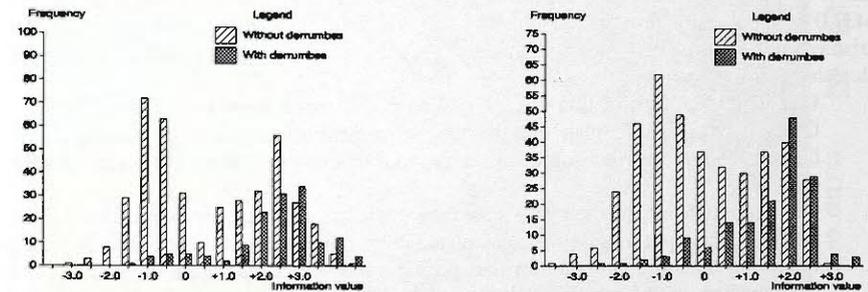
Figure 6.21: Frequency distribution of information values for the units calculated with a threshold of 1% (left) and 20% (right).

Both graphs of figure 6.21 show a bimodal distribution for the catchments without derrumbes. The ones from the tail above zero are considered to be areas susceptible to the occurrence of derrumbes.

Yin and Yan (1988) presented the following equation for estimation of the precision of the classification:

$$A = \frac{M_i}{N_i} \sqrt[3]{\left(1 - \frac{M - M_i}{N - N_i}\right)} \qquad [6.7]$$

in which:

A = precision of the predicted result,

N = total number of terrain units (catchments in this case) in the area,

N_i = number of terrain units with landslides,

M = number of terrain units predicted as unstable,

M_i = number of terrain units predicted as unstable which have landslides,

The precision of the result as calculated from this formula is 71%.

The final information values were classified into five classes, and the catchment map was recoded with the resulting scores. The resulting hazard map is given in figure 6.22. The mass movement features (derrumbes) used for the calculation are indicated. From this map it can be concluded that the Romeral zone (the area east of Chinchina) has a much higher score than the other two complexes. The terraces have the lowest values, as could be expected. The terrace (La Mesa) in the Romeral zone also has a relatively low score. The steep slopes along the road from Chinchina to Palestina have a higher score than the rest of the western hills, which is in good agreement with the result of previous analyses.

6.3.4.3 Pixel-based calculation

The information value method can also be applied at the pixel level, with individual pixels as terrain units. The disadvantage of using quadrangular units as (discussed in section 6.3.1) does not apply when the units are sufficiently small (in this case 12.5 x 12.5 m). The information value per pixel cannot be calculated in the same way as for larger terrain units, such as the catchment areas used in section 6.3.4.2. Since there are so many pixels (561 x 779 = 437,019) the construction and handling of a matrix, with the pixels on the y-axis and the variables on the x-axis, is not feasible. Instead, the information values for each input map are calculated for each variable class.

Calculating the information value based on pixels requires the following steps:

1. Crossing of each input map with the mass movement occurrence map, and calculating the area and number density of different types of mass movements for each variable class.

2. Calculating the information values for area and number density for each variable class.

3. Recoding the input map with the calculated information values for each class, resulting in an information value map for the specific variable classes within the map.

4. Combination of information value maps by simple addition, which gives the total information value per pixel.

5. Classification of the information values in a number of classes, and production of final map, which is then crossed with the mass movement occurrence map to evaluate the accuracy.

The information value method applied on a pixel basis is in fact very similar to the susceptibility determination presented in section 6.3.3. The only difference is that in the information value method the log value of the quotient of class density over map density is entered, whereas in the susceptibility method the difference in densities was used. The information values calculated from equation [6.5] are always smaller than the weight values calculated with equation [6.4]. Figure 6.23 displays the values obtained by the two methods for all variable classes, which have been ranked by increasing weight values. The first 25 variable classes in the curve have no active derrumbes and therefore have the same weights.
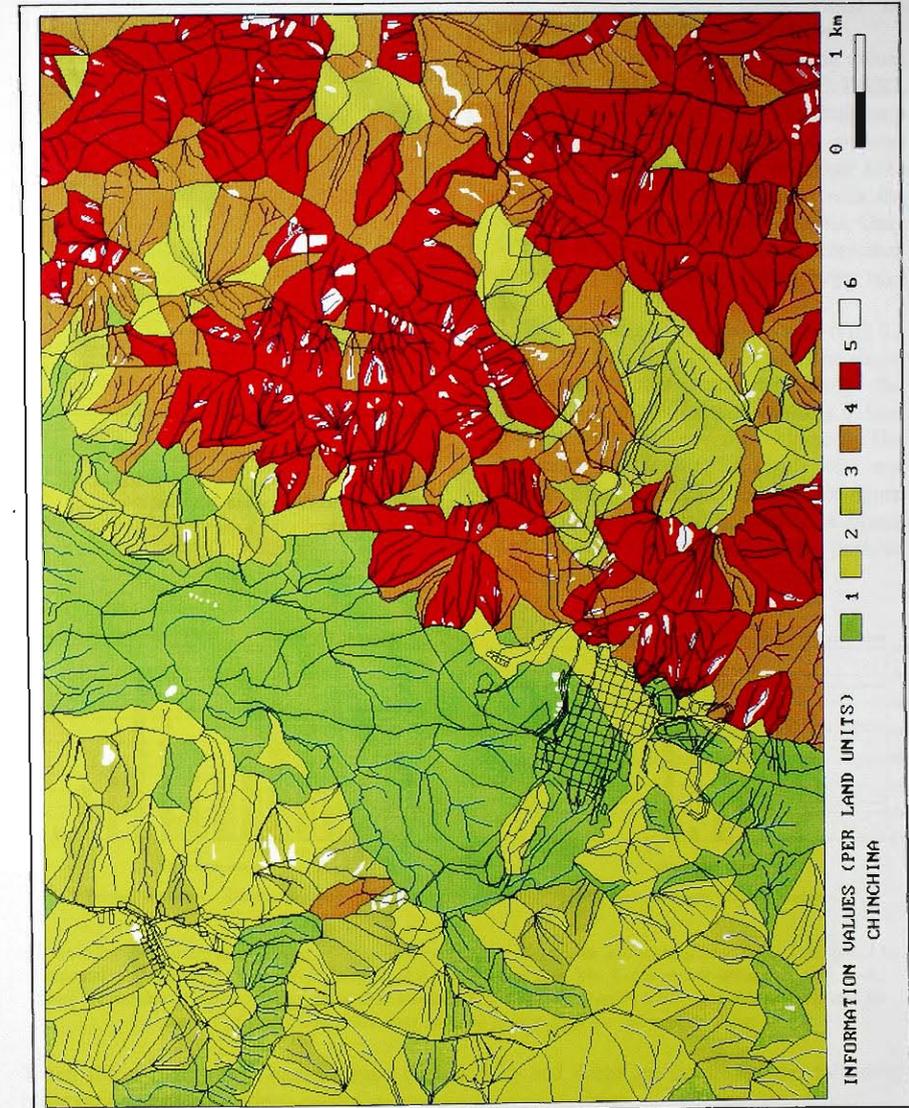
Figure 6.22: Classified information value map of the medium-scale study area for the occurrence of derrumbes producing using the information value method calculated on the basis of terrain units (catchment areas). The five classes have the following boundaries: stable (1 = <-1.5), relatively stable (2 = -1.5 to -0.5), doubtful (3 = -0.5 to 0.5), relatively unstable (4 = 0.5 to 1.5), and unstable (5 = >1.5).
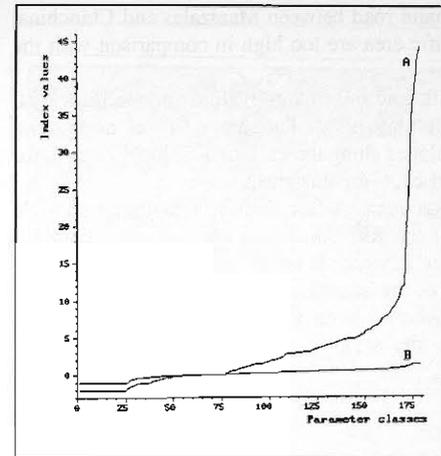
Figure 6.23: Comparison between weight values calculated according to equation [5.4] (A) and according to equation [5.5] (B)

Two different hazard maps based on information values have been made:

1. By summation of the information values for GEOL, SLOC2, LUSE, GEOC, DRS2, DRS1, F1, F2, R1, and R2. The frequency distributions of pixels with and without active derrumbes are given in figure 6.24 (left). The figure is in agreement with the results of the land unit based analysis. Only 5 % of the pixels occupied by derrumbes does not have information values larger than 0.

2. By crossing four input maps (GEOL, SLOC2, LUSE, and GEOC) into one single combination map and calculating the information values for the resulting unique combinations of variable classes. The frequency distributions of pixels with and without active derrumbes are given in figure 6.24 (right). This results in 95% of pixels with active derrumbes and positive information values.
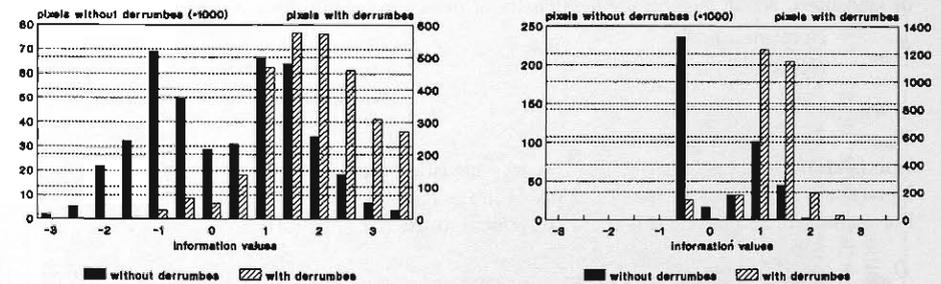
Figure 6.24: Frequency distributions of information values for pixels with and without derrumbes. Left: based on summation of individual maps. Right: Based on a combination map. The Y-axis on the left side of the graphs gives the number of pixels without derrumbes multiplied by 1000, the Y-axis on the right side of the graph the number of pixels with derrumbes, and the X-axis gives the information values.

When the two resulting hazard maps (figure 6.25 and 6.26) are compared the following observations can be made:

1. In the map based on summation of individual variable classes (figure 6.25) individual variable classes have an excessively strong influence on the total information value. Due to the high information values for buffers along faults and valley heads in the

159

Romeral zone and the buffer along the main road between Manizales and Chinchina, the total information values in that specific area are too high in comparison with the values in the rest of the area.

2. When a large number of input maps with low information values for the individual variable classes are summed, the result may be a "flattening off" of areas with moderate information values. The steep slopes along the Palestina-Chinchina road, for example, are placed in the lowest hazard class for this reason.

3. Figure 6.25 indicates a low hazard in some areas, where there is actually no possible hazard for derrumbes. The floodplain of the Rio Chinchina, and the terraces in the Romeral zone, both have a hazard class of 2, which is not in accordance with reality.

4. Figure 6.26 gives a better representation of the hazardous regions. Moreover, isolated areas outside of the Romeral fault zone where a hazard for derrumbes exists, such as the terrace slopes near Chinchina and the steep slopes between Chinchina and Palestina, are classified correctly.

6.3.5 Weight of evidence modelling

6.3.5.1 Introduction

This method was developed at the Canadian Geological Survey (Agterberg et al., 1990; Bonham-Carter et al., 1990) and was applied to the mapping of mineral potential. Sabto (1991) applied the method for landslide hazard analysis. The method consists of reducing each set of landslide-related factors on a map to a pattern of a few discrete states. In its simplest form the pattern for a feature is binary, representing its presence or absence within a pixel. According to Bonham-Carter et al. (1990), the first step is determining the prior probability of landslides, which is given by the density of pixels with landslides within the study area:

$$P_{prior} = \frac{Npix(slide)}{Npix(total)} \qquad [6.8]$$

in which:

P_{prior} = prior probability,
Npix(slide) = the number of pixels with a landslide occurrence,
Npix(total) = the total number of pixels in the map.

For mathematical reasons it is more convenient to use the odds (O):

$$O_{prior} = \frac{P_{prior}}{1 - P_{prior}} = \frac{Npix(slides)}{Npix(total) - Npix(slides)} \qquad [6.9]$$

Considering the relationship between a binary variable map (B_i) and a landslide map (S), the following combinations are possible:

B_i = Npix(B_i)/Npix(total)
B_i = Npix(total)-Npix(B_i)/Npix(total)
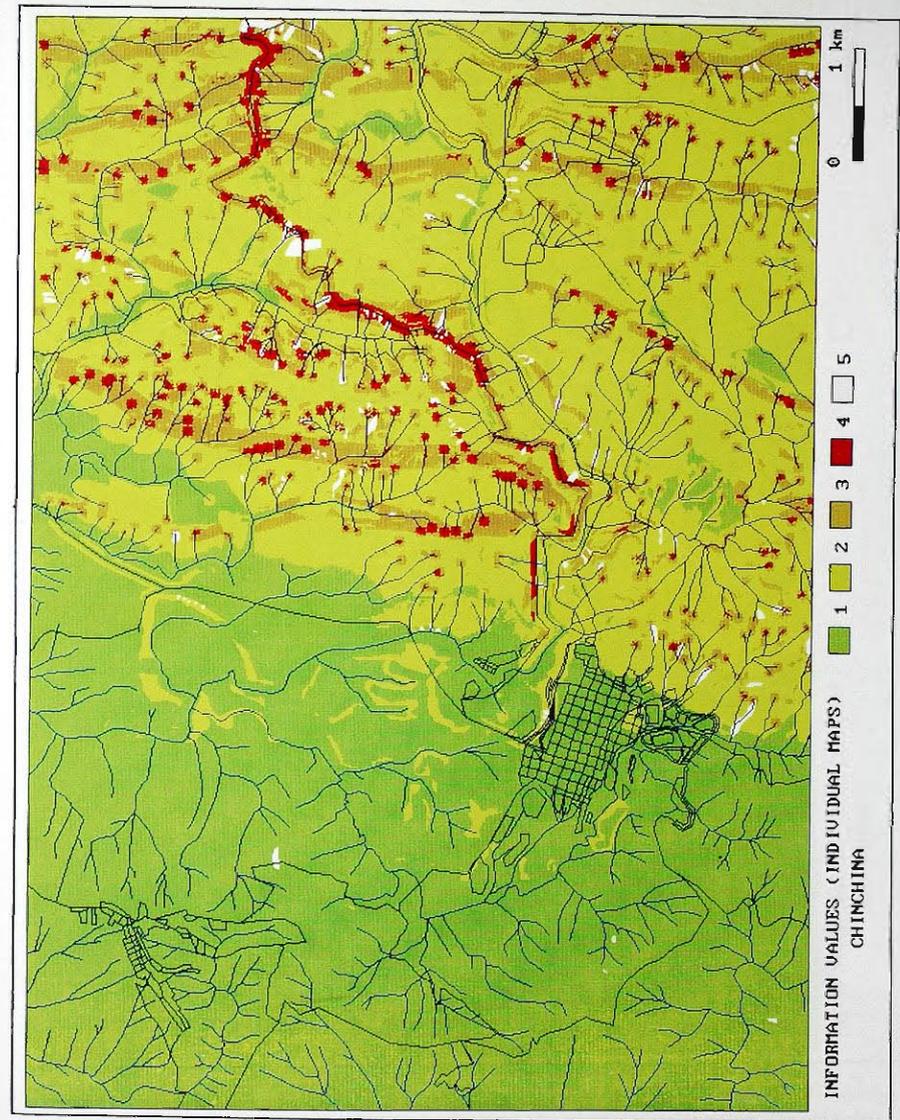
Figure 6.25: Classified information value map of the medium-scale study area for the occurrence of derrumbes made by summation of information value maps for individual variables. The five classes have the following boundaries: stable (1 = <-1.5) , relatively stable (2 = -1.5 to -0.5) , doubtful (3 = -0.5 to 0.5), relatively instable (4 = 0.5 to 1.5) and unstable (5 = >1.5). The occurrences of derrumbes are also indicated.
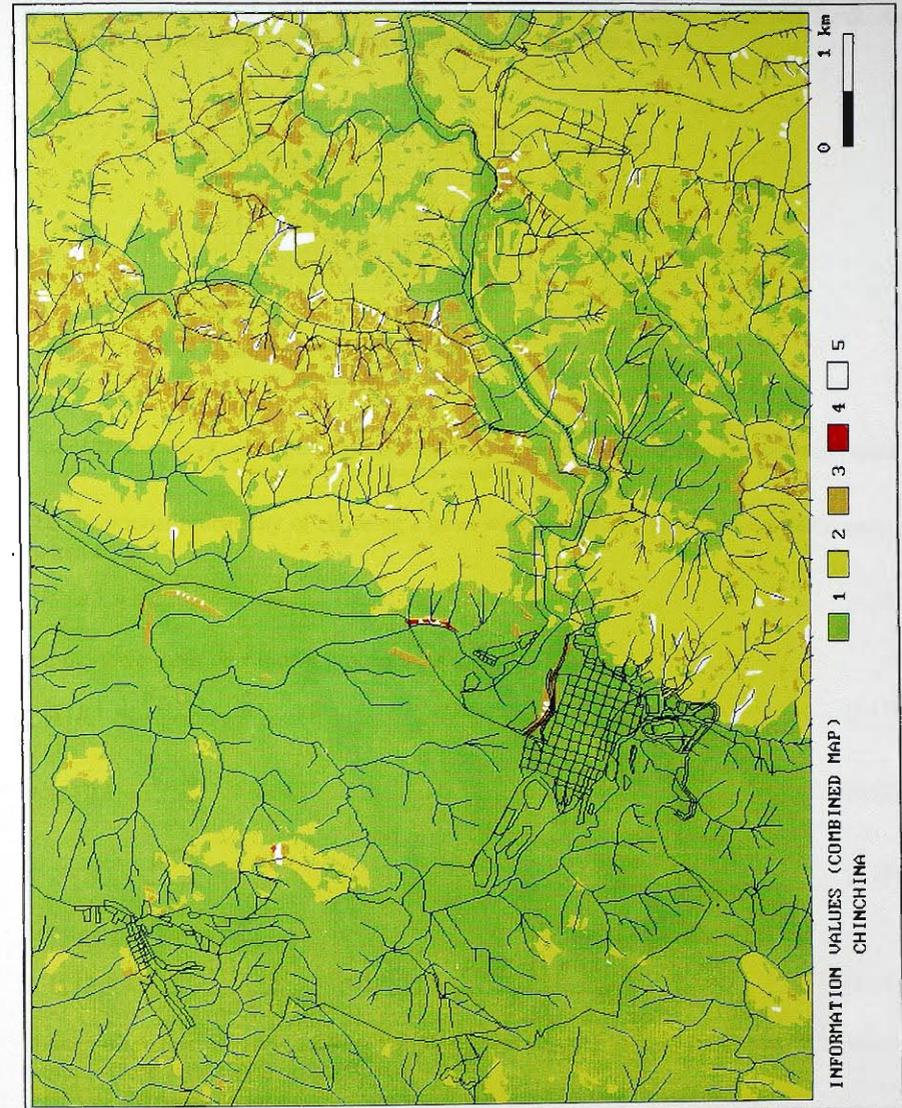
Figure 6.26: Classified information value map of the medium-scale study area for the occurrence of derrumbes based on the calculation of information values for unique combinations of variable classes. The same class boundaries as in figure 6.25 were used.

160b

Four combinations of B_i and S are possible in the map: $B_i \cap S$, $\overline{B_i} \cap S$, $B_i \cap \overline{S}$ and $\overline{B_i} \cap \overline{S}$. An example of the weight of evidence modelling is given in figure 6.27.


```
Npix(tot) =1000
Npix(s)  =10
Npix(Bi)  =200
[ 6.8] =10/1000=0.01
[ 6.9] =10/990=0.010101
[ 6.10]=5/200=0.025
[ 6.11]=195/200=0.975
[ 6.12]=5/800=0.00625
[ 6.13]=795/800=0.99375
[ 6.14]=0.5*0.01/0.2
       =0.025
and 0.5*0.01/0.8
       =0.00625
[ 6.15]=ln(0.5/0.197)
       0.931
[ 6.16]=ln(0.5/0.803)
       =-0.473
```

Pattern Bi   Landslide

Example of weight of evidence Modelling
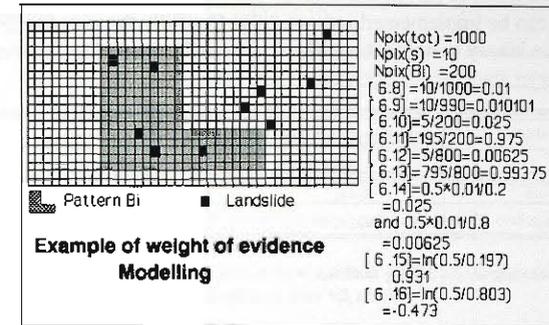
Figure 6.27: Example of weight of evidence modelling using an imaginary data set. The numbers between square brackets are the equation numbers from section 6.3.5.1.

The conditional probability of choosing a pixel with a landslide, given that the cell contains pattern B_i is:

$$P\{S \mid B_i\} = \frac{B_i \cap S}{B_i} \qquad\qquad [6.10]$$

and the three other conditional probabilities are:

$$P\{\overline{S} \mid B_i\} = \frac{B_i \cap \overline{S}}{B_i} \qquad\qquad [6.11]$$

$$P\{S \mid \overline{B_i}\} = \frac{\overline{B_i} \cap S}{\overline{B_i}} \qquad\qquad [6.12]$$

$$P\{\overline{S} \mid \overline{B_i}\} = \frac{\overline{B_i} \cap \overline{S}}{\overline{B_i}} \qquad\qquad [6.13]$$

According to Bayes rule:

$$P\{S \mid B_i\} = \frac{P\{B_i \mid S\}\, P\{S\}}{P\{B_i\}} \quad,\quad P\{S \mid \overline{B_i}\} = \frac{P\{\overline{B_i} \mid S\}\, P\{S\}}{P\{\overline{B_i}\}} \qquad\qquad [6.14]$$

Bonham-Carter et al. (1990) defined positive and negative weights (W_i^+ and W_i^-), which combine these conditional probabilities:

$$W_i^* = \log_e \frac{P\{B_i \mid S\}}{P\{B_i \mid \overline{S}\}} \qquad\qquad [6.15]$$

and

$$W_i^- = \log_e \frac{P\{\overline{B}_i | S\}}{P\{\overline{B}_i | \overline{S}\}} \qquad [6.16]$$

In GIS the method can be implemented rather easily. Consider the simple crossing of a binary landslide map with a binary variable map. The four possible resulting combinations are given in table 6.9.

Landslides		Variable class represented as binary pattern	
		1 (present)	0 (absent)
Present	1	Npix$_1$	Npix$_2$
Absent	0	Npix$_3$	Npix$_4$

Table 6.9: Cross-table example of a binary landslide map with a binary variable map. Npix$_{1-4}$ is the number of pixels for each combination.

The weights of evidence can be written in numbers of pixels as follows:

$$W_i^* = \log_e \frac{\dfrac{Npix_1}{Npix_1 + Npix_2}}{\dfrac{Npix_3}{Npix_3 + Npix_4}} \qquad [6.17]$$

and

$$W_i^- = \log_e \frac{\dfrac{Npix_2}{Npix_1 + Npix_2}}{\dfrac{Npix_4}{Npix_3 + Npix_4}} \qquad [6.18]$$

If more binary maps are used, the weights can be added, provided that the variable maps are conditionally independent with respect to landslide occurrence. The logarithm of the posterior odds can be calculated as follows:

$$\log_e O\{S | B_1^k \cap B_2^k \cap B_3^k ... B_n^k\} = \sum_{i=1}^{n} W_i^k + \log_e O_{prior}\{S\} \qquad [6.19]$$

and the posterior probability as:

$$P\{S\} = \frac{O}{(1 + O)} \qquad [6.20]$$

The contrast $C = W^+ - W^-$ gives a useful measure of the correlation between the variable map and the landslide occurrences. C becomes zero when a map has a distribution which is spatially independent of the points.

The main assumption for univariate statistical methods is that the maps should be conditionally independent. To test this independence a pairwise test can be executed

(Bonham-Carter et al, 1990). All possible pairs of variable maps should be evaluated separately. The pairwise test includes the calculation of observed and expected frequencies of landslides. Therefore the maps are crossed pairwise, and the resulting cross map is crossed again with the mass movement map. The combinations obtained from crossing two binary maps and a landslide map are given in table 6.10.

Landslides	Possible combinations of two binary maps			
	$B_1 \cap B_2$	$B_1 \cap \overline{B}_2$	$\overline{B}_1 \cap B_2$	$\overline{B}_1 \cap \overline{B}_2$
Present	Npix$_1$	Npix$_2$	Npix$_3$	Npix$_4$
Absent	Npix$_5$	Npix$_6$	Npix$_7$	Npix$_8$

Table 6.10: Possible combinations of two binary input maps (B$_1$ and B$_2$) and a landslide map.

Using the weight of evidence modelling, the logarithm of the odds for each unique overlap of two variable classes, is calculated by:

$$\log_e O(S | B_1 B_2) = W_1^* + W_2^* + \log_e O(S) \qquad [6.21]$$

$$\log_e O(S | B_1 \overline{B}_2) = W_1^* + W_2^- + \log_e O(S) \qquad [6.22]$$

$$\log_e O(S | \overline{B}_1 B_2) = W_1^- + W_2^* + \log_e O(S) \qquad [6.23]$$

$$\log_e O(S | \overline{B}_1 \overline{B}_2) = W_1^- + W_2^- + \log_e O(S) \qquad [6.24]$$

The predicted number of pixels in each unique overlap can be calculated, using:

$$m_i = P_i \, Npix_i \qquad [6.25]$$

in which:
m_i = the number of predicted landslides for the overlap of two classes,
P_i = the calculated probability for the overlap of the two classes,
Npix$_i$ = the number of pixels in each overlap (for B$_1 \cap$ B$_2$ this will be Npix$_1$ + Npix$_5$).
The conditional independence is tested with the following formula:

$$G^2 = -2 \sum_{i=1}^{8} x_i \log \frac{m_i}{x_i} \qquad [6.26]$$

in which:
x_i = the number of mass movement occurrences for the overlap of two classes (for B$_1$ $\cap$ B$_2$ this will be Npix$_1$).
The function G^2 has a χ^2 distribution with 2 degrees of freedom (Bonham-Carter et al., 1990). On the basis of the result of the χ^2 test the selection of the variable maps is made. The weight of evidence values are added and the posterior probability is calculated. After classification of the posterior probability, the expected number of landslide occurrences per probability class is calculated for each class and compared with the observed number of occurrences per probability class. The expected frequency per class is given by:

$$f_{i(e)} = P_i \, Npix_i \qquad [6.27]$$

in which:

$f_{i(e)}$ = expected number of occurrences per probability class i,
P_i = the probability per class i,
$Npix_i$ = the area (in pixels) of probability class i.

By crossing the predictor map with the mass movement map the actual number of mass movements can be calculated, and the χ^2 test can be applied:

$$\chi^2 = \sum \frac{(f_{i(o)} - f_{i(e)})^2}{f_{i(e)}} \qquad [6.28]$$

in which $f_{i(o)}$ = the observed frequency of landslides.

6.3.5.2 Results

The weight of evidence values were calculated for all variables listed in table 6.3. The method explained in the previous section was made so that it can be performed on variable maps with more than one class, as well, thus avoiding the use of separate calculations with bit maps for each class. All maps were crossed pairwise with the landslide map, which designates unique code numbers for each individual scarp or body. For different mass movement types and activities the number and area densities per variable class were calculated. The prior probabilities for different types and activities of mass movements were determined by crossing the landslide map with an empty variable map, containing only zero values (see table 6.11). The prior probabilities which were calculated for the number of landslides are very small. This is due to the fact that only one pixel was used to represent an individual landslide, instead of all pixels as is the case in the area density calculation. Although weight of evidence maps could be made for all categories given in table 6.11 only those for active derrumbes, based on numbers, will be presented.

	BASED ON AREA DENSITY					
Activity	All types	Rotational slides	Translational slides	Rotational flowslides	Translational flowslides	Derrumbes
All	$5.762.10^{-2}$	$1.174.10^{-2}$	$1.453.10^{-2}$	$5.462.10^{-3}$	$9.441.10^{-3}$	$1.532.10^{-2}$
Active	$1.576.10^{-2}$	$8.375.10^{-4}$	$4.563.10^{-3}$	$4.393.10^{-4}$	$2.444.10^{-3}$	$6.728.10^{-3}$
	BASED ON NUMBER DENSITY					
All	$2.178.10^{-3}$	$3.478.10^{-4}$	$7.391.10^{-4}$	$1.236.10^{-4}$	$2.700.10^{-4}$	$6.727.10^{-4}$
Active	$8.238.10^{-4}$	$6.407.10^{-5}$	$3.410.10^{-4}$	$2.517.10^{-5}$	$6.636.10^{-5}$	$3.226.10^{-4}$

Table 6.11: Prior probabilities for the occurrence of different mass movement types and activities for the medium scale area.

To investigate the conditional independence of the individual variable classes, the pairwise test discussed in section 6.3.5.1 should be applied to all possible combinations of variables. Combining all 178 variable classes (listed in table 6.3) would result in an astronomically large number of combinations. Therefore only a limited number of combinations was selected, using the most important variable maps (see table 6.4). With this limited number of combinations, pairwise crossing still involves a total of 1042 operations. In 703 of the 1042 cases the hypothesis that the two variable classes are conditionally

---

independent with respect to the occurrence of active derrumbes had to be rejected, when using a significance level of 1%. Table 6.12 gives an example of the results for the combinations of slope classes and geological units.

SLOPE CLASSES	GEOLOGICAL UNITS													
	1	2	3	4	5	6	7	8	9	10	11	12	13	14
1: 0-10°	161	4	91	119	124	0	22	2	1	2	9	14	13	3
2: 10-20	181	40	144	166	255	16	22	5	0	6	29	14	28	6
3: 20-30	204	23	148	188	255	26	44	12	14	16	19	25	28	8
4: 30-40	193	5	123	151	185	19	6	1	0	3	33	15	13	0
5: 40-50	198	4	93	148	161	0	10	0	0	4	7	4	13	0
6: 50-60	175	5	83	141	168	0	7	0	0	0	7	5	11	0
7: 60-70	163	7	92	144	148	0	14	0	0	0	9	0	11	0
8: 70-80	155	0	95	136	146	0	4	0	0	0	7	2	0	0
9: 80-90	0	8	0	0	0	0	4	0	0	0	0	0	0	0

Table 6.12: χ^2 values for specific combinations of geology and slope angle. The values are based on nr/km² and are calculated for active derrumbes. At a significance level of 1% all combinations with χ^2 values >9.21 are conditionally dependent with respect to the occurrence of active derrumbes.

All combinations of slope classes (SLOC2) with down- or cross-slope convexity classes (PROFC/PLANC) have extremely high χ^2 values. All combinations of geomorphological complex number 2 (Romeral zone) with any of the other maps, also proved to be dependent. In fact all combinations of variables with higher densities than the density of the individual variable classes result in high χ^2 values. Thus, when the individual combinations are used to construct the final posterior probability map, values for those combinations which are statistically dependent will be too high. To evaluate the effect of dependent variables on the final posterior probability values, four example combinations of input maps were used. Frequency distributions of weight values and percentages for three cases are given in figures 6.28 to 6.30 and two of the resulting maps are shown in figures 6.31 and 6.32:

1. Summation of the weight of evidence values for GEOL, SLOC2, LUSE, GEOC, DRS2, DRS1, F1, F2, R1, and R2. The resulting map gives only negative values due to the strong effect of the negative weight values for those variable classes of DRS1, DRS2, F1, F2, R1, and R2 with a distance more than 50 m from a road, fault, or valley head.

2. Summation of the weight of evidence values for GEOL, SLOC2, LUSE, GEOC, DRS2, F1, and R1. The frequency distribution of pixels with and without active derrumbes is given in figure 6.28, and the resulting map in 6.31. Eight percent of the pixels with derrumbes had negative weights.

3. Crossing of four input maps (GEOL, SLOC2, LUSE and GEOC) into a map with unique combinations, which was used in the probability calculation. The frequency distribution of pixels with and without active derrumbes is given in figure 6.29 and the map in figure 6.32. It resulted correct classification of 96% of the pixels with derrumbes.

4. The combination of the six input maps defined in section 6.3.2 (SLOC2, GEOL, GEOC, GEOS, R, F). The frequency distribution of pixels with and without active derrumbes is given in figure 6.30. The method resulted in 92.6% of the pixels with active derrumbes being classified correctly.
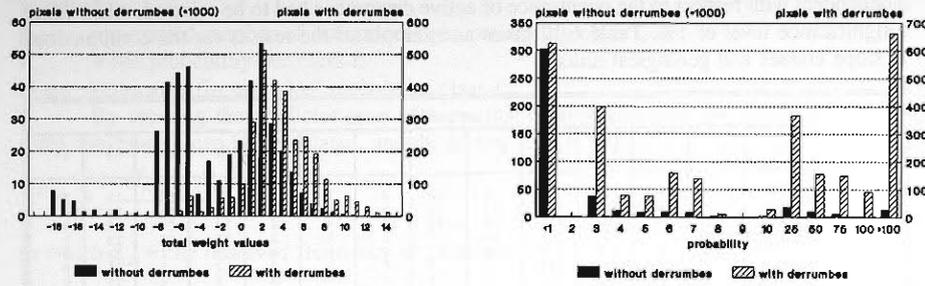
Figure 6.28: Results of weight-of-evidence modelling for a summation of seven input maps (GEOL, SLOC2, LUSE, GEOC, DRS2, F1 and R1). Left: Frequency distribution of final weight values. Right: Frequency distribution of permillage probabilities.
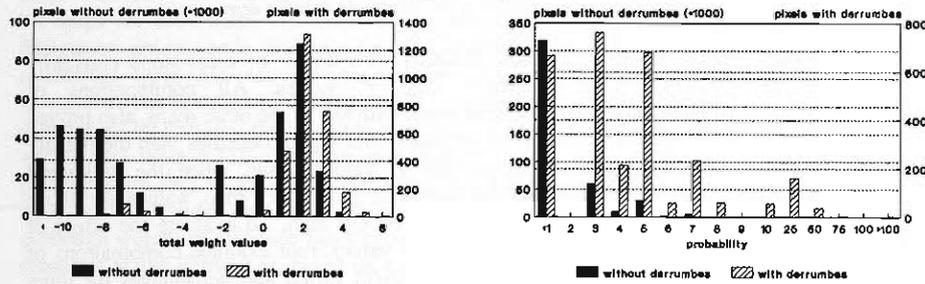
Figure 6.29: Results of weight-of-evidence modelling for a combination of four input maps (GEOL, SLOC2, LUSE, GEOC). Left: Frequency distribution of final weight values. Right: Frequency distribution of permillage probabilities.
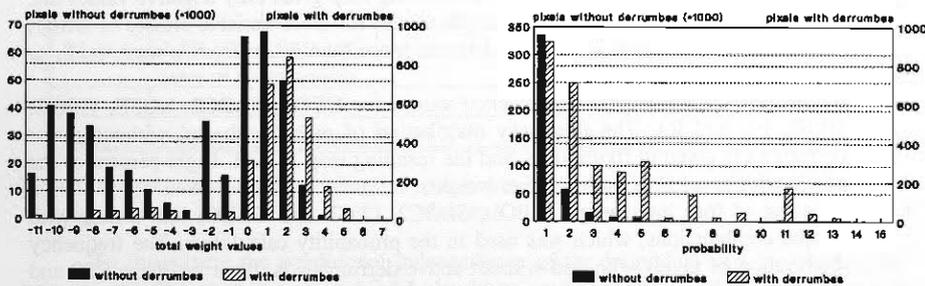
Figure 6.30: Results of weight-of-evidence modelling for a combination of six reclassified input maps (SLOC2, GEOL, GEOC, GEOS, R, F). Left: Frequency distribution of final weight values. Right: Frequency distribution of permillage probabilities.
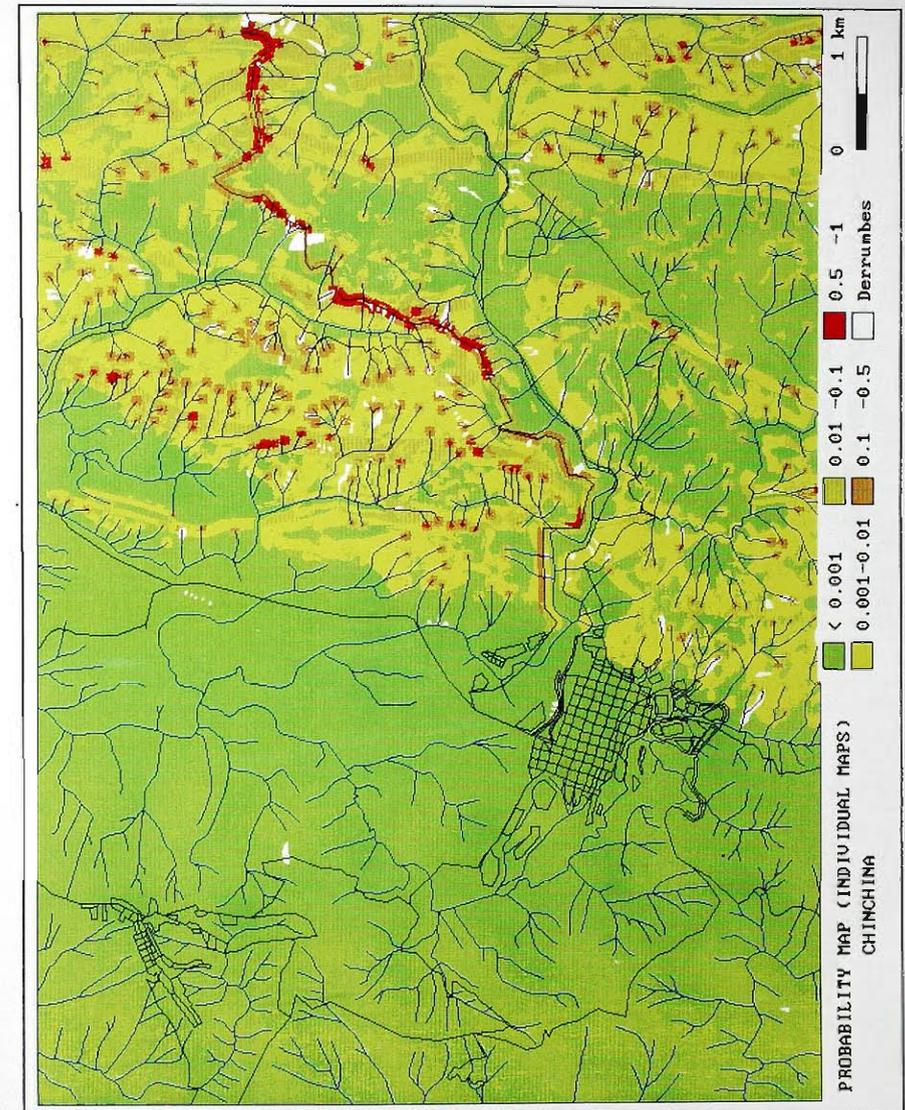
Figure 6.31: Classified probability values for the occurrence of derrumbes in the medium-scale study area made by summation of weight-of-evidence maps for individual variables.
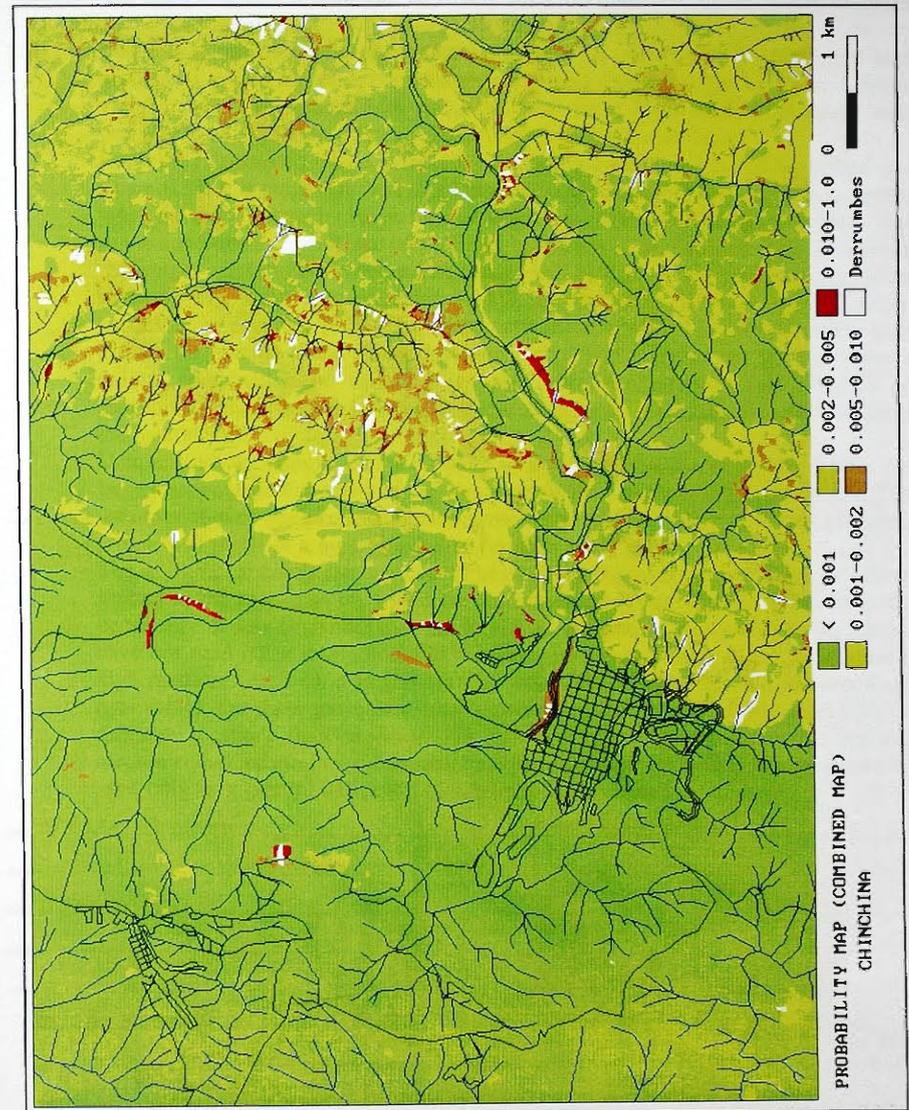
Figure 6.32: Classified probability values for the occurrence of derrumbes in the medium-scale study area made from a map with unique combinations of variable classes.

6.3.5.3 Discussion

The following conclusions can be drawn from the results of the weight-of-evidence modelling:

1. The use of conditionally dependent variable maps will result in extremely high probability values for those combinations which have high weight values in different variable maps. In figures 6.28 and 6.31 there are a large number of pixels with probabilities larger than 0.1; even some values of 0.99 were found.

2. From the relationship between the observed and predicted number of landslides (see figure 6.33) it is clear that there is a large mismatch for the higher probability ranges when the map is made by summation of weight values from different input maps. Due to the conditional dependence of variables in relation to the occurrence of derrumbes, the weight values in those dependent classes will be high. Several high weight values summed will result in a posterior probability that is far too high. The χ^2 value, according to equation [6.26], for example 2 in section 6.3.5.2 was extremely high (7680), due mainly to the strong deviation for the higher probability classes. When a unique combination of variables is used, after map crossing, the problem of conditional dependence is avoided, and the resulting χ^2 values are acceptable (2.9 for the example 4).

3. Unique variable maps made by crossing of many variable maps, however, have the large disadvantage that many of the combination areas become very small in size. The presence of even one pixel with mass movements, which can be due to map matching errors, will result in a high probability for such small units.

4. The resulting probability values cannot be used without great caution. They are at best limited to the time-span for which the mass movement map is valid. Even then, the occurrence of new landslides may not follow the prediction, because triggering factors have not been taken into account in the analysis. It may be that in the near future a high rainfall event with a large return period, which did not occur in the time-span over which the mass movement map shows information, may trigger landslides in different locations than expected. For this reason, the probability values are not recommended for use in a subsequent quantitative risk analysis. The values should be used only as a general indication of susceptibility to mass movement.
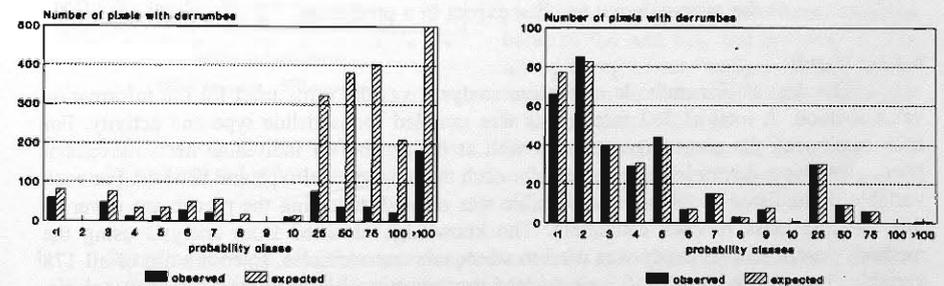
Figure 6.33: Comparison between the observed number of derrumbes and the number predicted based on the weight-of evidence modelling. Left: predictions based on summation of seven input maps. Right: predictions based on one combination made by crossing six reclassified input maps.

167

6.4 Multivariate statistical analysis

Multivariate statistical analyses of important causal factors for landslide occurrence may indicate the relative contribution of each of these factors to the degree of hazard within a defined land unit. The analyses are based on the presence or absence of stability phenomena within these units. Two different approaches were followed, which are slightly different from those presented in section 6.3.1:

1. A calculation based on terrain units. The data files containing the percentage cover of the variable classes in each catchment, prepared for the information value method (section 6.3.4.2), could be used here without modification.
2. A calculation based on pixels, in which a subset of the total number of pixels in the map was used.

6.4.1 Multiple regression

6.4.1.1 Introduction

The most common multivariate statistical method is multiple regression. It is used here to correlate landscape factors and mass movements, according to the following equation:

$$Y = b_0 + b_1X_1 + b_2X_2 + b_3X_3 + ...b_nX_n \qquad [6.29]$$

The dependent variable Y represents the presence (1) or absence (0) of a mass movement. It can also be expressed as the percentage of a terrain unit covered by landslides. The variables $X_1 - X_n$ are the independent variables, such as slope class, geological units, etc. The symbols $b_0 - b_n$ are the partial regression coefficients. The standardized partial regression coefficients, which are the partial regression coefficients expressed in units of standard deviation, indicate the relative contribution of the independent variables to the occurrence of landslides (Davis, 1986). The following statistics are used to evaluate the result of a calculation:

R^2 (adj):   amount of variance accounted for by the model. It adjusts for the number of independent variables in the regression.

SE: standard error of estimate. The square root of the residual mean square error. It measures the unexplained variability in the dependent variable.

MEA: absolute mean error. The average of the absolute values of the residuals, which is the average error one can expect in a prediction.

6.4.1.2 Results

The data set for multiple regression analysis was the same used for the information value method. A total of 552 catchments was sampled for landslide type and activity. For each catchment, the percentage cover as well as the number of individual mass movement phenomena were determined, separately for each mass movement type and activity. For each variable class, listed in table 6.3, a variable was created indicating the percentage cover of that variable class in each catchment. The knowledge obtained from analysis using the methods described previously was used to select relevant variables, since the use of all 178 variable classes listed in table 6.3 would lead to memory problems in the PC-based analysis. Table 6.13 lists the variables used. Features represented by continuous surfaces, such as slope angles, altitude, and distance from ridges, valley heads, and drainage, were resampled by crossing them with the catchment map. This way, variables such as internal relief, drainage

---

density, maximum, minimum, average and predominant slope, height, and distance were obtained.

To evaluate the importance of each of the variables for construction of the model, a series of stepwise multiple regression analyses was executed with the percentage of active and dormant derrumbes per unit as the dependent variable, as well as the presence/absence values using different threshold values (see section 6.3.4.2). In the stepwise regression analysis a confidence level of 80% and a threshold value of F = 4 were used for the decision to include or exclude the variables in the model.

Variables	Classes
GEOLOGY	1,3,4,5,11
GEOM. SUBUNITS	3,4,5,6,7,8
GEOM. COMPLEXES	1,2,3
LAND-USE	1,2,3,4,8
FAULTS	1
ROADS	1
SLOPE ANGLE	Predominant, maximum, minimum, average, median, perc>25, perc>35
DISTANCE TO RIDGES	Predominant, maximum, average, median, perc>50m, perc<50m
ALTITUDE	Difference, difference/hectare
DISTANCE TO VALLEY HEADS	Density, predominant, average, perc<50m.
DISTANCE TO DRAINAGE	Density, predominant, average, perc<50m.

Table 6.13: Variable classes sampled per catchment for multiple regression analysis.

The results were very poor. The R^2 values did not exceed 0.25, which means that, at best, only a quarter of the variance could be explained by the model. Another test was performed, using the presence or absence of derrumbes (1 or 0) as a dependent variable, but the result was not significantly better. Converting the variables into presence/absence using different threshold values also did also not lead to more acceptable results.
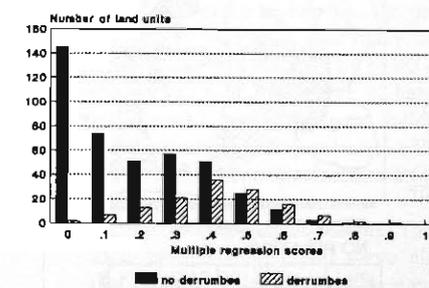
Figure 6.34: Frequency distribution of predicted values for units with and without derrumbes.

The fitted values according to the model for units (catchments) with and without landslides (0 and 1) are given in figure 6.34. This graph shows that the separation between stable and unstable land units is very poor. The highest score for predicted stable units is indeed on value 0, but the predicted unstable units have their maximum between 0.4 and 0.5, and not near 1. The multiple regression analysis gives poorer results than the other techniques discussed in the previous sections.

The use of terrain units for the sampling of variables in multiple regression analysis is met with a number of problems:

1. *Sampling method.* Variables are sampled in terrain units (catchments), which leads to a generalization. Two different methods of sampling can be applied:
    a. Presence/absence sampling. In this respect it is important to specify what threshold percentage of a certain variable in a terrain unit should be used to decide on presence or absence. Problems related to that were discussed

previously in section 6.3.4.2.

b. The problem of establishing a threshold value could be avoided by using the percentage cover of a variable in a terrain unit as a variable in the multiple regression analysis. In this case the dependent variable (occurrence of landslides) is also expressed as a percentage value. The multiple regression analysis is executed under the assumption that the percentage of landslides in a terrain unit will increase when the percentages of controlling factors also increase. This assumption was not supported by field evidence in the study area.

Sampling of variables in terrain units does not take into account the relationship between mass movement occurrence and variables at the same location within a unit. This generalization leads to a masking of the important relationships between landslides and terrain variables. Variables which were very important in pairwise analysis do not seem to be important when the relation is examined on the basis of terrain units. This problem is schematically displayed in figure 6.35 in which 10 imaginary terrain units are shown, 5 of which contain landslides. Spatial distribution of a variable is also shown. In the example on the left hand side, the variable occurs only in the units with the landslides, but not at the same locations. In fact none of the landslides is located within the variable area. In the sampling method applied, all units with landslides will obtain a value of 1 (presence) for the variable.
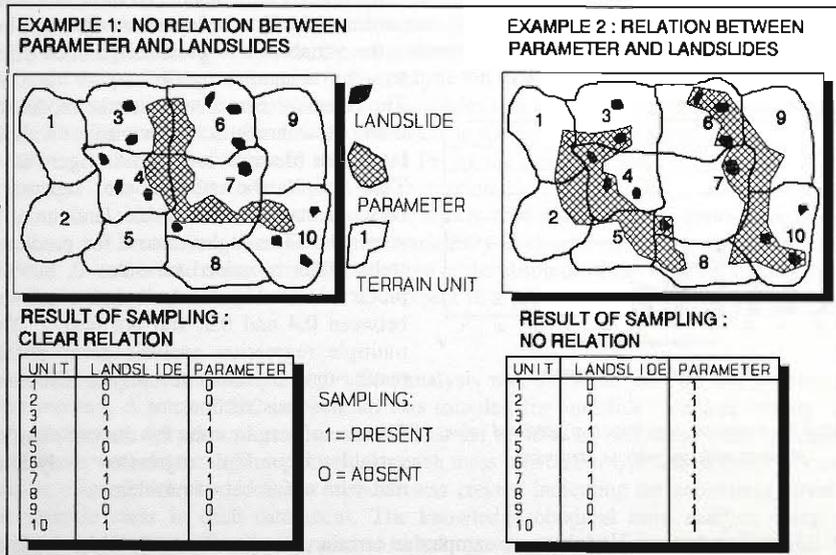
Figure 6.35: Problems related to the sampling of variables in terrain units for statistical analysis. Left: although there is no relation, the result of the sampling shows a clear relation. Right: although there is a clear relation, the result of the sampling shows there is no relation.

The resulting table shows a very high correlation between the landslides and the variable, which contrasts with reality. An opposite situation is also shown in figure 6.35. In this second example there is a high correlation between landslide occurrence and the variable. Practically all landslides occur within the variable area. However, the table which results from the presence/absence sampling method gives a very poor correlation. The units without landslides have a value of 1 for the variable as well.

2. *Size of unit.* Obviously the size, and shape, of the terrain units used for sampling will have a strong effect on the result. Larger units will give poorer results. Due to the limited memory capacity of a PC-based statistical package, the volume of input data must be limited. This will result in poorer results than when all data are used (as described in section 6.3). Generalization of data to terrain units using a GIS, mentioned in the literature (Carrara et al., 1990; 1991), is also related to the data structure used in the GIS. With vector-based GIS systems, sampling must be made over polygons, and not over pixels as is the case in raster-based systems.

3. *Result maps.* The results of the analysis are checked against the percentage cover of landslides in the terrain units. When the predicted and observed values are similar, the equation is considered valid. This is a kind of circular argument, which, however, occurs in all types of analysis treated so far. When terrain units are used as the basic units, it would be much simpler to calculate the landslide density per unit and use this value for the hazard map. The application of multivariate statistical techniques is useful in the detection of terrain units which are presently landslide free but which are predicted to be unstable. If the percentage of units wrongly classified as stable is equal to the percentage of units wrongly classified as unstable, then these percentages can be seen as errors in the model. When the percentage of units wrongly classified as unstable is much higher than the percentage of units wrongly classified as stable, this may be an indication that many of the landslide-free units are potentially unstable. Unfortunately, a hazard map based on terrain units does not provide information about the variation of the degree of hazard within a unit. In a terrain unit there may be hilltops with low hazard, and valley heads with high hazard. Only if very small land units are used, near pixel size, will the results be acceptable based on the medium-scale requirements (see section 2.6). In this case, however, the calculation matrix will become too large.

4. *Sample areas/prediction areas.* The assumption that a regression equation calculated in a sample area, could serve also for similar areas nearby (prediction area) is questionable. In the prediction area the regression equation should always be tested by calculating the landslide density per terrain unit. A landslide density map without application of multivariate analysis will give a good result as well.

5. *Complexity of the study area.* One of the main problems in the use of multivariate techniques in this study is the very complex geological and geomorphological situation in the study area. The occurrence of mass movements is governed by a complex set of factors, which may not even be equal over the whole area.

Multivariate analysis can be applied to evaluate the partial contribution of each variable for the occurrence of mass movements. The partial correlation coefficients give an indication on how much the mass movement density would change when one variable changes, and all other variables are kept constant. With a multiple regression analysis it is

difficult, however, to determine which specific combinations of variables will result in higher landslide hazard. A user with limited statistical background loses sight of what happens during the multivariate analysis. It is often perceived as "throwing the data into the 'black hat', or 'black box', and seeing what comes out".

6.4.2 Discriminant analysis

A second type of multivariate analysis carried out in this study is discriminant analysis. The objective of the analysis is to find the best discrimination between two groups: units or pixels with and those without mass movements. The analysis results in a discriminant function:

$$D_s = B_0 + B_1X_1 + B_2X_2 + B_3X_3 + ... B_nX_n \qquad [6.30]$$

Where the X_i are the values of the variables and the B_i the calculated coefficients. Before any further analysis can be performed, the success of the formula in separating the two groups must be tested. For this purpose three tests can be used:

1. The variability between the two groups and within the groups, and the total variability of the data, are calculated. The ratio of the variability between the two groups and the variability within the groups is called the *eigenvalue* (Statgraphics, 1991). It should be maximized for a good discriminant function.
2. The ratio of the variability between the two groups and the total variability is called "Wilk's λ". A small value indicates strong variation between groups and less variation within groups. A Wilk's λ of 1 indicates that there is equally great variation within groups as between groups (i.e., that the function does not discriminate).
3. The χ^2 (Chi-square) test to determine if the two groups are significantly different.

Because of the problems related to the use of terrain units mentioned in section 6.4.1.2, the analysis was only carried out on a pixel basis. With a statistical package (Statgraphics, 1991) 1000 points were randomly selected within the medium-scale study area. Unfortunately, only 13 of these were located within derrumbes. Therefore additional points within derrumbes were sampled from the label files connected to the landslide polygons. Such points were selected only within the scarp areas of active or dormant derrumbes. In this way 295 pixels in derrumbes and 983 pixels not in derrumbes were obtained. The total set was divided into two groups: one for the training set and the other for the prediction set. Before exporting the data to an external statistical package (Statgraphics, 1991) a matrix was created by reading the information from the variable maps using the X- and Y-coordinates of the sampling points. Nominal variables, such as land use, geology, and geomorphology, were recoded by their relative importance to the occurrence of derrumbes. This technique was preferred over the use of dummy variables for each separate class (Carrara et al., 1991) because the use of many dummy variables would increase the size of the matrix, as well as the time needed for calculation. The binary value for the presence or absence of derrumbes was selected as the dependent variable. Sixteen variables were entered in the discriminant function.

The results proved to be poor: the calculated eigenvalue was low (0.21), as was the canonical correlation (0.42), and the Wilk's λ was high (0.82). Group centroids were -0.25 and 0.87. With the exception of slope angle and geological unit, most variables had a very low discriminating power. Variables which show high correlations with the occurrence of

derrumbes in the univariate statistical techniques, such as the distance to valley heads and the distance to roads, had relatively low values. The results from the prediction set were very similar to those from the sample set: 72% of the points was correctly classified.

The landslide occurrence map (figure 6.5) shows that the density of derrumbes is much higher in the Romeral zone than in the other two complexes. In the full data set this obscures the relationships with important variables. For this reason a test was performed to see if the use of separate data sets from the three different geomorphological complexes (Romeral zone, terraces, and western hills) would improve the results. The data set was split into three separate files for the three geomorphological complexes. The results for the various tests are given in table 6.14.

Results from discriminant analysis did not prove to be successful. When the basic assumptions for applying discriminant analysis are taken into account (Davis, 1986), the following remarks must be made:

1. Not all of the sampling points with derrumbes were chosen randomly.
2. The probability of a pixel to be part of the group of no-derrumbes is much larger than to be part of the derrumbe group.
3. Not all variables are normally distributed. Geology, for example, in which the lithological units are ranked according to landslide density, is obviously not normally distributed as the units are not equally large.
4. The possibility is high that incorrectly classified pixels are used. Most input maps are made through photo-interpretation, with only a limited number of field observations.
5. Selection of single pixels as sampling points in mass movements does not result in a representative data set. Generally more variable classes will be present within a mass movement than is represented within the sampled pixel. This problem is not encountered when all pixels with landslides are used, as is the case in the univariate statistical methods.

From the foregoing, the conclusion can be drawn that the application of multiple regression and discriminant analysis for mass movement hazard assessment is met with a series of difficulties. The multivariate analysis techniques, however, are considered to be important, as they take into account the interrelationships of the landslide controlling factors, whereas these factors are considered independently in univariate statistical techniques. More investigation should be carried out in the development of pixel-based multivariate statistical techniques.

	A	B	C	D	E	F	G	H
Sampling points	603	603	1278	1278	390	390	157	157
Eigenvalue	0.214	0.212	0.157	0.181	0.131	0.124	0.378	0.314
Canonical correlation	0.420	0.418	0.359	0.391	0.340	0.332	0.523	0.489
Wilks λ	0.824	0.825	0.864	0.847	0.884	0.889	0.726	0.761
χ^2	122	121	186	211	46.7	45.14	47.41	41.10
X	0.31	0.28	-	-	0.29	-	0.15	-
Y	-0.03	-	-	-	-0.04	-	-0.21	
DTMC	-0.08	-	-	-	-0.14	-	-0.31	-
ASPCL	0.01	-	-	-	0.01	-	-0.17	-
SLOC2	0.53	0.52	0.60	0.55	0.41	-0.45	0.59	0.53
PLANC	-0.02	-	-	-	-0.10	-	-0.20	-0.26
PROFC	-0.19	-0.19	-	-	0.02	-	0.11	0.04
DRT	-0.13	-0.14	-	-	-0.48	0.49	-0.07	-
F1	-0.11	-0.14	-	-	0.27	-0.15	-0.39	-
F2	-0.23	-0.27	-	-	-	-	-0.55	-0.23
R	-0.32	-0.32	-	-0.30	-0.37	0.39	-	-0.41
DRS	-0.20	-0.19	-	-0.22	-0.32	0.28	-0.03	0.01
GEOC	-0.01	-	-	-	-	-	-	-
GEOL	0.44	0.44	0.64	0.58	0.42	-0.42	0.26	0.36
GEOM	0.06	-	-	-	0.03	-	0.46	0.47
LUSE	-0.08	-	-	0.03	-0.07	-	0.31	0.28
Predicted: 0 Observed: 1	25%	25%	24%	25%	33%	36%	25%	33%
Predicted: 1 Observed: 0	29%	31%	36%	32%	37%	38%	12%	12%

A: DE23TR: training set for all complexes, using all variables
B: DE23TR: training set for all complexes, using selected variables
C: De23TOT: total set for all complexes, with only two variables
D: DE23TOT: total set for all complexes, with five variables
E: DE23TR1: set for complex 1 (Romeral zone), with all variables
F: DE23TR1: total set for complex 1 (Romeral zone), with selected variables
G: DE23TR2: total set for complex 2 (western hills), with all variables
H: DE23TR2: total set for complex 2 (western hills), with selected variables

Table 6.14: Summary of the results of discriminant analyses for the presence or absence of derrumbes, carried out on a set of 983 randomly selected pixels without derrumbes, and 295 pixels selected from within derrumbes.

6.5 Deterministic landslide hazard analysis

6.5.1 Introduction

A very wide range of deterministic models for slope instability analysis is available nowadays, ranging from simple infinite-slope models to complex 3-D models (Graham, 1984). The only model which calculates slope instability on a pixel basis is the infinite-slope model. Most other models require the definition of a potential sliding surface within a profile, and the landslide above the sliding plane is subdivided into a series of slices.

The one-dimensional infinite-slope model describes slope stability in the simplest form. It is only applicable for the calculation of shallow translational slides. Slope stability is calculated for the pixels on a map, using information combined from several input maps, such as slope angle, soil depth, soil strength, and depth to groundwater. If the second dimension is neglected the model can be applied in a raster based GIS. Calculations for each individual pixel will result in safety factor values for all pixels, which can be used to create a hazard map.

The basic formula for the infinite slope model is (Graham, 1984):

$$F = \frac{c' + (\gamma - m\gamma_w)\, z\, \cos^2\beta\, \tan\varphi'}{\gamma\, z\, \sin\beta\, \cos\beta} \qquad [6.31]$$

in which:

F = safety factor,
c' = effective cohesion (KPa),
γ = unit weight of soil (KN/m³),
m = groundwater/soil thickness ratio z_w/z (dimensionless),
γ_w = unit weight of water (KN/m³),
z = depth of failure surface below the terrain surface (m),
z_w = height of water table above failure surface (m),
β = terrain surface inclination (°),
φ' = effective angle of shearing resistance (°).

When the effect of horizontal earthquake acceleration is included, equation [6.31] becomes:

$$F = \frac{c' + (z\gamma\cos^2\beta - z\rho a\cos\beta\sin\beta - \gamma_w z_w\cos^2\beta)\tan\varphi'}{z\gamma\sin\beta\cos\beta + z\rho a\cos^2\beta} \qquad [6.32]$$

in which:

ρ = bulk density in (kg/m³),
a = horizontal component of earthquake acceleration (m/s²).

For calculation purposes equation [6.32] was divided into two parts [6.33]:

$$F = \frac{c'}{z(\gamma\sin\beta\cos\beta + \rho a\cos^2\beta)} + \frac{\tan\varphi'\, z(\gamma\cos^2\beta - \rho a\cos\beta\sin\beta - \gamma_w m\cos^2\beta)}{z(\gamma\sin\beta\cos\beta + \rho a\cos^2\beta)} \qquad [6.33]$$

6.5.2 Seismic acceleration

6.5.2.1 Introduction

Analysis of slope instability employ the use of static (one acceleration value assumed) or dynamic (accounting for the temporal variation in acceleration during an earthquake) seismic acceleration values. The dynamic method, requiring the use of finite-element models, is beyond the scope of this work. Calculation of single acceleration values in relation to return periods for various sites in the terrain is also a difficult task, considering the limited availability of seismic data. Unfortunately, no seismic acceleration values are available for the study area, as accelerographs have not been installed. To calculate seismic acceleration, the following variables should be known:

- Magnitude, frequency of occurrence, and distance of seismic events;
- Material sequences for each point of the terrain, as well as geotechnical data such as density and seismic wave velocity;
- Groundwater levels;
- Topographic conditions.

Many equations have been suggested to calculate peak ground acceleration for hard rock in relation to the magnitude and focal distance of a seismic event (Hays, 1980; UNESCO, 1978). These equations are applicable only in those areas where they were developed. Many equations were developed for the western United States (Milne and Davenport, 1965; Davenport, 1972; Schnabel and Seed, 1972). Donovan (1973) used worldwide data to derive a general equation:

$$A_h = 1320\,e^{\,0.58M}(R + 25)^{-1.52} \qquad [6.34]$$

where

A_h = peak horizontal acceleration for hard rock (g),
M = magnitude (Richter scale),
R = hypocentre distance (km).

In Colombia Gonzalez (1992) uses the following empirical relation for an area in the department of Cundinamarca:

$$A_h = 0.0254\,(RY)^{0.2962} \qquad [6.35]$$

in which: RY = return period in years.

For the relationship between acceleration and intensity many different empirical equations have also been derived. Based on data from the western United States, Trifunac and Brady (1975) proposed an empirical relationship between seismic intensity values of 6 to 9 on the Modified Mercalli scale and acceleration:

$$\log_{10}A_h = -0.014 + 0.30\,I_{MM} \qquad [6.36]$$

in which:

A_h = peak horizontal ground acceleration in cm/s^2,
I_{MM} = the intensity on the Modified Mercalli scale.

Murphy and O'Brien (1977) derived statistical correlations between horizontal ground acceleration and Modified Mercalli intensity using a worldwide data sample.

$$\log_{10}A_h = 0.24\,I_{MM} + 0.26 \qquad [6.37]$$

A very simple estimation of the amplification of the seismic wave due to different materials can be obtained, derived from the work of Medvedev (1965):

$$N = 1.67\ [\ \log_{10}\ (v_0\ \rho_0\ )\ -\ \log_{10}\ (\ v_1\ \rho_1\ )\ ]\ +\ c \qquad [6.38]$$

in which:

N = increase in acceleration (dimensionless),
v_0 = seismic wave velocity of the material below the contact (m/s),
ρ_0 = bulk density of the material below the contact (kg/m^3),
v_1 = seismic wave velocity of the material above the contact (m/s),
ρ_1 = bulk density of the material above the contact (kg/m^3),
c = correction factor for the depth of the phreatic water level.

6.5.2.2 Results

Data collected after the 1979 earthquake in Manizales can be used to evaluate the applicability of the equations given above. Maximum acceleration at the surface can be estimated from the intensity map (see figure 3.12) using equation [6.36] or [6.37]. The acceleration values can also be calculated by multiplying N (equation [6.38]) by the maximum acceleration in hard rock, derived from equation [6.34].

Based on the values for the seismic intensities in Manizales due to the 1979 earthquake the calculated accelerations are between 0.071 and 0.282 g. The 1979 earthquake had a magnitude of 6.3 and a focal depth of 106 km and its epicentre was located some 75 km from Manizales. The distance to the hypocentre was 130 km. Acceleration values calculated on the basis of different relations from various authors are given in table 6.15.

Values for acceleration of hard rock in Manizales are mentioned by various authors. Geotecnia (1980) gives a value of 0.042 g which was calculated without reference to the equation used. Rodriguez et al. (1988) used data based on the general design conditions of the Colombian Earthquake-Resistant Building Code in a study of the Siria landslide. They presented a maximum acceleration of 0.25 g with a return period of 475 years. The values obtained from the relationship between acceleration and intensity are considerably higher than those obtained from the relationship between magnitude and distance to hypocentre.

Equation according to	A
Milne and Davenport (1965)	0.314
Davenport (1972)	0.014
Schnabel and Seed (1973)	0.030
Donovan (1973)	0.023
Gonzalez (1991)	0.054

Table 6.15: Acceleration values in Manizales calculated using different equations given in literature.

This means that there is a very strong amplification of the seismic waves due to topographic and geotechnical conditions. However, it is questionable whether the intensity map for Manizales is correct (see also section 3.2.3) and whether equations [6.37] and [6.38] can be applied for the study area.

All values from table 6.15 are in a narrow range, except for those of Milne and Davenport. The relationship given by Donovan (1973) was ultimately chosen to calculation maximum accelerations in this study.

In order to be able to calculate return periods for acceleration values, return periods are first selected for magnitudes. Based on the formula for the data from 1922 to 1979 in section 3.2.3, the average return period for an earthquake with a magnitude of 7.5 is 32 years. The average return period for a seismic event with a magnitude of 6.5 is approximately 7

years, taking into account that it may occur in a relatively large area. To calculate maximum acceleration in hard rock for these events one must assume a distance to the epicentre. A relatively short distance of 50 km was used, which is equal to the distance to the epicentre of the 1962 earthquake. The resulting acceleration values for the two events are given in table 6.16. The data used to calculate amplification for a standard profile in the Manizales area is given in table 6.17 (Geotecnia, 1980).

Mag MM	RY year	Dh (km)	De (km)	A_m (g)
7.5	32	120	50	0.036
5.5	7	100	50	0.018

Table 6.16: Acceleration (A_h), RY = Return period (year), Dh = Hypocentre depth, De = Epicentre distance.

Material	v m/s	ρ kN/m³
Fill	0.30	1.3
Volcanic ash	0.38	1.4
Manizales Formation	2.14	2.0
Quebradagrande F.	3.2	2.6

Table 6.17: Amplification values for a typical soil profile.

Based on the values in table 6.17 the amplification for different sequences of materials can be calculated from equation [6.38]:
- Fill-Ash-Manizales-Quebradagrande : $N = 0.48 + 1.5 + 0.23 = 2.21$
- Ashes-Manizales-Quebradagrande: $N = 0.48 + 1.73 = 2.22$
- Manizales-Quebradagrande: $N = 0.48$
- Fill-Ash-Quebradagrande: $N = 1.99 + 0.23 = 2.21$
- Ash-Quebradagrande: $N = 1.99$
- Fill-Quebradagrande: $N = 2.22$

For the presence/absence of a groundwater level within the upper layer the following estimative corrections were made (James, 1986):
- Groundwater < 1 m. : $N + 1$
- Groundwater 1-4 m. : $N + 0.5$
- Groundwater < 4 m. : N

With the data from tables 6.16 and 6.17 and with the engineering geological map presented in section 5.4.4.2, acceleration values can be calculated for each pixel for a given seismic event.

6.5.3 Evaluating possible failure conditions

The use of even a very simple slope stability model, such as the infinite-slope model, in the calculation of safety factors for translational slides within the large scale study area meets with serious difficulties:

1. *Soil sequences.* In constructing the engineering geological map (discussed in section, a number of assumptions had to be made. The ash thickness map (discussed in section 5.4.4.1), is based on particularly doubtful "common relation" (see figure 5.6). The values in this graph were obtained from measurements of ash thickness throughout the area (not just in Manizales) and from a slope map.

2. *Water table.* Water-table information was obtained from the ash thickness map and a water-table information was obtained from the ash thickness map and a two-dimensional hydrological model (section 5.4.4.3). Data were interpolated over the whole terrain using regression analysis, which gives a relationship between the deviation from a standard profile, and the ash thickness. Cumulative effects of groundwater along a slope were not taken into account. This would require rather complex calculations using neighbourhood operations which, at the time of analysis, were not available in the GIS package ILWIS.

3. *Geotechnical properties.* Values for the cohesion of ash, in existing geotechnical reports are rather high (table 4.16), and questionable. The angle of internal friction and the bulk-density (appendix 18) did show greater uniformity.

4. *Seismic acceleration.* Due to the lack of measurements the seismic acceleration values discussed in section 6.5.2.2 are also speculative.

Considering these uncertainties, calculation of safety factor maps without previous evaluation of these four factors, would be useless. Since the material thicknesses are the most crucial uncertainty in the analysis, an evaluation was made of the critical depth of translational landslides, by solving equation [6.33] for the case F = 1. Based on this equation a number of different scenarios were evaluated. The relation between the critical depth and surface slope angle is given in figure 6.36 for different values of cohesion and two different groundwater conditions using a standard φ´ of 30°. The "common relation" used to calculate ash thickness (figure 5.6) is also indicated in the graph. From the graph it can be concluded that under dry conditions no failures would take place in soils with cohesion values ranging from 5 to 15 KPa. Under fully saturated conditions (which is of course unrealistic) most of the soils with a cohesion of 5 and 10 KPa, and some with a cohesion of 15 KPa, would fail. The cohesion strongly influences the minimum depth under which a translational failure could occur, ranging from 1 m with a cohesion of 5 KPa to 4 m with a cohesion of 15 KPa. This shows that a cohesion value of 15 KPa is very unlikely.

In figure 6.37 the critical depth against the surface slope angle is plotted for different earthquake accelerations and groundwater/soil thickness ratios (z_w/z), given a constant c´ (10 KPa) and φ´ (30°). Larger acceleration values and higher groundwater levels reduce the critical depth. Comparison of the values with the "common relation" (M-line) leads to the conclusion that failure could take place starting from a situation without seismic acceleration and a m (z_w/z) value of 0.5. Higher groundwater levels and stronger seismic accelerations would lead to failures.

In figure 6.38 some of the values for the relationship between the depth of the sliding plane and the surface slope angle, derived from a set of translational landslides and derrumbes that were measured in the Manizales area, are plotted together with some critical depth lines for extreme conditions of c´ and m. It is clear from this figure that landslides and derrumbes occur over a very wide range of soil thicknesses and surface slope angles. Slope angles are generally larger than 25°, and soil thicknesses range from 1 and 7 m. With the exception of one, all points are located between the maximum possible limits of cohesion and groundwater/soil depth relations. The conditions under which failure occurs are very different, and the use of one value for cohesion or groundwater/soil depth relation would be a gross simplification.
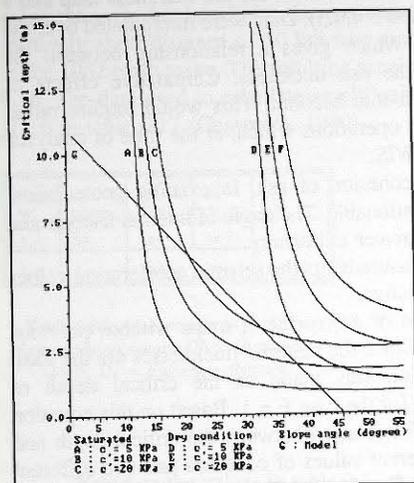
Figure 6.36: Critical depth plotted against surface slope angle for various combinations of values for cohesion and groundwater ($m = z_w/z$). Line G displays the relationship between ash thickness and slope angle used in this study.
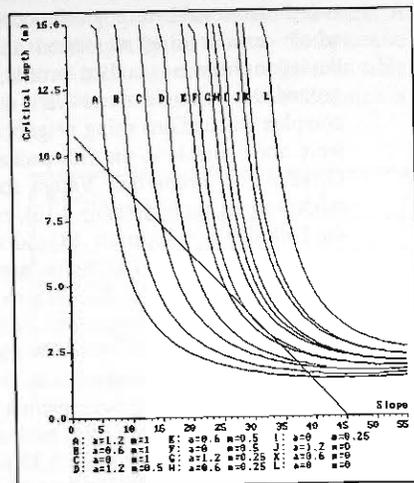
Figure 6.37: Critical depth plotted against surface slope angle for various combinations of values for seismic acceleration (a) and groundwater ($m = z_w/z$). Line M displays the relationship between ash thickness and slope angle used in this study.
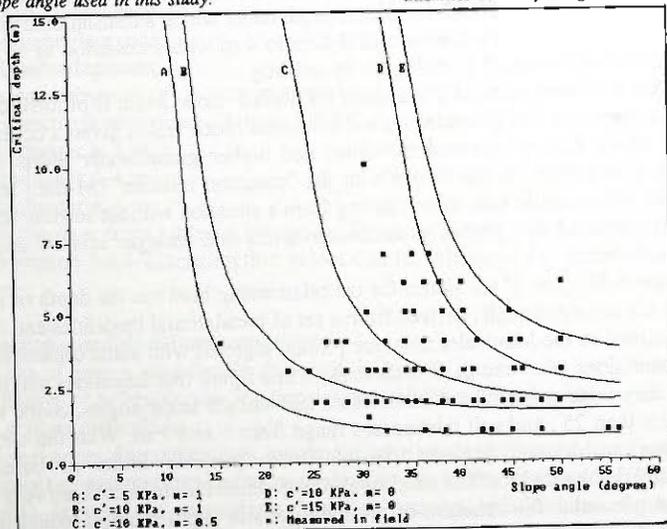
Figure 5.38: Values for the relationship between sliding plane depth and surface slope angle, measured for translational landslides in Manizales, plotted together with critical depth/slope angle relations calculated for some extreme values of cohesion (c´) and groundwater/soil depth ratio ($m = z_w/z$).

When figure 6.38 is compared with the model line for ash thickness in figure 6.36, it shows that ash deposits on steep slopes can be much thicker than predicted with the model line. This will be caused by variations in cohesion values, which can be considerably higher in some locations than in others.

A calculation was made to estimate the number of pixels in the map that would have safety factors lower than 1 when the different conditions mentioned above would be applied. The engineering geological map was modified so that it only displayed ash and or fill thickness of more than 1 m, which is considered the minimum possible failure depth (see figure 6.36). The results are given in table 6.18. From this table it can be observed that groundwater/soil depth ratios of 0.5 and 1 lead to an extremely large percentage of pixels with a safety factor less than 1. This situation is, of course, very unlikely. Groundwater/soil depth ratios are not constant for different ash thicknesses, as was shown in section 5.4.4.3. With small ash thicknesses this ratio may be as high as 1, and for thick ash it is seldom higher than 0.3. The influence of cohesion can also be evaluated from table 6.18. In the case of a cohesion of 5 KPa and an earthquake acceleration an unrealistically high percentage of the area is predicted to fail, even under dry conditions.

When the results from table 6.18 are compared with figures 6.36 to 6.38 it is clear that the map includes many other combinations of slope angle and ash or fill thickness than those predicted with the model (straight line in the figures). This is obvious when considering the large range of ash thickness versus slope angle derived from field measurements, as observed in figure 5.6. One reason for the deviation the occurrence of fill material on top of the ash. Fill thickness was calculated as the difference in DTMs between 1949 and 1989. For those pixels with a fill thickness value that value was added to the thickness value coming from the straight line. For those pixels where the terrain had been excavated, the excavation depth value was subtracted from the depth obtained from the straight line. The lower part of table 6.18 displays the results of calculations performed on the fill materials. It appears that at 3700 pixels the slopes always will fail, even in dry conditions and with high values for cohesion. This result must be due to errors in the DTMs and the slope maps. An evaluation of these errors will be given in sections 7.2.3.

C_m	a	m	Npix	PTot
5	0	0	7563	3
5	0	0.5	60598	22
5	0	1	156227	58
5	0.06	0	10712	4
5	0.06	0.5	90704	33
5	0.06	1	195839	72
5	0.12	0	47146	17
5	0.12	0.5	121917	45
5	0.12	1	240136	88
10	0	0	5207	2
10	0	0.5	12463	5
10	0	1	121736	45
10	0.06	0	7637	3
10	0.06	0.5	51921	19
10	0.06	1	163652	60
10	0.12	0	10629	4
10	0.12	0.5	94120	35
10	0.12	1	207271	76
15	0	0	3716	1
15	0	0.5	9394	3
15	0	1	75005	28
15	0.06	0	5415	2
15	0.06	0.5	8989	3
15	0.06	1	13086	5
15	0.12	0	7829	3
15	0.12	0.5	17984	7
15	0.12	1	169191	62

C_m	=	Cohesion (KPa)
a	=	Seismic acceleration (g)
m	=	Groundwater/Soildepth relation
Npix	=	Number of pixels with safety factor less than 1.
PTot	=	Percentage of the map with safety factor less than 1.

Calculation for pixels with fill only				
C_m	a	m	Npix	PTot
5	0	0	5325	2
10	0	0	3736	1
15	0	0	3716	1

Table 6.18: Percentage of pixels in the large-scale study area with ash and or fill material failing under different conditions.

6.5.4 Factor-of-safety maps

Before the safety-factor maps were calculated it was considered important to remove from the data set the impossible combinations, caused by errors in the input data. The process of removal is shown in figure 6.39, in which all combinations of terrain slope angle and ash and fill thickness, occurring in the map, are given as dots, together with the line (A) used to model ash thickness, and the curve showing critical depth for a cohesion of 10 KPa under dry conditions and without earthquake acceleration (line B). This map contains obviously many combinations of soil thickness and slope angle, which are caused by errors in calculating fill thickness from DTMs. In figure 6.39 (right) the combinations to the right hand side of the curve showing critical depth (B) have been displaced horizontally until they reached line B. This means that with any small increase of groundwater level or earthquake acceleration the terrain at these pixels will fail.
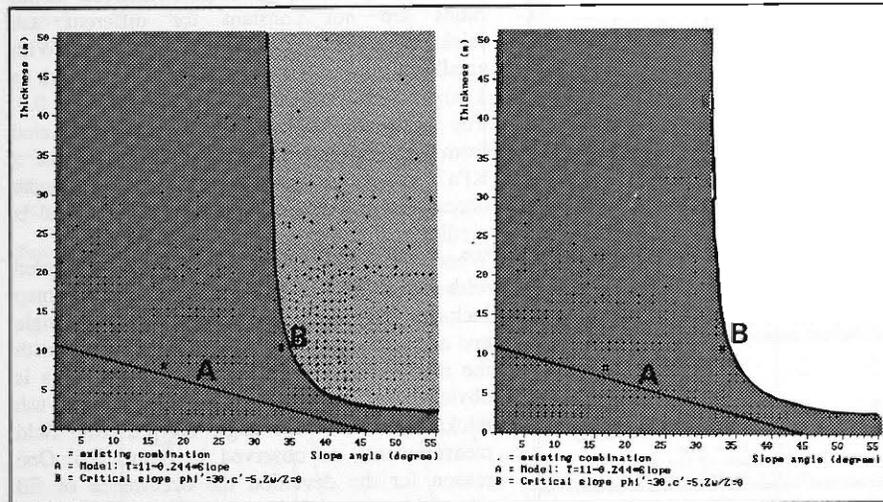
Figure 6.39: Removal of impossible combinations of ash and/or fill thickness and terrain slope angle. Left: All possible combinations of thickness and slope angle occurring in the map, together with the model line (A) for ash thickness and the curve for critical depth under dry conditions with a cohesion of 10 KPa (B). Right: Removal of all combinations that occur to the right of the critical line (B).

The following conclusions can be drawn:

1. The ash-thickness map based on the model line is a rather conservative estimation. Most of the pixels are stable under groundwater/soil thickness ratios smaller than 0.5, even when earthquake acceleration is taken into account. In reality soil thickness may be much greater than calculated in the model.

2. When fill thicknesses are used the situation is reversed. More than a realistic number of pixels with fill material will fail even under normal conditions.

3. The resulting soil thickness map is only a rough approximation of the real situation. More research should be carried out to obtain a better model for ash thickness, and the errors in the DTMs should be reduced by using a larger pixelsize.

Two examples of safety factor maps will be shown:

a. *Rainfall triggered landslides.* The following parameters were used: $c' = 10$ KPa, $\varphi' = 30°$, $\gamma = 14$ KN/m^3, $a = 0$, $m = z_w/z$ relation with return period of 25 years. For calculation of m see section 5.4.4.3.

b. *Earthquake triggered landslides.* The following parameters were used: $c' = 10$ KPa, $\varphi' = 30°$, $\gamma = 14$ KN/m^3, $a = 0.086$-0.12 g (return period of 32 years, with different values of amplification, depending on profile sequence and groundwater depth), and $m = z_w/z$ relation with a return period of 0.164 years).

The return period for groundwater depth/soil depth ratio of 0.164 used in the second example is related to the groundwater depth that occurs during 60 days per year. The groundwater maps were made according to the method described in section 5.4.4.3. The two examples showed results for the areas covered by fills to be different from those for the areas covered by ash. Figure 6.40 gives the percentage values for both examples.
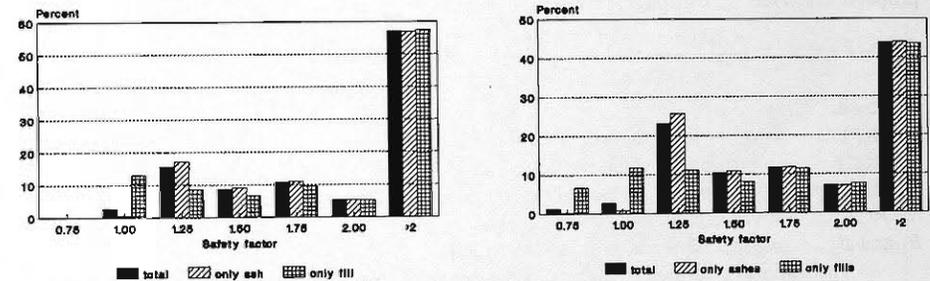
Figure 6.40: Relative frequency distribution of safety factor classes for different materials. Left: The example for rainfall triggered translational slides. Right: The example for earthquake triggered translational slides.

The following conclusions can be drawn from figure 6.40:

1. The maps calculated on the basis of rainfall and earthquake are very similar, because a higher groundwater table as well as a high value of seismic acceleration have the same influence on the factor of safety as visible in the diagram of critical thickness versus slope (see figure 6.37). The combined effect of both a high groundwater level and a high value for earthquake acceleration will have a much stronger effect, but the probability that these two triggering occur simultaneously is extremely low.

2. There are more pixels with a low safety factor for the map calculated on the basis of an earthquake event (see figure 6.40), especially in the class between 1 and 1.25.

3. Many more failures are calculated to occur in the fill material than in ash. This is caused in part by the errors in the DTMs, explained above. It is, however, also due to the fact that some of the fills are deposited on relatively steep slopes on which they will not be stable over a long period.

4.   The strong relationship between the parameter maps (soil thickness, groundwater) and the slope angle is seen clearly in the map, as most of the areas with low safety factors occur on steep slopes. The slopes north and south of the central part of Manizales, where most of the squatter areas are located, have an especially high frequency of unstable areas in both maps. The slopes in the northeastern sector of the city, where future urbanization is planned, show a tendency to become unstable after extreme rainfall as well as due to earthquake events.

The classified safety factor map calculated on the basis of rainfall is given in figure 6.41, and on the basis of an earthquake event in figure 6.42.

6.5.5 Failure probability maps

In the previous section, a method to calculate safety factors was explained, which uses average values for the various input parameters. Most of these factors contain a large degree of uncertainty. For this reason, the use of safety factors calculated from average values is not recommended. In this section the probability that the safety factor will be equal to or lower than 1 will be calculated. The method is based on the calculation of the variance of the safety factor, given by the following formula, which is partly based on the equations for error propagation given by Burrough (1986):

$$\mathrm{VAR}(F) = B_1^2 \left(\frac{\mathrm{VAR}(c')}{z^2} + \frac{c'^2 \mathrm{VAR}(z)}{z^4} \right) + B_2^2 \mathrm{VAR}(\tan \varphi')$$

[6.39]

in which:

$\mathrm{VAR}(F)$ = variance of the safety factor,
$\mathrm{VAR}(c')$ = variance of effective cohesion,
$\mathrm{VAR}(\tan \varphi')$ = variance of the tangent of the effective friction angle,
$\mathrm{VAR}(z)$ = variance of the ash thickness,
B_1 and B_2 = separate terms of equation [6.33].

The variances of the cohesion and the angle of internal friction for the ash deposits can be calculated from sampling point data. The standard deviations given in table 4.16 for ash deposits are in the order of 5 to 6 KPa for the cohesion, and 3 to 5° for the friction angle. The variances used here are: 25 KPa for c' and 0.005 for $\tan(\varphi')$.

Determining the variance of ash thickness is a great problem. The discussion of the ash thickness, presented in section 5.4.4.1, resulted in the conclusion that the ash cover cannot be modelled properly on the basis of the currently available data set. The large variation in ash thickness within each slope class is obvious from figure 5.6. The approach that was ultimately chosen to determine the variance of ash thickness is based on the critical depth calculations, presented in figure 6.36 and 6.37. Based on a variable groundwater table related to slope angle it is possible to draw approximate upper (A), and lower (B) curves for critical depths (see figure 6.43). In the lower slope angle range the variance (C) will be the lowest in near horizontal slopes. In this range deviations from the average ash thickness will be small. These will increase slightly in slope ranges of 5 to 15°, depending on the amount of erosion. Once the critical depth curve is reached the difference between the maximum and minimum critical depth will become very large, depending on differences in groundwater depth/soil thickness ratios (m). In the steeper slope ranges the variance becomes small again as the maximum and minimum curves approach each other.
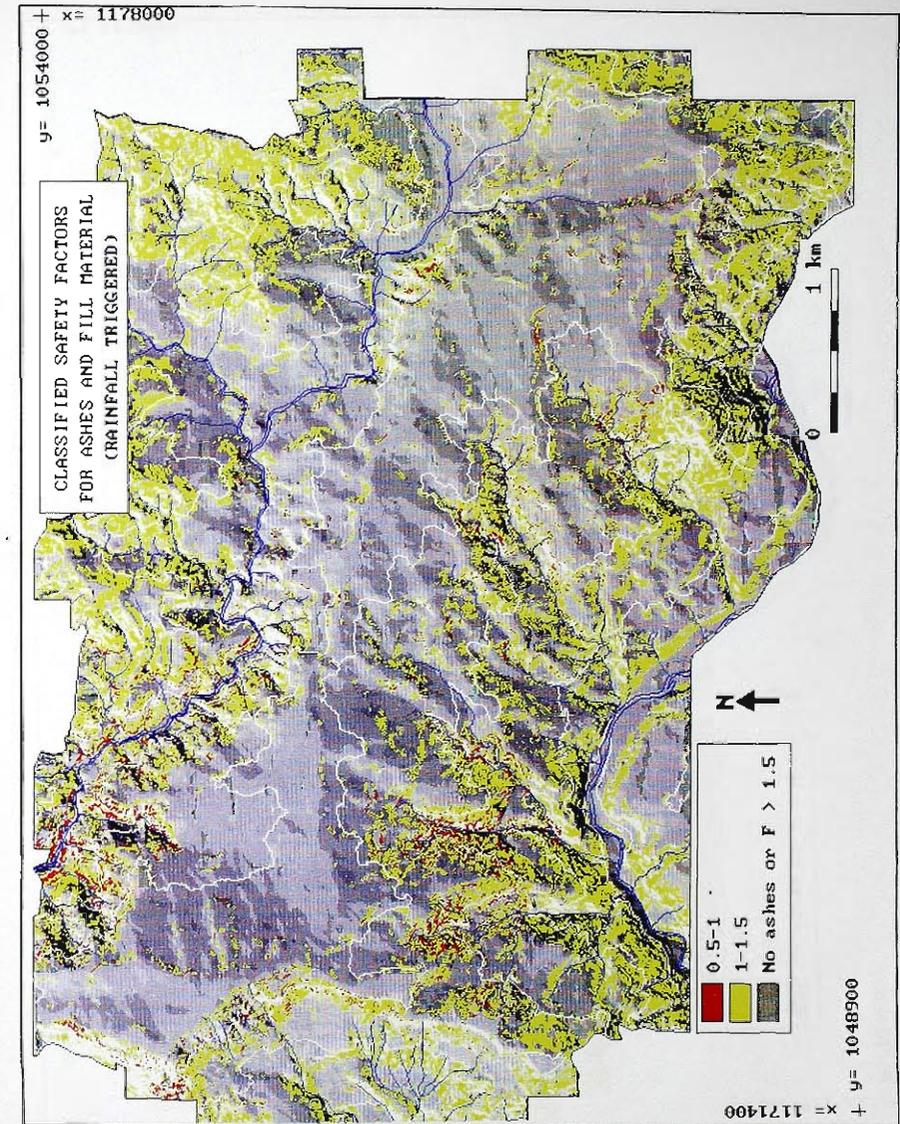
Figure 6.41: Classified safety-factor map for the large-scale study area calculated on the basis of groundwater levels related to a rainfall event with a return period of 25 years.

CLASSIFIED SAFETY FACTORS
FOR ASHES AND FILL MATERIAL
(EARTHQUAKE TRIGGERED)

0.5-1
1-1.5
No ashes or F > 1.5
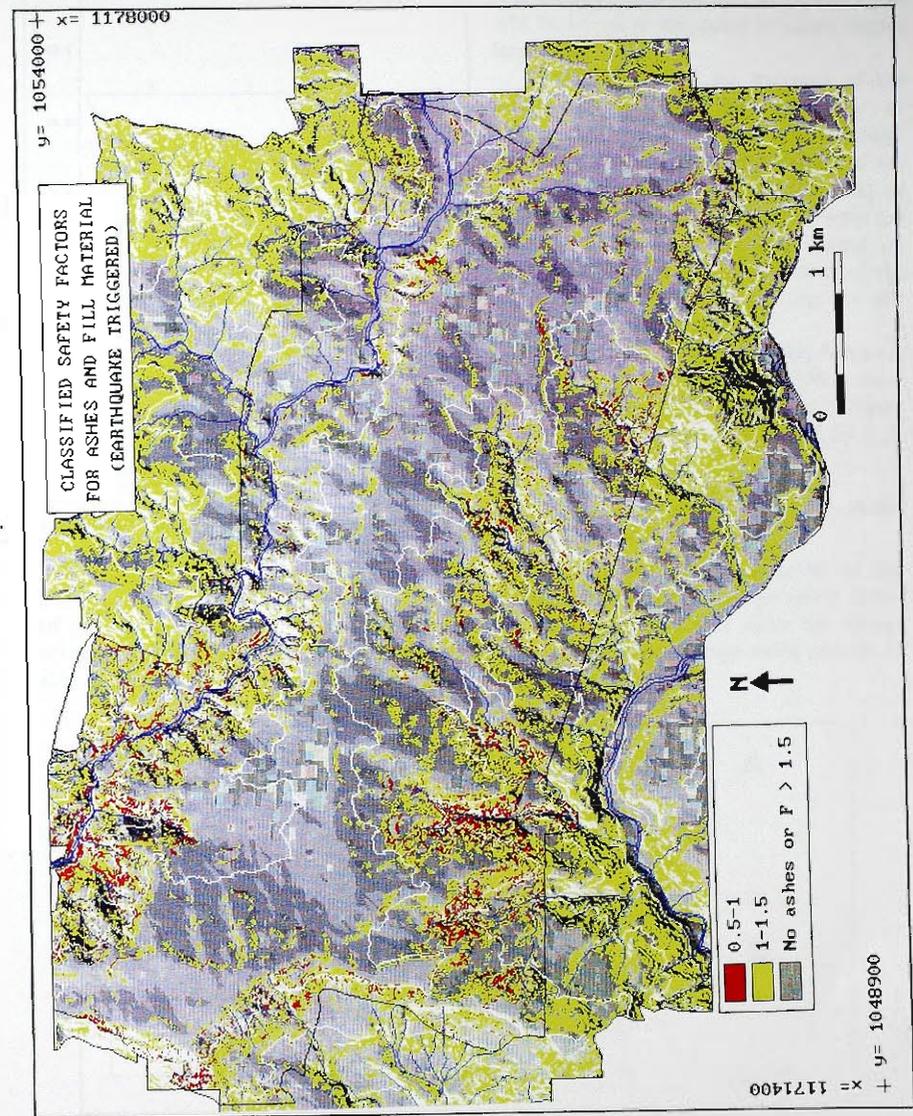
Figure 6.42: Classified safety-factor map for the large-scale study area calculated on the basis of groundwater levels related to a rainfall event with a return period of 0.164 years and an earthquake with a return period of 32 years.

184b
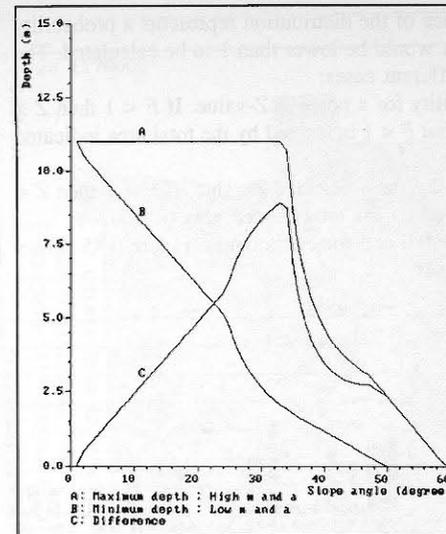
Figure 6.43: Minimum and maximum ash thicknesses
based on critical depth relations.

It is assumed also that due to erosion there will be no more ash cover at slope angles larger than 60°.

In calculating the variance of the safety factor, only the variances of cohesion, friction angle and soil thickness are taken into account. The variance of the groundwater depth/soil depth ratio (m) as well as of the seismic acceleration were too difficult to take into account. Based on these, partly hypothetical variances of the input factors, the variance map for the safety factor was calculated.

If the distribution of safety factors is assumed to be normal, the deviation from the mean value can be calculated (Blalock 1979). This deviation is expressed by a Z-value:

$$Z = \frac{1 - F}{\sqrt{\mathrm{VAR}(F)}} = \frac{1 - F}{\mathrm{STD}(F)} \qquad [6.40]$$

The Z-value can be considered as the distance between the average safety factor and ordinates which are Z-standard deviation units away. The total area under the normal curve is equal to 1. From a table of Z-values the area between the average value and the Z-value can be obtained. A graphical presentation is given in figure 6.44.
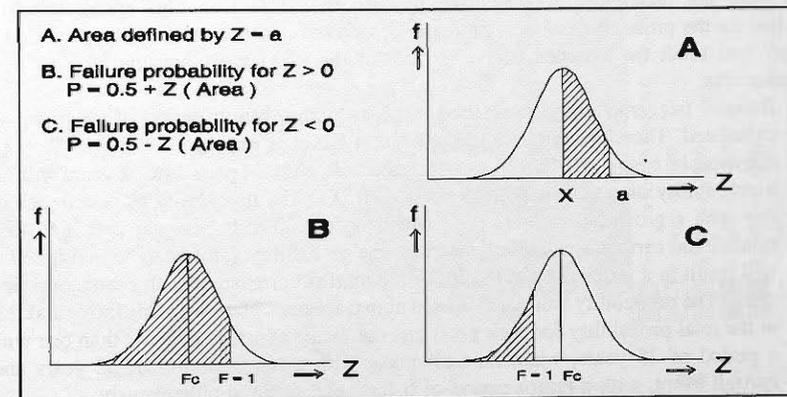
Figure 6.44: Normal distributions of F values. The shaded area under the curves represents the probability that the safety factor is lower than 1 (F_c = average safety factor).

This combined with the fact that the total surface of the distribution represents a probability of 1 allows the probability that the safety factor would be lower than 1 to be calculated. The failure probability can be calculated for two different cases:

1. Figure 6.44.B shows the failure probability for a positive Z-value. If $F < 1$ then $Z > 1$ (equation [6.40]) and the probability that $F < 1$ is formed by the total area indicated in the figure (0.5).
2. Figure 6.44.C shows the failure probability for a negative Z-value. If $F > 1$ then $Z < 1$ and the probability that $F < 1$ is formed by the total shaded area (< 0.5).

Probability maps were calculated for rainfall and for earthquakes. Figure 6.45 shows the distribution of the resulting probability classes.
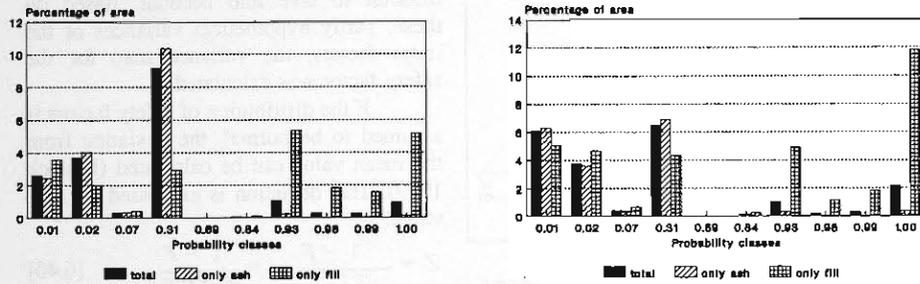
Figure 6.45: Classes for failure probability calculated using an infinite-slope model. Only probability values larger than 0 are displayed. Left: Calculation based on a rainfall event with a return period of 25 years. Right: Calculation based on a rainfall event with a return period of 0.164 years and an earthquake with a return period of 32 years.

In figure 6.45 the probabilities for the occurrence of groundwater peaks or earthquake events were not taken into account. The probability values from this figure should be multiplied by the probabilities based on the return periods. In this case a "design period" of 25 years was used; the assumed design period for the low-budget housing projects in the Manizales area.

- *Rainfall triggered event.* Groundwater peaks with a return period of 25 years were calculated. Therefore no extra multiplication factor is needed.
- *Earthquake triggered event.* An earthquake with a return period of 32 years will have a probability of occurrence in 25 years of 0.781. The probability of occurrence of a day with a groundwater level peak which occurs 60 days per year is 0.164. As the rainfall and earthquakes are independent, the probability values can be multiplied and will result in a probability of 0.128 for the joint occurrence of both events once in 25 years. The probability values calculated above are multiplied with this factor and result in the total probability for each pixel that the factor of safety is lower than one within a period of 25 years, when an earthquake with a return period of 32 years and a rainfall event, with a return period of 0.164 year, occur simultaneously.

The resulting probability maps are given in figures 6.46 and 6.47. The probability for failures for the 25 year period is higher for rainfall triggered slides than for earthquake triggered ones.
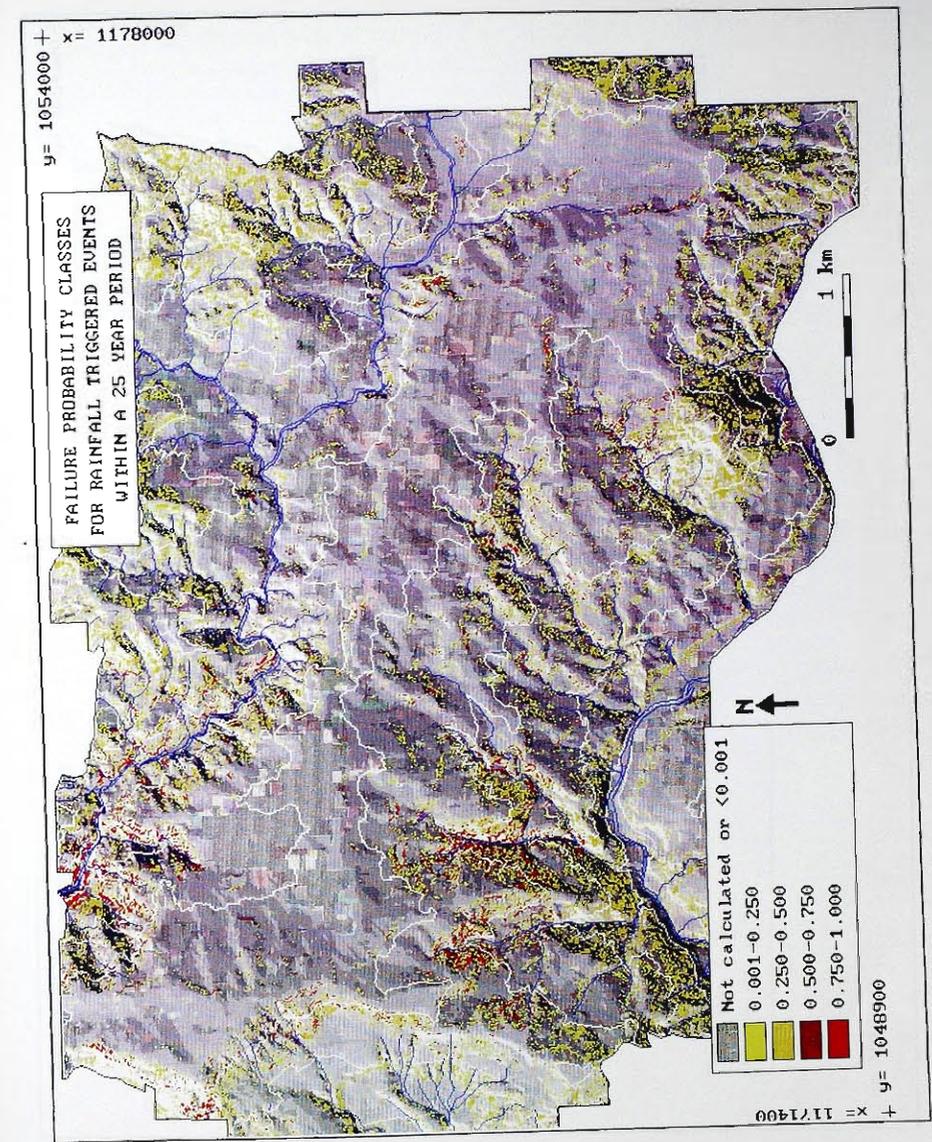
Figure 6.46: Failure probability for a design period of 25 years related to rainfall-triggered translational landslides.
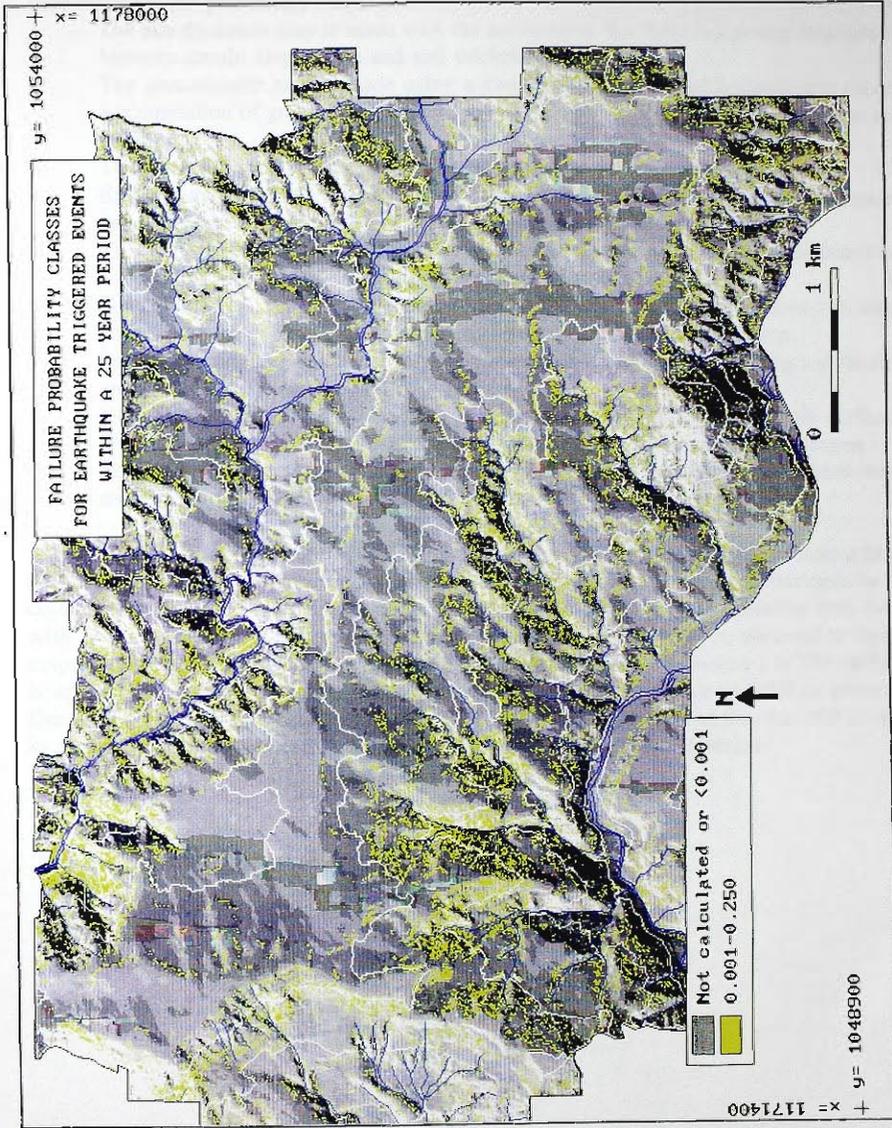
Figure 6.47: Failure probability for a design period of 25 years related to earthquake-triggered translational landslides.

186b

At this point it is important to repeat the large number of assumptions that have been used to create the probability maps:

1. The ash-thickness map is made with the assumption that there is a strong relationship between terrain slope angle and soil thickness.
2. The groundwater map is made using a simple two-dimensional hydrological model. Accumulation of groundwater related to slope length or concavity was not taken into account.
3. The vertical soil sequence was considered to be uniform throughout the area.
4. Errors in the calculation of urban landfill thickness were corrected with a hypothetical curve for critical soil thickness versus terrain slope angle.
5. The soil variables (cohesion, friction angle, density and saturated conductivity) are assumed to be uniform throughout the area.
6. For determining seismic acceleration values empirical relations, developed in other areas, were used. Topographic amplification was not taken into account.
7. For the probability calculation only the variance of ash thickness, cohesion and friction angle were taken into account.
8. No effects of the city itself, such as loading by houses, impervious terrain surfaces, leaking water pipes, or stabilization measures, were included in the calculations.
9. The infinite-slope model can only be used for translational landslides. Other mass movement types were not taken into account.

This list of assumptions makes clear that only general conclusions can be drawn from the resulting maps. It is questionable whether the results could be improved considerably by collecting more data. Inside an urban area, many variables are so heterogeneous that, even with a very detailed drilling program, sufficient information could not be obtained to create maps with the strict specifications for large-scale maps as outlined in section 2.6. The method is application only over relatively small areas at a very detailed scale (1:2000 or greater). Despite the many drawbacks, however, it is the only method, presented thus far, that results in a real hazard map, indicating failure probability within a specified period.

6.6 Landslide frequency analysis

The last method for landslide hazard assessment which will be illustrated is the landslide frequency analysis. A useful tool in analysing the frequency of rainfall-related mass movement occurrences is the calculation of rainfall thresholds, based on antecedent rainfall conditions. Antecedent rainfall can be calculated with the following formula (Crozier, 1986):

$$Pa_0 = kP_1 + k^2P_2 + \dots k^nP_n \qquad [6.41]$$

in which:

Pa_0 = antecedent rainfall for day 0,
P_1 = daily rainfall on the day before day 0,
P_n = daily rainfall on the nth day before day 0,
k = an empirical constant (< 1.0) which depends on the draining capacity of the material and the hydrological characteristics of the area (Capecchi and Focardi, 1988). Mostly values between 0.80 and 0.90 are used in the literature.

A daily rainfall record must be available over a relatively long period. For the Manizales area a continuous record exists for the period 1960-1990. A batch file was written for the calculation, and antecedent rainfall was calculated by moving a calculation window with a fixed length over the data. Antecedent rainfall was calculated for several periods (5, 10, 15, and 30 days before day 0). Return periods were calculated from the resulting daily antecedent rainfall record (see also figure 2.9).

The next step is the comparison of the antecedent rainfall record with landslide occurrences. Landslide occurrences were obtained in a tiresome manner from the daily records of the fire brigades of Manizales and Villa Maria. Only those landslide occurrences in which the fire-brigade had to assist in rescuing victims or performing evacuations are noted in these records. Most of the reported landslides occur in the rainy periods in April-May and October-November.

The landslide data were crossed with the antecedent rainfall data in order to determine threshold values in antecedent rainfall for a certain probability of landslide occurrence. An example of the crossing for one year is presented in figure 6.48. From this figure it can be seen that the relation is best with the antecedent rainfall for 15 days. However, not all peaks in antecedent rainfall contain a landslide occurrence and not all landslide occurrences are related to peaks in antecedent rainfall.

In order to evaluate the relationship over the complete period a plot was made of daily rainfall against antecedent rainfall for a period of 15 days, in which the occurrences of landslides are indicated with thick points (figure 6.49). It is clear from this table that no threshold values can be established as the landslide occurrences are found throughout the plot, even at values of low daily rainfall and antecedent rainfall.

This method is not considered to be useful for an area such as this, for the following reasons:

1. There is no complete record of landslide occurrence; only the catastrophic ones are known from fire-brigade records.
2. In an urban area such as Manizales, many of the landslides may not be rainfall related, but can also be caused by human activities, such as bulldozer, leaking water pipes, etc.
3. Rainfall in the Manizales area is rather variable in space (as mentioned in section 3.4).
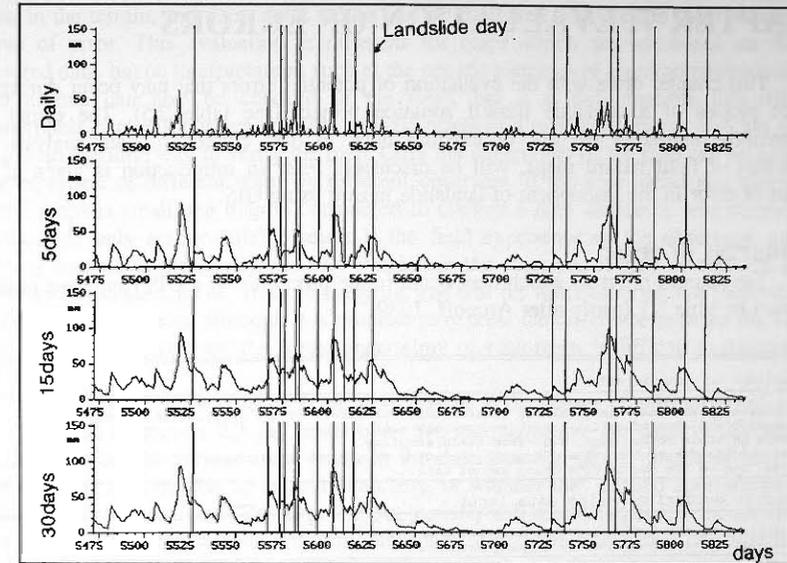
Figure 6.48: The relationship between landslide occurrences (vertical lines) and rainfall for a one year period. Daily rainfall is shown in the upper curve. Antecedent rainfall for 5, 15 and 30 days are displayed below.
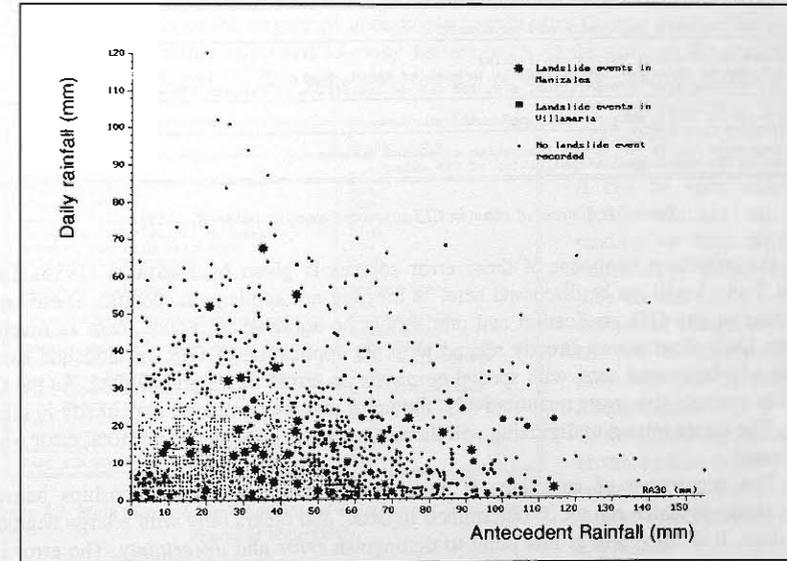
Figure 6.49: Plot of antecedent rainfall (using a window of 30 days) against daily rainfall for landslide- and non landslide events. No threshold values can be established.

CHAPTER 7: EVALUATION OF ERRORS

This chapter deals with the evaluation of potential errors that may occur during the various phases of a landslide hazard zonation project (see table 2.5). The errors and uncertainties related to the use of existing data, to data collection, data analysis and production of final hazard maps, will be discussed. First an introduction is given of the sources of error in the assessment of landslide hazard using GIS.

7.1 Sources of error

The sources of errors which may occur in the procedure of a GIS supported analysis are listed in table 7.1 (partly after Aronoff, 1989)

1. Errors in source data
- Geometric (positional) and semantic (classification) errors in the compilation of maps. - Geometric and classification errors in remotely sensed data. - Errors in other source data. e.g. from field sampling. - Inaccuracies due to the vague ("fuzzy") character of natural boundaries. - Errors due to the source data being out of date.
2. Errors occurring during data input
- Digitizing errors due to operator mistakes and limited precision of the digitizer. - Errors in attribute data entry (typing errors).
3. Errors in data storage
- Errors due to the limited precision with which coordinates and other numerical data are stored. - Errors arising from vector-to-raster conversion.
4. Errors in data analysis and manipulation.
- Propagation of errors during map overlay. - Errors due to incorrect use of formula (misuse of logic, etc). - Errors arising from interpolation, e.g. for the determination of terrain slope.
5. Errors in data output and application.
- Cartographic errors due to the limitation of output devices. - Incorrect or inappropriate application of GIS outputs.

Table 7.1: Sources of error in GIS-supported analysis (Aronoff, 1989).

An extensive treatment of these error sources is given by Burrough (1986). Error sources 2 and 3 will not be discussed here, as they are not application specific. These errors may occur in any GIS application and one should be attentive to reduce them as much as possible. Only those errors directly related with the application of GIS for landslide hazard analysis will be treated here, with special emphasis on errors in the source data. As the GIS is used to evaluate the errors quantitatively, the maps that are compared are already in digital format. The errors related to digitizing will therefore also be presented in the total error which is evaluated.

The occurrence of landslides is governed by complex interrelationships between factors, some of which cannot be determined in detail and others only with a large degree of uncertainty. It is important at this point to distinguish *error* and *uncertainty*. The error in a map can be assessed only if another map, or field information is available which is error-free, and with which it can be verified. Slope angles, for example, can be measured at several

points in the terrain, and these point values can be compared with a slope map to assess the degree of error. This evaluation is different for maps which are not based on factual, measured data, but on interpretation, such as the genetic elements of a geomorphological map. Such a map can also be checked in the field, but it is still possible that different geomorphologists will not agree on the specific origin of a certain landform. In other words, there is no absolute way to verify the map. Only the uncertainty of the map can be assessed, by comparison of different maps by different observers. If the area identically mapped in several maps is small, the map is considered to contain a high degree of uncertainty. This method will only render reliable result if the field experience of the observers, and the mapping method is identically. Usually this is not the case, and it may be that one of the observers has made a lot of errors in mapping, and that the other observer has mapped more reliably. For this reason, although it is possible to express the difference between the various maps in a quantitative way, the actual uncertainty of such maps is difficult to determine in a absolute manner.

The amount of uncertainty is strongly related to the degree of subjectivity of a map. As mentioned in section 2.3 the terms *objective* and *subjective* are used in this study to indicate whether the various steps taken in the determination of the degree of hazard are verifiable and reproducible by other researchers, or whether they depend upon the personal judgement of the researcher. The larger the subjectivity will be, the larger also the uncertainty, as the possibility increases that different individuals will come to different conclusions.

Many of the input maps used in landslide hazard analysis are based on aerial photo-interpretation and will therefore will contain a large degree of uncertainty. Table 7.2 gives a list of factors that are considered to be important in controlling slope instability and a qualitative description of the degree of uncertainty (partly after Carrara et al., 1992).

The degree of uncertainty is related to many factors, such as the scale of the analysis, the time and money allocated for data collection, the size of the study area, the experience of the researchers, and the availability and reliability of existing maps. From this list it can be seen that many factors contain an intermediate or high degree of uncertainty, either because they are based on a limited amount of factual data (such as soil characteristics) or they are made by subjective interpretation.

In the following sections the errors and/or degree of uncertainty for some of the factors listed in table 7.2 are illustrated.

Factor	Uncertainty
Slope angle	Low
Slope direction	Low
Slope convexity	Low
General lithological zonation	Low
Detailed lithological composition	High
General tectonic framework	Low
Detailed rock structure	High
Earthquake acceleration	High
Rainfall distribution	Intermediate
Geomorphological setting	Low
Detailed geomorphological situation	Intermediate
Present mass movement distribution	Intermediate
Present mass movement typology	Intermediate
Present mass movement activity	Intermediate/high
Past mass movement distribution	High
Soil type distribution	Low/intermediate
Soil characteristics	Intermediate/high
Soil thickness	High
Groundwater conditions	High
Land use	Low
Past climatological conditions	High

Table 7.2: Main factors in landslide hazard zonation and their estimated degree of uncertainty.

7.2 Errors in existing data

Many of the existing maps used in a landslide hazard assessment project contain a considerable amount of errors and uncertainties. These errors and uncertainties may be caused by the following reasons:

1. *Image interpretation.* The best examples of this in the study area are the geological maps. More than ten geological maps at various scales have been made for various parts of the study area, by professional geologists or students for various applications. The lithological distribution does not show large variation among these maps, as this is rather simple and can be verified in numerous outcrops. The faults drawn on these maps, however, are completely different, since they are mainly based on image interpretation. If all the faults extracted from these maps are drawn together, not more than 5% is equally mapped by all geologists.

2. *Use of different legends.* Soil maps, made by different organizations using different legends, did not match at all.

3. *Source data being out of date.* The detailed land-use maps of the area which were made in 1985, showed large differences with the present situation.

4. *Incomplete data.* When the cadastral data base of Manizales was checked by random sampling (Turkstra et al., 1991) is was found to be very incomplete. Another example of incomplete data are the landslide-records from the fire-brigades in the area, in which only the catastrophic landslides are indicated.

5. *Insufficient time allocated to data collection.* Some landslide occurrence maps for the entire Chinchina basin exist, which have been made by a two-weeks fieldwork, and which fail to display the most obvious features.

Considering these drawbacks in the use of existing data, it is strongly recommended never to use existing data without a thorough second evaluation.

7.2.1 Errors in topographic maps

In table 4.2 a list was given of the indispensable data that should exist for an area in order to be able to start a landslide hazard zonation, such as topographic maps. However, even such basic data may contain considerable errors. At the beginning of this study digital information was used derived from four adjacent 1:100.000-scale topographic maps (Lozano, 1989). Between the eastern and western pairs of maps there is a change in the coordinate systems, one of which is related to the capital Bogotá and the other to the city of Medellin. In order to digitize an area occurring in both coordinate systems, one of them has to be renumbered to the other. Unfortunately, the maps themselves do not contain a conversion factor, so the possibility exists that different conversion factors are used by persons that have digitized maps within different projects. The differences were found to be on the order of ten meters or more, so that the existing digitized information could not be used.

A much larger error was encountered when data from a 1:25,000 scale map were superimposed on the 1:100,000 scale digitized maps. After careful examination of the maps it was found that about 1 cm on the original 1:100,000-scale topographic map was "invented" in order to make the eastern and western pairs of maps fit. Of course the information digitized on the basis of this topographic map was useless, and all the previous digitizing work had to be repeated. In addition, also errors of countour labelling and incorrect location of drainage lines have been encountered and corrected.

7.2.2 Errors in slope maps

One of the crucial input maps in landslide hazard analysis is the slope map, derived from a digital terrain model (DTM). Unfortunately, the most detailed topographic maps which cover the entire study area are at a scale of 1:25,000 and have a contour interval of 50 m. It is obvious that the slope angles based on such a general map will differ strongly from reality. To evaluate the error an area was selected surrounding Chinchina for which a 1:5,000-scale topographic map with a contour interval of 5 m is available. DTMs were made via linear interpolation of contour lines and slope maps were derived from the DTMs using gradient filters. The two slope maps were combined and the differences between the slope angles calculated. The resulting map and frequency plot are given in figure 7.1 (page). From the histogram it can be concluded that approximately 65% of the slope map derived from the 1:25,000-scale map has slope angles that differ 10° or less from the slope map derived from the 1:5,000-scale map. The frequency of the differences between the two slope maps is not completely normally distributed. There are more steep slopes in the 1:5,000-scale slope map than in the 1:25,000 scale map. This is partly caused by the terrace slopes which are of limited height and which are not depicted in the 1:25,000-scale map. The hills surrounding Chinchina show a more or less equal distribution of too gentle and too steep slopes.
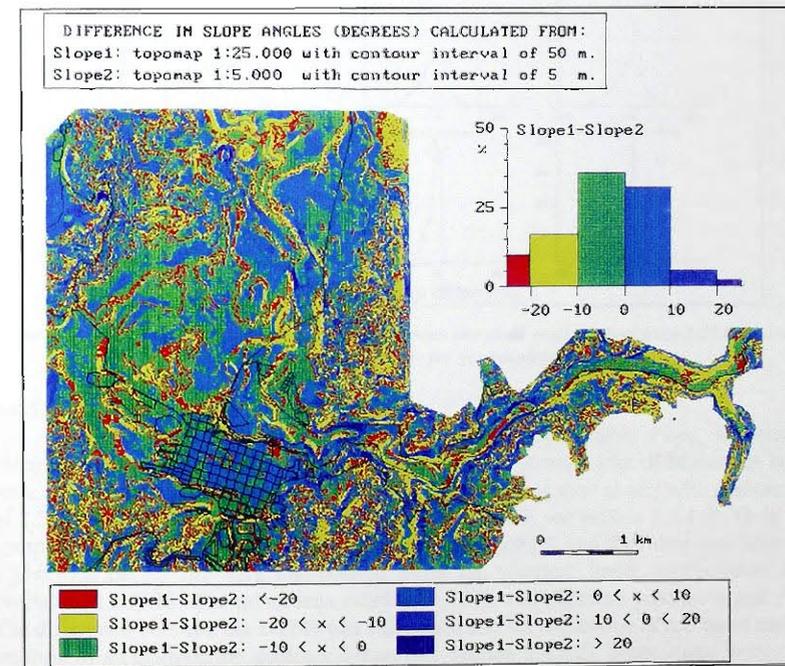
Figure 7.1 : Difference in slope angles calculated from two DTMs derived from topographic maps at different scales (1:25,000 and 1:5,000) and with different countour intervals.

A second evaluation was made by crossing the slope difference map with the map of the geomorphological units (GEOM) in the area. The result is given in figure 7.2, which shows the frequency distributions for the various geomorphological units. The steeper the curves are, the smaller is the difference between the two slope maps. The differences are naturally smallest in the flatter areas, such as the terrace levels and the anthropogenic units. In the anthropogenic units about 22% of the pixels have the same slopes. The largest differences are found in the denudational and denudational structural units, where the percentage of pixels with equal slope angles is less than 5% of the total. From these observations it is clear that a slope map, especially when it is made from relatively general maps, will contain large errors.
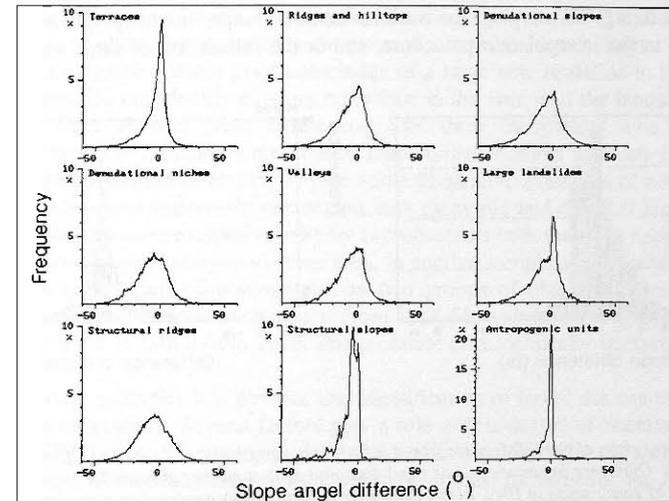
Figure 7.2: Frequency (in %) of difference (in ') between two slope maps (derived from 1:25,000- and 1:5,000-scale topographic maps) per geomorphological unit.

7.2.3 Comparison of detailed DTMs

Even if a DTM is made from very detailed topographic maps, the error in the calculated slope angles can be considerable. For the large-scale area of Manizales two DTMs were made from a large series of 1:2,000-scale topographic map sheets with contour intervals of 2.5 m from two different time periods (1949 and 1989, see section 5.2.1.3). Only the 10-m contours were digitized, the various map sheets were joined, and the rasterized contours (with a pixelsize of 8.5 m) were interpolated using the standard linear interpolation algorithm available in ILWIS. The urban area existing in 1949 was digitized separately and rasterized. The difference between the DTMs was calculated and served as one of the input maps for the creation of an engineering geological map (see section 5.4.4.2). Slope maps were calculated using 5 x 5 filters. During the analysis it was evaluated whether the pixels that had the same altitude in 1949 and 1989 could have different calculated slope angles due to errors in the

DTMs and slope maps. First the degree to which areas that were determined to be unchanged during the period 1949-1989 were really unchanged was evaluated. Large changes in topography between the two dates were not expected in the area that was already urbanized in 1949. However, figure 7.3 (left) shows that there were considerable changes. Only a small part of the area had a difference of 0 m. Subsequently, all pixels with equal altitudes in 1949 and 1989 were separated, and the differences in slope angles were calculated. Surprisingly, as shown in figure 7.3 (right), only 12% of the pixels with equal altitudes for the two dates also had the same slope angles. This does not indicate that there is a 88% error in the map, since it possible that, although the height of the pixel remained the same, the slope has actually changed, especially due to altitude changes of neighbouring pixels. Nevertheless, the slope map contains a large amount of error, which is an accumulation of errors in the original maps, in digitizing, in merging the various contour maps, in the pixelsize used during rasterization, in the interpolation procedure, and in the calculation of slope angles.
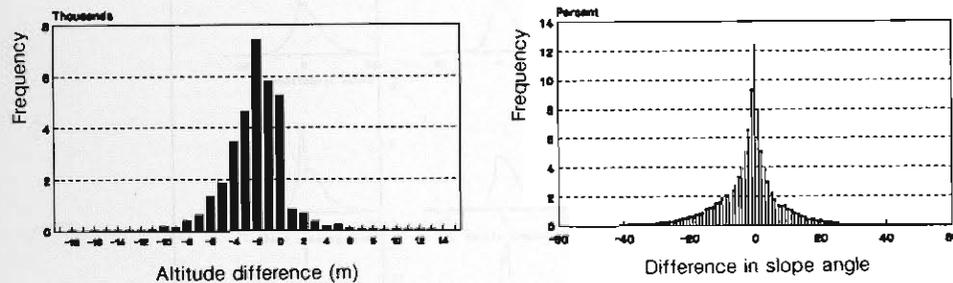
Figure 7.3: Comparison of two DTMs made from 1:2,000-scale topographic maps for two different times (1949 and 1989). Left: Difference in altitude (x-axis in m) displayed against number of pixels for the area which was already covered by construction in 1949. Right: Difference in slope angles displayed as a percentage of all pixels with equal altitude in 1989 and 1949.

Errors could have been reduced if all contours (with contour interval of 2.5 m) would have been digitized, and if smaller pixelsizes would have been used. However, this would have increased the time needed for digitizing considerably, and would have made the size of the raster files very large, leading to storage capacity problems and increasing calculation time on a PC.

7.3 Uncertainty in newly collected data

While it is easy to blame other persons for errors encountered in existing data, reduction of errors and uncertainties in newly collected data is the full responsibility of the researcher in a hazard mapping project. Before collecting new data it is important to have insight into those steps in data collection that lead to maps with a high uncertainty. In this section some of these aspects are evaluated.

7.3.1 Uncertainty in landslide maps

The landslide occurrence map is by far the most important map in a landslide hazard survey, since it gives the locations where landslides have occurred in the recent past. In many of the analysis techniques presented in chapters 2 and 6, the landslide occurrence map is the most important input map. Furthermore, the resulting hazard maps are compared with the actual distribution of landslides in order to check its accuracy. Therefore a landslide occurrence map should be as accurate as possible.

The process of mapping mass movements was presented in section 4.3.2.2. From this section it can be concluded that photo-interpretation plays a very important role in the creation of a mass movement inventory map, although it should always be followed by an extensive field check. It has been recognized in the literature that creation of mass movement occurrence maps contains a large subjective element. Fookes et al. (1991) discuss the results of a comparison of eight photo-interpretation maps of a landslide area in Papua New Guinea. Five of these took place without prior knowledge of a large new landslide in the area. Two of these five two did not identify existing landslides in the area, and the landslides mapped by the other three showed great differences. The three interpreters who had a-priori knowledge of the new landslide were able to map similar features at much greater detail. Carrara (1992) and Carrara et al. (1992) give some illustrative examples of comparisons of landslide maps for three regions. In one region with many old and dormant landslides, only 10% of the landslides were mapped equally by two observers with the same experience. Only one of them had the opportunity to visit the area. In another sample area, two landslide maps were made using two sets of photographs by two groups of observers. One group used 1:33,000-scale black and white photographs from 1954-55, and the other group used colour photographs at scale 1:10.000 from 1978. The landslide area identically interpreted was only 7.8%.

From these examples it is obvious that identification of landslides can contain a very high degree of uncertainty. Several factors play a role in this degree of uncertainty, such as the researcher's experience in photo-interpretation and field knowledge; the aim of the study; the characteristics of the study area; the age and type of mass movements; the scale, quality, and type of photos used; and the conversion of the information from the aerial photos to the base map. When working with GIS, digitizing error will exerbate the situation.

To evaluate the landslide interpretation within the study area several different landslide maps were compared. A test was done by comparing part of the landslide map at the medium scale, prepared by the author and presented in section 6.1.1 (figure 6.5), with a landslide map made by an ITC student at the MSc level. Both maps were based on detailed photo-interpretation and fieldwork, although the fieldwork time for the MSc-student was very limited. The photos used by the author were of 1:10,000-scale, while those used by the MSc-student were of 1:30,000-scale. The comparison of both digitized maps showed that only 8.6% of the total area occupied by landslides in both maps were mapped the same (which was only 1.2 % of the total area); 13.6% of the total area was mapped by either one of the two, while one map displayed 4.6% of landslides and the other 7.7%. The comparison of the two maps is given in figure 7.4.

Another comparison was executed between the landslide map made for the large scale area by the author (section 6.1.1) and a map made by graduate students of the Caldas University in Manizales, after extensive fieldwork. These two maps showed much larger similarities.

From these tests it can be concluded that landslide inventory maps contain a large degree of uncertainty. This can be reduced when detailed fieldwork is carried out, when clear criteria for landslide identification are used, when the interpretation is done by an experienced geomorphologist using large-scale aerial photos, and when the conversion and digitizing are done incorporating other types of information.

7.3.2 Variations in outlining geomorphological units

One of the input maps which is considered to be very subjective is the geomorphological map. Maps made by different geomorphologists will contain large differences, especially if the maps are made by photo-interpretation, with limited field checks. The differences will be greatest when the geomorphologists design their own legend.

To assess the variability in outlining geomorphological units a test can be made by comparing photo-interpretations done by several persons. A useful method of comparing various geomorphological interpretations is given by Middelkoop (1990).

During a workshop on the use of GIS in slope stability hazard assessment, 12 professionals working in the field of hazard mapping in the northeastern Andean countries were asked to interpret the same set of aerial photos. A stereo-photo triplet at a scale of 1:30,000 of the terraces and surrounding areas in Chinchina, and a legend of the main geomorphological units (table 4.7) were given to them, as well as an introduction to the geomorphology and geology of the area. Four groups were formed, and the photo-interpretation which they considered best of the group, was digitized directly without converting the photo-information to the topographic map. The resulting four maps were restructured so that they had the same legend numbers, and compared. The results are given in figure 7.5.

Only 10% of the area was assigned the same legend unit by all four groups. About 17% was mapped identically by three groups and 53% by two groups. The remaining 20% of the area was mapped differently by each group. The area mapped equally by all four groups consisted mainly of the terrace levels around Chinchina. The area with the largest differences were the steep slopes west of Chinchina.

The legend which was used has a relatively large number of classes. Therefore a second test was made by regrouping the classes into seven groups, mainly expressing the origin of the units. Naturally, the comparison of the four simplified maps now gave better results: 36% identically mapped by all four groups, 32% mapped by three, and 31% by two. Basically the terrace area was mapped equally. For the surrounding slopes, the main difference between the groups was that they mapped it either as denudational or denudational-structural, which is in itself a difficult item. It is obvious that the use of a more complicated legend, such as the one for geomorphological subunits (table 4.8) would most probably have resulted in even larger differences. On the other hand, the result would probably have improved considerably if sufficient time was spent on fieldwork, which was not the case here. The time which was available for the photo-interpretation and the field check was relatively short (3 days). If more time had been used the results probably would have been better.

From this example it can be concluded that a geomorphological map has a high degree of subjectivity, and depends strongly on the experience of the person that is making the map, as well as on the amount of time spent in the field for checking the interpretation.
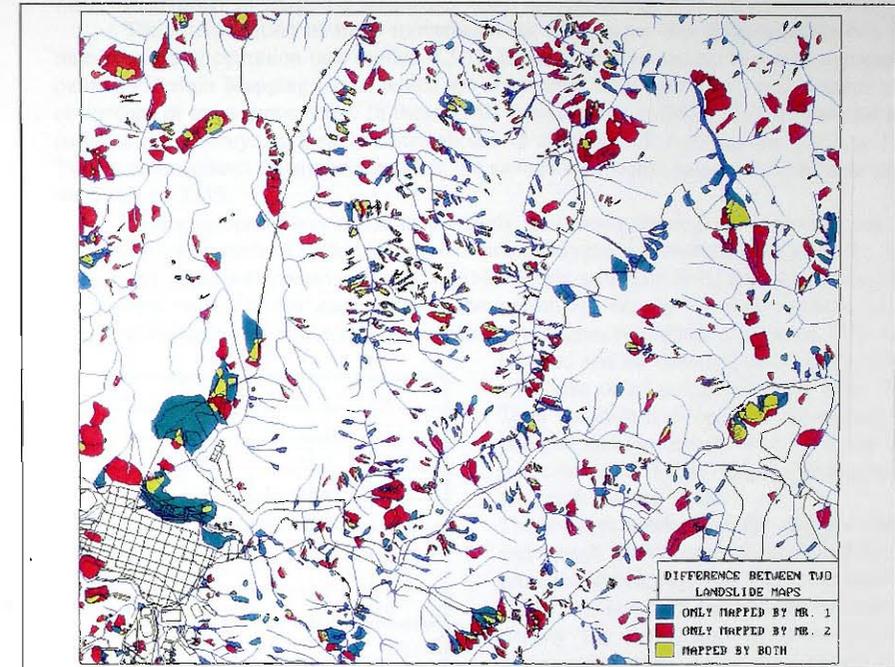
Figure 7.4: Overlay of two landslide maps for a part of the medium-scale study area.
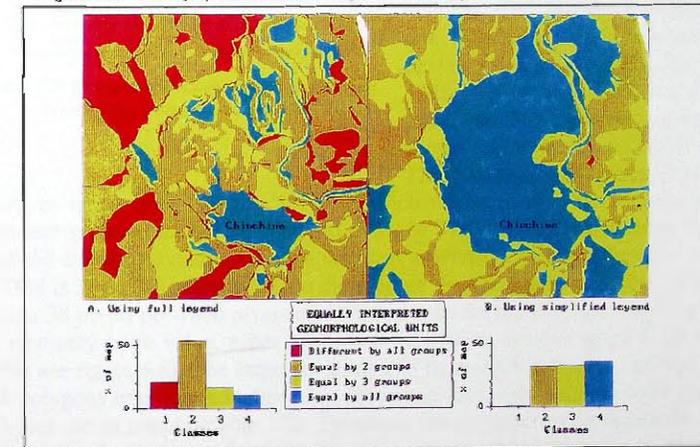
Figure 7.5: Comparison between geomorphological maps prepared by four different groups of earth scientists. Left: Number of groups that mapped an area identically using the full legend of table 4.7. Right: Number of groups that mapped an area identically using a simplified legend.

7.3.3 Uncertainty in mapping landslides from sample-areas

The interpretation of mass movements for large areas at a regional scale is a very time-consuming operation (see section 4.3.1). It would be time saving to use an approach of outlining Terrain Mapping Units, which are considered "homogeneous", with respect to the occurrence of mass movements. In these TMU sample areas could be used for detailed mass movement inventory. Each sample area should be characteristic for a certain TMU, or TMS. The mass movement density measured in the sample area would have to be similar to that of the TMU or TMS.

This assumption was tested in the study area, using the regional-scale data set. The TMU map was rasterized such that each individual polygon received a unique identifier. Each of these polygons was considered as a possible sample area. The TMU map was crossed with the process map, and for each polygon the permillage density for mass movements and erosional features was calculated. Subsequently, polygons belonging to the same TMS were grouped and the density was calculated for the total area of all polygons of the same TMS. Then the difference between the density in a polygon and the density over the entire TMS was calculated. Table 7.3 gives an example of the result for one TMS.

The average differences for polygon density and overall TMS density, were plotted for each process individually. The results are shown in figure 7.6, in which the average difference in density (in permillage) is given for eight different processes. From these graphs it can be seen that the density calculated in a polygon may deviate considerably from the one calculated over the whole TMS. These deviations are not equal for the different TMSs, TMUs and TMCs and for the different processes. The lower right graph of figure 7.6 shows the average deviation calculated per TMC, taking into account all processes. These deviations range from 0‰ for TMC 9 (which represent the glacier areas where no mass movement phenomena are mapped) to 67‰ in TMC 4 (the area around Manizales). The combined average deviation between the mass movement density calculated per polygon and per TMS is 38‰. This means that on the average the calculated landslide density per polygon deviates 38 pixels per 1000 pixels of the map, from the density calculated for the TMS. This is a relatively large value, especially when the typical density range is taken into account (<50‰ see figure 6.8). The large deviation can be explained by the fact that there are some TMS polygons with much higher mass movement densities than the other ones of the same TMS (see the example in table 7.3). Therefore, before selecting sample areas, one should be aware of the deviations in landslide densities within a TMS. In most cases it will be better to make a general landslide inventory of the entire study area, and not only within sample areas.

A	B	C	D	E
1	121	0	2	2
2	121	0	2	2
3	121	13	2	11
4	121	34	2	32
5	121	0	2	2
6	121	0	2	2
7	121	0	2	2

A: polygon number
B: terrain mapping subunit (TMS)
C: areal density of landslides in
   permillage per polygon
D: areal density of landslides in
   permillage per TMS
E: Difference between density per
   polygon and per TMS

Table 7.3: Example of the comparison of landslide densities per polygon and per TMS.
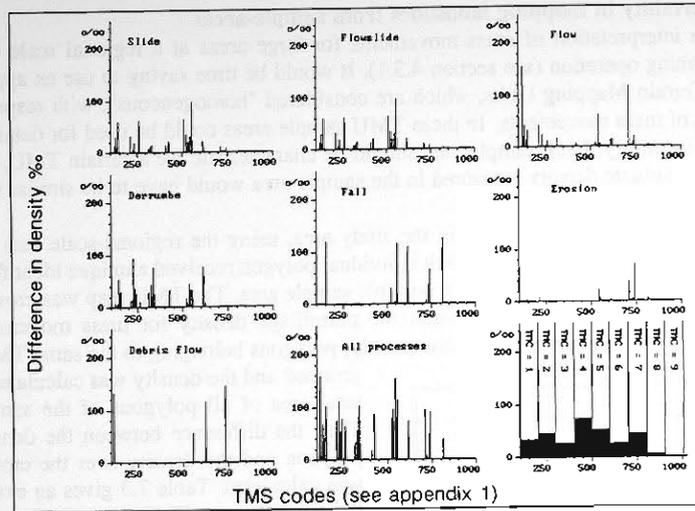
Figure 7.6: Differences in density of denudational processes calculated per polygon and per TMS expressed in ‰ (pixels with process/1000 pixels). The X-axis represents the terrain mapping subunits (TMSs) with the codes given in appendix 1. Graphs are given for eight different denudational processes. The lower right graph display the average density difference per Terrain Mapping Complex.

7.3.4 Evaluating the homogeneity of individual polygons

In delineating terrain mapping complexes, units, and subunits, it was stated in section 4.3.1 that the polygons themselves are considered to be homogeneous zones. Homogeneity increases from the TMCs towards the TMSs. The TMSs should be homogenous with respect to lithology, soil types, drainage density, internal relief and processes. This homogeneity was evaluated by crossing the isopleth map of various mass movements types, calculated for the regional-scale area, with the map of TMSs, used in the former section, where each polygon had a unique identifier. The minimum and maximum landslide densities from the isopleth map were calculated for each polygon, classified and displayed in a map.

There are polygons which have large internal variation in mass movement density. From this it can be concluded that homogeneity is a general and relative term, and should be considered at the scale at which it is used. Even at large scales the outlined units may still have variations in landslide density. The larger the unit, the more probable it is that there will be a greater density of mass movements in a particular part of the unit. Therefore, when such homogeneous units are used within a hazard analysis based on land units, such as in the multivariate analysis, the resulting values per polygon may be quite different than for specific parts within the same polygon. This problem could be solved by working on a pixel-level, as explained in section 6.3.1 and figure 6.12. Outlining of "homogeneous" units in a map is a difficult process, and will always lead to a considerable generalization. Therefore, methods based on the outlining of homogeneous units should only be applied at small-scales.

7.3.5 Errors in field descriptions

Errors introduced during data collection are not limited to maps based on "subjective" photo-interpretation. Data measured or estimated in the field may also show large deviations. An example of this is the identification and classification in the field of the various material types (see table 4.11). Distinguishing between the various types of pyroclastic materials proved to be especially difficult. The original legend of table 4.11 distinguished between fine ash, sandy ash and coarse sandy gravelly ash, and each of these groups was subdivided into weathered or unweathered. For a number of samples the correctness of this field classification was checked later by grain-size analysis and soil classification. Table 7.4 gives a summary.

Classif ication	LABORATORY		
FIELD	110 fine	120 sandy	130 lapilli
110	33	8	1
120	7	24	5
130	1	2	4

Table 7.4: Comparison of ash classification from the field and the laboratory. The number of samples is indicated.

The results showed that there is quite a large error in field classification of ash soils compared to laboratory analysis. Problems with weathering grade are important: weathered pyroclastics are classified as such in the field, but as fines in the laboratory. Especially important are mismatches of the fine and the sandy ash soils. This can be explained by the fact that pyroclastic material with 51% of sand and 49% of fines is classified as "sandy", and one which has 49% of sand and 51% of fines is classified as "fine" ash. Many of the ash samples turned out to be at the borderline between sandy and fine.

A second example is the uncertainty of describing landslide characteristics from a checklist. During the workshop mentioned previously, three groups of earth scientists independently prepared field descriptions of the same three landslides, using the landslide checklist presented in the appendix 4, and the description given in table 4.9. A comparison of the results for a few selected variables is given in table 7.5. From the table it is clear that there was no disagreement on the important parameters TYPE and SUBTYPE for these three mass movements. The activity classes were also estimated identically in most cases. The geometrical variables that can be measured, such as length and width, are very similar. Surprisingly, a factor that is difficult to determine, landslide depth, was also estimated very similarly by the three groups. The values for the slope angle before failure deviate rather strongly, as this is a rather subjective evaluation. Strong differences also occur for those variables that must be estimated or deduced, such as main cause and movement mechanism. In conclusion, it can be stated that the agreement is high for those variables that can be observed directly and poor for those which are based on subjective evaluation.

7.4 Errors in data processing

Summation of all inaccuracies presented in the former sections can result in a very low accuracy of the final product, especially in analyses in which many data layers are used, such as statistical analysis or deterministic modelling. An overview of the problems encountered in map overlaying is given by Burrough (1986). Each input map used in an analysis contains a considerable degree of *inherent error* (error or uncertainty in the contents of a map). Combination of several layers in a GIS will generate furthermore *operational errors*.

Variable	Description	Landslide 1: Rotational slide			Landslide 2: Derrumbe			Landslide 3: Flowslide		
		G.1	G.2	G.3	G.1	G.2	G.3	G.1	G.2	G.3
Type	Landslide type	1	1	1	4	4	4	2	2	2
Subtype	Subtype	1	1	1	2	2	2	1	3	3
Activity	Activity	2	2	2	2	2	1	3	3	3
SLOPEDIR	Slope direction	305	275	340	260	250	45	140	160	150
SLOANGLE	Slope angle	22	29	40	80	34	42	20	26	30
SLOPEUP	Length upslope	1	1	1	1	1	1	2	1	1
SLOPDOWN	Length downslope	1	3	1	1	1	3	0	1	1
SLOPROF	Slope in profile	1	3	3	1	3	3	3	1	2
SLOPLAN	Slope in plan	3	3	3	1	1	1	1	1	1
LSLENGTH	Landslide length	25	25	30	15	15	20	150	130	200
LSWIDTH	Landslide width	20	30	30	20	23	27	50	50	30
LSDEPTH	Landslide depth	8	7	7	8	5	5	9	10	10
MECHANIS	Movement mech.	1	2	1	1	1	1	3	3	4
MAINCAUS	Main causes	1/10	1	1/10	2	2/14	2	12/16	12/18	12
DAMAGE	Damage observed	0	3/9	3/9	1	1	1	1/3	3/9/1	1/3/7
STABIL	Stabilization	0	6	0	0	0	0	4/5	4/3/6	1/4/5
VULNER	Elements at risk	3/9	3/9	3/9	1	3	0	1/3	1	1/3/10
LANDUSE	Landuse before	6	6	6	3	3	5	6	6	6

Table 7.5: Comparison between descriptions of the same landslides made by three different groups (G.1,G.2 and G.3). The explanation of the variable codes is given in tables 4.9 and 4.10.

To evaluate the result of crossing multiple input maps, the susceptibility map made in section 6.3.3.4 (figure 6.19) was examined in more detail. This map was made by pairwise crossing of four input maps (slope classes, geology, land use and geomorphological complexes). The final map contained 689 unique combinations of variable classes for these four variables. Many of these combinations may not be important in the area, and may be caused by location and identification errors. The size of each of the combinations in number of pixels was obtained from a histogram calculation. Based on these values the cumulative percentage of combination classes was plotted against the logarithm of the number of pixels (see figure 7.7). This shows that approximately 50% of all combination classes is smaller than 100 pixels. These very small classes can be either very rare combinations of variable classes, or they can be considered as errors in the map, as it is unlikely that a certain combination of slope angle, landuse, geology and geomorphology will occur only in 1.5 ha (100 * 156.25 with a pixel size of 12.5 m) out of a total area of 68.2 km². All these combination with less than 100 pixels together occupied 1×10^4 pixels of the total of 4.37×10^5 pixels in the whole map, which is 2.3%

After crossing the map with the process map of active derrumbes (which was used as the basis for calculating weight values) only 121 pixels of the 2940 pixels with derrumbes (4%) was located in an combination class with less than 100 pixels. On this basis it can be concluded that the production of many small classes during map overlaying, apart from the inherent errors in the input maps, do not play a very large role in the accuracy of the final map. The method of creating new variable maps by crossing a number of classified input maps should only be used with caution. The best solution is the make only useful combinations of variables, based on field experience.
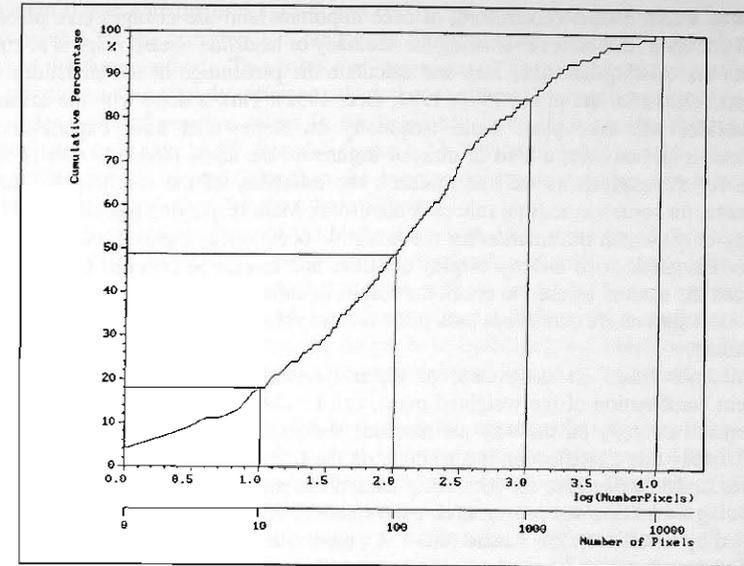
Figure 7.7: Plot of cumulative percentage of the 689 combination of variable classes for four input maps (slope angles, geology, land use and geomorphological complex) against the logarithm of the number of pixels.

7.5 Comparing accuracy of hazard maps

In general it is difficult to evaluate the accuracy of the hazard maps produced by the different analysis methods, discussed in chapter 6. A landslide hazard map must have predictive value for the near future, and can only be checked by comparing future landslides with the hazard classes assigned to the area in which they occur. Several problems are encountered, however:

- Most of the methods do not consider a time aspect, and the resulting hazard maps indicate merely the *susceptibility* to landsliding. These maps do not indicate if landslides within high hazard zones will occur once every year or once every 25 years.
- The landslide map used as a basis in most of the methods only displays information for a specified period of time (i.e. between the 1940s and 1990s). Landslide which occurred during this specified period may have been caused by triggering events which had only short return periods. If a triggering event occurs in the near future with a much larger return period (and a larger magnitude), it may very well be that areas which contain few or no landslides would also become unstable.
- The landslide map is made for the land-use situation present during the time that the mass movement map was made. New land-use changes in the near future in new areas may trigger landslides in areas indicated by a low hazard on the map. If a new road would be constructed, for example, the road construction itself could have a great influence on the occurrence of landslides. Thus the hazard map should be updated

once a new road is constructed, or once important land-use changes take place.

A common method for evaluating the accuracy of landslide hazard maps is to compare these with the existing landslide map and calculate the percentage of the landslides within each hazard class (Carrara et al., 1990, 1991; Gee, 1992). This is done with the assumption that landslides will take place more frequently on slopes that have experienced past movements. It is, however, a kind of circular argument: the same landslide map is used as the basis for the analysis as well as to check the reliability of the resulting hazard map. Furthermore, for some methods this check is not useful. Maps displaying landslide distribution or activity only contain information for the landslide occurrences themselves. The landslide density and isopleth maps directly display densities and cannot be checked by this method. Neither can the method be used to check the results of infinite-slope modelling, since the ash cover in most sites where derrumbes took place on steep slopes was considered to be removed by the failure.

Methods based on assignment of either qualitative or quantitative weights, and subsequent combination of the weighted maps, can be checked with landslide density. The result depends strongly on the way the resulting weights were classified in some discrete classes. Usually this classification is also done on the basis of landslide density by selecting increasing landslide densities for increasing hazard classes. In the medium-scale study area the following distinction was proven to be most suitable: very low hazard (< 0.2% of the class is occupied by landslides), low hazard (0.2-1 %), moderate hazard (1-4%) and high (> 4 %).

The best method for evaluating the reliability of hazard maps is to compare the percentages for the wrongly classified pixels with landslides, with the percentage of wrongly classified pixels without landslides, as was done in most of the statistical methods described in section 6.3 and 6.4. The percentage of pixels with landslides which are classified as stable, gives a clear indication of the error in the method. The percentage of pixels without landslides which are classified as unstable may indicate that they are actually potentially unstable. Table 7.6 gives a summary of the percentages correctly classified pixels with landslides for the various statistical methods, discussed in chapter 6.

Method	Correctly classified pixels with landslides
Susceptibility map	
• summation of individual maps	82 %
• stepwise combination of input maps	92 %
• using a combined parameter map	97 %
Information value method	
• based on mapping units	85 %
• summation of individual pixel maps	95 %
• using a combined parameter map	95 %
Weights of evidence modelling	
• summation of individual maps	92 %
• using a combination map composed of 4 factors	96 %
• using a combination map composed of 6 factors	93 %
Multiple regression analysis	No satisfying result obtained
Discriminant analysis	No satisfying result obtained

Table 7.6 Summary of percentage correctly classified pixels with landslides for the various statistical methods presented in sections 6.3 and 6.4.

Table 7.6 shows that the results for the susceptibility mapping, the information value method and the weight-of-evidence method based on pixels is quite good. Normally 90 or more percent of the mapped landslides also occur on pixels which had resulting weight values

---

larger than 0 (see equations [6.3],[6.4] and [6.5]), indicating that there occur factors which are favourable for the occurrence of landslides. There is not so much difference between the results of the three methods. This is not very surprising as they are based more or less on the same principle, using slightly different calculation equations. Susceptibility analysis produces a far wider range of positive values in the frequency distribution, due to the nature of the equation used (equation [6.4]). See also figure 6.23. This means that variable classes with a much higher density of landslides than the average density in the map will have a greater influence on the result than for the other methods.

What is striking in most of the histograms, both from those based on mapping units and those based on pixels, is that the frequency distribution of units or pixels with landslides has a more or less normal form, and that those without landslides have a marked bimodal form, with a maximum below 0 and a maximum above 0. This positive maximum is formed by those units or pixels which presently do not have landslides, but which occur in locations with a combination of factors favourable to landslides. These can be considered as hazard areas.

A very important factor in the analysis is the number of factor maps that are used. When factors are used which are dependent with respect to the occurrence of landslides, care should be taken not to sum the results of the individual factor maps. The number of observed and predicted landslides is very different when input maps are used which are dependent. This is not the case when a map is with unique combinations is prepared first, and used in the analysis. If the combination of variables is made on the basis of field experience, the result will be most reliable.

7.6 Production of hard-copy output

In the final section of this chapter some remarks will be given on the production of the final hazard maps with the use of GIS. The hazard maps presented in the chapter 6 were produced by a SHINKO thermal-wax printer and were not given at the required output scales mentioned in section 2.6. The following general considerations are important in the production of hazard maps using geographic information systems:

- *Reproduction costs.* If maps are printed at their original scale, the size would become too large, leading to excessive reproduction costs. Presentation of portions of the maps at the required scale was rejected in this study as this would make the map less illustrative as an output result of the particular mass movement hazard analysis method.
- *Pixel sizes.* The GIS system used in this study (ILWIS) is a raster-based system. All methods of analysis were carried out using raster maps, for which a particular pixel size had to be selected depending on the scale of analysis. For all three scales of analysis, the pixel size was selected in such a way that the raster map fitted as a whole on a colour screen with a dimension of 600 by 800 pixels. For this study many different methods of analysis had to be executed for three different data sets. This involved a very large volume of data, reaching the limit of what is possible on a personal computer. The total data volume for the three scales was approximately 600 Mbyte, which could be handled only by using data compression software. If the selected pixel size had been half as small as the ones used, the size of the individual maps and the total data volume would have been four times as large, leading to large

problems in data handling on a PC.

If the raster maps presented in the previous chapters were displayed at the required scales, the resulting cartographical output would have been unacceptable. Selecting small pixel sizes in the analysis of raster maps is recommended, as this is not only beneficial for the cartographic quality of the output products, but will also reduce errors during map analysis.

- *Vector or raster presentation.* Production of a cartographically acceptable output map from a GIS is much more problematic for raster maps than for vector maps (Aronoff, 1989). Vector maps allow the use of pen plotters, which can produce higher quality maps. In a raster-based GIS, however, the result maps from models may contain different values for each pixel. In that case the map cannot be converted to vector format and reproduced on a plotter.
- *Use of cartographical packages.* Most GIS systems have only limited capability for the production of cartographically acceptable results, using different fonts, hatchures, line thicknesses, line styles and symbols (Sumbukeni, 1991; Sijmons, 1992). The ILWIS system, which was used in this study, allows only the use of one font and line thickness. Colours can be used for lines and units, and these can be combined with user defined patterns. For better quality products the maps should be exported to external cartographic packages, such as THEMAK, Intergraph, or Apple Freehand.

7.7 Conclusions on error evaluation

From the foregoing sections it is clear that most of the input maps for a landslide hazard zonation study contain a great degree of uncertainty, either because they are based on subjective (photo) interpretation, or because they are based on a too limited set of observations. Large uncertainties may occur in the most crucial map used in landslide hazard analysis: the mass movement inventory map. It is very important that this map is made with as much precision as possible. An important aspect is the clear formalization of the decision criteria for the most important parameters such as landslide type and activity.

Considering the high degree of uncertainty of the input maps, the errors occurring during the analysis, such as the overlaying of many maps, are of lesser importance. Therefore, instead of putting more emphasis on the development of new and better analysis techniques, more research should be devoted to how the errors in the input data can be kept to a minimum. In future work a clear distinction should be made in the entire procedure of data collection, data entry and data analysis, which of the input maps is based on factual evidence (observations in the field, laboratory results, etc.) and which is inferred data. This way, within the course of a landslide hazard zonation project, newly obtained data can be introduced, and existing maps updated, resulting in more reliable hazard maps.

CHAPTER 8: CONCLUSIONS

The main objective of this study is the development of methodologies for landslide hazard zonation with the use of geographic information systems. This main objective was achieved through the following steps:

- Collection of information on existing methods for landslide hazard assessment;
- Identification of different scales of analysis and definition of their characteristic requirements and potentials;
- Identification of input data needed for each method of analysis;
- Design of procedures within a GIS for the execution of the various methods;
- Testing of each method using the same basic data set;
- Evaluation of potential sources of error in input data and analysis methods;
- Comparison of the various methods;

Any hazard evaluation involves a large degree of uncertainty. Prediction of natural hazards such as landslides, which are caused by interaction of factors which are not always fully understood and are sometimes unknown, confronts earth scientists with especially large problems. For large areas and at small, not detailed, scales it is very well possible to make general predictions: the number of landslides that have occurred in the past within a land unit is a good indication of what can be expected to occur in the near future. It is, however, much more difficult when predictions need to be made in more detail for areas presently free of landslides. In this situation, the earth scientist must rely on models based on the assumption that landslides are more likely to occur in places where a combination of conditions exists which has lead to landslides in the past. Most methods presented in the literature and evaluated in this study are based on this principle. This implies knowledge of causal factors, and the ability to represent these on a map, as well as detailed knowledge about past mass movements. Since hazard maps are used to make predictions over relatively large areas, collection of data for and preparation of these factor maps is a time-consuming operation, and cannot be based solely on factual, measured, field data. During the preparation of these factor maps, the subjective evaluation of field conditions by the earth scientist will play an important role. Since all earth scientists are not equally experienced, these maps will normally contain a considerable degree of uncertainty. It is clear that hazard maps prepared by very experienced geomorphologists will have the highest reliability, with or without the use of GIS. However, solutions must be found to upgrade the reliability of hazard maps in studies where less experienced earth scientists are responsible for the collection of basic data and subsequent analysis. For those cases it is important to give recommendations as to how the reliability of the end product can be increased, by reducing the uncertainty of the input factors as much as possible. This should be achieved by clear definition of criteria for the interpretation of landslides and their controlling factors, as well as by thorough fieldwork. Instead of "making a map by photo-interpretation followed by a field check", input maps for a hazard zonation should be prepared after "fieldwork preceded by photo-interpretation".

The most important input map for a mass movement hazard analysis, the mass movement inventory map, contains, apart from the uncertainties caused by subjective interpretation, a number of limitations which are important to recognize. First, it is only a momentary picture of a continuously changing distribution of landslides. During a certain period of time new landslides will occur, others will be reactivated, and some may even become invisible to the interpreter due to vegetation growth or human modification.

Therefore, it is important to include a multitemporal analysis of aerial photos in each hazard study at the large or medium scale, and to use landslide activity maps in the subsequent analysis. Another limitation of the landslide inventory map is that the magnitude of the events is usually not fully taken into account. Generally landslide hazard analysis is only executed for a specific combination of landslide type and activity. If sufficient information is available it would also be useful to include the size of the events in the analysis.

The use of GIS confronts the earth scientist with quantitative values for many uncertainties encountered in the input data, and can serve as an important tool in analyzing the sources of error. It can also help in reducing the errors occurring in the phase of transfer of the photo-information to a topographic map, and in the correct positioning of the various input layers. Apart from the large subjectivity present in the input factors, some of the methods for landslide hazard zonation, evaluated in this study, also contain a considerable subjectivity in the subsequent analytical phase. GIS can serve as an important tool in reducing the subjectivity during analysis. It offers map overlaying possibilities and calculation facilities far superior to conventional techniques. One of the major contributions of GIS may be the reducing the subjective element during the analysis phase, allowing the user to concentrate more on reducing errors stemming from the input data. It is especially useful in those situations where the causal factors for mass movements are not fully understood. The user can test hypotheses rapidly, and select the most important combination of factors by trial and error. When field knowledge is combined with the calculation facilities of GIS the result will be optimal. GIS should not be used to throw a large group of variables into a "the black box", to see what comes out, since such an approach is not based on a clear understanding of the causal mechanism of slope failures. Standard calculation methods are presented, but the user is fully responsible for the selection of relevant input data and the analytical model.

The methods presented in this study cannot be executed at each scale of analysis. Before starting a hazard study an earth scientist should be aware of the desired degree of detail of the hazard map, given the requirements of the study. When a degree of detail and a working scale have been defined, the cost-effectiveness of obtaining input data must be considered. In this study recommendations are given as to which kind of data can be collected at each working scale (regional, medium and large scale). The availability of data determines the type of analysis that can be executed. In table 8.1 a summary is given of conclusion of the author on the feasibility and usefulness of applying the methods discussed in this study for the various scales under consideration, and of the usefulness of GIS. The following recommendations are given:

- For very large areas at the regional scale the best method is the use of terrain classification based on satellite imagery followed by qualitative hazard analysis using relative weight values obtained from brief field visits.
- For modestly large areas at the regional scale it is advisable to use terrain classification based on satellite imagery and interpretation of landslides from aerial photos, followed by a density calculation of landslides per mapping unit.
- At the medium scale, the most useful method consists of the collection of important factors related to mass movement occurrence, followed by reclassification and combination into homogeneous units and calculation of quantitative weight values.
- For geomorphologically homogeneous areas at the large scale the best method is the application of simple slope stability models.
- For geomorphologically heterogeneous terrain at the large scale the use of detailed geomorphological mapping is considered the best solution.

Method	Regional scale	Medium scale	Large scale	Usefulness of GIS in the analysis
Landslide distribution analysis	2-3	3-3	3-3	Intermediate
Landslide density analysis	2-3	3-2	3-1	Intermediate/high
Landslide activity analysis	1-3	3-3	3-3	Intermediate/high
Landslide isopleth analysis	2-3	3-2	3-1	High
Geomorphological landslide hazard analysis	3-3	3-3	3-3	Very low
Qualitative landslide hazard analysis	3-3	3-2	3-1	Low/intermediate
Landslide susceptibility analysis	1-3	3-3	3-2	High
Information value method	1-1	3-3	3-2	High
Weights of evidence method	1-1	3-3	3-2	High
Multivariate statistical analysis	1-2	3-2	3-2	High
Deterministic landslide hazard analysis	1-1	1-2	2-3	High
Antecedent rainfall analysis	2-2	3-3	3-2	Very low

Table 8.1: Summary of the feasibility and usefulness of applying GIS-based techniques for landslide hazard zonation on the three scales under consideration. The first number indicates the feasibility (1 = low: it would take too much time and money to gather sufficient information in relation to the expected output; 2 = moderate: a considerable investment would be needed, which only moderately justifies the output; 3 = good: the necessary input data can be gathered with a reasonable investment related to the expected output). The second number indicates the usefulness (1 = of no use: the method does not result in very useful maps at the particular scale; 2 = of limited use: other techniques would be better, 3 = useful).

The hazard maps resulting from the evaluated methods generally suffer from a number of serious limitations, which should be considered:

- Practically none of these methods will result in hazard maps according to the definition of Varnes (1984), as they do not contain information on the time aspect. Most maps are merely susceptibility maps, displaying the likelihood for landsliding based on the observed density of landslides in areas with a certain combinations of factors. The time aspect can be taken into account in deterministic modelling at the large scale, but this method requires a large number of input factors which are very difficult to obtain.
- The relationship between the hazard map and land-use changes is difficult to assess. Generally one of the factors is the land-use situation for the same time period for which the landslide inventory map is available. The resulting hazard map therefore gives information only for that land-use situation. As soon as important land-use changes take place, such as the construction of a new road, the hazard map becomes outdated. Road construction itself is also a factor in the production of new landslides and should be incorporated into the analysis. The hazard map of an area where no road is planned will look different from the one on which the planned road is taken into account. The same is true for any other land-use change, such as construction of new settlements or changes in crops. Specific landslide hazard maps should therefore be made for each engineering or agricultural project.
- Hazard evaluation for different types of mass movement will require the use of different analysis methods. The occurrence of rapid translational landslides will be controlled by different factors than deep-seated landslides. The resulting hazard maps should be presented separately as they have a different meaning for different land-use

types. The presence of fossil deep-seated landslides will not have a similar importance in the construction of a new road as rapid surficial slides.

- The accuracy of hazard maps is often difficult to assess. The normal procedure is to compare the result with the field situation (i.e., with the landslide inventory map). Since this map was also used as the basis of the analysis, this can be considered a circular argument.

A landslide hazard map should not be an objective in itself. It is necessary input information in a risk evaluation, which should also take into account the vulnerability of the elements at risk (population, infrastructure, economic activities, etc.). Fully worked out examples of landslide risk studies have not yet been presented. At best a general outline is given of the procedure that should be followed. Without considering the problems of the evaluation of landslide vulnerability, which are also considerable, the present limitations of hazard maps make it impossible to come to a reliable quantitative landslide risk map. As hazard maps usually do not contain information on the probability and magnitude of landslides within a given period of time, the resulting risk maps can only be of a qualitative type.

In order to be able to produce a detailed landslide risk map more research should be done on the preparation of real landslide probability maps. The most important focus of the research should be in reducing the uncertainty of the input data, and development of methods which will take the uncertainty into account during the analysis procedure. In order to improve the accuracy of the input data, standardized techniques for data collection should be used and a clear separation should be made in input maps between factual data, derived from the field or the laboratory, and inferred data. In order to obtain more insight into the temporal changes in landslide activity it is of crucial importance that local agencies or universities develop landslide data bases, in which the location, date of occurrence, type, and damage caused by landslides in relation to triggering factors such as rainfall, earthquakes or human activities, are recorded.

GIS will play an increasingly important role in the analysis of landslide hazards. It is an important tool in evaluating the accuracy of the input data. With a good data base structure and standardized methods of data gathering the input maps can be greatly improved during the course of a project by the entry of newly collected data. In this way GIS will not only serve inexperienced earth scientists in the analysis of unknown causal factors of slope instability within a region, but it will also enable experienced professionals to create a detailed data base which can be of use for many more engineering geological applications other than landslide hazard assessment alone. GIS is very important in analyzing the complex combination of factors leading to slope instability. It allows the use of models which were previously available, but which could not be used because of the large amounts of time involved in their application. One of the most promising applications of GIS in landslide hazard assessment could be the further development of detailed slope instability models, in combination with groundwater models, applied over relatively small areas. Provided that it is used in combination with detailed field knowledge GIS will enhance the reliability and objectivity of the hazard maps, which therefore will become increasingly important in the decision-making process.

However, even if very reliable hazard and risk maps are produced, the time and money invested in them will only be worthwhile when they are actually used in the planning process, and not used only by scientists or politicians to impress the public after a catastrophe has occurred. Therefore, emphasis should be given to the practical application of the new knowledge acquired with the use of GIS in landslide hazard zonation.

SAMENVATTING

De zonering van aardverschuivingsgevaar heeft tot doel de onderverdeling van een gebied in zones met gelijke gevoeligheid of waarschijnlijkheid met betrekking tot het voorkomen van massabewegingen. Verschillende methodes hiervoor zijn bekend uit de literatuur. Alle methodes vereisen de combinatie en integratie van een groot aantal gegevens, welke meestal bestaan uit kaarten. De meeste methodes zijn erg tijdrovend, wanneer ze handmatig uitgevoerd moeten worden.

Deze studie evalueert de toepasbaarheid van geografische informatie-systemen (GIS), computersystemen voor het werken met geografische gegevens, in de zonering van aardverschuivingsgevaar. Na een inventarisatie van de bestaande methodes worden deze vergeleken en worden er aanbevelingen gedaan voor het gebruik van specifieke methodes in specifieke situaties. Negen verschillende methodes worden beschreven in hoofdstuk 2: analyse van de verdeling van massabewegingen, analyse van de dichtheid van massabewegingen, analyse van de activiteit van massabewegingen, geomorfologische gevarenanalyse, kwalitatieve gevarenanalyse, univariate statistische analyse, multivariate statistische analyse, deterministische analyse van hellingstabiliteit en analyse van de frequentie van massabewegingen. De mogelijkheden en specifieke eisen met betrekking tot de invoer-gegevens, worden behandeld voor elk van deze methodes. Drie schalen van analyse worden onderscheiden: een regionale schaal (<1:100,000), een middenschaal (1:50,000-1:25,000) en een grote schaal (>1:10,000). Er wordt aangegeven welke methode toepasbaar is op elk van de drie schalen en hoe GIS gebruikt kan worden bij de uitvoering daarvan.

De methodes zijn getest in het Rio Chinchina gebied in de Centrale Cordillera (Colombia), in de omgeving van de stad Manizales. Voor elk van de drie schalen is een studiegebied gekozen en een gegevensbestand verzameld. In hoofdstuk 3 wordt een introductie gegeven over de specifieke aspecten van het studiegebied in relatie tot het voorkomen van massabewegingen, zoals de geologische situatie, het breukpatroon, de seismische activiteit, de aanwezigheid van een bedekking met vulkanische as, de klimatologische situatie, ontbossing, de verbouw van koffie, de aanleg van wegen en de verstedelijking.

Onderwerpen gerelateerd aan de gegevensverzameling voor de bepaling van aardverschuivingsgevaar, gebruikmakend van GIS, worden behandeld in hoofdstuk 4. Voor elk van de drie schalen worden de minimale eisen met betrekking tot de types en volumes van gegevens gepresenteerd. Interpretatie van luchtfoto's en satellietbeelden is de belangrijkste bron van informatie. Deze moet op een gestructureerde manier uitgevoerd worden, gebruik makend van duidelijke besluitcriteria en een foto *checklist*. Nadruk wordt gelegd op het gebruik van multi-temporele luchtfoto-interpretatie om de veranderingen in massabewegingsactiviteit en landgebruik te bepalen. Veldwerktechnieken worden gepresenteerd voor het gebruik van checklists in de beschrijving van massabewegingsverschijnselen en de verzameling van gegevens over bodem en gesteente, waarbij simpele veldtests gebruikt worden.

Het gebruik van geografische informatie systemen vereist een speciale aanpak van de verzameling en invoer van gegevens. Hoofdstuk 5 behandelt de specifieke aspecten van gegevensinvoer en manipulatie voor de bepaling van aardverschuivingsgevaar, gebruikmakend van GIS. De structuur van de geografische databestanden voor de drie verschillende schalen wordt beschreven. Er worden voorbeelden gegeven van de manipulatie van digitale informatie, voorafgaande aan de analyse, met speciale nadruk op de constructie van een ingenieursgeologische kaart en de toepassing van een grondwatermodel voor de grote schaal.

Alle methodes, beschreven in hoofdstuk 2, werden getest met het gegevensbestand van het Rio Chinchina gebied. De resultaten van de analyse en de problemen die ontstonden tijdens de analyse, worden behandeld in hoofdstuk 6. Speciale aandacht is geschonken aan de univariate statistische analyse, omdat dit de meest nuttige methode is om de veldkennis van de aardwetenschapper te combineren met de rekenmogelijkheden van een GIS. Kwalitatieve analytische methodes profiteren in het algemeen niet optimaal van de GIS mogelijkheden en zijn erg afhankelijk van de subjectieve beslissingen van de aardwetenschapper. Wanneer er echter een beperkte hoeveelheid gegevens beschikbaar is, zijn het de enige bruikbare methodes. Deze methodes kunnen resulteren in goede gevarenkaarten, mits deze gemaakt zijn door ervaren geomorfologen. Bij multivariate analyse-technieken treden er problemen op in relatie tot het bemonsteren van variabelen. Deterministische modellen vereisen gedetailleerde invoergegevens, die niet verkregen kunnen worden voor grote gebieden.

Een evaluatie van de verschillende aspecten die leiden tot fouten in de analyse wordt gegeven in hoofdstuk 7. De kaarten die het meest gevoelig zijn voor fouten zijn die welke gebaseerd zijn op subjectieve foto-interpretatie. Fouten in bestaande kaarten en veldwaarnemingen kunnen echter ook aanzienlijk zijn. De nadruk zal in de toekomst gelegd moeten worden op de ontwikkeling van standaardmethodes voor data verzameling en een duidelijke onderscheiding in de invoerkaarten tussen gemeten en geinterpreteerde gegevens.

GIS kan beschouwd worden als een nuttig hulpmiddel bij de bepaling van aardverschuivingsgevaar (hoofdstuk 8). Het biedt veel voordelen voor meer gestructureerde gegevensverwerking en analyse. Bij het gebruik van GIS-systemen wordt men echter geconfronteerd met het grote belang van gedetailleerde, accurate en betrouwbare invoergegevens, die alleen verkregen kunnen worden door middel van gedetailleerd veldwerk.

RESUMEN

El objetivo de una evaluación de amenazas por inestabilidad de pendientes es la subdivisión de un área en zonas con igual susceptibilidad o probabilidad de ocurrencia de movimientos de masa. Muchos métodos diferentes han sido propuestos en la literatura. Estos métodos tienen en común la combinación e integración de una serie de mapas de entrada, lo que es un procedimiento que toma mucho tiempo si se hace manualmente.

Este estudio evalúa la aplicabilidad de los sistemas de información geográfica (SIG), que son sistemas computarizados usados en el manejo de datos geográficos, para el estudio de amenazas por inestabilidad de pendientes. Se hizo un inventario de los métodos corrientemente disponibles, para compararlos y dar recomendaciones de que método específico usarse en situaciones específicas.

En el capítulo 2 se discuten nueve métodos diferentes: análisis de distribución de movimientos de masa, análisis de densidad de movimientos de masa, análisis de actividad de movimientos de masa, análisis de amenaza geomorfológica, análisis cualitativo de amenazas, análisis estadístico univariado, análisis estadístico multivariado, análisis determinístico de inestabilidad de pendientes, y análisis de frecuencia de movimientos de masa. Se tratan los requerimientos específicos de los datos de entrada y las potencialidades de cada uno de estos métodos. Se distinguieron tres escalas de análisis: una escala regional (<1:100,000), una escala media (1:50,000 - 1:25,000) y una escala grande (>1:10,000). Se dan recomendaciones sobre qué método aplicar en cada una de las escalas y como un SIG puede ser incorporado.

Los métodos han sido probados en el área del río Chinchiná en la Cordillera Central de Colombia, cerca de la ciudad de Manizales. Las áreas de estudio fueron seleccionadas para cada una de las tres escalas arriba mencionadas y una serie de datos fueron colectados. El capítulo tres da una introducción de los aspectos específicos del área de estudio relacionados con la ocurrencia de movimientos de masa, tales como situación geológica, modelo de fallamiento y actividad sísmica, presencia de capas de cenizas volcánicas, la situación climática, deforestación, cultivos de café, construcción de carreteras y la urbanización. Se describen también varios ejemplos de fenómenos de movimientos de masa.

En el capítulo 4 se discuten los aspectos relacionados con la colección de datos necesarios para un análisis de amenaza por inestabilidad de pendientes usando un SIG. Se presentan los requerimientos mínimos para tipos y volúmenes de datos, así como también los estándares para la colección de los mismos en cada una de las tres escalas. La interpretación de fotografías aéreas e imágenes de satélite es la fuente principal de información para muchos de los mapas de entrada y deberá llevarse a cabo en una forma bién estructurada, usando criterios claros y listas de chequeo en las fotos. Se da énfasis a la fotointerpretación multitemporal mediante el uso de fotografías aéreas, para evaluar los cambios en la actividad de los movimientos de masa y modelos de uso del suelo. Se desarrollaron técnicas de trabajo de campo las cuales incluyen el uso de listas de chequeo para la descripción de fenómenos de movimientos de masa y la colección de datos de suelo y roca usando también simples pruebas de campo.

El uso de sistemas de información geográfica requiere una especial atención en la colección y al manejo de datos. En el capítulo 5 se tratan los aspectos especiales de entrada y manipulación de datos necesarios para un evaluación de amenazas por inestabilidad de pendientes usando un SIG. Se dan las estructuras de las bases de datos de mapas y atributos para las tres diferentes escalas. Se dan ejemplos de manipulación de datos pre-análisis con especial énfasis en la construcción de un mapa geológico ingenieril y la aplicación de un modelo de agua subterránea a escala grande. En el capítulo 6 todos los métodos de análisis son probados con datos del área del río Chinchiná. Se discuten los resultados de los análisis y se bosquejan los problemas que fueron encontrados. Se da especial énfasis a los análisis eatadísticos univariados y se concluyó que éste es el método más útil para combinar el conocimiento de campo de cada científico con las posibilidades de cálculo del SIG. Generalmente los métodos analíticos cualitativos no benefician totalmente las potencialidades de un SIG y son considerados como muy dependientes del juicio subjetivo del científico. Sin embargo, cuando los limitados datos de entrada están disponibles, éstos son los métodos más recomendables. Ellos pueden resultar en mapas de amenaza de buena calidad si son hechos por geomorfólogos experimentados. Las técnicas de análisis multivariados presentan problemas asociados con el muestreo de parámetros. Los modelos determinísticos requieren datos de entrada muy detallados los que no pueden proveerse cuando se trabaja en áreas grandes.

En el capítulo 7 se da una evaluación de las fuentes de error. Los mayores errores en los mapas provienen de una subjetiva interpretación de imágenes. Sin embargo, todos los errores en los mapas existentes y en las observaciones de campo también pueden ser considerables. En trabajos futuros deberá darse fuerte énfasis en el desarrollo de estándares para la colección de datos, como también una clara diferenciación de los mapas de entrada provenientes de datos reales e inferidos.

En las conclusiones el SIG es considerado como una herramienta útil (capítulo 8). Es sin embargo, una herramienta que, aparte de sus potencialidades para manipulación de datos, actualización y análisis, confronta el usuario con la importancia de tener mapas de entrada detallados, exactos y confiables, y una amplia experiencia de campo.

REFERENCES

Abramovsky, C. (1990)
    Historical urban development of Manizales.
    Unpublished map. Institut Geographique Alpine, Grenoble, France.
Agterberg, F.P., Bonham-Carter, G.F., and Wright, D.F. (1990)
    Stastistical pattern integration for mineral exploration
    in: Proceedings COGEODATA Symposium, Espo, Finland, Gaal, G. (ed).
Aitchison, G.D. and Grant, K. (1967)
    Proposal for the application of the P.U.C.E. programme of terrain classification and evaluation to
    some engineering problems.
    CSIRO Division of Soil Mechanics Research Paper no. 119.
AIS, Associación Colombiana de Ingenieria Sismica (1984)
    Codigo Colombiano de Construcciones Sismo-Resistentes.
    Estudio general del Riesgo Sismica de Colombia, Bogotá.
Akinyede, J.O. (1990)
    Highway cost modelling and route selection using a Getechnical Information System.
    Phd thesis, Technical University of Delft, The Nethrelands, 221 pp.
Alzate, J.B. and Escobar, A.E. (1992)
    Adquisition de datos para un SIG
    Proceedings 1er Simposio International sobre Sensores Remotes y Sistemas de Informacion Geografica
    para el Estudio de Riesgos Naturales, Bogotá, Colombia, 1992, pp. 449-465
Amaya, N.R. (1986)
    Estudio hidrológico de los rios que nacen en el Volcan Nevado del Ruiz y formulación de un modelo de
    simulación matemática sobre el comportamiento hidraulico de los flujos de lodo.
    FAO Report Project, TCP/COL/6651, United Nations Food and Agricultural Organization, Rome, 61 pp and
    appendices.
Anderson, M.G. and Richards, K.S. (eds) (1987)
    Slope stability. Geotechnical engineering and Geomorphology.
    Wiley & Sons, New York, 648 pp.
Angeles, M. de los et al. (1989)
    Relleno hidraulico: "Polideportivo la Sultana" (Manizales)
    Boletin de Vias. Universidad Nacional de Colombia, Seccional Manizales, Vol.XVI, No.68, pp. 13-74.
Anonymous, (1990)
    Geological Society Working Group report: Tropical residual soils.
Arcila, J. and Valencia, G. (1985)
    Danos provocados en cafetales por emanaciones del volcan Nevado del Ruiz.
    Avances technicos, CENICAFE, Chinchina, Colombia, Nr. 127, 4 pp.
Arcila, M. (1990)
    Aspectos geologico-geotecnicos del area de emplazamiento de las obras del aeropuerto de Palestina".
    Unpublished MSc thesis Universidad de Caldas, Manizales, Colombia, 78 p.
Aronoff, S. (1989)
    Geographical Information Systems: a Management Perspective.
    WDL Publications, Ottawa.
Asté, J.P., Gouisset, Y and Leroi, E. (1990)
    The French "INVI" project: national inventory of unstable slopes
    Internal Publication BRGM, Orleans, 6 pp.
ASTM, (1989)
    ASTM: Annual book of ASTM Standards.
    American Society for Testing and Materials.
Baez, E.E., Beltran, L.B. and Gonzalez, G. (1988)
    Inventory of mass movements observed in the Colombian road network during 1986
    Technical report ID-UN-018A.
    Research program on landslides in the Colombian road network
    Ministry of Public Works. Bogotá. 68 pp.
Bargagli, A. (1991)
    Screen digitizing, geometric corrections & monoplotting for SPOT, LANDSAT and normal aerial photographs
    on the ILWIS environment.
    Internal report, ITC, The Netherlands, 29 pp.
Barrero, L.D., Alvarez, A.J. and Kassem, T. (1969)
    Actividad ignea y tectónica en la cordillera Central durante el Meso-cenozoico.
    Boletin Geologico No 17 (1-3), Instituto de Geologia y Minas (INGEOMINAS), pp 145-173.
Barton, N., Lien R., and Lunde J. (1974)
    Engineering Classification of Rock Masses for the Design of Tunnel support.
    Rock Mechanics, Vol. 6, pp.183-236.
Belloni, L. and Morris, D. (1991)
    Earthquake-induced shallow slides in volcanic debris soils.
    Geotechnique 41, No. 4, pp. 539-551.
Bernknopf, R.L., Campbell, R.H., Brookshire, D.S. and Shapiro, C.D. (1988)
    A probabilistic approach to landslide hazard mapping in Cincinatti, Ohio, with applications for economic
    evaluation.
    Bulletin International Association of Engineering Geologists, Vol. 25, No.1, pp. 39-56.
Bertozzi, R., Locatelli, M. and Vianello, G. (1992)
    Model for the correlation between landuse dynamics and hydrogeological risk.
    Proceedings INTERPRAEVENT 1992, Bern, Band 3, pp 131-144.
Bieniawski, Z.T. (1973)
    Engineering classification of jointed rock-masses.
    Transactions of the South African Institute of Civil Engineers 15, pp 335-344.
Bill, R. and Frisch, D. (1991)
    Grundlagen der Geo-Informationssysteme.
    Wichmann, Karlsruhe, Band 1, 414 pp
Blalock, H.M. (1979)
    Social statistics
    Mac Graw Hill, 625 pp.
Bocco, G. (1991)
    Gulley erosion analysis using remote sensing and Geographic Information Systems. A case study in
    Central Mexico.

PhD thesis, University of Amsterdam, 1991, 120 pp.
Bonham-Carter, G.F., Agterberg, F.P., Wright, D.F. (1990)
Weights of evidence modelling: a new approach to mapping mineral potential.
Geological Survey of Canada Paper 8-9. Agterberg, F.P. and Bonham-Carter, G.F. (eds). Ottawa, Canada, pp.171-183.
Brabb, E.E. (1984)
Innovative approaches to landslide hazard and risk mapping.
Proceedings 4th International Symposium on Landslides, Toronto, Canada, Vol. 1, pp 307-324.
Brabb, E.E. (1987)
Analyzing and portraying geologic and cartographic information for land-use planning, emergency response, and decision making in San Mateo county, California.
Proceedings GIS '87- San Fransisco, California, 26-30 October 1987. pp 362-374.
Brabb, E.E., Pampeyan, E.H., and Bonilla, M.G. (1972).
Landslide susceptibility in San Mateo County, California,
US Geological Survey Miscellaneous field Studies Map. MF360, scale 1:62,500.
Brabb, E.E., Guzzetti, F., Mark, R. and Simpson, R.W. (1989)
The extent of landsliding in northern New Mexico and similar semi-arid regions.
In: *Landslides in a semi-arid environment*. Sadler and Morton (eds). Publications of the Inland Geological Society, Vol. 2, pp. 163-173.
Brass, A., Wadge, G. and Reading, A.J. (1989)
Designing a Geographical Information System for the prediction of landsliding potential in the West Indies.
Proceedings *Economic Geology and Geotechnics of Active Tectonic Regions*, University College, London, 3-7 April, 1989, 13 pp.
Brink, A.B., Mabbutt, J.A., Webster, R. and Becket, P.B.T. (1965)
Report on the Working Group on land classification and data storage.
MEXE Report, no. 940
Bromhead, E.N. (1986)
The stability of slopes.
Surrey University Press, Surrey, 373 pp.
Brown, W.M. (1992)
Information for disaster reduction: The National Landslide Information Center, US Geological Survey.
Proceedings 6th International Symposium on Landslides, Christchurch, New Zealand, 1992, Vol. 1, pp 891-892.
Brunsden, D., Doornkamp, J.C., Fookes, P.G., Jones, D.K.C. and Kelly, J.M.H. (1975)
Large scale geomorphological mapping and highway engineering design.
Quart. Journ. Engng Geol., 1975, Vol 8, pp. 227-253.
Burrough, P.A. (1986)
Principles of Geographical Information Systems for Land Resources Assessment.
Clarendon Press, Oxford 194 pp.
Calvache, M.L., (1986)
Depositos piroclasticos asociados a la erupción del 13 de noviembre de 1985 en el Nevado del Ruiz.
Internal report, Instituto de Geologia y Minas (INGEOMINAS), Manizales, Colombia 23p.
Calvache, M.L., (1986)
Estado de los glaciales del volcan Nevado del Ruiz a marzo 9 1986.
Internal report, Instituto de Geologia y Minas (INGEOMINAS), Manizales, Colombia, 12p.
Canutti, P., Frascati, F., Garzonio, C.A. and Rodolfi, G. (1979)
Dinamica Morfologica di un ambiente sogetto a fenomeni franosi e ad intensa attiva' agricola.
C.N.R. Publication no. 142., National Research Council, Firenze, Italy, pp. 81-102.
Canutti, P. et al. (1985)
Stabilita dei versanti nell'area representativa di Montespertoli (Firenze)
S.E.L.C.A. Firenze. 2 mapsheets.
Canutti, P. et al. (1986)
Slope stability mapping in Tuscany, Italy.
In: *International Geomorphology*. Part 1, pp. 231-239, Gardiner, V. (ed).
Wiley & Sons, New York.
Capecchi, F. and Focardi, P. (1988)
Rainfall and landslides: Research into a critical precipitation coefficient in an area of Italy.
Proceedings 5th International Symposium on Landslides, Lausanne, Switzerland, Vol. 2, pp. 1131-1136.
Carrara, A. (1983)
Multivariate models for landslide hazard evaluation
Mathematical Geology, 15, No. 3, pp. 403-427.
Carrara, A. (1988a)
Landslide hazard mapping by statistical methods. A "black box" approach.
Workshop on Natural Disasters in European Meditteranean Countries, Perugia, Italy, pp 205-224.
Carrara, A. (1988b)
Drainage and divide networks derived from high-fidelity Digital Terrain Models.
in: *Quantitative analysis of Mineral and Energy Resources*. C.F.Chung (ed). Reidel Publ. pp 581-597.
Carrara, A. (1992)
Landslide hazard assessment
Proceedings 1er Simposio Internacional sobre Sensores Remotos y Sistemas de Informacion Geografica (SIG) para el estudio de Riesgos Naturales, Bogotá, Colombia, pp. 329-355.
Carrara, A. and Merenda, L. (1974)
Metodologia per un censimento degli eventio franoso in Calabria.
Geologia Applicata e Idrogeologia, Vol. X, pp. 237-255.
Carrara, A., Pugliese Carratelli, E. and Merenda, L. (1977)
Computer-based data bank and statistical analysis of slope instability phenomena.
Zeitschrift für Geomorphologie N.F., Vol.21, No 2, pp. 187-222.
Carrara, A., Cardinali, M. and Guzzetti, F. (1992)
Uncertainty in assessing landslide hazard and risk
ITC-Journal 1992-2, pp. 172-183.
Carrara, A., Catalano, E., Sorriso Valvo, M., Reali, C. and Osso, I. (1978)
Digital terrain analysis for land evaluation.
Geologia Applicata e Idrogeologia, Vol. XIII, pp. 69-127.
Carrara, A., Cardinali, M., Detti, R., Guzzetti, F., Pasqui, V. and Reichenbach, P. (1990)
Geographical Information Systems and multivariate models in landslide hazard evaluation.
ALPS 90 Alpine Landslide Practical Seminar. 6th International Conference and Field Workshop on Landslides. Aug. 31-Sept.12, 1990, Milano, Italy. pp. 17-28.

Carrara, A., Cardinali, M., Detti, R., Guzzetti, F., Pasqui, V. and Reichenbach, P. (1991)
GIS techniques and statistical models in evaluating landslide hazard.
Earth Surface Processes and Landforms, Vol. 16, No. 5, pp. 427-445.
CENICAFE (1990)
Meteorological data of various stations in the Rio Chinchina catchment.
Unpublished reports, Centro Nacional de Investigación de Café, Chinchina, Colombia.
Chacon, F.B. and Orozco, M. (1989)
Aportes al conocimiento de las factores geologicos que inciden en los deslizamientos de Manizales.
Unpublished MSc thesis, Universidad de Caldas, Manizales, Colombia, 139 pp.
Chaplow, R. (1986)
Production of Borehole logs using a micro-computer.
Quarterly Journal of Engineering Geology, London, Vol. 19, pp. 291-299.
CHEC (1985)
Evaluacion de los recursos geotérmicos del area San Vicente- Manizales- Tolima. Geologia regional.
Unpublished report and map. Centro Hidroelectrico de Caldas, Manizales, Colombia, 112 pp.
CHEC (1990)
Meteorological data of various stations in the Rio Chinchina catchment.
Unpublished reports, Centro Hidroelectrico de Caldas, Manizales, Colombia.
Choubey, V.D. and Litoria, P.K. (1990)
Terrain classification and land hazard mapping in Kalsi-Chakrata area (Garhwal Himalaya), India.
ITC-Journal 1990-1, pp. 58-66.
Choubey, V.D., Chaudhari, S. and Litoria, P.K. (1991)
Landslide hazard zonation in Uttarkashi and Tehri districts, U.P. Himalaya.
Proceedings 6th International Symposium on Landslides, Christchurch, New Zealand, Vol 2, pp. 911-917.
Chowdury, R.N. (1978)
Slope analysis.
Developments in geotechnical engineering, vol 22.
Elsevier, Amsterdam, 423 pp.
Chowdury, R.N. (1984)
Recent developments in landslide studies: probabilistic models.
Proceedings 4th International Symposium on Landslides, Toronto, Canada, Vol.1, pp. 209-220.
Coates, D.R. (1977)
Landslide perspectives.
In: *Landslides*. D.R. Coates (ed). Geological Society of America, pp. 3-28.
Cooke, R.U. and Doornkamp, J.C. (1990)
Geomorphology in environmental management.
Oxford University Press, Oxford, England, 410 pp.
Corominas, J., Baeza, C. and Saluena, I. (1992)
The influence of geometrical slope characteristics and land use on the development of shallow landslides.
Proceedings 6th International Symposium on Landslides, Christchurch, New Zealand, 1992, Vol. 2, pp 919-924
Cortez, R. (1988)
Inventory of mass movements observed in the Colombian road network during 1986
Research program on landslides in the Colombian road network
Unpublished report, Ministry of Public Works. Bogotá. 79 pp.
Cotecchia, V. (1978)
Systematic reconnaissance mapping and registration of slope movements.
Bulletin International Association of Engineering Geologists, No. 17, pp 5-37.
CRAMSA (1990)
Unpublished geotechnial reports of the following sites: Barrio Velez, Barrio Estrada, La Floresta, Peralonzo, Villa Julia, Palogrande, Liceo Isabel la Catolica, Balcones de Chipre.
Corporacion Regional Autonoma de Manizales, Salamina y Aranzazu. Approx. 500 pp.
Crozier, M.J. (1973)
Techniques for the morphometric analysis of landslips.
Zeitschrift für Geomorphologie Vol. 17, No.1, pp. 78-101
Crozier, M. J. (1984)
Field assessment of slope instability
In: *Slope stability*. D. Brunsden & D.B. Prior (ed). Wiley & sons, New York, pp 103-142.
Crozier, M.J. (1986)
Landslides: causes, consequences & environment
Croom Helm, London, England, 245 pp.
Cruden, D. and Brown III, W.M. (1992)
Progress towards the World Landslide Inventory
Proceedings 6th International Symposium on Landslides, Christchurch, New Zealand, Vol.1, pp 59-64.
Dackombe, R.V. and Gardiner, V. (1983)
Geomorphological Field Manual.
Allen & Unwin, London, 248 pp.
Date, C.J. (1986)
An introduction to database systems, Volume I.
Addison-Wesley Publ. Comp., Reading, Massachusets, 250 pp.
Davenport, A.J. 1972
A statistical relation between shock amplitude, magnitude and epicentre distance and its application to seismic zoning.
West Ontario University, Engineering Sci. Res. Report, BLWT-4-72, 19 pp.
Davis, J.C. (1986)
Statistics and data analysis in geology.
Wiley & Sons, New York, 546 pp.
Dearman, W.R. (1976)
Weathering classification in the characterisation of rock: a revision.
Bulletin International Association of Engineering Geologists 13, pp 123-127.
Deere, D.U. and Deere, D.W. (1988)
The RQD Index in practice.
Proceedings Symposium on Rock Classification for Engineering Purposes. Philadephia, 1988.
ASTM Special Technical Publication 984, American Society for Testing Materials, pp. 91-101.
Demek, J. and C. Embleton (eds) (1978)
Guide to medium-scale geomorphological mapping
IGU Commission on Geomorphological Survey and Mapping

E. Schweizerbart'sche Verlagsbuchhandlung, Stuttgart, Germany, 348 pp.

Donovan, N.C. (1973)
A statistical evaluation of strong motion data including the February 9, 1971 San Fernando earthquake.
Proceedings 5th World Conference on Earthquake Engineering, Rome, Italy, Vol. 2, paper 155, 10 pp.

Echavarria, J.I., Hoyos, J.M., Lopez, M.C. and Peña, L.H. (1991)
Geologia del la cuenca del Rio Chinchina, Sector Manizales-Chinchina.
Unpublished MSc thesis, Universidad de Caldas, Manizales, Colombia, 190 pp.

Einstein, H.H (1988)
Special lecture: Landslide risk assessment procedure
Proceedings 5th International Symposium on Landslides, Lausanne, Switzerland, 1988, Vol.2, pp. 1075-1090.

Elbersen, G.W.W. and Catalan, R. (1986)
The use of portable computers in physiographic soil surveys
Proceedings XIII Congres International Society of Soil Scientists, Hamburg, Germany, 1986, Vol.III, pp. 1102-1103.

Enzico, D. 1989
Mapa preliminar de riesgos naturales en Manizales.
Unpublished map, Alcaldia, Manizales, Colombia.

Essa Nuru Alemu (1992)
GIS in rock slope stability analysis
Unpublished MSc thesis, ITC, Delft, The Netherlands, 62 pp.

Estudios y Asesorias (1986)
Aspectos hidraulicos de los flujos de lodo y agua en el area de influencia del Volcan Nevado del Ruiz.
Preliminary report to RESURGIR, Bogota, Colombia, 30 pp.

Federación Nacional de Cafeteros de Colombia (1985)
Mapas de uso del suelo para los municipios de Palestina, Chinchina y Manizales.
1:10.000 scale landuse maps, with legend.

Federación Nacional de Cafeteros de Colombia (1982)
Estudio de zonificacion y uso potencial del suelo en la zona cafetera del Departamento de Caldas.
Federación Nacional de Cafeteros de Colombia, Bogota, Colombia, 220 pp.

Florez, A. (1986)
Geomorfologia del area de Manizales-Chinchina, Cordillera Central de Colombia.
Analisis Geograficos Nr 9, Instituto Geografico Agustin Codazzi, Bogota, Colombia, 158 pp.

Fookes, P.G., Dearman, W.R. and Franklin, J.A. (1971)
Some engineering aspects of rock weathering with field examples from Dartmoor and elsewhere.
Quarterly Journal of Engineering Geology, 4, pp. 139-185.

Fookes, P.G., Dale, S.G. and Land, J.M. (1991)
Some observations on a comparitive aerial photography interpretation of a landslipped area.
Quarterly Journal of Engineering Geology, 24, pp. 249-265

Fournier D'Albe, E.M. (1976)
Natural disasters.
Bulletin International Association of Engineering Geologists, Vol. 14., p. 187.

Gagon, H. (1975)
Remote sensing of landslide hazards on quick clays of Eastern Canada.
Proceedings 10th International Symposium on remote sensing of environment. ERIM, Ann Arbor, Michigan, pp 803-810.

Galvis, J.R., Giraldo, H.G.G. and Jaramillo, J.O. (1980)
Sismo del 23 de Noviembre de 1979 en Manizales. Effectos estructurales.
Internal report, CRAMSA, Manizales, 12 pp.

Gardner, T.W., Conners Sasowski, K. and Day, R.L. (1990)
Automatic extraction of geomorphometric properties from digitial elevation data.
Zeitschrift für Geomorphologie N.F. Suppl. Band 60. pp 57-68.

Gee, M.D. (1992)
Classification of landslide hazard zonation methods and a test of predictive capability.
Proceedings 6th International Symposium on Landslides, Christchurch, New Zealand, Vol 2, pp 947-952.

Geotecnia LTDA (1980)
Investigacion geotecnica postsismica del sector de la avenida Santander entre la Calles 47 y 48
Unpublished report for the Corporacion Regional Autonoma de Manizales, Salamina y Aranzazu (CRAMSA), Manizales, Colombia, 30 pp.

Gilewska, S. (1976)
Different methods of showing the relief on detailed geomorphological maps.
Zeitschrift für Geomorphologie, 11 (4), pp. 481-490.

Gomez, J.R.Y. (1943)
El territorio de Manizales y la estabilidad de su suelo
Revista de la Academia Colombiana de Sciencias Exactas, Fisicas y Naturales. Vol. V, No. 19, pp 337-343.

Gonzalez, A.J. (1992)
Avalanche risk evaluation at Utica (Colombia)
Proceedings 1er Simposio Internacional sobre Sensores Remotos y Sistemas de Informacion Geografica (SIG) para el estudio de Riesgos Naturales, Bogotá, Colombia, pp.356-378.

Graham, J. (1984)
Methods of stability analysis.
In: Slope Instability. D. Brunsden and D.B. Prior (eds), Wiley & Sons, New York, pp. 171-215.

Grunder, M. (1980)
Beispiel einer anwendungsorientierten Gefahrenkartierung 1:25.000 für forstliche Sanierungsprojeckte im Berner Oberland (Schweiz)
Proceedings INTERPRAEVENT 1980, Bad Ischl, Austria, Band 4, pp. 353-360.

Hammond, C.J., Prellwitz, R.W. and Miller, S.M. (1992)
Landslide hazard assessment using Monte Carlo simulation
Proceedings 6th International Symposium on Landslides, Christchurch, New Zealand, Vol 2, pp 959-964.

Handszer, A.P. and Grand, M.M. (1989)
Naturaleza y dinamica de un flujo piroclastico en la zona de Nereidas. Departamento de Caldas (Colombia).
Proceedings 5th Colombian Geological Congress, Bucaramanga, 14-17 March, 1989. Vol. 1 pp.473-483.

Hansen, A. (1984)
Landslide Hazard Analysis. In: Slope Instability.
In: Slope Instability. D. Brunsden and D.B. Prior (eds), Wiley & Sons, New York, pp. 523-602.

Hansen, M.J. (1984)
Strategies for classification of landslides
In: Slope Instability. D. Brunsden and D.B. Prior (eds), Wiley & Sons, New York, pp. 1-25.

Hartlén, J. and Viberg, L. (1988)
General report: Evaluation of landslide hazard
Proceedings 5th International Symposium on Landslides, Lausanne, Switzerland, Vol. 2, pp. 1037-1057.

Hays, W.N. (1980)
Procedures for estimating earthquake ground motions.
U.S. Geological Survey Professional paper 1114, 77 pp.

Hearn, G.J. (1992)
Terrain hazard mapping at Ok Tedi mine, Papua New Guinea.
Proceedings 6th International Symposium on Landslides, Christchurch, New Zealand, Vol 2, pp 971-976.

Herd, D.G., (1974)
Glacial and volcanic geology of the Ruiz Tolima volcanic complex, Cordillera central, Colombia.
PhD dissertation, University of Washington, 77 pp.

Hermelin, M. (1990)
Bases fisicas para los planes de desarollo de los municipios de Risaralda.
AGID report nr. 13. Environmental geology and natural hazards of the andean region. p. 269-274.

Hermelin, M. (1992)
Medio ambiente, planes de desarollo y toma de decisiones.
Proceedings 1er Simposio Internacional sobre Sensores Remotos y Sistemas de Informacion Geografica (SIG) para el estudio de Riesgos Naturales, Bogotá, Colombia, pp. 646-663.

HIMAT (1990)
Meteorological data of various stations in the rio Chinchina catchment.
Unpublished reports, HIMAT, Bogotá, Colombia.

Hoek, E. and Bray, J.W. (1981)
Rockslope engineering.
Institute of Mining and Metallurgy, London, 358 pp.

Howe, D.R. (1982)
Data analysis for Data Base Design.
Edward Arnold, London, 301 pp.

Huang, S.L and Chen, B.K. (1991)
Integration of Landsat and terrain information for landslide study
Proceedings 8th Thematic Conference on Geological Remote Sensing (ERIM), Denver, Colorado, USA, Vol. 2, pp 743-754.

Huma, I. and Radulescu (1978)
Automatic production of thematic maps of slope instability.
Bulletin International Association of Engineering Geologists, No 17, pp. 95-99.

Hutchinson, J.N. (1988)
Morphological and geotechnical parameters of landslides in relation to geology and hydrogeology.
Proceedings 5th International Symposium on Landslides, Lausanne, Switzerland, vol. 1, pp 3-35.

IAEG, (1976)
Engineering geological maps. A guide to their preparation.
International Association of Engineering Geologists. The UNESCO press, Paris. 79 pp.

IGAC (1949)
Topographical map sheets 1 to 13 at a scale of 1:2.000 for Manizales
Instituto Geografico Agustin Codazzi, Bogotá, Colombia.

IGAC (1967)
Topographical map sheets 205-IV-A, 205-IV-C, 206-III-B and 206-III-D.
Instituto Geografico Agustin Codazzi, Bogotá, Colombia.

IGAC (1974)
Topographical map sheets 205, 206, 225 and 226 at 1:100.000 scale.
Instituto Geografico Agustin Codazzi, Bogotá, Colombia.

IGAC (1979)
Mapa de estudio general de suelos de los municipios de Manizales, Aranzazu, Neira, Palestina, Salamina, La Merced y Villamaria.Escala 1:100.000.
Instituto Geografico Agustin Codazzi, Bogotá, Colombia.

IGAC (1985)
Cartografia integrada del medio natural Chinchina-Manizales.
Analisis Geograficos no 8, Bogotá, 132p.

IGAC (1986)
Cartografia integrada de los medios naturales de la Cordillera central Colombiana. Plancha 225- El Ruiz
Analisis Geograficos no. 5, Bogotá, 92 pp.

IGAC (1987)
Topographical map sheets 1 to 3 at a scale of 1:5.000 for Chinchina.
Instituto Geografico Agustin Codazzi, Bogotá, Colombia.

IGAC, (1988)
Estudio geomorfologico, erosion, suelos y uso de la tierra en los municipios de Chinchina, Villamaria, Palestina, Neira, Filadelfia, Pacora y Aguadas, Caldas".
Report for CRAMSA, Manizales, Colombia

IGAC (1989)
Topographical map sheets 1,2,3,4,4a,5,6,7,8,9,10,11,12,13,14,14,15,16,17,18,19,20,21,22,23,24,25,26,27,28, 29,30,31,32 and 33 at a scale of 1:2.000 for Manizales
Instituto Geografico Agustin Codazzi, Bogotá, Colombia.

IGAC (1990)
Topographical map 1:10.000 of Manizales
Instituto Geografico Agustin Codazzi, Bogotá, Colombia.

INGEOMINAS (1985)
Mapa de riesgos volcanicos potenciales del Nevado del Ruiz
Instituto de Geologiá y Minas, Instituto de Geologia y Minas (INGEOMINAS), Bogotá, Colombia, 27 pp. + 1 map

INGEOMINAS (1987)
Mapas geologicos a escala 1:25.000
Instituto de Geologiá y Minas, Instituto de Geologia y Minas (INGEOMINAS), Bogotá, Colombia, 6 maps.

Ingeosuelos (1991)
Estudio de suelos de la hacienda la Esmeralda. Relleno sanitario para Manizales. Diseno.
Report for: Empresas Publicas de Manizales, Colombia, 74 pp.

Innocienti, L. (1992)
Data integration for landslide risk mapping in urban areas using GIS.
Unpublished MSc thesis, ITC, Enschede, The Netherlands, 88 pp.

Irmay, S. (1954)

On the hydraulic conductivity of unsaturated soils.
Trans. Amererican Geophysical Union 35, pp 463-468.

Irving, E.M. (1971)
La evolucion estructural de los Andes mas septrentionales de Colombia.
Boletin Geologico, No. 19 (2). Instituto de Geologia y Minas (INGEOMINAS), 90 pp.

ITC (1992)
ILWIS 1.3 User's manual.
International Institute for Aerospace Survey and Earth Sciences (ITC), Enschede, The Netherlands.

Ives, J.D. and Messerli, B. (1981)
Mountain hazards mapping in Nepal. Introduction to an applied Mountain Research project.
Mountain Research and Development, Vol. 1, No. 3-4, 1981, pp. 223-230.

James, M.E. (1986)
Estudio sismotectonico en el area del viejo Caldas.
Internal report nr. 2008, Instituto de Geologia y Minas (INGEOMINAS), Medellin, Colombia, 113 pp.

Kasa, H., Kurodai, M., Kojima, H. and Obayashi, S. (1992)
Study on landslide prediction model using satellite remote sensing data and geographical information.
Proc. 8th Thematic Conf. on Geological Remote Sensing, Denver, Colorado, USA, Vol. 2, pp 983-988.

Keefer, K. et al. (1987)
Real-Time Landslide Warning During Heavy Rainfall.
Science 238, pp. 921-925.

Kessler, J. and Oosterbaan, R. (1974)
Determining hydraulic conductivity of soils.
In: Drainage principles and applications. Publication 16, III, International Institute for Land Reclamation and Improvement, Wageningen, pp. 253-296.

Kienholz, H. (1977)
Kombinierte Geomorphologische Gefahrenkarte 1:10.000 von Grindelwald.
Geographica Bernensia G4, Geographisches Institut Universität, Bern, Switzerland.

Kienholz, H. (1978)
Maps of geomorphology and natural hazards of Grindelwald, Switzerland, scale 1:10.000.
Arctic and Alpine Research 10, pp. 169-184.

Kienholz, H. (1980)
Zur Anwendung des Luftbildes bei der mittelmässtaäbigen Gefahrenkartierung für regionalplanerische Zwecke in schlecht erschlossenen Gebirgsräumen anhand von Erfahrungen aus Kartierungen in den Colorado Rocky Mountains.
Proceedings INTERPRAEVENT 1980, Bad Ischl, Austria, Band 3, pp. 155-172.

Kienholz, H. (1984)
Hangstabilitäts- und Gefahrenbeurteilung im nepalischen Mittelgebirge
Proceedings INTERPRAEVENT 1984, Villach, Austria, Bands 2, pp 331-342.

Kienholz, H. (1992)
Risk assessment in mountains.
Proceedings 1er Simposio Internacional sobre Sensores Remotos y Sistemas de Informacion Geografica (SIG) para el estudio de Riesgos Naturales, Bogotá, Colombia, Vol.2., 20 pp.

Kienholz, H., Bichsel, M., Grunder, M. and Mool, P. (1983)
Kathmandu-Kakani area, Nepal: Mountain Hazards and Slope Stability Map.
United Nations University, Mountain Hazards Mapping Project: Map No 4. Scale 1:10.000.

Kienholz, H., Mani, P. and Kläy, M. (1988)
Rigi Nordlene. Beurteilung der Naturgefahren und Waldbauliche Prioritätenfestlegung.
Proceedings INTERPREAVENT 1988, Graz, Austria, Band 1, pp 161-174.

Kingsbury, P.A., Hastie, W.J. and Harrington, A.J. (1992)
Regional landslip hazard assessment using a Geographical Information System.
Proceedings 6th International Symposium on Landslides, Christchurch, New Zealand, Vol 2, pp. 995-999.

Klimazewski, M. (1982)
Detailed geomorphological maps
ITC-Journal 1982-3, pp. 265-272

Kobashi, S. and Suzuki, M. (1988)
Hazard Index for the judgement of slope stability in the rokko mountain region.
Proceedings INTERPRAEVENT 1988, Graz, Austria, Band 1, pp. 223-233.

Koirala, A. (1992)
Mass movement susceptibility of the area East of Manizales. Cordillera Central, Colombia.
Unpublished MSc thesis, ITC, Enschede, The Netherlands, 82 pp.

Koopmanschap, E. (1992)
A report from a practice at the ITC in Manizales, Colombia.
Unpublished report, ITC, Enschede, The Netherlands, 32 pp.

Kooter, B.M. (1988)
The EGIS project, Design and Partial Implementation of a Engineering Geological Information System.
Memoirs of the centre of Engineering Geology in the Netherlands, No. 53.
TU-Delft, Faculty of Mining and Petroleum Engineering, Delft, The Netherlands, 80 pp.

Kuiper, B. (1990)
CASA, a backanalysis program using circular methods.
Computer program. Department of geography, University of Utrecht, Utrecht, The Netherlands.

Lambe, T.W. and Whitman, R.V. (1969)
Soil mechanics
Wiley & Sons, New York, 553 pp.

La Rotta, E. (1991)
Evaluation of a deterministic hydrological model (HEC-1) in an Andean environment with scarce data. The case of Chinchine-Rio Claro.
Unpublished MSc thesis, ITC, Enschede, The Netherlands, 137 pp.

Lessing, P., Messina, C.P. and Fonner, R.F. (1983)
Landslide risk assessment.
Environmental geology, Vol. 5, No.2, pp. 92-99.

Lopez, H.J. and Zinck, J.A. (1991)
GIS-assisted modelling of soil-induced mass movement hazards: A case study of the upper Coello river basin, Tolima, Colombia.
ITC-Journal 1991-4, pp 202-220.

Lozano, E. (1989)
An ILWIS application in departemente of Caldas, Chinchina watershed Pava west and Pava east subwatersheds, Caldas, Colombia.
Unpublished MSc thesis, ITC, Enschede, The Netherlands, 53 pp.

Mählmann, E. (1991)
The SLOPE10 program for conversion of pantometer measurements to profile data.
Computer program. Department of geography, University of Utrecht, Utrecht, The Netherlands.

Malgot, J. and Mahr, T. (1979)
Engineering geological mapping of the West Carpathian landslide areas.
Bulletin International Association of Engineering Geologists, 19, pp 116-121.

Mani, P. and Gerber, B. (1992)
Geographische Informationssysteme in der Anlyse von Naturgefahren.
Proceedings INTERPRAEVENT 1992, Bern, Switzerland, Band 3, pp 97-108.

McDonald, H.C. and Grubbs, R.C. (1975)
Landsat imagery analysis: an aid for predicting landslide prone areas for highway construction.
NASA Earth Resource Survey Symposium, Houston, Texas, Vol. 1-b, pp 769-778.

McKean, J., Buechel, S. and Gaydos, L. (1991)
Remote sensing and landslide hazard assessment
Proceedings 8th Thematic Conference on Geological Remote Sensing (ERIM), Denver, Colorado, USA, Vol. 2, pp 729-742.

McMillan, A.A., Browne, M.A.E. and Robson, P.G. (1987)
The BGS Scottish Land Survey Borehole Computer Database- Practice and Use
British Geologist 10/4, p. 120.

Medvedev 1965
Engineering sismology.
National Technical Information Service (NTIS) (TT 65- 50011), 260 pp.

Meijerink, A. (1988)
Data acquisition and data capture through terrain mapping units.
ITC-Journal 1988-1, pp 23-44.

Mejia, G., Kohnke, H. and White, J.L. (1968)
Clay mineralogy of certain soils of Colombia
Soil Science Society America Proceedings, Vol. 32, no 5, pp 665-670.

Mendivelso, L.D., Aguilar, T.G.M., Robertson, K.G. and Nossin, J.J. (1992)
Sensores remotos aplicados al diagnostico y evaluacion de amenazas naturales en el piedemonte Llanero, Sector de Villavicencio, Meta, Colombia.
Proceedings 1er Simposio Internacional sobre Sensores Remotos y Sistemas de Informacion Geografica (SIG) para el estudio de Riesgos Naturales, Bogotá, Colombia, pp.78-98.

Middelkoop, H. (1990)
Uncertainty in a GIS: a test for quantifying interpretation output
ITC-Journal 1990-3, pp. 225-232.

Milne, W.G. and Davenport, A.G. (1965)
Earthquake probability.
Proceedings 4th World Conference on Earthquake Engineering, Santiago, Chile.

Mitchell, C.W. (1973)
Terrain Evaluation
Longman, London, 221 pp.

Mojica, J., Colenares, F., Villaroel, C., Macia, C. and Moreno, M. (1985)
Characteristicas del flujo de lodo occurido el 13 de Noviembre de 1985 en el valle de Armero (Tolima, Colombia). Historio y comentarios de los flujos de 1595 y 1845.
Geologia Colombiana, Universidad Nacional de Colombia, No 14, Separata especial, pp. 107-140.

Mool, P. (1992)
Mass movement susceptibility analysis at the medium scale using a GIS system (ILWIS) applied to an area East of Manizales (Colombia)
Unpublished MSc thesis, ITC, Enschede, The Netherlands, 140 pp.

MOPT-UN (1990)
Soil reports Estampilla and Estampillita, Manizales, Colombia. Research program on landslides in the Colombian road network.
Ministry of Public Works. Bogotá. 68 pp.

Mora, S.C. and Vahrson, W.G. (1992)
Determinacion "A priori" de la amenaza de deslizamientos utilizando indicadores morfodinamicos.
Proceedings 1er Simposio Internacional sobre Sensores Remotos y Sistemas de Informacion Geografica (SIG) para el estudio de Riesgos Naturales, Bogotá, Colombia, pp. 259-273.

Mosquera, D. (1978)
Geologia del cuadrangulo K-8.
Preliminar report. Instituto de Geologia y Minas (INGEOMINAS), Ibagué, Colombia, 63 pp.

Mulder, H.F.H.M. (1991)
Assessment of landslide hazard.
Nederlandse Geografische Studies. PhD thesis University of Utrecht. 150p.

Mulder, H.F.H.M. and Van Asch, T.W.J. (1987)
Quantitative approaches in landslide hazard zonation. In:
Geomorphologie et risques naturels, Travaux de l'Institute de Geografie de Reims, No. 69-72, pp 43-53.

Mulder, H.F.H.M. and Asch, T.W.J. van (1988)
A stochastical approach to landslide hazard determination in a forested area
Proceeding 5th International Symposium on Landslides, Lausanne, Switzerland, Vol. 2., pp.1207-1210

Muñoz, F.C. and Nieto, A.E. (1988)
Localizacion y estadistica de los eventos sismicos de alta y baja frequencias occurrida en el volcan Nevado del Ruiz de julio 20 1986 a Noviembre 15 de 1986.
In: International Workshop: A Model of Nevado del Ruiz Volcano. Williams. S.N. and Meyer, H. (eds) Manizales, Colombia, 28 March-1 April, 1988.28 pp.

Muñoz, F.C. and Nieto, A.E. (1989)
Fuentes de sismos de alta frequencia en el volcan Nevado del Ruiz, Colombia.
Proceedings 5th Colombian Geological Congress, Bucaramanga, 14-17 March, 1989. vol. 1 pp. 396-418.

Murphy, J.R. and O'Brien, L.J. (1977)
Analysis of a worldwide strong motion data sample to develop an improved correlation between peak acceleration, seismic intensity, and other physical parameters.
Computer Sciences Corporation, Report NUREG-0402 to the U.S. Nuclear Regulatory Commission. 68 pp.

Murphy, W. and Vita-Finzi, C. (1991)
Landslides and seismicity: an application of remote sensing
Proceedings 8th Thematic Conference on Geological Remote Sensing (ERIM), Denver, Colorado, USA, Vol. 2, pp 771-784.

Naranjo, J.L., Rojas, R. and Borrero, C.A. (1986)
Velocidad, descarga maxima y volumen del lahar del Rio Chinchina, Nov. 13/85

Revista CIAF, Vol. 11 nr 1-3, Bogotá, Colombia, pp 77-84.
Naranjo, J.L. and Rios, P.A. (1989)
    Geologia de Manizales y sus alrededores y su influencia en los riesgos geologicos.
    Revista Universidad de Caldas, Vol. 10 Nos. 1-3, 113 pp. Universidad de Caldas, Manizales, Colombia.
Navarro, E. James, M. and Arias, J. (1988)
    Evaluacion amenazas geologicas area Manizales-Valparaiso
    Internal report Instituto de Geologia y Minas (INGEOMINAS) for Interconexion Electria S.A., Medellin, 143p. + 6 maps.
Nemcok, A., Pasek, J. and Rybar, J. (1972)
    Classification of landslides and other mass movements.
    Rock mechanics 4, pp 71-78.
Neuland, H. (1976)
    A prediction model for landslips.
    Catena, 3, pp. 215-230.
Newman, E.B., Paradis, A.R. and Brabb, E.E. (1978)
    Feasibility and cost of using a computer to prepare landslide susceptibility maps of the San Fransico Bay Region, California.
    US Geological Survey Bulletin 1443, 29 pp.
Niehaus, D.J. (1992)
    Slope instability hazard assessment for natural disaster reduction, an approach using remote sensing analysis and Geographic Information Systems: a case study in the Central Cordillera of Colombia.
    Unpublished MSc thesis, ITC, Enschede, The Netherlands, 143 pp.
Niemann, K.O. and Howes, D.E. (1991)
    Applicability of digital terrain models for slope stability assessment.
    ITC-Journal 1991-3, pp. 127-137.
Okimura, T. and Kawatani, T. (1986)
    Mapping of the potential surface-failure sites on granite mountain slopes
    In: International Geomorphology. Gardiner (ed). Part 1, John Wiley & Sons, pp.121-138.
ORACLE (1988)
    Interactive application facility reference manual.
    ORACLE Data Base Management System, ORACLE Company. USA.
Osejo, J.M. (1992)
    Los sensores remotos en el inventario de amenazas naturales. (Aplicacion en la cuenca del Rio Rimac-Peru).
    Proceedings 1er Simposio Internacional sobre Sensores Remotos y Sistemas de Informacion Geografica (SIG) para el estudio de Riesgos Naturales, Bogotá, Colombia, pp. 128-144.
Othman, M.A., Hassan, N.R.N. and Aziz, H.M.A. (1992)
    A statistical approach to cut slope instability problems in Peninsular Malaysia.
    Proceedings 6th International Symposium on Landslides, Christchurch, New Zealand, Vol 2, pp 1379-1385.
Page, W. (ed) (1986)
    Geologia sismica y sismicidad del noroeste de Colombia ·
    Interconexion Electrica S.A., Medellin, 277p.
Palacios, A. (1991)
    Multiple purpose land evaluation in the Colombian coffee zone using GIS. Case study of the Caldas area.
    Unpublished MSc thesis. ITC, Enschede, The Netherlands, 114 p.
Parra, Cepeda and Thouret (1986)
    Mapa actualizada de amenaza volcanica potencial del Nevado del Ruiz
    Instituto de Geologia y Minas (INGEOMINAS), Manizales, Colombia 14 p.
Pearson, E., Wadge, G. and Wislocki, A.P. (1991)
    An integrated expert system/GIS approach to modelling and mapping natural hazards.
    Proceedings European conference on GIS (EGIS), session 26, pp. 763-771.
Penquet, D.J. and Marble, D.F. (1990)
    Introductory readings in GIS
    Taylor & Francis, London. 371 p.
Peralta, E.B. (1992)
    La aplicacion del Sistema de Analisis Geoambiental (SAGA) en la determinacion de riesgo de deslizamientos. El caso de Itaocara, Brasil.
    Proceedings 1er Simposio Internacional sobre Sensores Remotos y Sistemas de Informacion Geografica (SIG) para el estudio de Riesgos Naturales, Bogotá, Colombia, pp. 240-258.
Perrot, A. (1988)
    Cartographie des risques de glissement en Lorraine.
    Proceedings 5th Internation Symposium on Landslides, Lausanne, Switzerland, Vol. 2, pp 1217-1222.
Radbruch-Hall, D.H., Edwards, K. and Batson, R.M. (1979)
    Experimental engineering geological maps of the conterminous United States prepared using computer techniques.
    Bulletin International Association of Engineering Geologists, No. 19, pp. 358-363.
Ramirez, (1975)
    Historia de los terremotos en Colombia.
    Instituto Geografico Agustin Codazzi, Bogotá, Colombia, 250 p.
Raper, J.F. and Wainwright, D.E. (1987)
    The use of the geotechnical database "Geoshare" for site investigation data management.
    Quarterly Journal Engineering Geology, London, Vol. 20, pp. 221-230.
Reading, A. J. (1991)
    Stability of tropical residual soils from Dominica, West Indies.
    Engineering Geology 31, pp. 27-44.
Rengers, N. (1992)
    UNESCO-ITC project on mountain hazard analysis using GIS.
    Proceedings 1er Simposio Internacional sobre Sensores Remotos y Sistemas de Informacion Geografica (SIG) para el estudio de Riesgos Naturales, Bogotá, Colombia.
Rengers, N. and Soeters, R. (1980)
    Regional geological mapping from aerial photographs
    Bulletin International Association of Engineering Geologists, No. 21, pp 103-111.
Rengers, N., Soeters, R., Van Riet, P.A.L.M. and Vlasblom, E. (1990)
    Large-scale engineering geological mapping in the Spanish Pyrenees.
    Proceedings 6th Congress of the International Association of Engineering Geologists, Amsterdam, 1990, pp 235-243.
Rengers, N., Soeters, R. and Westen, C.J. Van (1992)
    Remote sensing and GIS applied to mountain hazard mapping.

Episodes, Vol.15, No.1, March 1992, pp.36-45.
Rhind, D. and Mounsey H. (1990)
    Understanding GIS.
    London, Taylor and Francis, 240 pp.
Rib, H.T. and Liang, T. (1978)
    Recognition and identification.
    In: Landslides and engineering practice. E.B. Eckel (ed). Special report no. 29., Highway Research Board, pp 34-80.
Rijtema, P.E. (1969)
    Soil moisture forecasting.
    Nota 513, I.C.W., Wageningen.
Rodriguez, E.A., Gonzalez, A.J., Beltran, L. and Villaraga, H. (1988)
    Analisis dinamico deslizamiento "La Siria".
    Research program on landslides in the Colombian road network. Report MOPT-UN 07.3.
    Ministry of Public Works. Bogotá. 54 pp.
Rojas, R., Borrerp, C.A. and Naranjo, J.L. (1986)
    Comparacion de mapas de contornos isopacos de las erupciones del volcan del Ruiz: R-7, R-4, R-2 y R-0.
    Revista CIAF, Vol. 11, Nr 1-3, 7 pp.
Romero, J.A., Florez, A. and Sanchez, H.A. (1989)
    Inventario inicial de riesgos naturales.
    Analisis Geograficos, nr. 16, Instituto Geografico Augustin Codazzi, Bogotá, Colombia, 56 pp.
Rosenbaum, M.S. and Warren, C.D. (1986)
    Creating a Geological Database for Planning Tunnels underr London.
    Quarterly Journal of Engineering Geology, London, Vol. 19, pp. 413-424.
Ruiz, C.E. (1981)
    Los rellenos hidraulicos, una experiencia regional.
    Boletin de Vias, Universidad Nacional de Colombia, Seccional Manizales, Colombia, Vol.IX, No.47.
Runqiu, H. and Yuanguo, L. (1992)
    Logical message model of slope stability prediction in the Three Gorges reservoir area, China.
    Proceedings 6th International Symposium on Landslides, Christchurch, New Zealand, Vol 2, pp 977-981.
Rupke, J. de Graaff, L.W.S., de Jong, M.G.G. and Verhofstad, J. (1987)
    A geomorphological mapping system at scale 1:10.000 for mountainous areas.
    Zeitschrift für Geomorphologie N.F., 31 Nr. 2, pp. 229-242.
Rupke, J., Cammeraat, E., Seijmonsbergen, A.C. and Westen, C.J.v (1988)
    Engineering geomorphology of the Widentobel catchment, Appenzell and Sankt Gallen, Switzerland. A Geomorphological inventory system applied to geotechnical appraisal of slope stability.
    Engineering Geology 26, pp 33-68.
Sabto, M. (1991)
    Probabilistic modelling applied to landslides in central Colombia using GIS procedures.
    Unpublished Msc thesis, ITC, Enschede, Netherlands, 26 pp.
Salgado, L.E. and Chacon, F.B. (1991)
    Mapa de fallas en la zona de influencia sismica del eje Cafetero de la Cordillera central de Colombia.
    Internal report, Universidad Nacional de Colombia, Seccional Manizales, 54 pp + 2 maps.
Salgado, L.E. and Hurtado, J.E. (1991)
    Mapa de isosistas de intensidades del terremoto de Noviembre 23 de 1979, para el municipio de Manizales.
    Internal report, Universidad Nacional de Colombia, Seccional Manizales, 17 pp + 1 map.
Salomé, A.I. and var Dorsser, H.J. (1982)
    Examples of 1:50.000 scale geomorphological maps of part of the Ardennes.
    Zeitschrift für Geomorphologie Bnd. 26, (4), pp. 481-489.
Salomé, A.I. and van Dorsser, H.J. (1985)
    Some reflections on Geomorphological Mapping Systems.
    Zeitschrift für Geomorphologie Bnd. 29, (3), pp. 375-380.
Sauchyn, D.J. and Trench, N.R. (1978)
    Landsat applied to landslide mapping.
    Photogrammetric Engineering and Remote Sensing 44, No.6, pp 735-741.
Schnabel and Seed (1972)
    Accelerations in rock for earthquakes in the western United States.
    Seismological Society of America Bulletin 62, pp 501-516.
Seijmonsbergen, A.C. (1992)
    Geomorphological Evolution of an Alpine area and its application to Geotechnical and Natural Hazard Appraisal.
    PhD Thesis, University of Amsterdam, 109 pp.
Seijmonsbergen, A.C., Van Westen, C.J., and Rupke, J. (ed) (1989)
    Geomorphological-, Geotechnical- and Natural Hazard maps of the Hintere Bregenzerwald area (Vorarlberg, Austria) Set of 12 maps + overlays + explanation.
    Gebr. Borntraeger, Stutgart, Germany.
Selby, M.J. (1982)
    Hillslope materials and processes.
    Oxford University Press, Oxford, 264 pp.
Sharpe, C.F.S. (1938)
    Landslides and related phenomena.
    Columbia Univ. Press, New York, 137 pp.
Sijmons, K. (1992)
    Cartographic representation and production of GIS data.
    Proceedings 1er Simposio Internacional sobre Sensores Remotos y Sistemas de Informacion Geografica para el estudio de Riesgos Naturales, Bogotá, Colombia, pp. 664-672.
Simões, M.G., Vieira, H.M. and dos Santos, U.P. (1992)
    Evaluation and mapping of landslide hazard on desorderly occupied areas through GIS and remote sensing techniques.
    Proceedings 1er Simposio Internacional sobre Sensores Remotos y Sistemas de Informacion Geografica (SIG) para el estudio de Riesgos Naturales, Bogotá, Colombia, pp. 289-303.
SODEIC LTD (1987)
    Estudio de la subcuenca del rio Chinchina: mapas de erosion, socioeconomica y infraestructura, hidrologia, climatologia y sedimentologia
    Internal report for CRAMSA, Manizales, Colombia, 192 pp & maps.
Soeters, R., Rengers, N. and Van Westen, C.J. (1991)
    Remote sensing and geographical information systems as applied to mountain hazard analysis and environmental monitoring.

Proceedings 8th Thematic Conference on Geologic Remote Sensing (ERIM), April 29-May 2, 1991, Denver, USA,
Vol. 2, pp. 1389-1402.
Sowers, G.F. and Royster, D.L. (1978)
Field instrumentation.
In: *Landslides and engineering practice*. Eckel E.B. (ed). Special report no. 29., Highway Research
Board, pp 81-111.
SPOT (1986)
SPOT XS 9 aug 86, path/row 643/340, incidence angle 14.1 degrees Left. Western part.
SPOT XS 9 aug 86, path/row 644/340, incidence angle 18 degrees Left. Eastern part.
SPOT XS 5 sep 86, path/row 643/340, incidence angle 26.1 degrees Right. Western part.
SPOT image, France
Stakenborg, J.H.T. (1986)
Digitizing alpine morphology. A digital terrain model based on a geomorphological map for computer-
assisted applied mapping.
ITC-Journal 1986-4, pp 299-306.
Statgraphics (1991)
Statgraphics Reference Manual, version 5.0. STSC, Inc. USA.
Stephens, P.R. (1988)
Use of satellite data to map landslides.
Proceedings 9th Asian Conference on Remote Sensing, Bangkok, pp. J.11.1-J11.7.
Stevenson, P.C. (1977)
An empirical method for the evaluation of relative landslide risk.
Bulletin International Association of Engineering Geologists, No. 16, pp 69-72.
Sumbukeni, H. (1992)
Symbolosation system for geomorphological map design in a GIS environment.
Unpublished Msc thesis, ITC, Enschede, 140 pp.
Thouret, J.C. (1989a)
Geomorfologia y Crono-estratigrafia del Macizo Volcanico Ruiz-Tolima (Cordillera Central Colombiana)
In: *Studies on tropical Andean Ecosystems*. Van der Hammen, T., Diaz-Piedrahita and Alvarez, V.J.
(eds). Vol. 3 (seg. parte), pp. 257-277.
Thouret, J.C. (1989b)
Suelos de la Cordillera Central, transecto Parque Los Nevados.
In: *Studies on tropical Andean Ecosystems*. Van der Hammen, T., Diaz-Piedrahita and Alvarez, V.J.
(eds). Vol. 3 (seg. parte), pp. 293-441.
Thouret, J.C. and Fabre, D. (1989)
Procesos morfodinamicos sobre las vertientes de la Cordillera Central
In: *Studies on tropical Andean Ecosystems*. Van der Hammen, T., Diaz-Piedrahita and Alvarez, V.J.
(eds). Vol. 3 (seg. parte), pp. 279-291.
Thouret, J.C., Gourgand, A. and Calvache, M.L. (1989)
The eruption of the Nevado del Ruiz on the 13th of November 1985.
In: *Studies on tropical Andean Ecosystems*. Van der Hammen, T., Diaz-Piedrahita and Alvarez, V.J.
(eds). Vol. 3 (seg. parte), pp. 217-255.
Tomlin, C.D. (1990)
Geographic Information Systems and cartographic modelling.
Prentice Hall, New Jersey, 249 pp.
Trifunac, M.D. and Brady, A.G. (1975)
On the correlation of seismic intensity scales with the peaks of recorded strong ground motion.
Bulletin Seismological Society of America 65, p 139-162.
Turkstra, J., Alvarez, V.J. and Mendez, D. (1991)
An application of Geographical Information Systems in urban planning. A case study of Manizales,
Colombia.
Report: ITC & IGAC, Enschede, The Netherlands, 125 pp.
UNESCO (1978)
The assessment and mitigation of earthquake risk
UNESCO Natural hazard series no. 1, United Nations Educational, Scientific and Cultural Organization,
341 pp.
Universidad Nacional de Colombia, Seccional de Manizales, (1986)
Plan integral de desarollo urbano Manizales, Manizales, Colombia.
Internal report Universidad Nacional de Colombia- Seccional Manizales & Munucipio de Manizales.
Vol. 1. 150 pp.
Valencia, C.E. (1988)
Geotectonica regional del antiguo Caldas con enfasis en la aplicacion a la ingenieria sismica.
Unpublished MSc thesis. Universidad de los Andes, Bogotá, Colombia, 54 pp.
Valencia, L.M. (1990)
Recommendations for the production and revision of Colombian maps 1:100.000 utilizing remote sensing
data.
Unpublished MsC thesis, ITC Enshede, 100 pp.
Valenzuela, C.R. (1988)
ILWIS overview.
ITC Journal 1988-1, pp. 4-14
Van Asch, T.W.J. (1984)
Landslides: The deduction of strength parameters of materials from equilibrium analysis.
Catena, Vol. 11, pp.39-49.
Van Asch, T.W.J, Van Westen, C.J., Blijenberg, H. and Terlien, M. (1992)
Quantitative landslide hazard analyses in volcanic ashes of the Chinchina area, Colombia.
Proceedings 1er Simposio Internacional sobre Sensores Remotos y Sistemas de Informacion Geografica
para el estudio de Riesgos Naturales, Bogotá, Colombia 10-12 march 1992, pp. 433-443.
Van Dijke, J.J. and Van Westen, C.J. (1990)
Rockfall hazard: a geomorphological application of neighbourhood analysis with ILWIS.
ITC-Journal 1990-1, pp. 40-44.
Van Dorsser, H.J. and Salome, A.I. (1983)
Mapping in physical geography: three maps of a formerly glaciated lowland.
Geologie en Mijnbouw, Vol. 62., No. 4, pp. 601-610.
Van Duren, I. (1992)
Landuse interpretation of the Chinchina area.
Unpublished report ITC. 2 maps + legends.
Van Westen, C.J. (1989)
ITC-UNESCO project on G.I.S. for Mountain Hazard Analysis

Proceedings First South American Symposium on Landslides, 7-10 August 1989, Paipa, Colombia, pp 214-224.
Van Westen, C.J. and Alzate, J.B. (1990)
Mountain hazard analysis using a PC-based GIS
Proc. 6th Int. Congr. Int. Assoc. Eng. Geol., Vol. 1, pp. 265-272.
Van Westen, C.J. and Alzate, J.B. (1990)
Analisis de Amenazas en areas montañosas, utilizando un SIG basado en un computador personal.
in: Hermelin (ed) AGID Report No 13: Environmental Geology and Natural Hazards of the Andean Region,
pp 527-536.
Van Westen, C.J. 1992a
Scale Related GIS techniques in the analysis of landslide hazard.
Proceedings 1er Simposio Internacional sobre Sensores Remotos y Sistemas de Informacion Geografica (SIG)
para el estudio de Riesgos Naturales, Bogotá, Colombia, pp. 484-498.
Van Westen, C.J. 1992b
Medium scale hazard analysis using GIS.
Proceedings 1er Simposio Internacional sobre Sensores Remotos y Sistemas de Informacion Geografica (SIG)
para el estudio de Riesgos Naturales, Bogotá, Colombia, Vol. 2, 15 pp.
Vargas, G. (1990)
Estructuras y deformacion en la faja creatica en los alrededores de Manizales, Caldas
Thesis, Universidad de Caldas, Manizales, 66p.
Vargas, G.C. (1992)
Methodologie pour l'etablissement de cartes de sensibilité aux mouvements de terrain fonde sur
l'utulisation d'un couple stereographique SPOT XS/TM. Application à la region de Paz del Rio (Colombie)
Proceedings 1er Simposio Internacional sobre Sensores Remotos y Sistemas de Informacion Geografica (SIG)
para el estudio de Riesgos Naturales, Bogotá, Colombia, pp. 201-220.
Varnes, D.J. (1978)
Landslide types and processes.
In: Landslides and engineering practice. E.B. Eckel (ed). Special report no. 29., Highway Research
Board, pp 20-47.
Varnes, D.J. (1984)
Landslide Hazard Zonation: a review of principles and practice
Commission on Landslides of the IAEG, UNESCO, Natural Hazards No 3, 61 pp.
Verstappen, H.Th. and van Zuidam, R.A. (1975)
ITC System of Geomorphological Survey.
ITC Textbook VII-2, ITC, Enschede, 52 pp.
Vis, M. (1989)
Processes and patterns of erosion in natural and disturbed Andean forest ecosystems
PhD Thesis, University of Amsterdam, The Netherlands, 114 pp.
Wadge, G. (1988)
The potential of GIS for modelling of gravity flows and slope instabilities.
International Journal on GIS, Vol. 2., No. 2, pp. 143-152.
Wagner, A., Olivier, R. and Leite, E. (1988)
Rock and Debris Slide Risk Maps Applied to Low-Volume Roads in Nepal. Proceedings 4th International
Conference on Low Volume Roads. Transportation Research Record 1106. pp 255-267.
Ward, T.J., Ruh-Ming Li and Simons, D.B. (1982)
Mapping landslide hazards in forest watershed.
Journal of Geotechnical Engineering Division, Proceedings of the American Society of Civil Engineers,
Vol 108, No. GT2, pp.319-324.
Wentworth, C.M., Ellen, S.D. and Mark, R.K. (1987)
Improved analysis of regional engineering geology using GIS.
Proceedings GIS'78, San Fransisco, USA, 26-30 october, 1987, pp. 636-649.
Wickham, G.E., Tiedemann, H.R. and Skinner, E.H. (1972)
Support determination based on geologic predictions.
Proceedings Rapid Excavation and Tunneling Conference, AIME, New York, 1972, pp. 43-64.
Wieczorek, G.F. (1984)
Preparing a detailed landslide-inventory map for hazard evaluation and reduction.
Bull. Ass. Eng. Geol. Vol.21, no. 3, pp 337-342.
Wright, R.H. and Nilsen, T.H. (1974)
Isopleth map of landslide deposits, southern San Fransico Bay region, California.
US Geological Field Studies Map MF-550.
Wright, R.H., Campbell, R.H. and Nilsen, T.H. (1974)
Preparation and use of isopleth maps of landslide deposits.
Geology, No.2, pp 483-485.
Yin, K.L. and Yan, T.Z. (1988)
Statistical prediction model for slope instability of metamorphosed rocks
Proceedings 5th International Symposium on Landslides, Lausanne, Switzerland, Vol. 2, pp 1269-1272.
Zaruba, Q. and Mencl, V. (1969)
Landslides and their control.
Academia & Elsevier, Prague, 205 pp.
Zevenbergen, L.W. and Thorne, C.R. (1987)
Quantitative analysis of land surface topography.
Earth Surface Processes and Landforms, Vol. 12, pp. 47-56.
Zuidam, R.A.van (1986)
Terrain classification
ITC-textbook, ITC, Enschede, The Netherlands.

APPENDICES

APPENDIX 1: Legend of the TMU map

CRITERA FOR DIFFERENT INFORMATION LAYERS:

* A Terrain Mapping Unit is a homogeneous unit with respect to genesis, geology, geomorphology and soils
* A Terrain Mapping Unit can be outlined in a stereo-image on the basis of photomorphic properties.

The following criteria were used:

```
TMU complexes  :  - Altitude and predominant genetic origin
TMU's          :  - Geology
TMU subunits    :  - Internal relief and drainage density
Elements       :  - Form and genesis
Facets         :  - Genesis and morphography
Processes      :  - Processes
```

TERRAIN MAPPING UNIT COMPLEXES

100   Units of fluvio-glacial and fluvio-volcanic origin occurring throughout the area restricted to the main valleys.

200   Units of denudational origin with thick mantles of unlithified material with less evidences of recent uplift
    (occurring in the W of the area between 900 and 1300m)

300   Units of denudational structural origin subjected to intense recent uplifting consisting of N-S oriented valleys and ridges
    (occurring in the Romeral fault zone, between 1300 and 2200 m)

400   Units of denudational structural origin consisting of plateau remnants with clear evidence of recent uplifting
    (occurring in the surroundings of Manizales between 1700 and 2300 m)

500   Units of denudational origin consisting of a uniformly dissected planation surface
    (occurring E of the Romeral fault between 2200 and 3000 m.)

600   Units of denudational origin consisting of rugged topography in lava flows
    (occurring in the E between 3000 and 3600 m)

700   Units of glacial origin consisting of glacially eroded older lavaflows
    (occurring in the E between 3600 and 4200 m)

800   Units of glacial and volcanic origin consisting of glacially eroded younger lavaflows
    (occurring in the E between 4200 and 4800 m)

900   Units of glacial origin consisting of actual glaciers and very recently deglaciated lava flows.

The subdivision in Terrain Mapping Units is as follows:

TERRAIN MAPPING UNITS AND SUBUNITS

100   Units of fluvio-glacial and fluvio-volcanic origin occurring throughout the area restricted to the main valleys.
    110 Units in predominantly alluvial materials
        111 Affected by 1985 Ruiz mudflows
        112 Not affected
    120 Units in predominantly debris-flow materials
        121 Flat
        122 Dissected
        123 With colluvial cover
        124 Terrace slope
    130 Units in pyroclastic flow materials
        131 Flat
        132 Dissected
        133 With colluvial cover
        134 Terrace slope

200   Units of denudational origin with thick mantles of unlithified material with less evidences of recent uplift (occurring in the W of the area between 900 and 1300m)
    210 Units in sedimentary, low-resistant rocks
        211 Flat
        212 Low relief and low drainage density
        213 Low relief and high drainage density
        214 High relief and low drainage density
        215 High relief and high drainage density
    220 Units in intrusive resistant rocks
        221 Flat
        222 Low relief and low drainage density
        223 Low relief and high drainage density
        224 High relief and low drainage density
        225 High relief and high drainage density
    230 Units in high-grade metamorphic, less resistant rocks
        231 Flat
        232 Low relief and low drainage density
        233 Low relief and high drainage density
        234 High relief and low drainage density
        235 High relief and high drainage density

    240 Units in meta-sedimentary rocks with varying resistance
        241 Flat
        242 Low relief and low drainage density
        243 Low relief and high drainage density
        244 High relief and low drainage density
        245 High relief and high drainage density
    250 Units in resistant igneous rocks
        251 Flat
        252 Low relief and low drainage density
        253 Low relief and high drainage density
        254 High relief and low drainage density
        255 High relief and high drainage density

300   Units of denudational structural origin subjected to intense recent uplifting, consisting of N-S oriented valleys and ridges (occurring in the Romeral fault zone, between 1300 and 2200 m)
    310 Units in partly metamorphosed resistant intrusive rocks
        311 Flat
        312 Low relief and low drainage density
        313 Low relief and high drainage density
        314 High relief and low drainage density
        315 High relief and high drainage density
    320 Units in highly metamorphosed less resistant intrusive rocks
        321 Flat
        322 Low relief and low drainage density
        323 Low relief and high drainage density
        324 High relief and low drainage density
        325 High relief and high drainage density
    330 Units in meta-sedimentary rocks with varying resistance
        331 Flat
        332 Low relief and low drainage density
        333 Low relief and high drainage density
        334 High relief and low drainage density
        335 High relief and high drainage density
    340 Units in resistant igneous rocks
        341 Flat
        342 Low relief and low drainage density
        343 Low relief and high drainage density
        344 High relief and low drainage density
        345 High relief and high drainage density

400   Units of denudational structural origin consisting of plateau remnants with clear evidence of recent uplifting (occurring in the surroundings of Manizales between 1700 and 2300 m)
    410 Plateau remnants in mixed lahar, alluvial, and pyroclastic flow material with a thick ash cover
    420 Slopes in mixed lahar, alluvial, and pyroclastic material
        430 With low relief and low drainage density
        440 With low relief and high drainage density
        450 With high relief and low drainage density
        460 With high relief and high drainge density
        470 Near vertical slopes, mostly fault scarps
        480 Slopes with colluvial cover

500   Units of denudational origin consisting of a uniformly dissected planation surface (occurring E of the Romeral fault between 2200 and 3000 m)
    510 Units in highly resistant lavas
        511 Relatively young dome with high relief and low drainage density
        512 Relatively young collapsed dome with low relief and low drainage density
    520 Units in meta-sedimentary rocks with varying resistance
        521 Flat
        522 Low relief and low drainage density
        523 Low relief and high drainage density
        524 High relief and low drainage density
        525 High relief and high drainage density
    530 Units in resistant igneous rocks
        531 Flat
        532 Low relief and low drainage density
        533 Low relief and high drainage density
        534 High relief and low drainage density
        535 High relief and high drainage density
    540 Units in less resistant intrusives
        541 Flat
        542 Low relief and low drainage density
        543 Low relief and high drainage density
        544 High relief and low drainage density
        545 High relief and high drainage density
    550 Units in less resistant metamorphic rocks
        551 Flat
        552 Low relief and low drainage density
        553 Low relief and high drainage density
        554 High relief and low drainage density
        555 High relief and high drainage density

600   Units of denudational origin consisting of rugged topography in lava flows (occurring in the E between 3000 and 3600 m)
    610 Units in lavas subjected to intense denudation which have lost their original flow morphology
        611 Flat
        612 Low relief and low drainage density
        613 Low relief and high drainage density
        614 High relief and low drainage density
        615 High relief and high drainage density
        616 Near vertical slopes
        617 Large landslide in lavas

620 Units in lavas subjected to less intense denudation in which the original flow morphology is still recognizable
  621 Flat
  622 Low relief and low drainage density
  623 Ligh relief and low drainage density
  624 High relief and high drainage density
  625 Near vertical slopes
  626 Slopes with colluvial cover
700 Units of glacial origin consisting of glacially eroded older lava flows (occurring in the E between 3600 and 4200 m)
710 Plateaus underlaid by lavas without clear flow morphology
  711 Low relief and low drainge density covered by morainic deposits
  712 Low relief and low drainge density covered by colluvial cover
  713 Low relief and low drainge density without cover
720 Clearly recognizable lava flows
  721 Flat
  722 Low relief and low drainage density
  723 High relief and low drainage density
730 Valley floors between lava flows
  731 Low relief and low drainage density covered with morainic deposits
  732 Low relief and low drainage density with colluvial cover
740 Valley slopes between lava flows
  741 Glacial cirque; high relief and high drainage density
  742 Glacial valley slopes: smooth; high relief and low drainage density
  743 Glacial valley slopes: dissected; high relief and high drainge density
  744 Glacial valley slopes: with morainic deposits: high relief and low drainage density
800 Units of glacial and volcanic origin consisting of glacially eroded younger lava flows (occurring in the E between 4200 and 4800 m)
810 Clearly recognizable lava flows
  811 Flat
  812 Low relief, smooth surface
  813 Low relief, rough surface
  814 High relief, smooth surface
  815 High relief, rough surface
  816 Near vertical slopes
  817 Slopes with colluvial cover
820 Valley floor between lava flows
  821 Low relief and low drainge density in morainic deposits
  822 Low relief and low drainge density in colluvial
  823 Low relief and high drainge denity in peat 824 With low relief and low drainage density without soil cover
830 Volcanic domes with subsequent glacial erosion
  831 Intact
  832 Collapsed
840 Crater
  841 Active crater
  842 Inactive crater
850 Volcanic cone
860 Volcanic neck
900 Units of glacial origin consisting of actual glaciers and very recently deglaciated lavaflows.
910 Glacier not affected by 1985 eruption
920 Glacier affected by 1985 eruption
930 Deglaciated during 1985 eruption

APPENDIX 2: Geomorphological checklists

RUN$	PHOTO%	POINTNR.%	PROBLEM$
Photorun on which the point is found	Photo number	Number of point to be checked	Description of problem that has to be solved

Format of the list for field checking points of doubt from photo-interpretation.

RUN	PHOTO	POINTNR.	GS#	SLOPEANGLE	SLOPE LENGTH	CONVEXITY
Photo run	Photo number	Observation point nr.	Geomorphological subunit code	Measured slope angle in degrees	Slope length class	Slope convexity class

Format of a checklist for the collection of semi-quantitative morphometric data in the field for the geomorphological subunits.

APPENDIX 3: Explanation of landslide checklist

Variable	Class	Explanation	Variable	Class	Explanation
Observer	Name	Name of observer	Activity	1-3	Landslide activity
Project	Name	Project name	Maincaus	0-15	Main cause of failure
OP	nr	Observation point	Damage	0-9	Observed damage
Run	Name	Photo run	Stabil	0-7	Stabilization measures
Photo	nr	Photo number	Vulner	0-9	Elements at risk
Slidenr	nr	Landslide number on photo	Landuse	1-13	Land use before failure
Day/Month	DD/MM	Date of observation	Scarpstat	0-2	State of scarp
Location	Name	Location description	Scarpveg	0-3	Vegetation on scarp
Altitude	m	Altitude	Scarpform	0-2	Form of scarp
Slopedir	degr.	Direction of original slope	Scarparea	0-3	Area of scarp
Slopeangle	degr.	Inclination of original slope	Waterout	0-1	Water seepage from scarp
Slopeup	1-4	Slope length downslope of scarp	Translen	m	Length between end of scarp and beginning of body
Slopedown	1-4	Slope length upslope of scarp			
Sloprof	1-3	Convexity of slope in profile	Bodystat	1-4	State of body
Sloplan	1-3	Convexity of slope in plan	Bodyform	0-3	Form of body
Lslength	m	Landslide length from top of scarp to end of scarp	Bodyarea	0-3	Area of body
			Bodyhyd	0-3	Water condition of body
lswidth	m	Maximum landslide width	Bodyveg	0-3	Vegetation on body
lsdepth	m	Maximum landslide depth	Slidemat	code	Material in which sliding took place
Type	1-5	Landslide type	Layernr		Layer nr in soil profile
Subtype	0-3	Landslide subtype	Top	cm	Depth of top of layer
Mechanism	1-6	Landslide mechanism	Bottom	cm	Depth of bottom of layer
			Material	code	Material type

Overview of variables from the landslide checklist.

APPENDIX 4: Landslide checklist

LANDSLIDE OBSERVATION SHEET
Observer: Project:

	SCARPSTAT		POINT	
	SCARPVEG		PHOTORUN	
	SCARPFORM		PHOTONR.	
	SCARPAREA		SLIDENR.	
	WATEROUT		DAY	
	TRANSLEN		MONTH	
	BODYSTATE		YEAR	
	BODYFORM		ALTITUDE	
	BODYAREA		SLOPEDIR	
	BODYHYD		SLOPEANGLE	
	BODYVEG		SLOPEUP	
	SLIDEMAT		SLOPEDOWN	
	POINT		SLOPEPROF	
	LAYERNR		SLOPLAN	
	TOP		LSLENGTH	
	BOTTOM		LSWIDTH	
	MATERIAL		LSDEPTH	
	POINT		TYPE	
	LAYERNR		SUBTYPE	
	TOP		MECHANISM	
	BOTTOM		ACTIVITY	
	MATERIAL		MAINCAUSE	
	POINT		DAMAGE	
	LAYERNR		STABIL	
	TOP		VULNER	
	BOTTOM		LANDUSE	
	MATERIAL			

LOCATION:

APPENDIX 5: Soil checklist

SOIL OBSERVATION SHEET
Observer: Project:

GENERAL INFORMATION

OP	RUN	PHOTONR	DAY	MONTH	YEAR	ALTITUDE

LOCATION	SECTOR	SLOPE DIR	SLOPE ANGLE	OUTCROP HEIGHT

DATA ON SOIL LAYERS

	PERMEABILITY		LAYER	
	SORTING		TOP	
	CONSISTENCY		BOTTOM	
	REL.DENSITY		MATERIAL	
	% BOULDERS		COLOUR	
	% COBBLES		LAYERING	
	% GRAVELS		CEMENTATION	
	% SAND		TEXTURE	
	% FINES		MOIST	

POCKET PENETROMETER READINGS

LN	PP	LN	PP	LN	PP	LN	PP	LN	PP

SHEAR VANE TEST   **LINE COUNTINGS**

LN	PEAK	DUMMY	RESID	LN	TOTAL	BOULDERS	COBBLES

SOIL SAMPLES

LN	SAMPLE	REQUIRED TEST

APPENDIX 6: Calculated thickness of soil materials and weathered rock obtained from soil observations

Mat	n	AVG thick SOIL	STD thick SOIL	MIN thick SOIL	MAX thick SOIL	AVG thick W.ROCK	STD thick W.ROCK	MIN thick W.ROCK	MAX Thick W.ROCK	Cortez thick SOIL	Cortez thick W.ROCK
610	2	200	0	200	200	1500	0	1500	1500	300	-
710	2	200	0	200	200	800	0	800	800	1200	2000
730	16	500	400	100	1400	1650	1150	300	4000	800	2000
810	15	200	150	20	500	600	150	400	800	-	2000
820	4	400	0	400	400	900	450	400	1500	-	-
830	83	450	450	10	2000	300	500	100	3000	400	2000
910	7	200	100	100	300	800	400	300	1500	-	-
920	40	400	400	50	1500	800	1300	100	5600	400	3500
930	14	350	200	180	750	800	600	100	1700	1000	1400

Calculated average, standard deviation, minimum and maximum values for thickness of residual soils and weathered rock for the various lithological types (see table 4.11 for list of material codes). The last two columns display estimations given by Cortez (1988).

APPENDIX 7: Soil characteristics estimated in the field.

Mat	N	SORT	LAY	CEM	PERM	MOIST	CONS	RELDENS	COLOR
111	30	4	1	1	3	2	3	0	10YR4/6
112	27	4	1	1	3	2	3	0	10YR5/6
121	9	4	3	1	5	1	0	1	2.5Y4/4
122	1	3	3	1	4	2	0	2	2.5Y6/4
131	5	2	3	1	5	1	0	1	2.5Y3/2
132	6	2	3	1	4	2	0	2	2.5Y4/2
210	3	1	2	1	5	1	0	2	2.5Y6/4
221	5	1	2	1	5	2	0	3	2.5Y6/4
311	27	1	1	2	4	2	4	0	2.5Y4/3
312	15	1	1	1	3	2	4	0	2.5Y8/4
314	4	1	1	1	3	1	5	0	2.5Y6/4
321	8	1	1	1	4	2	0	4	2.5YR6/2
322	5	2	1	1	3	2	0	3	2.5YR5/4
323	1	3	1	3	3	2	0	4	2.5YR6/4
410	23	1	1	1	4	3	2	0	10YR5/6
420	6	2	1	1	4	2	0	2	10YR6/4
430	3	1	1	1	4	2	0	2	10YR5/6
611	5	3	1	1	2	2	4	0	2.5Y7/6
711	7	3	1	1	3	2	3	0	2.5Y5/6
731	7	2	1	1	2	2	2	0	7.5YR5/6
811	7	2	1	1	4	2	2	0	10YR5/6
821	5	3	1	1	2	2	3	0	7.5YR5/8
831	20	2	1	1	2	2	2	0	7.5YR5/8
911	2	2	1	1	1	3	2	0	5YR7/6
921	14	2	1	1	2	2	2	0	10YR5/8
931	3	2	1	1	2	2	4	0	5YR5/8
1011	5	3	3	2	2	2	3	0	2.5YR7/3
1021	1	3	1	2	2	2	2	0	10YR4/6
1031	9	4	1	2	1	2	2	0	10YR4/5

Mat	= Material code (see table 3.11)	N	=	Number of observations
SORT	= Sorting code	LAY	=	Layering code
CEM	= Cementation code	PERM	=	Permeability code
MOIST	= Moisture condition code	CONS	=	Consistency code
RELDENS	= Relative density code	COLOR	=	Color according to Munsell scale

Soil material description using estimated field characteristics. See tables 4.11 and 4.12 for explanation of codes.

APPENDIX 8: Pocket penetrometer and shear vane results

MATERIAL CODE	Pocket penetrometer test				Shear vane test		
	N	ppavg kgf/cm²	PPMIN kgf/cm²	PPMAX Kgf/cm²	N	PEAKAVG KPa	RESIDAVG KPa
111	5	3.150	1.700	4.500	4	13.78	3.95
112	14	2.977	0.500	4.500	2	7.25	3.91
121	5	4.500	4.500	4.500	-		
131	1	2.145	1.500	2.700	-		
221	2	0.835	0.300	1.000	-		
311	9	3.308	1.000	4.500	-		
312	9	3.822	1.250	4.500	-		
321	1	4.250	4.000	4.500	2	7.30	3.2
322	3	4.500	4.500	4.500	-		
410	2	1.734	1.000	3.500	-		
420	4	3.881	1.600	4.500	-		
430	2	3.470	2.000	4.500	-		
731	4	4.375	2.700	4.500	2	10.60	3.1
811	2	4.425	4.200	4.500	-		
831	7	3.487	1.250	5.000	2	3.85	1.8
911	2	2.755	1.750	4.000	-		
912	2	2.262	0.750	3.500	-		
921	7	3.317	1.250	4.500	2	20.40	5.6
1021	1	1.950	1.250	2.750	-		
1031	4	4.162	3.000	4.500	-		

N   = Number of observations
PPAVG   = Average pocket penetrometer reading (kgf/cm²)
PPMIN   = Minimum pocket penetrometer reading (kgf/cm²)
PPMAX   = Maximum pocket penetrometer reading (kgf/cm²)
PEAKAVG = Peak shear vane strength (KPa)
RESIDAVG = Residual shear vane strength (KPa)

Recalculated pocket-penetrometer values for different soil types.

APPENDIX 9: Estimated grain-size distributions
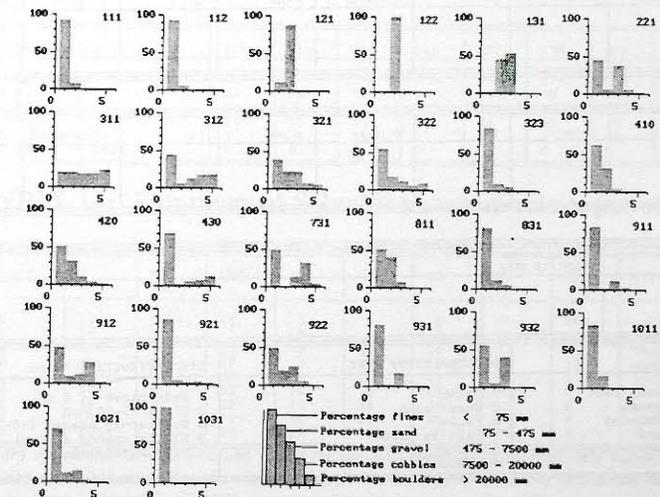
Histograms showing the estimated grain-size distributions for each soil type.

APPENDIX 10: Rock checklist

```
┌─────────────────────────────────────────────────────────────────┐
│ ROCK OBSERVATION SHEET                                           │
│ Observer:              Project:                                 │
├─────────────────────────────────────────────────────────────────┤
│ GENERAL INFORMATION                                             │
├──────┬──────┬─────────┬────────┬────────┬────────┬──────────────┤
│ OP   │ RUN  │ PHOTONR │ DAY    │ MONTH  │ YEAR   │ ALTITUDE     │
├──────┴──────┴─────────┴────────┴────────┴────────┴──────────────┤
│ LOCATION        │ OUTCROP DIR │ OUTCROP ANGLE │ OUTCROP HEIGHT  │
├─────────────────────────────────────────────────────────────────┤
│ DATA ON LITHOLOGICAL GROUPS                                      │
├──────────┬───────────┬──────────┬──────────┬──────────┬─────────┤
│HOMOGENEOUS│PERCENTAGE OF│MATERIAL │LITHOLOGICAL│WEATHERING│WEATHERING│
│ZONE (LG) │OUTCROP    │CODE Table 4.11│CODE   │ZONE (1 to 6)│DEPTH (Cm)│
├──────────┴───────────┴──────────┴──────────┴──────────┴─────────┤
│ DISCONTINUITY MEASUREMENTS                                       │
├──────┬────────────┬─────────────┬──────────┬──────────┬─────────┤
│ LG   │DN (discont.nr)│DIP DIRECTION│DIP ANGLE│TYPE (1-6)│SPACING (1-5)│
├──────┴────────────┴─────────────┴──────────┴──────────┴─────────┤
│ SCHMIDT HAMMER VALUES                                            │
├────┬────────┬──────┬────┬────────┬──────┬────┬────────┬─────────┤
│ LG │SH value│ANGLE │ LG │SH value│ANGLE │ LG │SH value│ANGLE    │
├────┴────────┴──────┴────┴────────┴──────┴────┴────────┴─────────┤
│ POINT LOAD TESTS                                                │
├────┬────────┬──────┬────┬────────┬──────┬────┬────────┬─────────┤
│ LG │P (Bar) │D (mm)│ LG │P (Bar) │D (mm)│ LG │P (Bar) │D (mm)   │
├────┴────────┴──────┴────┴────────┴──────┴────┴────────┴─────────┤
│ ROCK SAMPLES                                                    │
├────┬──────────┬─────────────────────────────────────────────────┤
│ LG │SAMPLE NR │ REQUIRED TEST                                   │
└────┴──────────┴─────────────────────────────────────────────────┘
```

WEATHERING	DISCONTINUITY TYPE	DISCONTINUITY SPACING
1 Unweathered fresh rock	1 Joint	1 Very close (< 5 cm)
2 Slightly weathered	2 Shear zone	2 Close (5-30 cm)
3 Moderately weathered	3 Fault	3 Moderately spaced (30-100 cm)
4 Highly weathered	4 Bedding plane	4 Widely spaced (1-3 m)
5 Completely weathered	5 foliation	5 Very widely spaced (>3 m)
6 Residual soil	6 Schistosity	

Explanation of rock parameters

APPENDIX 11: Lithological composition of rock material types

Lithological descriptions	610	710	730	810	820	830	910	920	930
Conglomerate	0	0	0	0	0	0	0	5	0
Coarse-grained Sandstone	0	0	0	0	0	0	0	2	0
Medium-grained Sandstone	0	0	0	0	0	0	0	10	0
Fine-grained Sandstone	0	0	0	0	0	0	0	3	0
Meta-sandstone	0	0	0	0	0	6	0	2	0
Greywacke	0	0	0	0	0	0	0	2	0
Chert and carbonaceous lutite	0	0	0	0	0	0	0	2	0
Chert and siliceous lutite	0	0	0	0	0	0	0	3	0
Lutite,chert,sandstone combined	0	0	0	0	0	0	0	6	0
Claystone and sandstone combined	0	0	0	0	8	0	0	31	0
Carbonaceous lutite	0	0	0	0	0	0	10	4	0
Siliceous lutite	0	0	0	0	0	0	0	6	0
Carbonaceous and siliceous lutite	0	0	0	0	0	0	20	6	0
Grey claystone	0	0	0	0	0	0	0	3	0
Brown claystone	0	0	0	0	14	0	0	8	0
Brown and red claystone	0	0	0	0	7	0	0	0	0
Quartz-graphitic schist	0	0	0	0	17	0	10	0	0
Graphitic schist	0	0	0	0	0	10	40	1	0
Chloritic schist	0	0	0	0	0	6	20	0	0
Sericitic schist	0	0	0	0	0	17	0	1	0
Amphibolitic schist	0	0	0	0	0	11	0	1	0
Quartz-micaceous schist	0	0	0	17	47	50	0	0	0
Micaceous quarz-diorite	0	0	0	83	0	0	0	0	0
Andesitic lavas	100	0	0	0	0	0	0	0	0
Diabase	0	0	0	0	0	0	0	0	79
Basic igneous rock	0	0	0	0	0	0	0	1	21
Porphyritic andesite	0	100	0	0	0	0	0	0	0
Acid igneous rock	0	0	4	0	0	0	0	0	0
Intermediate igneous rock	0	0	4	0	7	0	0	0	0
Sills (pegmatite)	0	0	0	0	0	0	0	1	0
Dioritic gabbro	0	0	92	0	0	0	0	0	0
All values in percentages									

APPENDIX 12: Percentage of weathering classes per rock type.

Class	Weathering	610	710	720	810	820	830	910	920	930
1	Fresh	20 %	2 %	8 %	0 %	0 %	0 %	0 %	1 %	12 %
2	Slightly	33	18	36	0	14	33	0	17	12
3	Moderately	33	65	16	33	22	33	20	41	44
4	Highly	14	15	16	50	21	17	50	32	32
5	Completely	0	0	16	17	43	17	30	9	0
6	Residual soil	0	0	8	0	0	0	0	0	0

APPENDIX 13: Summary of Schmidt hammer values per material type

Material	N	N <>0	AVG	STD	%VW	%W	%M	%St	Strength
610	10	10	64	3	0	0	0	100	strong
710	10	10	43	5	0	0	80	20	moderate
730	128	125	33	9	2	16	77	5	moderate
810	24	23	39	8	4	0	83	12	moderate
820	99	70	22	9	29	51	20	0	very_weak
830	96	95	33	11	1	23	69	7	moderate
910	36	27	22	10	25	44	31	0	very_weak
920	1046	895	22	10	14	32	50	4	moderate
930	177	171	38	10	3	9	79	9	moderate

Summary of Schmidt hammer rebound values for the most important rock materials within the study area. Explanation of the columns: Material= material code (table 4.11), n = number of Schmidt hammer readings, n<>0 = readings higher then 10, AVG = average Schmidt hammer value, STD = standard deviation, %VW = percentage very weak, %W = percentage weak, %M = percentage moderate, %S = percentage strong, strength = qualitative rock material strength based.

APPENDIX: 14 Frequency distributions of Schmidt hammer values for different lithologies within material type 920

Class 1: 0 - 5   Class 8: 35 - 40
Class 2: 5 - 10   Class 9: 40 - 45
Class 3: 10 - 15   Class10: 45 - 50
Class 4: 15 - 20   Class11: 50 - 55
Class 5: 20 - 25   Class12: 55 - 60
Class 6: 25 - 30   Class13: 60 - 65
Class 7: 30 - 35   Class14: 65 - 70
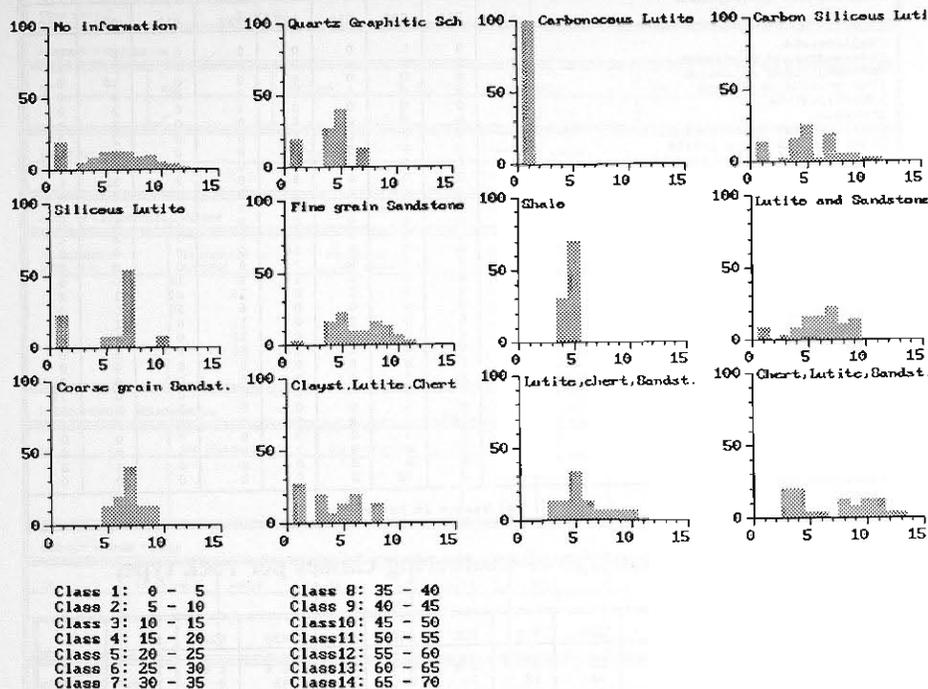
APPENDIX 15: Summary of discontinuity spacing per rock material types.

	Material codes (see table 4.11)								
Material	610	710	730	810	820	830	910	920	930
Average	30-100	30-100	30-100	<5	5-30	<5	5-30	5-30	5-30
Minimum	30-100	30-100	<5	<5	5-30	<5	<5	<5	<5
Maximum	30-100	30-100	>300	5-30	5-30	>300	5-30	>300	>300
All values are in centimeters									

APPENDIX 16: Summary of grain-size distributions for several material types.

MATE RIAL	N	Grav AVG	Sand AVG	Fine AVG	Grav STD	Sand STD	Fine STD	Grav MIN	Sand MIN	Fine MIN	Grav MAX	Sand MAX	Fine MAX
110	33	1	33	66	1	16	16	0	4	13	12	87	96
120	37	1	66	32	1	12	16	0	52	0	13	100	48
130	6	15	72	13	13	13	11	0	50	0	35	91	34
220	9	18	49	31	15	30	27	0	15	4	59	96	84
240	2	0	53	47	0	3	3	0	50	44	1	56	50
310	29	15	36	45	15	23	24	0	8	13	52	87	91
320	12	6	61	33	5	23	21	0	24	0	35	99	74
400	9	2	41	57	1	13	13	0	24	37	10	61	76
620	3	0	69	31	0	12	12	0	44	18	0	82	56
720	2	0	22	78	0	4	4	0	75	16	1	84	25
730	6	0	22	78	0	14	14	0	4	58	1	41	96
810	6	5	66	29	4	15	14	0	44	12	21	88	51
820	1	0	91	9	0	0	0	0	91	9	0	91	9
830	14	9	12	79	7	8	21	0	2	14	82	34	98
910	2	13	16	62	11	12	34	0	4	28	25	28	96
920	12	2	15	83	1	8	9	0	3	66	13	31	96
930	4	2	21	77	1	7	11	0	14	58	6	36	86
1010	3	0	18	82	0	16	18	0	2	57	0	43	98
1020	1	7	20	63	3	2	0	0	0	0	0	0	0
1030	4	0	5	95	0	2	3	0	3	90	0	10	97

Summary of grain-size distributions for several material types (table 4.11). All values are in percentages

APPENDIX 17: Summary of soil classifications for several material types.

MATERIAL CODE	N	LL AVG	PL AVG	PREDOMINANT USCS CODE	PREDOMINANT SOIL GROUPS
110	40	63	37	cl, mh	sandy lean clay, sandy elastic silt
120	31	41	26	sc, sm	clayey sand, silty sand
130	5	–	–	sw, g?	sw or sp
220	3	27	16	cl, sc	sandy lean clay, clayey sand with gravel
240	2	64	42	sm	silty sand,
310	61	51	28	ch, cl, gc, gm, mh, sc	sandy fat clay, sandy lean clay, clayey gravel with sand, silty gravel with sand, gravelly elastic silt with sand, clayey sand
320	8	26	17	gc, mh, sc	clayey gravel with sand, sandy elastic silt, clayey sand
400	10	48	27	mh, ml, sm	sandy elastic silt, sandy silt, silty sand
500	8	57	31	ch, mh	sandy fat clay, sandy elastic silt
730	6	52	36	mh, ml	sandy elastic silt, sandy silt
810	2	–	–	sc	clayey sand
830	13	50	32	mh	sandy elastic silt
910	2	49	35	gm	silty gravel with sand
920	12	75	44	mh, ml	sandy elastic silt, sandy silt
930	4	66	37	mh, ml	sandy elastic silt, gravelly silt
1010	8	54	32	ml	sandy silt
1030	4	83	54	mh	sandy_elastic_silt

Summary of soil-classifications for several meterial types. N = number of samples, LL = liquid limit, PL = plastic limit.

APPENDIX 18: Summary of density values for several material types.

Material	DRY N	DRYAVG	DRYSTD	DRYMIN	DRYMAX	WET N	WET AVG	WET STD	WET MIN	WET MAX
110	11	1.0372	0.3592	0.6300	1.8100	15	1.3796	0.2757	1.0300	1.8300
120	13	1.1554	0.1394	0.9400	1.3800	13	1.4633	0.2199	1.1220	1.8500
130	4	1.0233	0.3671	0.6431	1.4100	4	1.4538	0.3967	1.0391	1.8700
310	0	-	-	-	-	9	1.5624	0.2311	1.2500	2.0800
410	0	-	-	-	-	2	1.1150	0.0050	1.1100	1.1200
830	6	1.2433	0.2692	0.9100	1.6800	10	1.5800	0.2950	1.1400	2.0600
920	2	1.1017	0.0962	0.9100	1.2000	6	1.5400	0.1678	1.3300	1.7600
1010	0	-	-	-	-	3	1.3866	0.2577	1.0300	1.6300
1020	2	1.0450	0.0250	1.0200	1.0700	2	1.5350	0.0050	1.5300	1.5400
1030	4	0.9325	0.0973	0.8600	1.1000	4	1.5725	0.1372	1.4900	1.8100

Summary of density values for several material types occurring in the area. DRY N = number of samples for dry density testing, DRYAVG = average dry density, DRYSTD = standard deviation for dry density, DRYMIN = minimum dry density, DRYMAX = maximum dry density, WETN = number of samples for wet density, WETAVG = average wet density, WETSTD = standard deviation of wet density, WETMIN = minimum wet density, WETMAX = maximum wet density. ALl density values are in g/cm³.

APPENDIX 19: Summary of density values for several rock material types.

MATERIAL CODE	N	DRYDENSITY (AVG) g/cm³	BULDENSITY (AVG) g/cm³
610	1	2.55	2.70
710	1	2.29	2.61
730	7	3.04	3.08
810	3	2.68	2.72
830	7	2.76	2.90
910	3	2.77	2.66
920	18	2.48	2.77
930	5	2.99	3.99
1010	1	1.68	2.41

APPENDIX 20: Summary of clay mineralogical content for several material types.

MAT	N	Q	F	M	K	V	H	C	D	2:1-2:2	AM	CEC AVG	CEC STD	CLAY AVG
110	7	0	0	1	1	0	1	1	0	1	3	19	4	44
310	3	0	0	1	2	0	1	1	0	0	1	16	2	30
730	3	0	0	1	1	1	2	0	0	1	1	32	14	40
810	3	0	0	1	1	1	2	0	0	0	3	16	6	19
830	3	0	0	0	2	0	2	0	0	0	0	18	1	30
920	0	1	1	0	3	0	0	1	0	0	0	15	2	40
930	1	0	0	1	0	2	1	0	0	1	1	28	0	25
1020	1	0	0	0	2	0	2	2	0	1	1	27	0	29
1030	4	0	0	2	1	0	0	1	1	0	1	21	8	69

Summary of clay mineralogy for various soiltypes. 0 = Not present, 1 = traces, 2 = present, 3 = common. Columns: Q = Quartz, F = Feldspate, M = Mica, K = Kaolinite, V = Vermiculite, H = Halloysite, C = Cristobalite, D = Dickite, CEC AVG = Average Cation Exchange Capacity in mEq/100gr, CEC STD = Standard deviation of CEC, CLAY AVG = Average percentage of clay.

APPENDIX 21: Meteorological data base structure.

STATIONS.TBL
| Stat# | Station$ | X! | Y! | Altitud% | Yearmin% | Yearmax% |

METEO MAP

RAINAVG.TBL
| Stat# | Pjan& | Pfeb& | Pmar& | Papr& | Pmay& | Pjun& | Pjul& | Paug& | Psep& | Poct& | Pnov& | Pdec& | Pyear& |

TEMPAVG.TBL
| Stat# | Tjan& | Tfeb& | Tmar& | Tapr& | Tmay& | Tjun& | Tjul& | Taug& | Tsep& | Toct& | Tnov& | Tdec& | Tyear& |

ETPAVG.TBL
| Stat# | Ejan& | Efeb& | Emar& | Eapr& | Emay& | Ejun& | Ejul& | Eaug& | Esep& | Eoct& | Enov& | Edec& | Eyear& |

RAINCOMP.TBL
| Year# | Month# | Day# | Montevideo$ | Cenicafe& | Uribe& | SanCancio& | Marmato& | Agronomia& | etc.... |

DAYRAIN.TBL
| Stat# | Month# | Day# | r71& | r72& | r73& | r74& | r75& | r76& | r77& | r78& | r79& | r80& | r81& | r82& | etc... |

ANTERAIN.TBL
| Stat# | Year# | Month# | Day# | Rain# | R05# | R10# | R15# | R30# |

APPENDIX 22: Land-use data base structure.

PARCELS.TBL
| Parcel% | Farm% | Area& | Slope# | Water# | Useprin% | Plantyr% | Densprin% | Usesec% | Denssec& |

| Water# | Availability$ |

| Usesec% | Useprin% | Landuse$ |

| Slope# | Slopeclass$ |

FARMS.TBL
| Farm% | Nrpoly% | Area& | Peri& | Municip# |

| Municip# | Municipality$ |

WORKERS.TBL
| Farm% | Permanent% | Normal% | Maximum% |

PERSONS.TBL
| Farm% | Person# | Relation# | Sex# | Study# | etc.. |

| Study# | Education$ |

| Sex# | Male/female$ |

| Relation# | Relationtype$ |

MACHINES.TBL
| Farm% | Codem# | Nrmach# | Capacity& | State& |

| State& | State mac |

| Codem# | Type machine |

HOUSES.TBL
| House% | Farm% | Consttype# | Methconst# |

| Methconst# | Method constr$ |

| Consttype# | Type constr$ |

APPENDIX 23: Socioeconomic data base structure.


```
BLOCK.TBL
Block% Sector# Area& Peri&

CITY BLOCKS
MANIZALES

BLOCK1.TBL
Block% Predios# Lotes# Arlotes& Construcc# Pconstruc# Arconstruc& Prophoriz# Condomini#

BLOCK2.TBL
Block% M-institut# M-comercio# M-industri# A-institut& A-comercio& A-industri& Lot-vacio#

BLOCK3.TBL
Block% Area-vacant& Avalu-total% Prom-pisos& Prom-ptos& Ptos-min% Ptos-max%

BLOCK4.TBL
Block% Estrat-min# Estrat-max# Viviendas# Avivienda& Avalu-vi-min% Avalu-vi-max%

BLOCK5.TBL
Block% Prom-pt-vi% Ptos-V-min% Ptos-V-max% Alcobas% Banos% Locales#
```

APPENDIX 24: Descriptive landslide statistics for the medium scale data set

Landslide type	Area M^2	Density permillage	Number	NR/KM^2	percentage of total number
ALL LANDSLIDES					
- Without distinction	39.541×10^5	57.89	1111	16.26	100
- Only active ones	10.816×10^5	15.84	408	5.97	36.7
- Only scarps of actives	7.494×10^5	10.97	345	5.05	31.1
ROTATIONAL SLIDES					
- Without distinction	8.333×10^5	12.20	205	3.00	18.4
- Only active ones	5.884×10^4	0.86	30	0.44	2.7
- Only scarps of actives	3.580×10^4	0.52	26	0.38	2.3
TRANSLATIONAL SLIDES					
- Without distinction	1.004×10^6	14.70	348	5.10	31.3
- Only active ones	3.169×10^5	4.64	161	2.36	14.5
- Only scarps of actives	2.578×10^5	3.77	147	2.15	13.2
FLOW SLIDES					
- Without distinction	9.593×10^5	14.05	211	3.09	19.0
- Only active ones	1.848×10^5	2.71	51	0.75	4.60
- Only scarps of actives	1.053×10^5	1.54	31	0.45	2.8
FLOWS					
- Without distinction	1.085×10^5	1.59	14	0.20	1.3
- Only active ones	5.984×10^4	0.88	5	0.07	0.45
- Only scarps of actives	4.575×10^3	0.07	2	0.03	0.18
DERRUMBES					
- Without distinction	1.049×10^6	15.36	333	.4.88	30.0
- Only active ones	4.612×10^5	6.75	161	2.36	14.5
- Only active scarps	3.462×10^5	5.07	139	2.04	12.5

Calculated landslide densities for different types and activites within the medium-cale study area. Indicated are: the area in m^2, the permillage of the total area, the number of occurrences, the number per km^2 and the percentage of the total number of mass movements

Appendix 25: Summary of landslide characteristics from checklist

VARIABLE	all	1-0	2-0	4-0	1-1	1-2	2-1	2-2	4-2	0-1	0-2
type	1	1	2	4	1	1	2	2	4	1	3
subtype	1	1	1	2	1	2	1	2	2	1	2
newtype	11	11	21	42	11	12	21	22	42	11	32
sloangle	6	6	6	7	6	7	6	6	7	6	6
slopedir	8	2	4	8	6	2	1	7	8	8	8
slopeup	1	1	1	1	1	1	1	1	1	1	1
slodown	1	1	1	1	1	1	1	1	1	1	1
sloprof	1	1	3	1	1	1	3	2	1	1	1
sloplan	2	2	2	2	2	3	3	2	2	2	2
lslength	1	1	1	2	1	1	1	1	1	1	1
lswidth	2	2	2	2	2	1	2	1	2	2	1
lsdepth	1	1	1	1	2	1	1	1	1	1	1
mechanis	1	1	1	1	1	1	1	4	1	1	1
activity	2	2	2	3	2	2	2	3	3	2	2
maincaus	8	8	8	8	2	2	8	8	8	8	8
damage	3	3	3	3	3	3	3	3	3	3	3
stabil	0	0	0	0	0	0	0	0	0	0	0
vulner	3	1	3	1	1	1	3	1	1	3	3
landuse	2	2	6	6	2	5	6	2	6	2	6
scarpsta	1	1	1	1	1	1	1	1	1	1	1
scarpveg	2	2	2	1	2	1	2	2	1	2	2
scarpfor	1	1	2	2	1	1	2	2	2	1	2
scarpare	1	1	1	1	1	1	1	1	1	1	1
waterout	1	1	2	2	1	1	2	1	2	1	2
bodystat	1	1	3	4	1	1	3	3	4	1	3
bodyform	2	2	2	0	3	2	2	2	0	2	2
bodyarea	2	2	2	0	2	1	2	2	0	2	1
bodyhyd	1	1	2	0	1	1	2	1	0	1	2
bodyveg	0	0	0	0	0	0	0	0	0	0	0
observat	211	127	43	33	100	25	27	13	30	13	72

Predominant variable classes for different landslide types, calculated from data obtained via checklists. The column header numbers are combinations of type and subtype: 1-0 = All slides, 2-0 = All flowslides, 4-0 = All derrumbes, 1-1 = Rotational slides, 1-2 = Translational slides, 2-1 = Rotational flowslides, 2-2 = Translational flowslides, 4-2 = Translational derrumbes, 0-1 = All rotational movements, 0-2 = All translational movements. The explantion of the parameter codes can be found in tables 4.9 and 4.10.

APPENDIX 26: Variable classes for statisctical analysis

```
GEOL
Lithological units
1  = inch      Gneissic intrusive of Chinchina
2  = kclp      Schists of Lisboa/Palestina
3  = kd        Volcanic member of the Quebradagrande formation
4  = kdg       Gabbro, diorite of Chinchina
5  = kis       Metasedimentary Quebradagrande Formation
6  = qal       Alluvial sediments
7  = qdfmix    Mix of old debris flow material, alluvial, and ashes
8  = qdw       Weathered debris flow material
9  = qlac      Lake deposits
10 = qlahar    Lahar deposits
11 = qpf       Pyroclastic flow deposits
12 = qpfmix    Mix of pyroclastic flow and debris flow
13 = tadp      Andesitic intrusive of Palestina
14 = toi       Tertiary sediments
```

```
GEOM                                       SLOC2
Simplified Geomorphological mainunits      Classified slope angles
1  = Alluvial units                                min  max
2  = Fluvioglacial/volcanic terraces       1   0  - 10 degrees
3  = Volcanic units and pyroclastic flow levels  2  10 - 20
4  = Denudational units: Hilltops          3  20 - 30
5  = Denudational units: Slopes            4  30 - 40
6  = Denudational units: Niches            5  40 - 50
7  = Denudational units: Hills             6  50 - 60
8  = Denudational units: Colluvial_slopes  7  60 - 70
9  = Denudational units: Large landslide   8  70 - 80
10 = Denudational-Structural: Faultscarp   9  80 - 90
11 = Anthropogeneous area
```

```
GEOS                                       SLOC
Simplified geomorphological subunits       Classified slope angles
1  = alluvial & fluvio-volcanic units             min max
2  = denudational hilltops, ridges and flat areas 1   0 - 2 degrees
3  = denudational slopes and slope deposits    2   2 - 4
4  = denudational niches                       3   4 - 6
5  = mainly fluvial valleys                    4   6 - 10
6  = large mass movements and erosion          5  10 - 13
7  = denudational-structural ridges and niches 6  13 - 17
8  = denudational-structural slopes            7  17 - 21
9  = anthropogenic landforms                   8  21 - 26
                                               9  26 - 33
                                              10  33 - 90
```

```
GEOC                                       PROFC
Geomorphological complexes                 Classified downslope convexity
1  = Western hills zone                     1   <   - 0.004
2  = Romeral fault zone                     2  -0.004 - 0
3  = Terraces                               3   0  - 0.004
                                            4   >     0.004
```

```
LUSE                                       PLANC
Simplified landuse classes                 Classified accrosslope convexity
1  = bare                                   1   <   - 0.004
2  = grass                                  2  -0.004 - 0
3  = shrubs                                 3   0  - 0.004
4  = technified coffee without shade trees  4   >     0.004
5  = technified coffee with shade trees
6  = traditional coffee
7  = other crops                           CATS
8  = forest                                Classified catchment areas
9  = constructions                          1   < 10 hectare
                                            2  10 - 20
ASPCL                                       3  20 - 30
Classified slope directions.                4  30 - 40
     minimum      maximum                   5  40 - 50
1       0           45                      6  50 - 60
2      45           90                      7  60 - 70
3      90          135                      8  70 - 80
4     135          180                      9  80 - 90
5     180          225                     10  > 90 hectares
6     225          270
7     270          315
8     315          360
```

SLLC
Classified distance from ridge
```
1    0  -  50    metres
2   50  - 100
3  100  - 150
4  150  - 200
5  200  - 250
6  250  - 300
7  300  - 350
8  350  - 400
9  400  - 450
10     > 500
```

DTMC
Classified altitude
```
1     < 1200    metres above sea level
2   1200  1300
3   1300  1400
4   1400  1500
5   1500  1600
6   1600  1700
7   1700  1800
8   1800  1900
9   1900  2000
```

CITY
Classified distance from edge of city
```
1   0          within the city itself
2   0 - 25     m distance from city border
3  25 - 50     m distance from city border
4   >50        m distance from city border
```

DR1, DR2, DR3, DR4, DR5, DRT
DR12, DR13, DR14,
DRS1, DRS2, DRS3, DRS,
R1, R2, R3, R
Classified distance from drainage, valley heads,
faults or roads
```
1   < 25       m distance from object
2  25 - 50     m distance from object
3   > 50       m distance from object
```

F1, F2, F3, F,
Classified distance from faults and/or lineaments
```
1    < 50      m distance from object
2   50-100     m distance from object
3  100-150     m distance from object
4  150-200     m distance from object
5   > 250      m distance from object
```

APPENDIX 27: The 33 highest ranking weight values for the occurrence of different mass movement types. Only number density for active features is given (See section 6.3.3.2)

All slides		Rotational slides		Translational slides		Rotational flowslides		Translational flowslides		Derrumbes	
Var	Val	Var	Val	Var	Val	Var	Val	Var	Val	Var	Val
DRS2-1	75	DRS1-1	4	DRS1-1	17	DR4-2	3	GEOM-8	24	R1-2	51
R1-2	63	F3-3	2	DRS2-1	14	GEOL-14	1	SLLC-7	12	DRS2-1	49
R1-1	58	R2-1	2	R1-1	12	F1-4	1	DRS2-1	10	SLOC2-7	46
DRS-1	57	R-1	2	R1-2	12	F2-3	1	DRS-1	8	R1-1	45
SLOC2-7	55	F1-2	2	GEOL-8	11	DRS2-1	1	F1-4	8	DTMC-9	38
SLOC2-6	36	F2-3	2	SLOC2-6	10	F-4	1	SLLC-6	7	DRS-1	31
DTMC-9	33	R1-2	2	SLLC-7	9	GEOL-4	1	F1-3	7	SLOC2-6	27
DRS2-2	29	DRS-1	2	DRS1-1	9	F2-2	1	DRS1-1	7	DRS2-2	19
DRS1-1	28	DR4-1	1	R-1	7	F2-4	1	LUSE-8	6	F1-2	13
F1-2	26	R1-1	1	R2-1	7	DR4-1	1	SLOC2-7	6	DRS-2	11
F1-3	25	F-3	1	R-2	6	ASPCL-1	1	F1-2	6	F1-3	11
F1-4	24	F2-4	1	DRS2-2	6	DR3-2	1	F-4	5	SLOC2-5	11
DRS-2	20	F1-3	1	DRS1-1	6	GEOS-6	1	F-3	4	F1-4	11
GEOM-8	18	F-2	1	R2-2	5	CATS-1	0.5	F1-1	3	LUSE-3	9
F1-1	18	R-2	1	DRS-2	5	LUSE-3	0.5	F-2	3	F1-1	9
F-3	17	DRS1-2	1	F1-2	5	F-3	0.5	DR2-2	3	F3-4	8
SLOC2-5	16	SLLC-3	1	F1-3	5	SLOC-3	0.5	DRS2-2	3	R-2	7
F-2	16	SLOC-7	1	F3-3	5	GEOM-5	0.5	DR2-1	3	F-2	7
R-2	16	F1-1	1	SLOC2-5	5	SLOC2-4	0.4	DRS1-2	3	LUSE-8	7
DR3-2	15	F3-1	1	F1-1	5	F1-3	0.3	SLLC-5	3	F-3	7
F3-3	15	F3-2	1	F1-4	5	SLOC-9	0.3	DRS-2	2	DR5-2	7
F-4	15	F-4	1	F3-2	4	LUSE-9	0.3	LUSE-3	2	GEOL-1	6
SLLC-7	15	DR2-2	0.7	F3-4	4	F1-2	0.3	SLLC-4	2	SLOC2-4	6
R-1	15	F3-4	0.7	F-3	4	SLOC2-5	0.3	SLOC-3	2	F-4	6
LUSE-3	14	GEOS-5	0.6	DR2-1	3	PLANC-3	0.3	CITY-3	2	SLOC-9	6
SLLC-6	14	CATS-3	0.6	DR3-1	3	DR2-1	0.3	F3-3	2	GEOL-11	6
F3-4	13	GEOM-7	0.6	SLOC2-7	3	F3-4	0.3	F3-2	2	DR3-2	6
DR2-2	12	DTMC-5	0.6	SLOC2-4	3	DTMC-3	0.3	F-1	2	F3-3	6
DR2-1	11	F1-4	0.6	GEOS-5	3	ASPCL-6	0.2	GEOL-4	2	R-1	5
SLOC2-4	11	LUSE-6	0.6	DR2-2	3	DR2-2	0.2	GEOL-8	1	DR2-2	5
F-1	10	DRS2-1	0.6	F-2	3	F1-1	0.2	GEOL-14	1	GEOS-5	5
R2-2	10	DR1-1	0.5	GEOS-9	3	DRS-2	0.2	SLOC-2	1	F-1	4
GEOS-5	10	DR2-1	0.5	city-2	3	DR3-1	0.2	SLOC2-4	1	SLOC-10	4

APPENDIX 28: Weight values calculated for active derrumbes. (See section 6.3.3.2)

The first column indicates the weight value for number density, and the second column shows the weight values for area density.

Nr/km2	%	VAR	CLASS
-5.72	-6.76	sloc2	9
-5.72	-6.76	sloc2	8
-5.43	-6.06	sloc	1
-5.40	-7.25	sllc	8
-5.40	-7.25	sllc	7
-4.83	-4.23	sloc	2
-4.17	-5.27	sloc	3
-4.06	-5.45	sloc2	1
-3.89	-5.57	sloc	4
-3.50	-6.72	dtmc	1
-3.17	-6.75	geos	9
-3.17	-6.75	geos	8
-2.57	-6.75	geol	9
-2.57	-6.75	geol	14
-2.57	-6.75	geol	8
-2.51	-6.75	geom	4
-2.51	-6.75	geom	10
-2.51	-6.75	geom	11
-2.51	-6.75	geom	8
-2.51	-6.75	geom	9
-2.43	-6.75	cats	7
-2.43	-6.75	cats	9
-2.43	-6.75	cats	6
-2.34	-6.72	drs3	2
-2.34	-6.72	drs3	1
-2.34	-6.72	drs1	2
-2.34	-6.72	drs1	1
-2.27	-6.28	geom	7
-2.26	-2.57	sllc	1
-2.22	-3.50	geos	2
-2.21	-6.13	geoc	1
-2.18	-5.74	geos	1
-2.10	-6.14	geol	2
-2.04	-2.12	geol	13
-1.79	-5.10	dtmc	2
-1.71	-2.15	profc	2
-1.67	-2.48	drl3	3
-1.64	-2.30	drt	3
-1.64	-2.53	drl2	3
-1.64	-5.54	geol	6
-1.63	-1.95	planc	2
-1.59	-2.34	drl4	3
-1.59	-4.83	f2	1
-1.58	-1.21	drs2	3
-1.57	-1.52	aspcl	2
-1.54	-5.86	geoc	3
-1.51	-3.69	cats	4
-1.51	-1.03	drs	3
-1.49	-6.11	geol	12
-1.43	-2.09	drl	3
-1.41	-4.89	cats	5
-1.34	-4.26	geol	10
-1.21	-0.97	f1	5
-1.18	-0.71	f	5
-1.07	-4.58	geom	1
-1.06	-5.22	sllc	6
-0.99	-0.54	f3	5
-0.99	-3.30	dtmc	3
-0.95	-0.87	luse	4

-0.84	-1.86	sloc2	2
-0.84	-0.41	r	3
-0.84	-3.42	aspcl	6
-0.78	0.68	geol	3
-0.76	-6.37	city	1
-0.72	-3.64	sloc	5
-0.72	-0.33	geos	6
-0.71	-0.75	r1	3
-0.67	-3.70	geom	2
-0.61	-4.32	luse	2
-0.59	-0.36	dr2	2
-0.58	-4.06	geol	7
-0.55	-4.30	geom	3
-0.49	-4.72	f2	2
-0.48	-5.82	dr4	1
-0.42	-5.18	dr4	2
-0.37	3.05	cats	3
-0.36	-1.05	aspcl	1
-0.29	0.12	dr3	3
-0.27	-0.63	luse	9
-0.20	1.39	aspcl	3
-0.14	-3.14	luse	7
-0.13	0.42	r2	3
-0.12	0.09	dr5	3
-0.12	-2.85	profc	3
-0.11	-1.93	sloc	6
-0.05	0.25	city	4
0.04	-0.10	luse	5
0.01	0.03	drs3	3
0.01	0.17	dr4	3
0.01	0.30	f2	5
0.02	3.22	f3	1
0.05	0.16	drs1	3
0.21	2.09	aspcl	7
0.25	0.45	dtmc	4
0.31	1.28	aspcl	5
0.31	-4.29	r2	1
0.34	-4.38	f2	1
0.46	0.53	cats	2
0.53	-2.90	planc	3
0.54	3.11	planc	4
0.56	0.72	cats	1
0.69	5.45	dtmc	7
0.80	-1.41	geos	3
0.80	4.96	geol	5
0.81	-4.68	f2	3
0.82	1.18	geos	7
0.90	4.89	dtmc	6
0.93	3.06	profc	4
0.96	3.06	dtmc	5
1.09	6.00	geos	4
1.11	-5.21	sllc	5
1.12	-4.87	dr5	1
1.28	1.96	planc	1
1.31	7.62	geol	4
1.36	4.56	geom	5
1.41	5.16	geom	6
1.58	-1.66	drl4	1
1.64	-1.61	drt	2

1.68	5.19	geoc	2
1.71	5.69	sloc2	3
1.76	-1.50	drl3	2
1.85	0.89	aspcl	4
1.90	3.15	profc	1
1.91	-1.46	drl2	2
1.97	-1.62	drl	2
2.02	-3.00	r2	2
2.08	4.03	sllc	2
2.09	6.30	drt	1
2.16	0.93	dtmc	8
2.23	-3.97	cats	10
2.33	6.95	drl4	1
2.64	0.67	f3	2
2.67	7.68	drl3	1
2.77	-3.26	dr3	1
2.79	5.44	luse	6
2.88	-1.21	luse	1
3.01	-3.09	city	2
3.08	-0.60	sloc	7
3.24	9.11	drl2	1
3.81	-3.58	city	3
4.06	-0.73	sllc	4
4.07	10.65	drl	1
4.07	3.75	sllc	3
4.13	3.95	dr2	1
4.23	5.66	sloc	8
4.36	9.21	sloc	10
4.47	4.84	f	1
5.00	13.44	geos	5
5.19	1.88	dr2	2
5.40	2.43	r	1
5.56	0.53	f3	3
5.68	-0.40	dr3	2
5.87	2.62	geol	11
6.13	9.68	sloc	9
6.22	4.74	f	4
6.22	9.03	sloc2	4
6.28	11.80	geol	1
6.97	-0.79	dr5	2
6.99	3.03	f	3
7.26	16.33	luse	8
7.27	1.95	f	2
7.37	3.87	r	2
7.70	3.75	f3	4
8.78	10.53	f1	1
8.93	21.27	luse	3
10.62	10.37	f1	4
10.95	7.00	sloc2	5
11.32	7.50	f1	3
11.35	7.10	drs	2
12.70	5.96	f1	2
19.37	14.41	drs2	2
27.55	16.96	sloc2	6
31.24	23.24	drs	1
38.10	56.11	dtmc	9
45.14	49.71	r1	1
46.55	9.56	sloc2	7
49.36	38.73	drs2	1
50.60	51.77	r1	2

APPENDIX 29: Hazard information values for derrumbes using different threshold values for the inclusions within a terrain unit (see section 6.3.4.2)

Map	T	Var1	Var2	Var3	Var4	Var5	Var6	Var7	Var8	Var9	Var10	Var11	Var12	Var13	Var14
dr1	1	+.038	+.035	-.002	–	–	–	–	–	–	–	–	–	–	–
dr1	10	+.071	+.060	+.001	–	–	–	–	–	–	–	–	–	–	–
dr1	20	+.091	+.084	+.005	–	–	–	–	–	–	–	–	–	–	–
dr2	1	+.015	+.018	0.000	–	–	–	–	–	–	–	–	–	–	–
dr2	10	+.034	+.030	0.000	–	–	–	–	–	–	–	–	–	–	–
dr2	20	-.048	+.031	0.000	–	–	–	–	–	–	–	–	–	–	–
dr5	1	+.116	+.124	0.000	–	–	–	–	–	–	–	–	–	–	–
dr5	20	0.000	0.000	0.000	–	–	–	–	–	–	–	–	–	–	–
drt	1	+.006	+.005	-.002	–	–	–	–	–	–	–	–	–	–	–
drt	10	+.017	+.015	+.003	–	–	–	–	–	–	–	–	–	–	–
drt	20	+.036	+.040	0.000	–	–	–	–	–	–	–	–	–	–	–
drs	1	+.099	+.088	0.000	–	–	–	–	–	–	–	–	–	–	–
drs	20	+.125	0.000	0.000	–	–	–	–	–	–	–	–	–	–	–
drs1	1	-.394	-.438	0.000	–	–	–	–	–	–	–	–	–	–	–
drs1	20	0.000	0.000	0.000	–	–	–	–	–	–	–	–	–	–	–
drs2	1	+.245	+.237	0.000	–	–	–	–	–	–	–	–	–	–	–
drs2	20	0.000	+.231	0.000	–	–	–	–	–	–	–	–	–	–	–
drs3	1	0.000	-.496	0.000	–	–	–	–	–	–	–	–	–	–	–
drs3	20	0.000	0.000	0.000	–	–	–	–	–	–	–	–	–	–	–
geoc	1	-.470	+.150	-.363	–	–	–	–	–	–	–	–	–	–	–
geoc	90	-.430	+.176	-.634	–	–	–	–	–	–	–	–	–	–	–
r	1	+.039	+.030	0.000	–	–	–	–	–	–	–	–	–	–	–
r1	1	+.294	+.293	0.000	–	–	–	–	–	–	–	–	–	–	–
r1	20	+.283	+.407	0.000	–	–	–	–	–	–	–	–	–	–	–
r2	1	-.016	+.002	0.000	–	–	–	–	–	–	–	–	–	–	–
r2	20	-.079	-.076	+.002	–	–	–	–	–	–	–	–	–	–	–
plancc	1	+.007	0.000	+.002	+.007	–	–	–	–	–	–	–	–	–	–
plancc	20	+.117	-.045	-.314	+.070	–	–	–	–	–	–	–	–	–	–
profcc	1	+.010	0.000	+.002	+.008	–	–	–	–	–	–	–	–	–	–
profcc	20	+.125	-.031	-.223	+.067	–	–	–	–	–	–	–	–	–	–
f	1	+.058	+.035	+.061	+.049	+.001	–	–	–	–	–	–	–	–	–
f1	1	+.152	+.121	+.147	+.127	0.000	–	–	–	–	–	–	–	–	–
f1	20	+.345	+.341	0.000	0.000	-.004	–	–	–	–	–	–	–	–	–
f2	1	-.190	-.199	-.227	-.229	+.001	–	–	–	–	–	–	–	–	–
f2	20	+.106	-.115	0.000	0.000	0.000	–	–	–	–	–	–	–	–	–
cats	1	-.074	+.115	-.065	+.072	-.458	–	–	–	–	–	–	–	–	–
cats	99	-.074	+.115	-.065	+.072	-.458	–	–	–	–	–	–	–	–	–
sllc	1	+.002	+.015	+.088	+.167	+.148	+.144	-.018	–	–	–	–	–	–	–
sllc	25	-.003	+.085	+.089	0.000	0.000	0.000	0.000	–	–	–	–	–	–	–
aspcl	1	-.065	-.058	-.006	+.022	+.065	+.040	+.022	+.007	–	–	–	–	–	–
aspcl	10	-.105	-.074	+.038	+.106	+.133	-.012	+.004	+.010	–	–	–	–	–	–
aspcl	20	-.119	-.056	-.007	+.090	+.118	-.006	-.002	-.006	–	–	–	–	–	–
dtmc	1	-.115	-.108	-.018	+.082	+.123	+.173	+.144	+.065	+.106	–	–	–	–	–
dtmc	20	0.000	-.278	-.029	+.079	+.117	+.181	+.054	+.186	+.584	–	–	–	–	–
dtmc	25	0.000	-.226	-.030	+.068	+.106	+.150	+.019	+.186	0.000	–	–	–	–	–
sloc2	1	+.003	+.013	+.081	+.144	+.175	+.254	+.027	0.000	0.000	–	–	–	–	–
sloc2	10	-.076	+.035	+.124	+.202	+.155	+.407	0.000	0.000	0.000	–	–	–	–	–
sloc2	20	-.128	-.012	+.164	+.209	+.311	+.584	0.000	0.000	0.000	–	–	–	–	–
sloc	1	-.026	-.031	-.046	+.024	+.022	+.040	+.065	+.100	+.128	+.164	–	–	–	–
sloc	10	-.128	-.272	-.231	-.177	-.158	-.046	+.777	+.146	+.186	+.199	–	–	–	–
sloc	20	-.342	-.200	-.522	-.357	-.530	-.225	-.096	+.186	+.233	+.192	–	–	–	–
luse	1	+.183	+.030	+.144	-.013	+.007	+.132	-.021	+.220	-.112	–	–	–	–	–
luse	10	-.018	-.004	+.091	-.014	+.032	+.146	-.079	-.262	-.040	–	–	–	–	–
luse	20	+.164	-.053	-.371	+.001	-.001	+.201	-.684	0.000	+.019	–	–	–	–	–
geom	1	+.112	-.074	-.143	-.028	+.092	+.069	-.278	+.283	-.593	+.216	0.000	–	–	–
geom	10	+.102	-.079	-.229	-.015	+.096	+.084	-.241	+.283	0.000	-.018	0.000	–	–	–
geom	20	+.027	-.083	-.115	-.123	+.114	+.075	-.250	+.283	0.000	-.018	0.000	–	–	–
geos	1	-.004	-.051	+.035	+.023	+.040	+.052	+.055	-.416	-.563	–	–	–	–	–
geos	10	-.025	-.138	+.054	+.033	+.055	+.059	+.070	0.000	0.000	–	–	–	–	–
geos	20	-.098	-.226	+.096	+.019	+.050	-.132	+.075	0.000	0.000	–	–	–	–	–
geol	1	+.242	-.383	-.031	+.126	+.116	-.144	+.006	0.000	0.000	+.209	+.128	-.573	-.034	-.399
geol	20	+.273	-.413	-.038	+.151	+.132	-.238	+.015	0.000	0.000	+.164	+.010	-.985	+.040	-.607
geol	40	+.298	-.487	-.023	+.195	+.160	-.717	+.007	0.000	0.000	-.115	-.195	-.759	+.083	-.778